Uned Ymchwil Arennol Cymru
Wales Kidney Research Unit

CARDIFF UNIVERSITY
PRIFYSGOL CAERDYDD

The role of miRNAs in peritoneal dialysis associated fibrogenesis

Melisa Lopez-Anton, MSc

Thesis presented for the degree of Philosophiae Doctor

May 2016

Wales Kidney Research Unit, Division of Infection & Immunity,

School of Medicine, Cardiff University

EuTRiPD™
European Training & Research in Peritoneal Dialysis

MARIE CURIE ACTIONS

Declaration

This work has not previously been accepted in substance for any degree and is not concurrently submitted in candidature for any degree.

Signed..... (candidate) Date .....

STATEMENT 1

This thesis is being submitted in partial fulfillment of the requirements for the degree of PhD

Signed..... (candidate) Date .....

STATEMENT 2

This thesis is the result of my own independent work/investigation, except where otherwise stated. Other sources are acknowledged by explicit references.

Signed..... (candidate) Date .....

STATEMENT 3

I hereby give consent for my thesis, if accepted, to be available for photocopying and for inter-library loan, and for the title and summary to be made available to outside organisations.

Signed..... (candidate) Date .....

STATEMENT 4: PREVIOUSLY APPROVED BAR ON ACCESS

I hereby give consent for my thesis, if accepted, to be available for photocopying and for inter-library loans after expiry of a bar on access previously approved by the Graduate Development Committee.

Signed..... (candidate) Date .....

To my parents and sister,

for your support, understanding and love.

Acknowledgements

Firstly, I would like to express my gratefulness to my supervisor Prof Donald Fraser along with my co-supervisors Dr Timothy Bowen, Prof Philip Taylor and Prof Nicholas Topley for offering me the opportunity to study a PhD in their laboratory and their continuous guidance. I would particularly like to thank Prof Donald Fraser and Dr Timothy Bowen for their close supervision, extraordinary patience, helpfulness and understanding in times of stress and difficulties with my experiments. In addition, I am grateful for the time Prof Donald Fraser gave to attend all EuTRiPD academies that were scheduled during my PhD.

I am thankful to Dr Mark Lambie, who helped us in the design and analysis of the GLOBAL miRNA study; to Dr Chantal Colmont, who spent so many hours in the -80 freezers looking for the samples for the study. I would also like to thank all the people that have been involved in the fluid GLOBAL registry used in this thesis. I am grateful to Prof Claus P. Schmitt and ESR Maria Bartosova for their invitation to Heidelberg University (Germany) to undertake a secondment and use the International Pediatric PD Biopsy Study samples for this thesis. I am also appreciative to them for sending me frozen HPMCs during the period ethical approval was not in place at University Hospital of Wales. I would also like to thank Prof Rob Beelen and ESR Evelina Ferrantelli for their contribution in developing the uremic PD mouse model and sharing the samples with Cardiff University for this project. I am grateful to Dr Peter Rutherford and Dr Clifford J Holmes for organizing my secondment in Baxter (Chicago, IL, U.S.).

I am thankful to Dr Usman Kalid and Dr Szabolcs Horvath for organising me to attend a kidney transplant from a living donor (and to the transplant technician that helped me when I had to leave the room soon after the surgery started). A general thanks to all the kidney transplant unit team for their help with collecting the omentum samples from donors that made my research possible.

Thanks to all the people that shared the laboratory and study office with me during my PhD; to all those who shared advise, guidance, scientific and non-scientific conversations; to all those who shared lab-coats and marker pens with me (…and were

not able to find them later); to all those who shared weekends at the lab, laughs and joy for good results and tears, particularly after the challenge of western blots; to all those who throw paper balls at me or shouted loud enough to make me realise there was a study office full of people behind me; to all those who shared coffees pretending they needed one when I needed one.

Thanks to all the people inside and outside the laboratory that listened to my problems and motivated me to continue; to all those friends that are still there for me even though I left Spain a while ago; to all the new friends I have made: to my housemates Albert, Felix and Adriana for reminding me I have a house not just laboratory, for making the house a home, for opening the door with a big smile, for being brave and not renting my room to somebody else while I was writing my thesis; to Fernando and Hector for always being there when I needed them; to Olga for her constant advice, help, time and laughs; to Malena for her support, for listening to me, for her endless WhatsApp voice messages; to Anna Rita for letting me be part of her experience here, for being an important part of mine, for sharing rooms, conferences, academies, nerves, laughs and so many good and bad times; to David for having the courage of sharing these last months with me.

I am thankful to Timothy Gribaudi for his support, encouragement and love during the first years of this thesis; for helping me to apply for this position; for proofreading many documents and recording many talks he never understood.

I am most grateful to my parents and sister because without their sacrifice, education, support and encouragement this thesis would have never been possible; for being there for me even though they are in a different country; for trying to understand me in such a complicated and different context; for loving me in difficult moments; for supporting me with hard decisions; for wanting to learn English just to come to visit me. I am grateful to *my Titi* who has always been there for me; she has been like a mother and a friend to me. A very big thank you to *my Peke*, for unconditionally always being there for me, for helping me to think twice before making decisions and supporting me regardless of what I decide.

Thesis Summary

Peritoneal dialysis (PD) is a life-saving form of renal replacement therapy for those with End Stage Kidney Disease. Peritoneal fibrosis is a considerable problem for PD patients, and mesothelial cells, which line the peritoneal cavity, play a central role in response to injury and fibrogenesis within the peritoneum. Mesothelial cells may undergo mesothelial to mesenchymal transition (MMT) contributing to peritoneal fibrosis and treatment failure. miRNAs are important regulators of fibrosis but their roles in peritoneal fibrosis are largely unknown. Here, a detailed characterization of the MMT process was performed in primary human mesothelial cells (HPMCs) in response to Transforming Growth Factor beta-1 (TGF-β1). Hybridization array showed mesothelial miR-21 and miR-31 expression was up-regulated by TGF-β1 which was validated by RT-qPCR in different PD associated MMT models. Mesothelial cells cultured *ex vivo* from PD patients exhibited phenotypic changes consistent with a progressive MMT process that correlated with an increase in miR-21 and miR-31 expression. Association of miRNA expression and MMT markers in 33 peritoneal biopsies from patients undergoing PD treatment and in PD effluent from 230 PD patients confirmed these results. *In silico* analysis combined 4 target prediction algorithms (Targetscan, miRanda, miRDB and Diana-microT) for miR-21 and integrated the resulting outcome with mRNA arrays comparing omentum vs PD effluent-derived HPMCs with epithelial (E) and non-epithelial (NE) phenotype. 13 possible miR-21 targets during the MMT process associated to PD therapy were identified and model scrutinized. Four of these were confirmed to be miR-21 targets. Functional gene analysis indicated that selected targets may be downstream modulators of Snail and cooperate driving MMT during peritoneal fibrosis. Taken together, these data provide a detailed characterisation of mesothelial miRNA expression and responses to TGF-β1, and identify miR-21 and miR-31 as promising biomarkers for peritoneal fibrosis associated to PD therapy.

Glossary of Abbreviations

AGE	Advanced glycosylation end-products
AKI	Acute kidney injury
ANOVA	Analysis of variance
APC	Antigen presenting cells
APD	Automated peritoneal dialysis
BCR	Baseline characteristics reported
BMI	Body mass index
CAPD	Continuous ambulatory peritoneal dialysis
CBS	Central biotechnology service
CDK	Cyclin-dependent kinase
CDS	Coding DNA sequence
CKD	Chronic kidney disease
CTGF	Connective tissue growth factor
CV	Coefficient of variation
E	Epithelial
ECM	Extracellular matrix components
EGF	Epidermal growth factor
EMT	Epithelial to mesenchymal transition
EPS	Encapsulating peritoneal sclerosis
ESR	Early stage researcher
ESRD	End-stage renal disease
FBS	Fetal bovine serum
FFPE	Formalin-fixed paraffin embedded
FGF	Fibroblast growth factor
GDF	Growth/differentiation factors
GDP	Glucose degradation products
GEF	Guanine nucleotide exchange factor

GFR	Glomerular filtration rate
GFS	Global Fluid Study
HD	Haemodialysis
HGF	Hepatocyte growth factor
HPMC	Human peritoneal mesothelial cells
ICAM-1	Intercellular adhesion molecule-1
IL	Interleukin
ILK	Integrin-linked kinase
IRC	Inter-run calibrators
JNK	Jun-N-terminal kinase
LCM	Laser capture microdissection
MCs	Mesothelial cells
MET	Mesenchymal to epithelial transition
MHC	Major histocompatibility complex
MMP	Matrix-metalloproteinases
MMT	Mesothelial to mesenchymal transition
NE	Non-epithelial
PAI	Plasminogen activator inhibitor
PAZ	Piwi, Argonaute and Zwille
PBS	Phosphate buffered saline
PCR	Polymerase chain reaction
PD	Peritoneal dialysis
PDCD4	Programmed cell death protein 4
PDE	PD effluent
PDGF	Platelet-derived growth factor
PET	Peritoneal equilibration test
PM	Peritoneal membrane
PTEN	Phosphatase and tensin homolog

qPCR	Quantitative polymerase chain reaction
RAGE	Receptor for advanced glycation end
RFP	Red florescence protein
RISC	RNA-induced silencing complex
ROS	Reactive oxygen species
RRF	Residual renal function
RRT	Renal replacement therapy
RT	Reverse transcription
SARA	Smad anchor for receptor activation
SBE	Smad-binding elements
SV	Speed-Vac
TF	Tissue factor
TFPI	TF pathway inhibitor
TGF-β1	Transforming growth factor β1
TGIF	TG-interacting factor
TIMP	Tissue inhibitor metalloproteinases
TNF-α	Tumour necrosis factor alpha
tPA	Tissue plasminogen activator
TRBP	Transactivating response RNA-Binding Protein
uPA	Urokinase plasminogen activator
uPAR	Urokinase plasminogen activator receptor
UTR	Untranslated región
VCAM-1	Vascular cellular adhesion molecule-1
VEGF	Vascular endothelial growth factor
WKTB	Wales Kidney Tissue Bank

Publications and Presentations arising from this thesis

Publications

Lopez-Anton M, Bowen T, Jenkins R. Roles for microRNAs in the regulation of peritoneal cavity homeostasis during peritoneal dialysis. (Biomed Res Int. 2015; 2015:929806).

Herlihy SE, Starke HE, **Lopez-Anton M**, Cox N, Keyhanian K, Fraser D, Gomer RH. Peritoneal dialysis fluid and some of its components potentiate fibrocyte differentiation (Perit Dial Int. 2016 Jul-Aug; 36(4):367-73).

Liuzzi AR, Kift-Morgan A, **Lopez-Anton M**, Brook AC, Friberg IM, Zhang J, Roberts GW, Donovan KL, Colmont CS, Toleman MA, Bowen T, Johnson DW, Topley N, Moser B, Fraser D, and Eberl M. Human γδ T-cells and MAIT cells expand at the site of microbial infection, amplify inflammatory responses and induce local tissue remodeling. (J Immunol. 2016 Sep 15; 197(6):2195-207).

Lopez-Anton M, Lambie M, Lopez-Cabrera M, Schmitt CP, Bartosova M, Schaefer B, Davies S, Stone T, Jenkins R, Taylor PR, Topley N, Bowen T, Fraser D. MicroRNAs-21 promotes fibrogenesis in peritoneal dialysis by targeting PDCD4. (Manuscript under review).

Lopez-Anton M, Rudolf A, Witowski J, Fraser D, Bowen T. Telomere length profiles in primary human peritoneal mesothelial cells. (Manuscript under review preparation).

Presentations

- Oral presentation, European Training & Research in Peritoneal Dialysis (EuTRIPD), Summerschool, Amsterdam and Zandvoort, Netherland, July 2012. Title 'The potential of microRNAs for peritoneal dialysis research'.
- Oral presentation, EuTRIPD, Winterschool, Amsterdam, December 2012, Netherland. Title 'The role of microRNAs in peritoneal dialysis associated fibrogenesis'.

- Oral presentation, PD-research in UK, Sheffield, UK, May 2013. Title 'The role of microRNAs in peritoneal dialysis associated fibrogenesis'.
- Oral presentation, EuTRiPD, Summerschool, Vienna, Austria, June 2013. Title 'The role of microRNAs in peritoneal dialysis associated fibrogenesis'.
- Poster presentation, Kidney Research Meeting, University of Durham, UK, September 2013. Title 'European Training & Research in Peritoneal Dialysis (EuTRiPD)'
- Oral and Poster presentation, European Peritoneal Dialysis (EuroPD) Congress and EuTRiPD midterm meeting, Maastricht, Netherlands, October 2013. Title 'Evaluation of mesothelial cell microRNA profile in an *in vitro* model of peritoneal fibrosis'
- Oral presentation, EuTRiPD Academy, Cardiff Springschool, UK, March 2014. Title 'The role of microRNAs-21 and -31 in peritoneal dialysis-associated fibrogenesis'.
- Oral presentation, Second best price, South West UK RNA annual meeting, Exeter, UK, May 2014. Title 'The role of microRNAs-21 and -31 in peritoneal dialysis-associated fibrogenesis'.
- Oral presentation, Congress of the international society for peritoneal dialysis (ISPD), Madrid, Spain, September 2014. Title 'The role of microRNAs-21 and -31 in peritoneal dialysis-associated fibrogenesis'.
- Oral presentation, EuTRiPD Summerschool, Lund, Sweden, May 2015. Title 'The role of microRNAs-21 and -31 in peritoneal dialysis-associated fibrogenesis'.
- Poster presentation, 52nd ERA-EDTA congress, London, UK, May 2015. Title 'The role of microRNAs-21 and -31 in peritoneal dialysis-associated fibrogenesis'.
- Poster presentation, microRNA and non-coding RNA in cancer conference, Keystone, Colorado, USA, June 2015. 'Regulation of mesothelial to mesenchymal transition by miRNAS'
- Oral and Poster presentation, EuroPD Congress and EuTRiPD meeting, Krakow, Poland, October 2015. 'microRNA-21 and -31 indicate peritoneal membrane characteristics during Peritoneal Dialysis therapy'.

- Abstract submitted for oral presentation, Mesothelium meeting, Manchester, UK, July 2016. Title 'The role of peritoneal mesothelial cells in peritoneal dialysis associated fibrogenesis'.
- Abstract submitted for oral presentation, Southwest UK RNA annual meeting, Bristol, UK, May 2016. Title 'Regulation of mesothelial to mesenchymal transition by miRNAS'

Contents

Chapter 1 - Introduction

1.1. Chronic Kidney Disease (CKD)

The kidneys are two bean-shaped organs localized at the back of the abdomen which in healthy adults are each approximately 10 cm in length, 6 cm wide and 3 cm thick. The kidneys are involved in regulatory functions including (i) removal of excess organic molecules, such as waste products of metabolism, from the blood; (ii) electrolyte regulation; (iii) acid-base balance maintenance; (iv) blood pressure control (*via* salt and water balance); (v) hormone (calcitriol and erythropoietin) and (vi) enzyme (renin) production. Incapacity to sustain blood homeostasis due to kidney injury may cause disease and ultimately lead to death. Kidneys are, therefore, responsible for monitoring blood water and molecule balance, sustaining salt and ion concentrations, maintaining pH and secreting toxic and waste products *via* urine generation. Urine production takes place in the nephrons, which are the functional units of the kidney, and work by blood filtration in the glomerulus followed by selective secretion and reabsorption of different molecules and water in the downstream nephron segments.

The factors contributing to impaired renal function are variable and can trigger either a gradual damage in renal capacity over months or years, called chronic kidney disease (CKD), or a quick decline progression in less than three months, termed acute kidney injury (AKI). Severe deterioration in renal performance may be called uraemia, which is characterized by symptoms generated by toxic and waste product accumulation. CKD is characterized by non-specific signs comprising (i) elevated blood pressure, (ii) pallor, (iii) volume overload, (iv) pericarditis, (v) asterixis (hand tremor), and (vi) muscle cramps; as well as symptoms including (i) loss or decreased appetite, (ii) easy fatigability, (iii) generalized weakness, (iv) involuntary weight loss or gain, (v) nausea and vomiting, (vi) metallic taste, (vii) generalized itching, (viii) difficulty breathing, (ix) edema (interstitial fluid), (x) intractable hiccups, (xi) frothy urine, (xii) loss of libido (e.g., erectile dysfunction), and (xiii) restless legs (Pereira et al, 2005). The glomerular filtration rate (GFR) is a test that estimates how much fluid passes in total from blood to urinary space across the glomerular filtration barrier located at the start of each nephron each minute and, therefore, indicates kidney function (Pereira et al,

2005). The National Kidney Foundation produced clinical practice guidelines *via* the Kidney Disease Outcomes Quality Initiative (NKF-KDOQI) programme to classify CKD into 5 stages according to renal excretory function as estimated by GFR (Levey et al, 2003) (Table 1.1).

Stage	GFR*	Description	Treatment
1	>90	Normal kidney function and associated abnormalities found[#]	Observation Blood pressure control
2	60-89	Moderate reduction in kidney function and associated abnormalities found[#]	Observation Blood pressure monitoring Risk factors control
3	(A) 45-59 (B) 30-44	Tolerably reduced kidney function	Observation Blood pressure monitoring Risk factors control
4	15-29	Severe reduced kidney function	Planning for End-Stage Renal Disease (ESRD)
5	<15 Dialysis requirement	Very severe or ESRD	Treatment need

Table 1.1: CKD classification into 5 stages according to NKF-KDOQI and GFR. *GFR values are expressed in mL/min and are normalized to an average surface area per 1.73 m^2. [#]Both of these stages are generally asymptomatic and require constant detection of protein in urine (proteinuria), albumin (albuminuria), red blood cells (haematuria) or structural abnormalities.

UK prevalence of stage 3-5 CKD was found to be 8.5% in a cross-sectional study including over 130.000 adults. (Stevens et al, 2007). GFR is not analyzed in a relevant proportion of the community and an underestimation of the real CKD prevalence in UK can be inferred in the measure indicated above (Stevens et al, 2007). The estimated cost of CKD to the NHS in England (2009-2010) was 1.4 £ billion / year and represented 1.3% of the total NHS annual budget (Kerr et al, 2012). Through Europe, prevalence of CKD stage 1-5 and 3-5 varies between countries (adjusted CKD stages 1-5 prevalence: 3.31% in Norway and 17.3% in northeast Germany; adjusted CKD stages 3-5 prevalence: 1.0% in central Italy and 5.9% in northeast Germany) (Brück et al, 2016).

1.1.1. End-Stage Renal Disease (ESRD)

CKD stage 5 is also called End-Stage Renal Disease (ESRD) defined by a GFR <15ml/min, taken to be the point at which renal replacement therapy (RRT) may be required for the patient. There are two main classes of RRT once ESRD is reached (i) renal transplant or (ii) dialysis. Although kidney transplant is the optimum choice for many ESRD patients, there are not sufficient kidney donors and all patients are not suitable for kidney transplant. Historically, an average of 23% of ESRD patients receive a renal transplant (Grassmann et al, 2005), and while transplant numbers continue to increase and outcomes continue to improve following transplantation, the majority of patients requiring RRT continue to depend on dialysis treatment to keep them alive. This treatment is based on an artificial replacement of the kidney function by promoting solute diffusion and osmosis through a semipermeable membrane. There are two dialysis methods (i) haemodialysis and (ii) peritoneal dialysis.

1.1.1.1. Haemodialysis (HD)

Haemodialysis (HD) is a therapy based on two fluids, dialysate and blood, moving in opposite directions separated by a semipermeable membrane (Figure 1.1). This flow is sustained within an artificial external kidney, called a dialyzer, designed to keep a high concentration gradient, enhancing the effectiveness of the process (Pereira et al, 2005). Consequently, this treatment cleans the blood of toxic substances and water excess, and regulates pH and electrolyte composition before blood is reintroduced into the body. HD is a highly effective technique but limitations include abrupt changes in (i) fluid, (ii) waste products, and (iii) electrolyte concentrations; (iv) need of access to the vascular system, and (v) use of anticoagulants during the procedure to prevent blood clotting. Haemodialysis machines monitor important parameters for the patient and can be home or hospital-based, with the latter being more common.

The most frequent adverse effects experienced by patients on HD therapy are summarized in Table 1.2 and include (i) regular travel for in-centre treatment, (ii) dietary and fluid intake restrictions, (iii) low blood pressure (hypotension) with associated nausea and dizziness, (iv) blood clot formation, (v) higher sepsis risk, (vi) muscle cramps, (vii) itchy skin, (viii) dry mouth, (ix) sleep disorders, (x) bone and joint pain, (xi) loss of

libido (e.g., erectile dysfunction), (xii) anxiety, (xiii) tiredness, and (xiv) difficulties to travel associated to arrangement access to dialysis facilities (NHS choices information webpage: http://www.nhs.uk/pages/home.aspx; 2016, April 1) (Pereira et al, 2005; Saxena & West, 2006). Nevertheless, this therapy also has many advantages when compared to peritoneal dialysis including (i) shorter period of time and fewer days a week of treatment, (ii) trained health professional assistance that can quickly detect possible issues, (iii) higher emotional support, (iv) it may be especially suitable for people who are visually impaired, have dementia or poor state of health, (v) home haemodialysis is possible but less common than in centre therapy, and (vi) equal effectiveness to PD (Table 1.2) (NHS choices information webpage; http://www.nhs.uk/pages/home.aspx; 2016, April 13) (Pereira et al, 2005; Saxena & West, 2006).

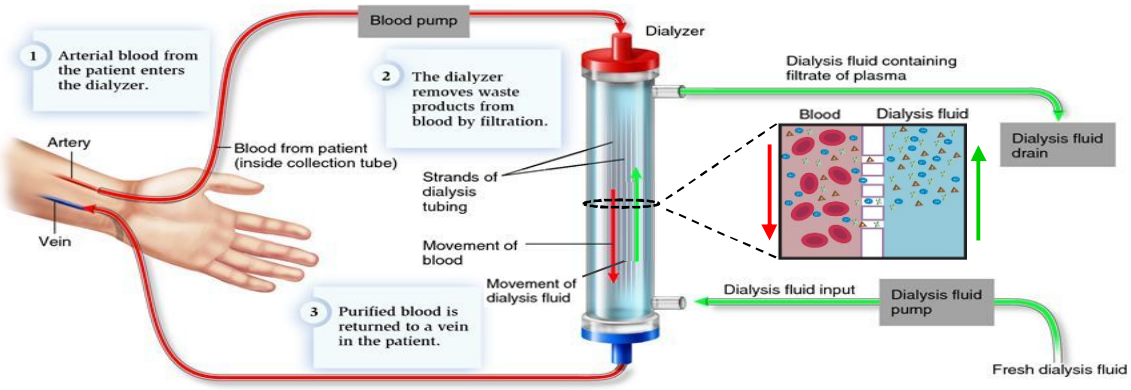

Figure 1.1. Haemodialysis diagram. (Figure modified from NHS choices information webpage; http://www.nhs.uk/pages/home.aspx; 2016, April 13).

1.1.1.2. Peritoneal Dialysis (PD)

Peritoneal dialysis (PD) is an alternative therapy to HD that uses the peritoneal membrane, which is a natural, vascularized and semipermeable membrane that lines the abdomen as an intrinsic, regular, dialyzer (Figure 1.2). During this treatment a sterile dialysate solution is introduced into the peritoneal cavity of the patient, *via* permanent abdominal catheter insertion, promoting capillary osmotic and diffusive transport of water and small solutes towards the instilled fluid. Dialysate solutions can have different compositions depending on patient requirements and remain in the cavity for a period

of hours to allow dialysis to occur. During this time the high concentration gradient created by the dialysate allows diffusion and osmosis movements of different substances and water between the blood and the PD solution through the peritoneal membrane. Eventually, the fluid containing blood toxic substances, small solutes and water excess is drained out and discarded, and replaced with fresh dialysate. The full therapy cycle is called a '*PD exchange'*, and the effectiveness of the therapy depends on the (i) gradient concentration, (ii) membrane surface, and (iii) membrane permeability (Pereira et al, 2005).

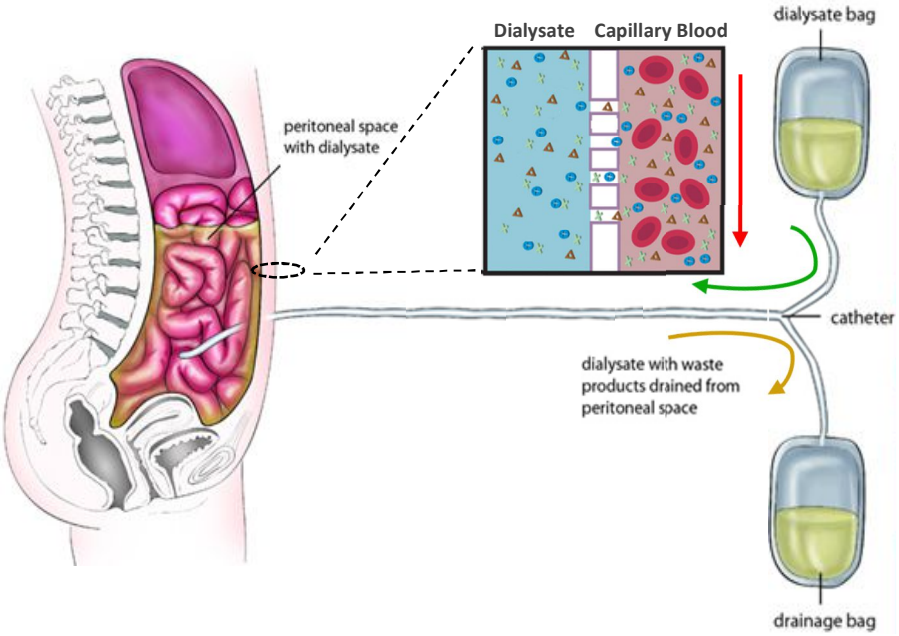

Figure 1.2. Peritoneal dialysis diagram. (Figure modified from NHS choices information webpage; http://www.nhs.uk/pages/home.aspx; 2016, April 13).

The most frequent problems experienced during PD therapy are summarized in Table 1.2 and include (i) permanent abdominal catheter insertion, (ii) peritonitis risk, (iii) need for therapy to be performed daily, (iv) gradual thickening and scarring of the peritoneum, (v) fewer but still diet and fluid intake restrictions, (vi) can trigger a reduction in protein levels, lack of energy and malnutrition, (v) weight gain, and (vi) higher risk of developing hernia (NHS choices information webpage; http://www.nhs.uk/pages/home.aspx; 2016, April 13) (Pereira et al, 2005; Saxena & West, 2006). Of note, this therapy comprises many advantages for patients such as the fact that is (i) mostly home-based with smaller, portable, machines, (ii) possible to perform in any clean area without special assistance, (iii) traveling freedom, (iv) recommended for people who still have some residual kidney function and (v) for

children aged two or younger, (vi) lower cost, (vii) better quality of life, and (viii) equally effective when compared with HD (Table 1.2) (NHS choices information webpage; http://www.nhs.uk/pages/home.aspx; 2016, April 13) (Pereira et al, 2005; Saxena & West, 2006).

	Advantages	Disadvantages
HD	Treatment employs shorter period of time and fewer days a week (~ 3 days/week ~ 4 hours/session)	Often carried out in dialysis clinic implying regular travel
	Need of trained health professionals that can quickly detect possible issues	Dietary and fluid intake restrictions
	Higher emotional support (the patient is in contact with other people receiving the same treatment)	Low blood pressure (hypotension) with associated nausea and dizziness (caused by fluid levels drop)
	Recommended for people who are visually impaired, dementia or poor state of health	Higher sepsis risk (caused by blood spreading bacteria and multiple organ failure)
	Home haemodialysis is possible but less common than in centre therapy	Muscle cramps (caused by fluid levels drop)
	Equally effective than PD	Itchy skin (caused by mineral raise between sessions)
		Dry mouth (caused by fluid levels drop)
		Sleep disorders
		Bone and joint pain
		Loss of libido and erectile dysfunction
		Anxiety
		Tiredness
		Difficulties to travel associated to arrangement access to dialysis facilities
PD	Mostly home-based with smaller, portable, machines	Permanent abdominal catheter
	Need of personal training but possible to performed in any clean area without special assistance	Peritonitis risk (bacterial peritoneal infection)
	Freedom to travel	Needs to be performed daily
	Recommended for people who still have some limited kidney function; better RRF preservation	Peritoneum gradual thickness and scarring
	Recommended for children aged two or younger	Fewer diet and fluid intake restrictions
	Lower cost	Can trigger a reduction in protein levels, lack of energy and malnutrition
	Better quality of live	
	Equally effective than HD	Weight gain (caused by sugar reabsorption and increasing caloric consumption)
		Higher hernia developing risk

Table 1.2: Table summarizing described advantages and disadvantages of HD and PD as ESRD therapies. (NHS choices information webpage; http://www.nhs.uk/pages/home.aspx; 2016, April 13) (Pereira et al, 2005; Saxena & West, 2006).

The number of ESRD patients increases between 6-7% annually with PD being the therapy experienced by 11% of RRT patients worldwide (Grassmann et al, 2005; Jain et al, 2012). In United States, PD treatment is growing fast due to a change in reimbursement policy and is expected to grow more during the following years (Golper, 2013). In Europe, RRT statistics vary between countries, and the UK is one of the nations with a higher percentage of patients on PD (Byrne et al, 2010). Nevertheless, PD therapy showed a slow decline during the last fifteen years in UK while RRT prevalence increased 4.4% (Byrne et al, 2010).

1.2. Peritoneal Anatomy and Histology

1.2.1. The peritoneum and the peritoneal cavity

Etymologically, the word *peritoneum* has a Greek *via* Latin origin in which *peri-* indicates around whereas *-ton-* relates to stretching and meaning stretched around. The peritoneum is the widest serous membrane, lines the visceral organs (visceral peritoneum or mesentery) and the abdominal cavity (parietal peritoneum) and comprises a total surface extension comparable to the skin (1-2 m^2) (Pereira et al, 2005; Yung et al, 2006). The space limited by these two membranes is the peritoneal cavity, which contains a serous liquid (< 50 ml) that favours membrane movement. During PD, the parietal peritoneum is largely engaged (80 %) in the efficient dialysis of water and solutes.

The peritoneum also folds into other substructures named (i) ligaments, (ii) mesenteries, and (iii) omentum which connect organs with each other and to the abdominal wall (Pereira et al, 2005). From these, the omentum can be also subdivided into two parts, namely the (i) lesser (covering liver, stomach curvature and part of the duodenum) and the (ii) greater (laying the visceral peritoneum) omentum, with significant function as a fat store and in immunity. The anatomist Ranvier described for first time the presence of small white masses or *'milky spots'* of cells in omental tissue (1874). These conglomerates where posteriorly characterized as clusters of macrophage and leukocyte cells (Krist et al, 1995). *Milky spots* have been associated with

immunocompetent cell migration towards the peritoneal cavity and local cell proliferation under both stimulated and unstimulated conditions (Cui et al, 2002). Interestingly, the frequency and dimension of these omental spots rise in patients receiving PD therapy (Beelen et al, 2005). Omentum also contains peritoneal mesothelial and fibroblast cells highly similar to those found at the peritoneal membrane, and has been extensively used as a primary cell source for research (Stylianou et al, 1990; Witowski & Jörres, 2006).

1.2.2. The peritoneal membrane

Histologically, the peritoneum is also called peritoneal membrane and consists of a mesothelial layer (mesothelium) sustained by a thin basal membrane and a submesothelial stratum of connective tissue (Nagy & Jackman, 1998). The mesothelium is a large cobblestone monolayer of ~ 1 x 10^9 mesothelial cells (MCs) with ~ 25 µm of diameter and which apical surface is densely covered by microvilli (Nagy & Jackman, 1998). The structural integrity of the mesothelium is maintained *via* cell-cell and cell-matrix interactions by tight, adherent and gap junctions as well as desmosomes. The thin, underlying basal membrane is generated by MCs and contains a network of collagen IV, proteoglycans and glycoproteins (Nagy & Jackman, 1998). Below these layers, the submesothelial stratum supports a higher network complexity that includes (i) extracellular matrix components (ECM) such as collagen, elastin, fibronectin and (ii) glycosaminoglicans (hyaluronan) as well as large and small (iii) blood vessels, (iv) draining lymphatics and (v) cellular elements like fibroblasts, resident macrophages, mast and adipose cells all of which contribute to maintain the homeostasis of the peritoneal membrane (Nagy & Jackman, 1998).

1.2.3. The mesothelium

Embryologically, the mesothelium originates from the embryonic mesoderm that surrounds the celom of the embryo and lines all serosa cavities (i) pleural (or chest cavity), (ii) pericardial (heart) and (iii) peritoneal (abdomen) (Mutsaers, 2004). During development, the mesothelium becomes a significant source of mesenchymal cells for tissue and organ generation including heart (Schlueter & Brand, 2013), lung (Que et al, 2008), gut (Wilm et al, 2005), liver (Ijpenberg et al, 2007) and fat (Chau et al, 2014). Adult mesothelium has a low proliferative rate (0.16 - 0.5 %) which is greatly increased after injury (30 – 80 %) and mesothelial cells retain the capacity to alter their phenotype *via* epithelial-to-mesenchymal transition (EMT) in response to different wound repair stimulus (Mutsaers, 2004; Yáñez-Mó et al, 2003). In the past, the principal function attributed to adult mesothelium was to favour slippery, non-adhesive movement of organs and tissues (Mutsaers, 2004). Nevertheless, nowadays adult mesothelial cells have been implicated in a broad spectrum of functions including (i) defensive barrier and non-adhesive surface, (ii) antigen presentation, (iii) inflammation regulation, (iv) coagulation and fibrinolysis, (v) extracellular matrix production, (vi) fluid and cell transport, and (vii) tumour cell adhesion and growth.

1.2.4. The mesothelial cell

Mesothelial cells are one of the largest peritoneal cell populations, ~ 1 x 10^9 cells (Nagy & Jackman, 1998). Their morphology varies between areas from flat squamous to cuboidal cells associated with higher activity (Mutsaers, 2002). Apical MCs surface is covered with highly versatile microvilli which enhance cell luminal area *via* length and/or number increase depending on physiological requirements (Mutsaers, 2002; Nagy & Jackman, 1998). Human peritoneal MCs (HPMCs) are ~ 0.5 – 2 µm thick, ~ 25 µm in diameter and maintain mesothelium structural integrity *via* cell-cell and cell-matrix interactions (Nagy & Jackman, 1998). MCs cell-cell contacts include (i) tight junctions, which are sealing protein complexes between adjacent MCs containing membrane proteins (e.g., Claudin, Occludin) and cytoplasmic proteins (e.g., Zona Occludens 1, ZO1) connecting transmembrane proteins with actin cytoskeleton and signalling proteins; (ii)

adherens junctions, which are an adhesion '*belt*' between MCs containing membrane proteins (E-cadherin) and cytoplasmic proteins (e.g., β-catenin, p120 catenin) connecting E-cadherin with actin cytoskeleton and signalling proteins; (iii) desmosomes, which function as an adhesion '*patch*' between MCs containing membrane proteins (desmosomal cadherin) and cytoplasmic proteins (e.g., desmoplakin) connecting transmembrane proteins with intermediate filaments; and (vi) gap junctions, which connect neighbouring MCs allowing ions and small molecule transfer between them while providing adherence (Lamouille et al, 2014; Mutsaers, 2004; Nagy & Jackman, 1998).

MCs are singular cells, able to co-express mesenchymal (vimentin and desmin) and epithelial (cytokeratin) intermediate filaments (Ferrandez-Izquierdo et al, 1994). MCs also share properties with vascular endothelium, expressing adhesion molecules that include ICAM-1, VCAM-1 and Platelet Endothelial Cell Adhesion 1 (PECAM-1) and cooperate in leukocyte migration (Jonjić et al, 1992). All the characteristics mentioned above mean that MCs are a versatile multifunctional cell type, with multiple implications in development and disease.

1.2.5. Physiological functions of the mesothelium

1.2.5.1. (i) Defensive barrier and non-adhesive surface

The mesothelium offers a defensive fence towards mechanical injury and foreign entities. MCs are firmly attached between each other and secrete matrix '*coat*' (glycosaminoglycans; mainly hyaluronan (HA)) that covers their surface, guarding the cells from abrasive harm and infective factors. Hyaluronan synthesis is increased with injury and contributes to cell differentiation, impedes adhesion formation and tumour cell propagation (Mutsaers, 2002). Mesothelial cells can also secrete phosphatidylcholine, the main component of lamellar phases and cellular surfactant, which reduces abrasion acting as a lubricant within serosal membranes (Mutsaers, 2002; 2004).

1.2.5.2. (ii) Antigen presentation

Mesothelial cells are prone to encounter any pathogenic organism or other injurious stimulus present in the peritoneal cavity due to their location lining the peritoneal cavity. MCs have the ability to secrete pro-inflammatory molecules including IL-6, IL-8, monocyte chemoattractant protein-1 (MCP-1) and RANTES following contact with infective agents or their secreted products (Kinnaert et al, 1996). These molecules contribute to inflammatory processes, triggering endothelial activation, which is required for leukocyte migration to the peritoneal cavity. Particular immune responses are developed *via* T cell antigen presentation and activation. This task is generally achieved by professional antigen presenting cells (APCs) including dendritic cells, macrophages, monocytes and B cells *via* major histocompatibility complex (MHC) class II molecules. Nevertheless, this immune network can be further assisted by non-professional (APCs) *via* intercellular adhesion molecule-1 (ICAM-1). At the peritoneum, the immune system is helped by MCs, which can also display MHC class II and intercellular adhesion molecule-1 (ICAM-1) upon stimulation and mediate antigen-T cell recognition mainly *via* ICAM-1 (Hausmann et al, 2000; Valle et al, 1995). Additionally, MCs can also secrete interleukin (IL)-15 which is a pleiotropic cytokine that has been involved in immune response initiation and T-cell growth (Hausmann et al, 2000).

1.2.5.3. (iii) Inflammation regulation

MCs have important functions during serosal inflammation including synthesis of (i) cytokine and chemokine molecules, (ii) growth factors, (iii) ECM proteins, (iv) intracellular adhesion molecules, and the ability of acting as (v) antigen presenters (Hausmann et al, 2000; Valle et al, 1995). Activated macrophages secrete inflammatory mediators comprising TNF-α, IL-1β and INF-γ which trigger MCs cytokine release including transforming growth factor β1 (TGF-β1), monocyte chemotactic protein-1 (MCP-1; or chemokine C-C motif ligand 2, CCL2), RANTES (or chemokine C-C motif ligand 5, CCL5) and IL-8 (or chemokine C-X-C motif ligand 8, CXCL8) and adhesion molecules including ICAM-1, vascular cellular adhesion molecule-1 (VCAM-1), E-cadherin, N-cadherin, CD49a, CD49b, CD44 and CD29 (Cannistra et al, 1994; Jonjić et al, 1992; Liberek et al, 1996; Mutsaers et al, 2015; Offner et al, 1996); enhancing leukocyte mobilization,

adherence and migration through the mesothelium to harmed areas (Liberek et al, 1996).

Peritoneal inflammatory responses can be challenged not only by infections but also *via* sterile dialysis fluid exposure, which promotes inflammation, cell proliferation, migration and ECM synthesis. These processes are led by the synthesis and secretion of growth factors including TGF-β1, platelet-derived growth factor (PDGF), fibroblast growth factor (FGF), hepatocyte growth factor (HGF) and different members of the epidermal growth factor (EGF) (Mutsaers et al, 2015). Indeed, long-term PD therapy facilitates chronic sterile peritoneal inflammation and the development of long-term peritoneal injury *via* fibrotic processes.

1.2.5.4. (iv) Coagulation and fibrinolysis

Fibrin deposition is an early important process in peritoneal wound healing and is tightly regulated by MCs. These cells have the ability to produce and regulate both pro-coagulant and fibrinolytic enzymes. Coagulation is mainly mediated *via* MC production of tissue factor (TF), a key initiator of the coagulation cascade that activates thrombin, which then cleaves fibrinogen into fibrin (Bottles et al, 1997). Conversely, TF pathway inhibitor (TFPI) impedes TF function and is also produced by MCs (Bajaj et al, 2000). Fibrinolytic capacity is also regulated by MCs, *via* tissue plasminogen activator (tPA), urokinase PA (uPA), uPA receptor (uPAR), plasminogen activator inhibitor (PAI)-1 and PAI-2 (Ivarsson et al, 1998). Thus, fibrin clearance depends on the counterbalance between the different players of the fibrinolytic system expressed at a certain time and site.

Pro- and anti-fibrinolytic pathways are coordinated by different inflammatory molecules, comprising lipopolysaccharide, tumour necrosis factor alpha (TNF-α), interleukin (IL)-1 and fibrogenic mediators including TGF-β1 and thrombin (Mutsaers, 2004; Tietze et al, 1998). During PD therapy, peritoneal mesothelial denudation disturbs fibrinolytic MCs regulation and promotes fibrin aggregation which ultimately, forms adhesions and plaques among the peritoneal membranes (Sulaiman et al, 2002).

1.2.5.5. (v) Extracellular Matrix Production

MCs produce diverse ECM components that are necessary for cell function and peritoneal membrane restoring. ECM molecules synthesized by MCs include collagen type I, III, and IV, elastin, fibronectin, laminin, proteoglycans (Mutsaers et al, 2015; Yung et al, 2006); and molecules contributing to maintain ECM homeostasis *via* secretion of matrix metalloproteinases and tissue inhibitors of metalloproteinases (Ma et al, 1999). MCs stimulated *in vitro* with different cytokines and growth factors including TGF-β1, IL-1β, EGF and PDGF (Leavesley et al, 1999; Yang et al, 1999a; Zhang et al, 2005) as well as PD effluent from patients exhibit ECM up-regulation (Perfumo et al, 1996).

1.2.5.6. (vi) Fluid and cell transport

The feasible routes for solute and water transfer within the peritoneal capillaries plasma and the PD fluid involves (i) the capillary endothelium, (ii) the peritoneal interstitial space, and (iii) the mesothelium (Devuyst & Rippe, 2014). The mesothelium is implicated in the movement and transfer of fluid and cells thought the serosa wall *via* microvilli, pinocytic vesicles, intracellular junctions and stomata (MCs junction cavities of 3-12 µm in diameter) (Mutsaers, 2004; Nagy & Jackman, 1998). Although the mesothelium does not entail an active barrier for water transport, it has been hypothesized that interstitial fibrosis *per se* accounts for trans-peritoneal ultrafiltration reduction (Devuyst & Rippe, 2014). Therefore, it is important to stress that peritoneal mesothelial MMT process (See 1.5) contributes to peritoneal fibrosis and ultrafiltration failure being an important factor for therapy long-term continuation.

1.2.5.7. (vii) Tumour cell adhesion and growth

The MC hyaluronan coat together with the secretion of other glycosaminoglycans and surfactants contributes to impeding tumour cell adhesion, dissemination and growth. Damaged mesothelium, nevertheless, helps tumor cell adhesion *via* mesothelial adhesion molecule up-regulation due to inflammatory mediators, local growth factors and tumoral CD44 molecules binding to hyaluronan (Harada et al, 2001; Lessan et al, 1999).

1.3. Peritoneal Dialysis Solutions What does biocompatibility mean?

The term biocompatibility makes reference to the ability of a material, device or system to perform without clinically significant host response (*Biocompatibility Conference*, 1998). Applied to PD solutions, *'biocompatibility'* involves the biological effect that the solution exerts on the normal functioning of peritoneal cells unchanging anatomical and physiological peritoneal characteristics once treatment ends (Di Paolo et al, 1995; Holmes, 1993). Indeed, PD solutions have a bio-incompatible essence traditionally characterized by high glucose concentrations, glucose degradation products (GDPs), lactate buffers, high osmolality and low pH (Table 3.1). These non-physiological properties cause peritoneal sterile chronic inflammation and healing mechanisms that trigger the development of structural and functional peritoneal membrane modifications (Sherif et al, 2006; Williams et al, 2002) (Figure 1.3 and 1.4; Table 1.3). These changes are contemplated as higher contributors of peritoneal ultrafiltration loss and dialytic ability (Margetts & Churchill, 2002). Additionally, these changes indirectly lead to patient systemic effects including fluid retention, left ventricular hypertrophy, heart failure, higher cardiovascular morbidity and mortality risk (Table 1.3. Modified from Chan & Yung 2007).

1.3.1. Glucose, Glucose Degradation Products (GDPs) and Advanced Glycation Products (AGEs)

Glucose has traditionally been the master osmotic agent in PD due to several factors including low price, safety, efficacy as osmotic colloid agent, and that it is easy to sterilise by heat. Nevertheless, a good amount of data implicates conventional, glucose-based solutions, as the main factor triggering PM alterations. Long-term PD patients are constantly subjected to PD solutions with 15 – 40 x physiological glucose concentrations to generate an appropriate osmotic gradient (Chan & Yung, 2007). Nevertheless, high glucose levels *per se* have been shown to trigger some of the above mentioned effects in MCs including (i) increased synthesis of MCP-1, TGF-β1, laminin,

	Affected cells	Effect on peritoneal resident or infiltrating cells	Effect on peritoneal membrane	References
Glucose	Mesothelial Cells	Increased synthesis of MCP-1, TGF-β1, laminin, and fibronectin	Inflammation and fibrosis	(Ha et al. 2001; Medcalf et al. 2001; Wong et al. 2003)
		Decreased tight junctions expression and epithelial markers	Mesothelial disintegration and membrane permeability	(Ito et al. 2000)
		Reduced perlecan synthesis	Increased membrane permeability	(Yung et al. 2004)
		Increased mitochondrial damage		(Ishibashi et al. 2002)
		Inhibition of cell proliferation	Impaired re-mesothelialization	(Gotloib et al 1999)
		Increased lactate dehydrogenase release		(Medcalf et al. 2001)
	Fibroblasts	Increased synthesis of matrix proteins and hyaluronan	Peritoneal fibrosis	
		Stimulation of proliferation	Peritoneal fibrosis	
		Increased insulin receptors and IGF-1	Peritoneal fibrosis	
		Induction of chemokines and cytokines	Inflammation	
	Leukocytes	Decreased phagocytosis	Impaired peritoneal host defense	
		Altered cytokine secretion	Impaired peritoneal host defense	
GDPs	Mesothelial cells	Reduced cell proliferation and viability, ROS formation	Impaired cell growth, GDP toxicity	(Witowski et al. 2000)
		Inhibition of re-mesothelialization	Mesothelial denudation	(Morgan et al. 2003)
		Decreased epithelial and increased mesenchymal markers synthesis	Impaired cellular functions, MMT	(Leung et al. 2005; Bajo et al. 2011)
		Increased expression of pro-inflammatory and pro-angiogenic factors: TGF-β1, IL-1β, IL-6, VEGF	Inflammation, Angiogenesis	(Inagi et al. 1999; Witowski et al. 2000; Leung et al. 2005)
	Fibroblasts	Inhibition of cell growth	Impaired wound healing	
	Leukocytes	Increased number of rolling leukocytes	Inflammation	
AGEs	Mesothelial cells	Increased VEGF and TGF-β1 synthesis	Peritoneal fibrosis	(Schwenger et al. 2006; Yang et al. 2015)
		Decreased synthesis of epithelial and increase synthesis of mesenchymal markers	Impaired cellular functions, MMT	(Yang et al. 2015)
		Accumulation in cells	Fibrosis	(Nakayama et al. 1997)

Table 1.3: Effect of glucose, glucose degradation products (GDPs) and advanced glycosylation end-products (AGEs) on specific peritoneal cell populations including mesothelial cells, fibroblasts and leukocytes. Monocyte chemoattractant protein-1 (MCP-1); transforming growth factor-β1 (TGF-β1); insulin-like growth factor-1 (IGF-1); reactive oxygen species (ROS); interleukin-1β (IL-1β); interleukin-6 (IL-6); vascular endothelial growth factor (VEGF). (Modified from Chan & Yung 2007).

and fibronectin (Ha et al, 2001; Medcalf et al, 2001; Wong et al, 2003); (ii) decreased expression of tight junctions and epithelial markers (Ito et al, 2000), (iii) reduced perlecan synthesis (Yung et al, 2004), (iv) increased mitochondrial damage (Ishibashi et al, 2002), (v) inhibition of cell proliferation (Gotloib et al, 1999), and (vi) increased lactate dehydrogenase release (Medcalf et al, 2001) (Table 1.3. Modified from Chan & Yung 2007).

In addition, conventional PDF are heat sterilized under acidic pH to avoid glucose caramelization but still resulting in the generation of breakdown glucose products or glucose degradation products (GDPs) which further accumulate during storage. Numerous PDF GDPs have been identified and characterized suggesting differential biological activities. These studies showed that GDPs, acidic pH and the use of a lactate buffer are probably the main factors associated with traditional glucose-founded PD fluids driving peritoneal damage (Table 1.3. Modified from Chan & Yung 2007). Within the alterations driven by GDPs in MCs it is important to point (i) reduced cell proliferation and viability, ROS formation (Witowski et al, 2000); (ii) inhibition of re-mesothelialization (Morgan et al, 2003), (iii) decreased synthesis of epithelial and increased synthesis of mesenchymal markers (Bajo et al, 2011; Leung et al, 2005) and, (iv) increased expression of pro-inflammatory and pro-angiogenic factors including TGF-β1, IL-1β, IL-6, VEGF (Inagi et al, 1999; Leung et al, 2005; Witowski et al, 2000) (Table 1.3. Modified from Chan & Yung 2007).

Glucose and GDPs can also mediate non-direct peritoneal injury *via* non-enzymatic glycosylation (glycation); binding to local proteins and generating advanced glycation end-products (AGEs). *In vivo*, catalysis degree is determined by protein and sugar concentrations as well as the time of exposure (Lamb et al, 1995). The reaction by which AGEs are formed is called *Maillard* and consists in non-enzymatic reaction of glucose with protein primary amino groups rising glycated residues termed *Amadori* products (Friedlander et al, 1996). These early products are reversible but through a set of dehydration and fragmentation processes give rise to stable, highly insoluble, covalent molecules called AGEs (Friedlander et al, 1996). AGEs not only trigger intra- and extra-cellular protein cross-linking but also interact with cellular membrane receptors (receptors for AGEs; RAGEs) to modify intracellular signalling. RAGEs are expressed in

multiple peritoneal cells including MCs, macrophages and fibroblasts suggesting important consequences for peritoneal homeostasis (Boulanger et al, 2002; Nakamura & Niwa, 2004). Therefore, soluble and structural protein glycation (AGEs) play important roles in long-term PD due to the high glucose concentrations in the peritoneum and have been associated with harmful consequences in MCs including (i) increased VEGF and TGF-β1 synthesis (Schwenger et al, 2006; Yang et al, 2015), (ii) decreased synthesis of epithelial and increased synthesis of mesenchymal markers (Yang et al, 2015), and (iii) accumulation in cells (Nakayama et al, 1997) (Table 1.3. Modified from Chan & Yung 2007). Indeed, AGEs presence is increased in PD effluent and peritoneal biopsies from long term PD patients and associates with filtration and ultrafiltration failure (Devuyst et al, 2010; Margetts & Bonniaud, 2003).

The principal systemic effect of PD fluids is to support blood cleaning, water and uraemic waste products removal, *via* diffusive and osmotic movements. Nevertheless, conventional PD solutions have some downside effects associated to the therapy including (i) fluid and sodium retention, (ii) left ventricular hypertrophy, (iii) hyperglycaemia, (vi) hyperinsulinemia, (v) hyperlipidaemia, and (vi) abdominal obesity (Figure 1.3) (García-López et al, 2012). Newer PD fluids have been refined expecting to diminish the disadvantageous consequences of long-term exposure to PD fluids and will be discussed during the next section.

1.3.2. Newer PD solutions

Iterative refinement of PD solutions has occurred, aiming to solve the challenges associated with conventional fluids and intending to be more 'biocompatible'. Newer PD solutions are based on the modification of one or more of the traditional perceived inadequacies associated with conventional fluids including (i) novel osmotic agents, (ii) alternative buffers, (iii) more physiological pH, and (iv) reduced GDP content (García-López et al, 2012). Nowadays, two novel osmotic agents are available at the market: icodextrin (Extraneal) and amino acids based (Nutrineal) (Table 3.1). Icodextin is an iso-osmolar mixture of glucose polymers with variable molecular weights that uses lactate as a buffer and is glucose-free (UFR = 2.27% glucose/initial hours) (Posthuma et al, 2001). This osmotic agent has slow absorption compared with glucose and is especially

appropriate for fluid and sodium removal during long dwells (8-12 h) (Ho-dac-Pannekeet et al, 1996). Nevertheless, Icodextrin use is still not approved in some countries and its use has been limited to one daily exchange due to increased maltose circulating levels (García-López & Lindholm, 2009). Amino acid-based solutions are also lactate buffered and glucose free (UFR = 1.36% glucose) (Grzegorzewska et al, 1999). This osmotic agent was particularly designed to improve nutrition by acting as a source of amino acids. Nonetheless, its use has also been restricted to single daily exchange to decrease acidosis (Grzegorzewska et al, 1999). Most last-generation solutions are glucose-based and use lactacte (Balance), bicarbonate (BicaVera) or a combination of both (Physioneal) as a buffer (Table 3.1). These solutions introduced the use of multi-chamber PD bags to favour glucose sterilization and storage with minimal GDP generation (pH 3-4) due to physical separation from the remaining electrolytes. Once mixed, the fluid has neutral/nearly-neutral pH.

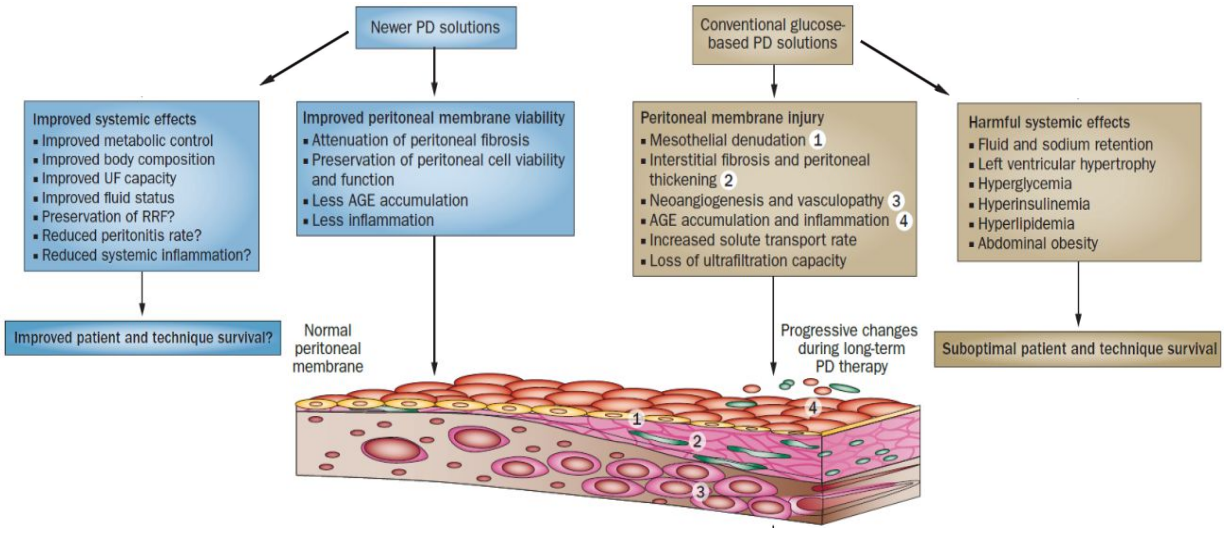

Figure 1.3. Schematic figure summarizing the effects of new and conventional PD solutions on the peritoneal membrane. AGE, advanced gycaltion end products; PD, peritoneal dialysis; RRF, residual renal function; UF, ultrafiltration (Modified from Gracía-López et al. 2012).

Some studies suggest that new PD solutions preserve better the peritoneal membrane and prolong the time on therapy compared with conventional solutions. Nevertheless, the evidence that last-generation of PD solutions can improve patient survival compared with classical PD fluids is not solid. When considering the potential benefits of new solutions it is important also to recognise that (i) icodextrin elicits greater ultrafiltration, improving patient fluid balance; and (ii) the use of non-glucose solutions during the long-dwell reduces the mean blood glucose levels of patients (Figure 1.3) (García-López et al, 2012). Nevertheless, there is still controversy regarding their potential to improve (i) preservation of RRF, (ii) peritonitis rate, and (iii) systemic inflammation (Figure 1.3) (García-López et al, 2012). Further large, randomized, controlled studies comparing these PD solutions with conventional fluids and reporting their specific effects and patient outcomes would be necessary to finally elucidate their full therapeutic potential.

1.3.3. Membrane changes during PD therapy

PD therapy involves constant exposure of the peritoneal membrane to bioincompatible PD solutions and a high basal inflammatory state. This results in a long-term alteration of the peritoneal cavity homeostasis characterized by progressive fibrosis (Margetts & Bonniaud, 2003; Williams et al, 2002), inflammation (Witowski et al, 2000), MCs denudation (Baroni et al, 2012), angiogenesis and vasodilation (Jiménez-Heffernan et al, 2008; Krediet et al, 2000), and MCs morphological and structural changes associated to a mesothelial to mesenchymal transition or (MMT) (Aguilera et al, 2005; Aroeira et al, 2007; Yáñez-Mó et al, 2003). Ultimately, the combination of these processes drives ultrafiltration failure and may necessitate a patient therapy switch (Aroeira et al, 2007).

The success of long-term PD therapy depends on the maintenance of the structural and functional integrity of the peritoneal membrane, across which solute transfer occurs. Although different cell types are involved in the loss of peritoneal membrane homeostasis there is particular interest in peritoneal mesothelial cells (MCs), one of the most numerous cell types of the peritoneal cavity. PD failure has been largely associated with the TGF-β1-driven conversion of MCs to myofibroblasts, *via* mesothelial-

to-mesenchymal transition (MMT) and mesothelial cell loss (see 1.5) (Selgas et al, 2006). This phenotypic conversion leads to increased synthesis of extracellular matrix components and release of pro-inflammatory and pro-angiogenic factors (Loureiro et al, 2011) (Figure 1.5).

1.3.3.1. Encapsulating Peritoneal Sclerosis (EPS)

Encapsulating Peritoneal Sclerosis (EPS) is a rare but severe disorder associated with prolonged PD therapy that may result in severe membrane fibrosis, intestinal obstruction, malnutrition and a high mortality rate. EPS patients also undergo a reduction in solute or fluid removal during PD therapy which is characteristic of membrane failure. The insults driving this condition are controversial, but it has been associated with recurrent or non-resolved peritonitis, malignancies, tuberculosis, autoimmune disease, β-blockers, intraperitoneal disinfectants and liver transplantation (Kawaguchi et al, 2000). Some authors defend the *'two hit'* hypothesis to develop this condition, which will comprise prolonged PD therapy together with peritonitis or quick therapy cessation (Honda & Oda, 2005). Satisfactory outcomes for patients with EPS may often be hampered by advanced disease at the time of diagnosis and by the frequent occurrence of comorbidity, for example a malnutrition state. Nowadays, EPS diagnosis is mainly performed *via* gastrointestinal dysfunction symptoms and computed tomography scanning (Kawaguchi et al, 2000) but the sensitivity of these diagnostics is deficient highlighting the necessity to develop earlier sensitive diagnostic tools for EPS (Yiannoullou et al, 2015).

1.4. The complexity of TGF-β1 in Peritoneal Dialysis

Peritoneal dialysis is a successful but non-physiological therapy. Repeated injurious stimuli lead to a programme of wound healing responses in which, in common with similar processes in other contexts, TGF-β1 plays a central regulatory role. TGF-β1 is a highly pleiotropic factor associated with the development of peritoneal injury including MMT, fibrosis and angiogenesis described in long-term PD patients. During PD, uraemia, PD solution bioincompatibility and inflammation have been associated with local TGF-β1 production in both animal models and humans (Margetts et al, 2005; Margetts et al, 2001; Zweers et al, 1999). *In vitro*, these solutions cause MCs alterations that are characterized by an increased expression of different factors including TGF-β1 (Ha et al, 2001; Wong et al, 2003; Yang et al, 2015). Animal PD models blocking TGF-β1 signalling *via* SMAD7 (Guo et al, 2007; Nie et al, 2007), BMP7 (Loureiro et al, 2010; Yu et al, 2009) or TGF-β1 direct inhibition (Loureiro et al, 2011) have found beneficial effects on mesothelial MMT and peritoneal injury/fibrotic responses. Human studies have highlighted that it is challenging to make reliable inferences from measurements of TGF-β1 in PD effluent due to (i) low fluid concentration and (ii) detection of the predominant inactive form of TGF-β1 (see 1.4.1), which is probably not indicative of tissue active TGF-β1 levels (Margetts & Bonniaud, 2003).

Studies in rat (Margetts et al, 2001) and mouse (Margetts et al, 2005) models of adenoviral-mediated active TGF-β1 gene transfer to the peritoneum highlighted the importance of TGF-β1 in PD therapy. In these *in vivo* models, peritoneal TGF-β1 overexpression closely mimicked structural and functional alterations observed in the peritoneum of long-term PD patients (Margetts et al, 2005; Margetts et al, 2001). These alterations included MMT, fibrosis, angiogenesis, higher solute transport, and ultrafiltration failure. Extended TGF-β1 overexpression in mouse peritoneum using a helper-dependent adenovirus also showed bowel encapsulation and peritoneal adhesions resembling those observed in EPS patients (Liu et al, 2009). TGF-β1-driven peritoneal MMT, fibrosis and angiogenesis depends on downstream SMAD signalling pathway (see 1.4.1.), although other pathways are also implicated in this process (see 1.4.1.). The multifaceted function of TGF-β1 during PD therapy is wide playing

evidencing the importance to identify downstream effectors coordinating early versus late stages in PD treatment. This knowledge will be crucial to implement PD treatment *via* targeting defined targets into TGF-β1 pathway to combat side effects during PD therapy.

1.4.1. TGF-β1 signalling from membrane to nucleus

The TGF-β cytokine family comprises growth and differentiation factors including activins, bone morphogenetic proteins (BMPs), growth/differentiation factors (GDFs) and TGF-βs (Shi & Massagué, 2003). Among all TGF-β cytokine family of factors, TGF-β1 and BMP7 equilibrium may be especially important to sustain peritoneal MCs phenotype during fibrosis (Loureiro et al, 2010; Vargha et al, 2006). TGF-β1 is member of the TGF-β/Activin/Nodal subfamily while BMP7 is a member of the BMP/GDF/MIS subfamily. Non-active, monomeric TGF-β1 cytokine contains different disulfide-bond interlocked β strands termed 'cyteine knot' (Sun & Davies, 1995). Active dimeric TGF-β1 is formed and stabilized *via* hydrophobic and disulfide bridges. Both factors act through transmembrane heterotetramer receptors (type I/type II) with intrinsic serine/threonine kinase activity (Shi & Massagué, 2003; Weiskirchen & Meurer, 2013). TGF-β receptor serine/threonine kinase family includes 12 different members, 7 type I and 5 type II, and generate different transmembrane heterotetramers for particular factors triggering specific signalling (Groppe et al, 2002). Active TGF-β1 dimeric stoichiometry indicates interaction with two (type I/type II) receptor complexes and is regulated *via* soluble ligand trap proteins and membrane-anchored accessory protein receptors (Shi & Massagué, 2003). Active BMP7 has also dimeric stoichiometry indicating similar interaction with specific receptors and regulation (Groppe et al, 2002; Shi & Massagué, 2003).

Upon TGF-β1 ligand binding to its primary receptor (type II, TGFBR2), signalling receptor (type I) is recruited, trans-phosphorylated and activated (Shi & Massagué, 2003). TGF-β1 activated receptor type I (also actividin receptor-like kinase 5, ALK5) has serine-threonine capacity to phosphorylate Smad2 and Smad3 (Shi & Massagué, 2003). Gene knockout studies in mice have shown that TGF-β1 null mice is embryonic lethal (Sanford et al, 1997) or die shortly after birth by multifocal inflammatory disease (Shull

et al, 1992) while heterozygous mice display mixed inflammatory infiltrations and hyperplastic lesions (Boivin et al, 1996). Additionally, TGFBR2 (Oshima et al, 1996) and ALK5 (Larsson et al, 2001) knockouts die at the embryonic stage, displaying abnormal yolk sac hematopoiesis and vasculogenesis. Similarly, in mice genetic Smad2 deletion is embryonic lethally (Nomura & Li, 1998), while null Smad3 mice are born with impaired immunity (Yang et al, 1999b). In contrast to TGF-β1, BMP-7 activated receptor type I (ALK3) phosphorylates the R-Smads Smad1, Smad5 and Smad8. Receptor activated (R-Smads) access and recognition by the receptors is facilitated by Smad anchor for receptor activation (SARA) proteins (Tsukazaki et al, 1998). Following phosphorylation, R-Smads associate with Smad4, a common Smad (Co-Smad) partner and a shared Smad pathway mediator (Shi & Massagué, 2003). The consequent R-Smad/Co-Smad complexes shuttle to the nucleus and activate target gene transcription in conjunction with other nuclear factors associated with MCs MMT (Smad2/3) or MMT reversion (Smads1/5/8). Transcription factor Smad3/4 directly binds DNA Smad-binding elements (SBEs) and GC-rich sequences within TGF-β target genes with a low energy binding fashion (Davis et al, 2010; Massagué et al, 2005). In addition, Smads can also interact with various DNA-binding cofactors into the transcriptional complex stabilizing Smads interaction (Feng & Derynck, 2005). There are over 30 Smad-interacting cofactors in mammals drawing a complicated and diverse picture of TGF-β1-driven gene responses depending on time, cell type and microenvironment (Feng & Derynck, 2005). TGF-β1 and BMP-7 signalling can be inhibited by Smad6 and Smad7, which act by blocking R-Smad phosphorylation and nuclear translocation by competitive interaction with the Co-Smad (Smad 4) together with receptor complex degradation *via* ubiquitin ligase recruitment (Gui et al, 2012; Shi & Massagué, 2003; Weiskirchen & Meurer, 2013). Smad signalling termination can be achieved *via* activated R-Smads (i) de-phosphorylation by phosphatases (Randall et al, 2002), (ii) ubiquitination and proteasomal degradation (Shi & Massagué, 2003), and (iii) histone phosphorylation and consequent changes in gene architecture (Shi & Massagué, 2003).

TGF-β1-induced EMT is not only a consequence of Smad-dependent pathways but also of so-called Smad-independent TGF-β1 signalling. Other pathways activated by TGF-β include mitogen-activated protein kinases (MAPKs), ERKs 1/2, JNK, and p38, along

with NF-κB, TAK-1 and PI3-K/Akt signalling, which together may tune TGF-β1-driven Smad responses and hence EMT. TGF-β1 activated Smads are firmly controlled by a network of pathways that can modulate the initial Smad wave and contribute to the diversity of TGF-β1 effects (Derynck & Zhang, 2003; Massagué, 2000). Thus, ERKs 1/2, JNK, NF-κB and TAK-1 appear to contribute to TGF-β1-triggered EMT (Strippoli et al, 2012; Strippoli et al, 2008), while p38 signalling has been shown to antagonize TGF-β1-effects *via* ERKs 1/2, NF-κB and TAK-1 activity modulation (Strippoli et al, 2010). It is therefore, the integration of these complex signals in context which ultimately determines cellular responses to TGF-β1 stimulus.

1.4.2. TGF-β1 effects in context

TGF-β1 signalling is involved in the control of (i) cell proliferation, (ii) apoptosis, (iii) fibrosis and scar formation, (vi) immune response regulation, (v) angiogenesis, and (vii) epithelial to mesenchymal transition (EMT). The signalling machinery underlying the different scenarios enumerated above is fundamentally the same. Specific cellular context and phenotype are a key component in shaping pathway outcome.

1.4.2.1. (i) Cell proliferation control

For most cells including, epithelial, endothelial, myeloid and lymphoid, TGF-β is a negative regulator of cell proliferation. TGF-β1 proliferative-regulatory mechanisms are the result of a combination of cooperative Smad-dependent gene responses, comprising (i) transcriptional activation of cyclin-dependent kinase (CDK) inhibitors (Toyoshima & Hunter, 1994) and (ii) c-Myc downregulation and inhibition (Pietenpol et al, 1990). CDKs regulate the cell cycle and are tightly controlled *via* cyclins and CDK inhibitors (CKIs), which act by enhancing or limiting CDKs activity respectively. In human peritoneal MCs TGF-β1 induces the expression of two CKIs, $p21^{CIP1}$ and $p27^{KIP1}$ (Ksiazek et al, 2007). Enhanced $p21^{CIP1}$ and $p27^{KIP1}$ expression impedes cyclin-CDK association blocking G1 phase progression. On the other side, c-Myc regulates cell cycle *via* gene transcription regulation including cyclin-D and transcription factor E2F, which are also involved in G1 to S transition as well as transcriptionally repressing $p21^{CIP1}$ and $p27^{KIP1}$.

1.2.5.2. (ii) Apoptosis

TGF-β1 has also been shown to induce apoptosis, or programmed cell death, in numerous cell types. TGF-β1 pro-apoptotic regulatory mechanisms are a result of TGF-β1's capacity to activate genes triggering apoptosis. In MCs, TGF-β1 may induce apoptosis *via* connective tissue growth factor (CTGF) (Szeto et al, 2006) or Smad2 (Lv et al, 2012) mediation of Bax expression up-regulation and down-regulation of anti-apoptotic Bcl2 gene expression. Nevertheless, these studies do not show strong evidence for a predominant proapoptotic effect of TGF-β1 and further confirmatory research is needed in the particular context of PMCs.

1.2.5.3. (iii) Angiogenesis

The term angiogenesis describes the development of capillaries from blood vessels during physiological and pathological processes comprising embryonic development, wound healing and tumour growth. This process is controlled by different cytokines and growth factors, including TGF-β1. TGF-β1 drives VEGF expression in vascular endothelial cells (Ferrari et al, 2006; Hicklin & Ellis, 2005). VEGF is involved in angiogenesis and activates tyrosinase kinase receptors 1 (VEGFR-1) and 2 (VEGFR-2) (Hicklin & Ellis, 2005). VEGF, VEGFR-1 and VEGFR-2 are necessaries for angiogenesis and their lack has been associated with embryonic lethality (Carmeliet et al, 1996).

In the peritoneum, TGF-β1 overexpression leads to enhanced VEGF expression, angiogenesis and ultrafiltration failure (Margetts et al, 2013; Margetts et al, 2001). Local VEGF production is increased during PD treatment and has been associated with peritoneal angiogenesis and long-term technique failure (Aroeira et al, 2005). It has been suggested that mesenchymal MCs can produce VEGF *in vitro* and contribute to angiogenesis increasing local VEGF levels (Aroeira et al, 2005). Indeed, TGF-β1 is a well-known inducer of mesenchymal MCs transformation that has been shown to increase VEGF expression in primary peritoneal MCs and pleural Met5A cell line (Young et al, 2015).

1.2.5.4. (iv) Immune response regulation

TGF-β1 is the TGF-β isoform that is principally expressed in the immune system. TGF-$\beta1^{-/-}$ mice manifested multiple foci of inflammation which associated with up-regulated cytokine generation (Kulkarni et al, 1993). Nevertheless, TGF-β1 pleiotropism obscured specific and direct immune cells that were cytokine targets. Mice expressing TGF-$\beta RII^{-/-}$ under a CD4 promoter in T cells (hence exhibiting abrogation of TGF-βRII in $CD4^+$ and $CD8^+$ T cells) developed an autoimmune response triggered by non-controlled $CD4^+$ T-cell differentiation into effector cells (Gorelik & Flavell, 2000). Clinically, these observations resemble those noticed in some Sézary disease patients in which $CD4^+$ T cells display low TGF-βRII expression, triggering an enhanced uncontrolled T cell proliferation (Capocasale et al, 1995). *In vitro*, TGF-β1 prevents activation and differentiation of naïve T cells abolishing Th1 and Th2 cytokine production (Lúdvíksson et al, 2000). TGF-β1 can differentiate $CD4^+CD25^-$ T cells into Tregs (Chen et al, 2003) and, together with Il-17, iTreg into pro-inflammatory Th17 cells *in vitro*. TGF-β1 also regulates macrophage and monocyte proliferation, chemo-attraction, enhances monocytic cytokine expression and phagocytic macrophage capacity.

1.2.5.5. (v) Fibrosis and Scarring

After injury, wound healing is controlled by multiple pro-fibrotic and anti-fibrotic cytokines and factors. Among them, TGF-β1 is considered to be a key fibrotic response mediator. Indeed, TGF-β1 deficient mice present defective wound repair, comprising low re-epithelialization and collagen synthesis (Böttinger et al, 1997). Complete TGF-β1 knockout mice displayed critical weight loss, general inflammatory response and tissue necrosis with consequent organ failure and death (Kulkarni & Karlsson, 1993). In the peritoneum, TGF-β1 stimulates fibroblasts and mesenchymal cells to proliferate and generate ECM contributing to the fibrotic response, both *in vivo* and *in vitro*. Similarly, TGF-β1 inhibits the synthesis of matrix-metalloproteinases (MMPs), enzymes degrading ECM components, and enhances tissue inhibitor metalloproteinases (TIMPs) and Plasminogen activator inhibition (PAI-1). CTGF is a cytokine released by MCs upon TGF-β1 stimulation (Leung et al, 2009), and a downstream mediator of pro-fibrotic signals on fibroblasts (Grotendorst, 1997). TGF-β1 also induces MCs epithelial to mesenchymal transformation, which contributes to fibrosis and wound healing.

1.2.5.6. (vi) Epithelial to mesenchymal transition (EMT)

Epithelial to mesenchymal transition (EMT) is a cellular mechanism that permits a polarized epithelial cell to experience complex biochemical alterations leading to mesenchymal cell phenotype conversion. The molecular changes occurring during this transformation include (i) activation/inhibition of transcription factors, (ii) expression/repression of particular cell surface proteins, (iii) cytoskeletal rearrangements, (iv) production of ECM degradative enzymes, and (v) specific miRNA expression. These changes lead to the acquisition of new cellular abilities comprising (i) increased migratory capability, (ii) invasiveness, (iii) anti-apoptosis, and (iv) elevated ECM expression.

EMT is a highly complicated and regulated process that entails structural and molecular rearrangements orchestrated by a particular expression regulation (Aguilera et al, 2005; Aroeira et al, 2007). This process is initiated with the loss of inter-cellular junctions and down-regulation of adhesion molecules followed by front-back polarity rearrangements, α-SMA expression acquisition, and enlarged migratory capabilities. Down the line, cells acquire the ability to degrade the basal membrane up-regulating matrix metalloproteinases (MMPs) expression and invading the submesothelial compartment. EMT culmination is achieved *via* basement membrane disruption and mesenchymal cell migration from its original location.

EMT in physiological contexts

The principle of cellular division as a mechanism to increase cell numbers generating tissues and organs was raised 150 years ago (Virchow, 1858). Pivotal in this inference was the comprehension that whole body cells raised from a unique cell, the zygote. This concept established the basis to sequentially understand that (i) cells adopt different phenotypic status through development, (ii) specific adult epithelial cells are plastic and maintain the ability to develop late EMT processes, or (iii) to develop a reverse process called mesenchymal to epithelial transition (MET), and (iv) terminally differentiated cells can also activate an EMT program depending on microenvironment stimulus (Kalluri & Weinberg, 2009; Lamouille et al, 2014). Thus, EMT mechanisms are now classified into three different subtypes: (type 1) implantation, embryogenesis and organ development; (type 2) tissue regeneration and organ fibrosis, and (type 3) cancer

progression and metastasis (Kalluri & Weinberg, 2009). The particular signals that determine each specific EMT are not well defined yet but TGF-β1 signalling has been involved in all these processes.

Type 1: Implantation, embryogenesis and organ development

Specifically, TGF-β1 has been shown to play critical roles in EMT associated to cardiac valve development as indicated by knockout mice (Mercado-Pimentel & Runyan, 2007). Moreover, TGF-β superfamily members have been involved as key molecules triggering EMT during most morphogenetic events (Yang & Weinberg, 2008). TGF-β1 superfamily control of vertebrate embryonic development includes (i) mesoderm formation (Nodal), (ii) neural crest formation (BMP), (iii) cardiac valve formation (TGF-β1, 2, 3, BMP), and (iv) secondary palate formation (TGF-β3) (Yang & Weinberg, 2008).

Type 2: Tissue regeneration and organ fibrosis

This mechanism starts as a repair-related episode triggered after trauma, injury and/or *via* an inflammatory microenvironment, causing an increase in EMT, ECM expression and organ fibrosis. Perpetuation of the EMT process may be subsequently controlled by local inflammation, ending with inflammatory signal reduction and, conversely, leading to tissue fibrosis and organ destruction under persistent inflammation. EMT type 2 has been described in kidney, liver, lung and peritoneum and was highlighted *via* transgenic mice (Margetts et al, 2013). More broadly, TGF-β1 has been described to be a major inducer of EMT in kidney, liver, biliary tract, lung and peritoneum (Kasai et al, 2005; Margetts et al, 2013; Nitta et al, 2008; Zeisberg et al, 2003).

Type 3: Cancer progression and metastasis

Cancer acquisition of invasiveness capabilities has also been linked to cellular EMT program activation. In this context, TGF-β1 is a relevant inhibitor of cell proliferation and primary tumorigenesis (Bierie & Moses, 2006). Nevertheless, TGF-β1 has also been described to be elevated in particular cancer types during late stages contributing to induce EMT program (Bierie & Moses, 2006; Padua & Massagué, 2009).

1.5. MMT in peritoneal dialysis

MCs have a mesodermal genesis and possess features from epithelial, mesenchymal and endothelial cells. Consequently, some authors suggested adapting the classical 'EMT' terminology for the particular mesenchymal MCs conversion by a more adequate term: mesothelial to mesenchymal transition (MMT). The first description of MMT in PD patients was shown by Yáñez-Mó et al. 2003, who identified this conversion in peritoneal tissue and PD effluent derived cells (Yáñez-Mó et al, 2003). Studies undertaken at that time described that omentum-derived MCs treated with TGF-β1 *in vitro* acquired myofibroblastic characteristics by an MMT-like process (Yang et al, 2003). Mesenchymal MCs have higher migratory and invasive capabilities, allowing them to infiltrate the submesothelial stratum (Aroeira et al, 2007; Yáñez-Mó et al, 2003). Indeed, peritoneal biopsies from PD patients manifest the existence of submesothelial, fibroblast-like, cells expressing cytokeratins, E-cadherin and ICAM-1 which are characteristic MCs markers (Aroeira et al, 2007; Jiménez-Heffernan et al, 2004). In these biopsies, α-SMA expression was particularly patent in the higher-submesothelial stroma where often co-stained with cytokeratins (Jiménez-Heffernan et al, 2004).

MCs transformation was determined in an *in vivo* rodent model of intraperitoneal adenoviral vector driving the active form of TGF-β1 (Margetts et al, 2005). In this model TGF-β1 induced peritoneal fibrosis, characterized by accumulation of α-SMA positive interstitial cells, neoangiogenesis and increased peritoneal membrane solute transport (Margetts et al, 2005; Margetts et al, 2001). Consistently, an *in vivo* Smad3 knockout mouse model showed peritoneal fibrosis protection with lower collagen deposition and reduced MMT, indicating Smad2/3 signalling importance during TGF-β1-driven MMT (Patel et al, 2010a). Indeed, Smad7-triggered Smad2/3 inhibition stops MMT and decreases peritoneal fibrosis (Shi & Massagué, 2003; Weiskirchen & Meurer, 2013). Smad2/3 pathway inhibition mediated by hepatocyte growth factor (HGF) and BMP-7 has also been associated with MMT blockage (Loureiro et al, 2010; Yu et al, 2009). Briefly, HGF up-regulates the expression of SnoN and TG-interacting factor (TGIF), two transcriptional co-repressors that bind activated Smad2/4 and Smad3/4, repressing Smad-mediated transcription (Dai & Liu, 2004; Tan et al, 2007; Yang et al,

2005). Additionally, BMP-7 stimulates Smad1/5/8 signalling which antagonizes TGF-β1-induced Smad2/3 and downstream MMT (Loureiro et al, 2010; Weiskirchen & Meurer, 2013).

In vivo, MMT arises from the combination of multiple signals, initiated by different factors, which increases the difficulty in defining an order or classification of events (Aroeira et al, 2007; Selgas et al, 2006). These molecules bind to specific cellular receptors and stimulate different intricate signal transduction networks including TGF-β1, integrin-linked kinase (ILK), notch, phosphatidylinositol-3-kinase (PI3K)/Akt and the mammalian target of Rapamycin (mTOR) (PI3K/Akt/mTOR), extracellular signal-regulated kinases 1/2 (ERKs1/2), TGF-β-activated kinase-1 (TAK-1) and c-jun-N-terminal kinase (JNK) signalling pathways. These networks coordinate the loss of inter-cellular adhesion structures, cytoskeletal rearrangements and the gain of migratory and invasive capabilities characteristics of the MMT process (Aroeira et al, 2007; Patel et al, 2010a; Selgas et al, 2006; Strippoli et al, 2012; Zhu et al, 2010). Thus, TGF-β1-induced MMT does not only act *via* Smad-dependent pathways but also *via* so-called Smad-independent TGF-β1 signalling. Consequently, TGF-β1-associated peritoneal MMT occurs as a consequence of Smad-dependent and -independent signalling, indicating the possible need of abolishing both signals to block MMT.

1.5.1. Origin of peritoneal myofibroblasts during peritoneal dialysis: an open debate

Myofibroblasts, or activated fibroblasts, may be broadly characterized as the major effector cells of fibrosis. Myofibroblast differentiation is induced by cytokines, including TGF-β1, and characterized by α-SMA expression. The term myofibroblast designates a particular type of activated fibroblast, with cellular characteristics halfway between those of fibroblasts and of smooth muscle cells. The first description of myofibroblasts came from Gabbiani et al. 1972, who identified them in different models of open wounds (Gabbiani et al, 1972). Today, myofibroblasts have been implicated in practically all remodelling and healing contexts, and are recognised as key protagonists in human pathologies. Their crucial role in wound healing and tissue remodelling includes synthesis of extracellular matrix components, growth factors and cytokines, guiding the tissue inflammatory response, and physical remodelling of the tissue *via* their contractile capabilities.

The source of myofibroblasts is a polemic topic in kidney research (Fragiadaki & Mason, 2011; Grgic et al, 2012; Humphreys et al, 2010; Kriz et al, 2011; LeBleu et al, 2013; Quaggin & Kapus, 2011; Zeisberg & Duffield, 2010). Overall, in kidney, there is little evidence that renal epithelial cells migrate to the interstitium and become myofibroblasts *in vivo* (Humphreys et al, 2010). Nevertheless, proximal tubular epithelial cells (PTECs) have been shown to display mesenchymal characteristics and become local producers of collagens as part of their response to injury. Additionally, kidney myofibroblasts have been described to arise from different extra-renal sources including local resident cells, bone-marrow derived cells, endothelial cells via EnMT and pericytes (Humphreys et al, 2010; LeBleu et al, 2013). Their specific contribution is currently subject to intense research. A possible explanation for the lack of PTECs full EMT reported in these observations may be that the chronic, slow-developing human disease process, in which cycles of epithelial injury and healing can alternate is more prone to mobilize the EMT program rather than acute and robust UUO models. Nevertheless, it is commonly recognized that myofibroblasts comprise a diverse cell population that may arise from several origins, which may differ between organs and/or through organ areas.

Therefore, traditional extrapolation of conclusions from kidney fibrosis research studies into the peritoneal fibrosis field should be avoided. Instead, the aforementioned literature emphasizes the importance of particular tissue and organ microenvironments governing the distinct contributions and origins of myofibroblast subpopulations.

Myofibroblastic origin of cells during peritoneal fibrosis associated to PD therapy is also a controversial question that can be divided into three different hypothesis.

Hypothesis 1:

Mesothelial cells are the source of myofibroblasts associated to PD therapy fibrogenesis

Long-term exposure of peritoneal mesothelial cells to non-biocompatible PD solutions during dialysis therapy induces peritoneal injury, MMT and myofibroblastic conversion (Margetts et al, 2005; Yáñez-Mó et al, 2003). This transition is characterized by a loss of epithelial morphology and markers, including cytokeratin and E-cadherin, accompanied by an increase in migratory phenotype and mesenchymal markers, such as snail and α-SMA expression. Although the MMT is a progressive step-wise process, ultimately, MCs may completely switch to myofibroblasts or active fibroblasts losing any possible trace of their initial identity (Margetts et al, 2005). Indeed, TGF-β1 and LacZ adenoviral gene co-administration to pleural rat mesothelium induced pleural fibrosis and progressive mesothelial cell migration into the fibrotic tissue (Decologne et al, 2007).

Hypothesis 2:

Submesothelial fibroblasts cells are the source of myofibroblasts associated to PD therapy fibrogenesis

Long term PD treatment induces peritoneal fibrogenesis where the major precursors of myofibroblasts are submesothelial fibroblasts (Chen et al, 2014). This hypothesis is supported by *in vivo* genetic lineage analysis in which MCs ($Cyto^+$) were labelled *via* red florescence protein (RFP) expression employing Wilms tumor-1 homolog (Wt1)-CreERT2 mice. Different peritoneal fibrosis mouse models showed MCs ($Cyto^+/RFP^+$) did not significantly contribute to the myofibroblast population during fibrogenesis (Chen et al, 2014). Nevertheless, it is important to mention that mesothelial cell MMT cannot be completely disqualified by the Chen *et al.* 2014 study due to genetic

labelling weaknesses. Indeed 24% of all peritoneal RFP^+ cells were $Wt1^+/RFP^+$ while only 65% of submesothelial fibroblasts were label-tracked (Chen et al, 2014). Additionally, the Wt1-CreERT2 mice model used for the study is not peritoneal MCs specific as $Wt1^+$ precursor cells may differentiate to MCs, submesothelial cells, hepatic stellate cells and perivascular mesenchymal cells in liver models using analogous lineage tracing approaches (Asahina et al, 2011; Li et al, 2013). Indeed, the liver models above mentioned showed MCs ($Wt1^+$) were able to contribute to the myofibroblast population *via* MMT (Asahina et al, 2011; Li et al, 2013). Ultimately, Chen *et al.* 2014 also showed that MCs ($Cyto^+$) were significantly labelled in a Col1a1-GFP transgenic reporter mice ($Col1a1\text{-}GFP^{Tg}$) after hypochlorite injury and AdTGF-β1 intraperitoneal injection (Chen et al, 2014). Despite the fact that $Cyto^+$ cells did not show migration or α-SMA expression, collagen expression in injured MCs indicated fibrotic phenotype transition. Indeed, this observation is consistent with Patel et al. 2010 who identified a 'non-invasive peritoneal MMT process' characterized by the presence of activated, collagen and growth factor producing, MCs which were not transformed into submesothelial myofibroblasts but critically contributed to peritoneal fibrosis (Patel et al, 2010b). Therefore, it will still be crucial to replicate these data in more clinically relevant animal models using specific peritoneal MCs labelling before drawing conclusions from this single study.

Hypothesis 3:

Myofibroblasts came from multiple sources during PD therapy fibrogenesis

This last hypothesis integrates the prior hypotheses with compelling data for diverse myofibroblast origins during peritoneal fibrosis including (i) mesothelial cell MMT differentiation ($Cyto^+/FSP\text{-}1^+$), (ii) bone-marrow-derived circulating cells or fibrocytes ($CD45^+/FSP\text{-}1^+$), (iii) endothelial to mesenchymal (EnMT) conversion ($CD31^+/FSP\text{-}1^+$), and (iv) activated resident interstitial fibroblasts ($-/FSP\text{-}1^+$) (Herlihy et al, 2015; Loureiro et al, 2011). The specific contribution of each myofibroblastic source is obscure in human patients and the only population percentage data published come from a PD mouse model in which MMT ($Cyto^+/FSP\text{-}1^+$, 37%), fibrocytes ($CD45^+/FSP\text{-}1^+$, 34%), EnMT ($CD31^+/FSP\text{-}1^+$, 5%), and resident fibroblasts ($-/FSP\text{-}1^+$, 24%) contributed to fibrosis (Loureiro et al, 2011). Thus, although there is controversy regarding

myofibroblast relative source contributions, mesothelial cells are suggested to be the predominant origin of myofibroblasts associated to fibrosis in PD treatment and therefore were the focus for this study.

As well as the stimuli leading to fibrosis and the source of myofibroblasts, a third key question are the downstream regulatory molecules responsible for changes in cellular behaviour and hence tissue remodelling. miRNAs are an important class of downstream regulator that are strongly implicated as effectors of TGF-β1 responses in other contexts, but have not previously been examined in depth in peritoneal fibrosis or in mesothelial cells. miRNAs are short non-coding RNAs that regulate gene expression at the post-transcriptional level. Aberrant miRNA levels associated with PD therapy may affect the regulation of a multitude of mRNA species resulting in significant cellular effects including mesothelial cell MMT process. Indeed, recent studies suggest that miRNAs are likely to be important in the regulation of mesothelial cell phenotype and homeostasis in the peritoneal cavity during PD therapy (Chen et al, 2012a; Zhang et al, 2012). Consequently, miRNA alterations associated with PD therapy may be valuable in understanding peritoneal cavity changes and predicting the clinical course of PD patients.

1.6. miRNA Discovery

miRNAs were initially discovered in *C. elegans* as critical developmental regulators over two decades ago (Lee et al, 1993; Wightman et al, 1993). Victor Ambros and his colleagues identified lin-4, a gene important in *C. elegans* larval development that did not encode a protein but two transcripts of 61 and 22 nt. Lin-4 mutants were restrained by first larval stage (L1) not being able to reach the adult form. Conversely, the lin-14 gene was known to contribute to cell lineage differentiation by specific temporal-graded activity. Subsequently, lin-4 was shown to act as negative regulator of LIN-14 protein level, originating a timely reduction in LIN-14 after L1 stage (Lee et al, 1993; Wightman et al, 1993). In their original descriptions of this phenomenon, the authors suggested that small lin-4 transcripts enclosed sequences matching with repeated elements in the 3’ untranslated region (UTR) of lin-14 mRNA, indicating that

lin-4 controls lin-14 translation through partial RNA complementarity (Lee et al, 1993; Wightman et al, 1993). Further analysis of lin-4 transcripts revealed that the longer transcript (61 nt) was predicted to stem loop fold which was suggested to act as a precursor of the shorter lin-4 transcript (22 nt) that also exhibited lin-14 mRNA antisense complementarity (Lee et al, 1993).

A seven-year gap then occurred before the next key ncRNA discovery. In 2000, Reinhart and Slack identified let-7, a gene important in C. *elegans* larval development which encoded a 21 nt ncRNA complementary to the 3'UTR of different genes including lin-14, lin-28, lin-41 and daf-12 (Reinhart et al, 2000; Slack et al, 2000). Let-7 loss caused persistence of larval cell fates in adult stages while let-7 up-regulation showed development of adult fates in larval stages indicating let-7 regulation of temporal developmental processes (Reinhart et al, 2000; Slack et al, 2000). Let-7 conservation analysis demonstrated that it was highly conserved in a wide range of animal species, indicating that let-7 regulation may broadly contribute to control temporal transitions in development (Pasquinelli et al, 2000).

miRNA post-transcriptional gene regulation has been described in animals, plants, bacteria and viruses (Bartel, 2004; Pfeffer et al, 2004; Shmaryahu et al, 2014). The term miRNA was established in 2001 (Ruvkun, 2001). Since then, alterations in miRNA expression have been described in a wide range of *in vitro* and *in vivo* models (Landgraf et al, 2007). miRBase 21 (June 2014) is the main miRNA database and considers a total number of 1881 human miRNAs precursors and 2588 mature sequences (Kozomara & Griffiths-Jones, 2014). Last miRBase version deleted duplicated, dubious and mis-annotated miRNA sequences (Kozomara & Griffiths-Jones, 2014). Certainly, the increase in high throughput sequencing studies will further continue updating miRBase *'high confidence'* datasets to identify new important miRNAs contributing to post-transcriptional cell regulations.

1.6.1. miRNA biogenesis and regulatory functions

miRNAs can be located in their own genes (intergenic) or in introns and exons of protein coding genes (intronic). Intergenic miRNAs are controlled by independent promoters while intronic miRNAs can be controlled by the host gene promoter or by their own promoter (Lagos-Quintana et al, 2001; Ramalingam et al, 2014; Wang et al, 2009). In addition, miRNAs can also occupy nearby positions called genomic clusters which are co-regulated and expressed *via* a common primary transcript (pri-miRNA) unit (Altuvia et al, 2005). A recent paper also identifies that intronic miRNAs clusters can be independently utilized *via* alternative splicing, leading to generation of different pri-miRNAs (Ramalingam et al, 2014).

miRNAs biogenesis begins in the nucleus where these small RNAs are transcribed by the RNA polymerase (Pol II) or Pol III enzyme (Borchert et al, 2006; Lee et al, 2004) as a long, poly-adenylated primary miRNA (pri-miRNA) molecule (Lee et al, 2002). The pri-miRNA transcript is a single stranded RNA of a few thousand nt with a stem-loop structure that is processed by a protein complex called 'microprocessor'. The microprocessor is composed by Drosha, a nuclear RNase III endonuclease; DiGeorge syndrome critical region gene 8 (DGCR8) cofactor that assists Drosha in pri-miRNA recognition to generate a precursor miRNA (pre-miRNA) and other regulatory factors including p68 and p72 (Lee et al, 2003). Of note, intronic-coded miRNAs that are transcribed as part of precursor mRNA (pre-mRNA) molecules are processed *via* pre-mRNA splicing to produce the miRNA in a manner that is not fully understood yet (Macfarlane & Murphy, 2010).

Pre-miRNAs are 60-70 nt stem-loop hairpin molecules that are actively transported to the cytoplasm by export receptor Exportin-5 and a Ran-GTP (Grishok et al, 2001; Yi et al, 2003). In this complex, Exportin-5 stabilizes nuclear pre-miRNA impeding its degradation and assists in pre-miRNA translocation to the cytoplasm while Ran-GTP to Ran-GDP hydrolysis allows pre-miRNA release once in the cytoplasm (Grishok et al, 2001; Yi et al, 2003).

miRNA/miRNA* duplexes (~22-25 nt) are generated by Dicer complex, a cytoplasmic RNase III that cleaves pre-miRNA into a small double stranded RNA duplex

(Bernstein et al, 2001). Dicer complex contains a long N-terminal ATPase/Helicase domain, a DUF283 domain, two C-terminal tandem RNase III nuclease domains and a Piwi, Argonaute and Zwille (PAZ) domain, named after three proteins that bind the 3' end of small RNAs (Bernstein et al, 2001). One single mature miRNA stand is preferentially incorporated into the RNA-induced silencing complex (RISC). The RISC complex contains the trans-activating response RNA-Binding Protein (TRBP) that recruits Argonaute 2 (AGO2) and other proteins (Chendrimada et al, 2005). Initially, it was thought that RISC-loaded the miRNA strand that had lowest 5' terminal thermodynamic stability while the partner strand was degraded. Nevertheless, different studies have challenged this hypothesis, showing that the partner strand can also target mRNAs *via* RISC complex incorporation (Finnegan & Pasquinelli, 2013).

miRNA-RISC complex binds to 3' un-translated regions (3'UTRs) of specific target genes by partial complementarity, which results in repression of translation and/or degradation of the target mRNA (Pasquinelli, 2012). Both regulatory systems require the presence of one of the Ago proteins. These proteins contain four domains: (i) N-terminal, (ii) PAZ (Piwi-Argonaute-Zwille) domain which hooks the 3' end of the selected miRNA, (iii) MID domain which has large 5' miRNA end specificity and terminal four bases discrimination capacity, and (iv) a PIWI element which has endonuclease activity, mediating RNA cleavage (Kim et al, 2009). The mRNA degradation process is mediated *via* miRNA-mRNA partial Watson-Crick base pair complementarity, in which the 5' miRNA nucleotides in the 2^{nd} to 8^{th} positions, termed the seed sequence, are especially important (Bartel, 2009). mRNA degradation takes place *via* AGO2-mediated endonucleolytic cleavage (Gu & Kay, 2010) or deadenylase-mediated mRNA poly(A) tail removal stimulated by partial miRNA complementarity (Wu & Belasco, 2008).

miRNAs control the expression of the majority of protein coding genes in the human genome, thereby affecting most biochemical pathways implicated in cellular homeostasis. Additionally, one miRNA may regulate the expression of hundreds of target mRNAs, profoundly affecting cell phenotype and function. Studies on miRNA expression in different model systems and body fluids have also emphasized their potential as therapeutic targets and disease biomarkers (Brown & Naldini, 2009; Cortez et al, 2011; Kota et al, 2009; Turchinovich et al, 2011) (Figure 1.4 and 1.5A).

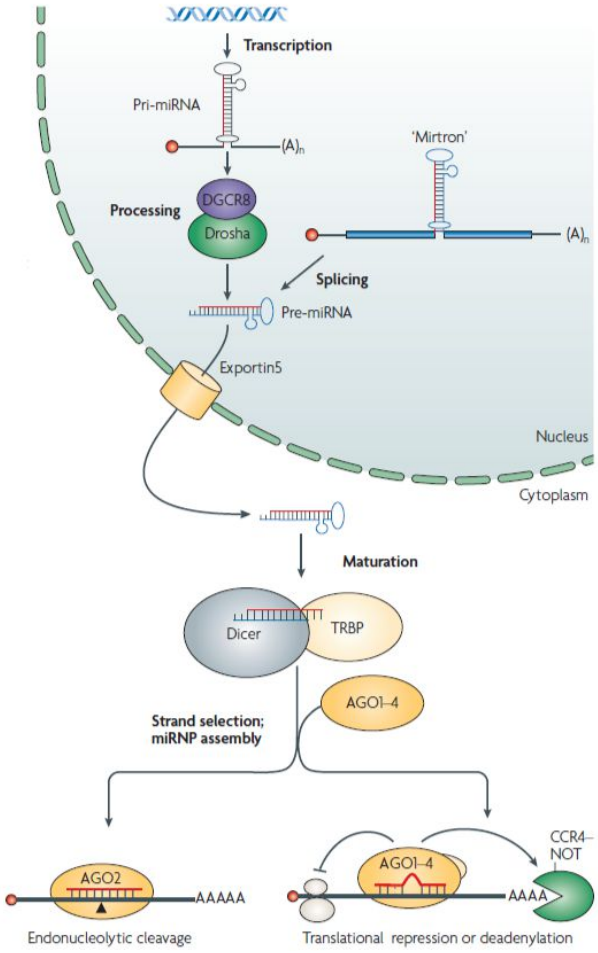

Figure 1.4. miRNA biogenesis and ribonucleoprotein complexes assembly. miRNAs are transcribed as precursor molecules (pri-miRNAs) from independent miRNA genes or protein-coding introns. Individual pri-miRNA may comprise various different miRNAs and fold into stem-loop structures that are processed in two steps catalysed by the RNase III type endonucleases Drosha and Dicer as a part of larger protein complexes containing additional accessory proteins. Drosha complex processes pri-miRNAs to ~70nt hairpins called pre-miRNAs which are transported to the cytoplasm by Exportin5 where they are further processed by Dicer complex to ~20pb miRNA duplexes. miRNAs are assembled into ribonucleoprotein (RNP) complexes which contain Argonaute (AGO) proteins and are essential for inducing miRNA mediated repression (Modified from Filipowicz et al, 2008).

1.6.2. miRNAs in TGF-β1 signalling and EMT processes

TGF-β1 alters miRNA expression *via* R-Smad (i) intronic or intergenic transcriptional miRNA regulation, and (ii) promoting Drosha association with miRNA containing SMAD binding elements (SBE) hairpins and miRNA maturation (Davis et al, 2008; Davis et al, 2010). On the other hand, miRNAs can also regulate TGF-β1 signalling *via* direct interaction with (i) downstream members of the pathway, and (ii) TGF-β1 target genes. This section reviews some of the best-described examples of miRNAs that are induced downstream TGF-β1 signalling and are known to contribute to the EMT process to highlight the importance and potential of miRNAs controlling mesenchymal cell fate (Table 1.4).

miRNA	Target	Function	References
miR-200 family (miR-200a, b, c, miR-141, miR-429)	*ZEB1, ZEB2, SIRT*	TGF-β1 down-regulates all miR-200 members allowing ZEB1 and ZEB2 accumulation, which are two E-cadherin transcriptional repressors. miR-200a also targets SIRT1 affecting epigenetic EMT regulation and promotion.	(Gregory et al. 2008; Eades et al. 2011)
miR-205	*ZEB1, ZEB2*	TGF-β1 down-regulates miR-205 allowing ZEB1 and ZEB2 accumulation, which are two E-cadherin transcriptional repressors and promoting EMT.	(Gregory et al. 2008)
miR-192	*ZEB1, ZEB2*	TGF-β1 down-regulates miR-192 allowing ZEB1 and ZEB2 accumulation, which are two E-cadherin transcriptional repressors and promoting EMT.	(Krupa et al. 2010)
miR-155	*RHOA*	TGF-β1 up-regulates miR-155 decreasing RHOA protein levels contributing to cell migration, cytoskeletal re-organization and promoting EMT.	(Kong et al. 2008)
miR-491-5	*PAR3*	TGF-β1 up-regulates miR-491-5 decreasing PAR3 protein levels which are critical for the integrity of the tight junctions and promoting EMT.	(Zhou et al. 2010)
miR-10b	*HOXD10*	TGF-β1 up-regulates Twist and downstream miR-10b decreasing HOXD10 protein levels which is a critical transcripiton factor regulating invasiveness and metastasis.	(Ma et al. 2007)
miR-24	*NET1A*	TGF-β1 up-regulates miR-24 decreasing NET1A protein levels, a RHO-GEF that activates RHOA.	(Papadimitriou et al. 2012)
miR-21	*PDCD4, SPRY1, TIAM1, PTEN*,	TGF-β1 up-regulates miR-21 decreasing PDCD4, SPRY1, TIAM1, PTEN protein levels which are implicated in EMT processes.	(Asangani et al. 2008; Yao et al. 2011; Thum et al. 2008; Brønnum et al. 2013; Cottonham et al. 2010; Meng et al. 2007; Dey et al. 2012)
miR-31	*TIAM1, LATS2, STK40*, etc.	TGF-β1 up-regulates miR-31 decreasing TIAM1, LATS2 and STK40 protein levels, which are implicated in EMT, G1/S cell cycle inhibition, and cytokine /chemokine expression.	(Cottonham et al. 2010; Liu et al. 2010; Xu et al. 2013)

Table 1.4. miRNAs in TGF-β1 signalling and EMT processes. (Table summarizing section 1.6.2.).

TGF-β1 downregulates miR-200 family (miR-200a, miR-200b, miR-200c, miR-141 and miR-429), miR-205 and miR-192 allowing Zinc finger E-box binding homeobox 1 (ZEB1) and ZEB2 accumulation, two miRNA downstream targets involved in E-cadherin transcriptional repression (Gregory et al, 2008; Krupa et al, 2010). TGF-β1 driven miR-200a downregulation also triggers histone deacetylase silent information regulator-1 (SIRT1) overexpression, implicated in E-cadherin gene silencing (Eades et al, 2011).

TGF-β1 facilitates tight junction and cell polarity loss *via* miRNA up-regulation, including miR-155 and miR-491, which target RHOA and polarity protein PAR3 respectively (Kong et al, 2008; Zhou et al, 2010). Additionally, RHOA signalling is TGF-β1 regulated *via* miR-24 increase, which targets neuro-epithelial cell-transforming-1A (NET1A) that activates RHOA (Papadimitriou et al, 2012). TGF-β1 also up-regulates miR-10b *via* Twist transcription factor; and inhibits homeobox D10 (HOXD10) transcription factor increasing RHOC mediated invasiveness and metastasis (Ma et al, 2007).

miR-21 and miR-31 were the most strongly induced miRNAs in a three dimension colon EMT model triggered by TGF-β1. Both miRNAs were found to regulate the expression of T-lymphoma invasion and metastasis 1 (TIAM1), a guanine nucleotide exchange factor (GEF) for the Rac GTPase that has been implicated in cell invasion (Cottonham et al, 2010). TGF-β1 is known to promote an EMT process while up-regulating miR-21 in a wide spectrum of cell types. Between the numerous validated miR-21 targets by several independent groups it is important to mention that miR-21 can down-regulate tumour suppressor (i) programmed cell death protein 4 (*PDCD4*) (Asangani et al, 2008; Brønnum et al, 2013; Yao et al, 2011); (ii) Sprouty homologue 1 (*SPRY1*) (Brønnum et al, 2013; Thum et al, 2008); and (iii) phosphatase and tensin homolog (*PTEN*) (Dey et al, 2012; Meng et al, 2007) transcripts contributing to mesenchymal phenotype and stimulating cell motility, migration and invasion. *PTEN* has also being shown to be directly targeted by miR-216a and miR-217 downstream of TGF-β1 stimulation (Kato et al, 2009). miR-31 has been less extensively studied but also described to target different important transcript molecules including (i) large tumor suppressor 2 (*LATS2*) (Liu et al, 2010), and serine/threonine kinase 40 (*STK40*) (Xu et al, 2013) which have been involved in G1/S cell cycle transition, EMT processes and cytokine/chemokine expression respectively.

1.6.3. miRNA-changes during PD therapy

The cellular homeostasis of the peritoneal cavity is dramatically affected during long-term PD therapy (Bos et al, 1991; Fernandez de Castro et al, 1994). Aberrant miRNA levels associated to PD therapy may affect the regulation of a multitude of mRNA species, resulting in significant cellular effects. In the context of PD, continuous dialysis fluid exchanges allows easy access to monitor peritoneal cells and miRNA expression in PD effluent (PDE), presenting the enticing possibility of monitoring peritoneal cavity homeostasis during PD treatment. Additionally, the development of micro-sample analysis techniques, together with structural and functional similarities of human peritoneal physiology compared with rodent models may permit *in vivo* scrutiny of PD characteristics (González-Mateo et al, 2009).

Only two articles describing miRNAs in PD therapy were published before this research project started in September 2012 (Table 6.1) (Chen et al, 2012a; Zhang et al, 2012). Chen et al. 2012 selected the following candidate miRNAs based on a report on EMT and kidney disease (Li et al, 2010): miR-15a, miR-17-92, miR-21, miR-30, miR-192, miR-216a, miR-217 and miR-377 (Chen et al, 2012a). Total PDE-derived cells from 110 PD patients (82 new, 28 prevalent) showed significant miRNA up-regulation of miR-15a, miR-21 and miR-192 when comparing new, prevalent and UF failure while miR-17, miR-30 and miR-377 expression was similar between groups (Chen et al, 2012a). miR-30 significantly correlated with GFR and no detectable expression of miR-216a and miR-217 was found in patient samples (Chen et al, 2012a). By contrast, Zhang et al. 2012 used their unpublished data of miRNA expression profiles in HPMCs of PD patients and HMrSV5 cells treated with TGF-β1 to focus their studies on miR-589 (Zhang et al, 2012). miR-589 down-regulation was confirmed in HPMCs from PD patients and HMrSV5 cells treated with TGF-β1, in which overexpression of miR-589 attenuated the MMT changes induced by TGF-β1 (Figure 1.5C) (Zhang et al, 2012).

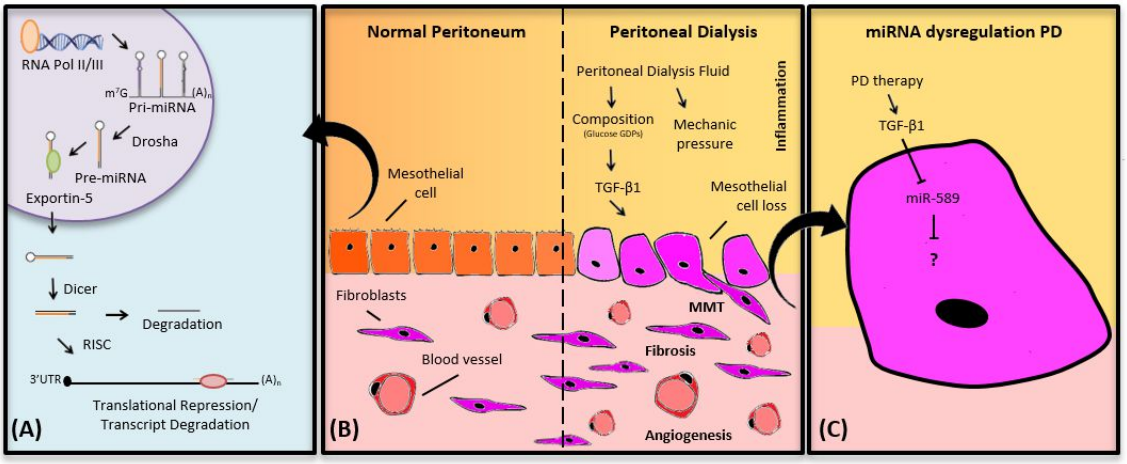

Figure 1.5 miRNA dysregulation in Peritoneal dialysis. (A) miRNA biogenesis pathway. miRNAs are transcribed by RNA polymerase (Pol II) or Pol III as primary miRNA (pri-miRNA) transcripts that are processed by Drosha to generate precursor miRNAs (pre-miRNAs). Pre-miRNA hairpins are transported by Exportin-5 to the cytoplasm, where mature miRNAs are generated by Dicer, and incorporated into the RNA-induced silencing complex (RISC). miRNA-RISC complexes bind to the 3' un-translated regions (3'UTRs) of target mRNAs by partial complementarity, resulting in repression of translation and/or mRNA degradation. **(B)** Peritoneal mesothelial-to-mesenchymal transition (MMT) is associated with PD therapy. Healthy peritoneal mesothelial cells (PMCs; left hand side) undergo morphological changes during PD-driven MMT, invading the submesothelium where they contribute to to angiogenesis, fibrosis and increase extracellular matrix components (ECM) deposition during PD therapy (right hand side). **(C)** Dysregulated miRNA expression resulting from PD therapy. Only miRNAs for which specific evidence in HPMCs existed by the beggining of this project on September 2012 are shown. Figure 6.1 at the general discussion reproduces this Figure **(C)** with additional, up to date, bibliography (Figure modified from Lopez-Anton et al. 2015).

1.6.4. miRNAs as biomarkers of the PD cavity during PD therapy

miRNAs have shown a sound potential as biomarkers in several fields and are easy to detect in different body fluids in which may associate with proteins, microvesicles, exosomes or necrotic bodies (Kosaka et al, 2010). PDE-derived miRNAs may be particularly suitable as biomarkers due to their specific pattern of expression, potential for easy detection, stability, and reliability (Akat et al, 2014; Di Leva et al, 2014; Liang et al, 2007; Lorenzen et al, 2012). PD-miRNA research is in early stage but there is a particular interest regarding miRNA as biomarkers to help individualizing PD treatment. Few studies have investigated the role of microRNAs in the peritoneum as discussed previously (see 1.6.3, Figure 1.5C) and later (see Chapter 6, Figure 6.1, Table 6.1), and have primarily focused on candidate miRNA evaluation (rather than unbiased profiling approaches) measuring miRNAs that may be associated with mesothelial EMT. These *in vitro* and *murine* models provide some association (Bao et al, 2015; Chen et al, 2012a; Lin et al, 2015; Liu et al, 2015; Zhang et al, 2012; Zhang et al, 2013) and functional

data (Liu et al, 2014; Xiao et al, 2015; Yu et al, 2014; Zhou et al, 2013), but their utility as PDE biomarkers has yet to be established. Ultimately, unbiased multi-center miRNA expression analysis of PDE samples combined with robust function data would be essential for the establishment of miRNA-biomarkers associated to PD therapy.

1.7. Aims

The overall purpose of this work was to study miRNAs in the context of PD.

My specific research objectives were:

1. To identify miRNAs expressed in peritoneal mesothelial cells and changes seen in peritoneal mesothelial MMT. To confirm miRNA changes in different models of peritoneal dialysis associated fibrogenesis.

   Hypothesis: *peritoneal mesothelial cells undergoing MMT display associated changes in miRNA expression.*

2. To develop a robust technique for extracting miRNAs from PD effluent and quantifying them. To evaluate the use of miRNAs as biomarkers in PD effluent from patients.

   Hypothesis: *miRNAs can be measured in PD effluent from patients and correlate with clinical parameters*

3. To determine the function of candidate miRNAs identified in aims 1 and 2 in peritoneal mesothelial MMT.

   Hypothesis: *differentially expressed miRNAs control the expression of a panel of mRNA targets and contribute to the MMT process*

Chapter 2 – Methods

2.1. Samples

2.1.1. PD Effluent: Fresh Overnight and Global Fluid Study Samples

Fresh overnight PDE samples from different stable patients were collected from the Renal Unit in the University Hospital of Wales. Patient ethical approval and informed consent for the use of their PDE for research purposes was obtained in all cases. These samples were collected for methodological parameters optimization needed for this study and developed in Chapter 4.

The Global Fluid Study is an international, multicenter, prospective, observational cohort study of 959 patients. This biobank was designed to examine potential local and systemic biomarkers for the maintenance of the structural and functional integrity of the peritoneal membrane on long-term PD therapy. The study has been previously described by Lambie et al. 2013. Samples from a single center were used, to exclude center effects. Stable PD patients were recruited from University Hospital of North Staffordshire, Stoke-on-Trent, UK. The sample size of the study was the maximum feasible by the registry (n=230) and the samples analyzed were, in all cases, the first sample collected from each patient once enrolled for study. Dialysate cytokine levels had been measured previously by electrochemiluminescence (Lambie et al, 2013). 4-hour dwell dialysate samples (peritoneal equilibration test; PET) were stored at - 80°C and thawed on ice. 600 µl aliquots were centrifuged at 12,000 *x g* (relative centrifugal force, RCF) at 4°C for 20 min prior RNA extraction. Ethical approval for this study was obtained from the Multi-Centre Research Ethics Committee for Wales.

2.1.2. Tissue Samples: Human Peritoneal Membrane Study

Formalin-Fixed, paraffin-embedded (FFPE) peritoneal membrane samples from 43 pediatric patients (1.83-19.16 years old) included in the International Pediatric PD Biopsy Study were used in this analysis. Patient samples were age and sex-matched. Average PD duration and submesothelial thickness was equivalent between PD patients

and controls respectively. Patients with previous peritonitis, systemic diseases and abdominal surgery other than catheter insertion, revision or kidney transplantation were excluded. Comprehensive individual clinical data were collected and assessed before analysis to exclude disparity regarding disease susceptibility or comorbidity. Approval was obtained from local ethics committees, and written informed consent obtained from patient and parents. FFPE samples were cresyl violet stained and the mesothelial and submesothelial compact zone were manually microdissected from a total of 40 µm section using a Leica RM 2165 rotary sliding microtome and a Leica S8 APO stereo microscope prior RNA isolation. Experiments performed on these samples were physically performed at the Department of Nephrology, Heidelberg University, Germany during a short stay, and are the result of an established collaboration with ESR Maria Bartosova and Prof Claus Schmitt, who are partners of the EU project EuTRiPD that funded this research.

2.1.3. Tissue Samples: Mouse Peritoneal Membrane Study

Uraemic PD mouse model was developed by ESR Evelina Ferrantelli at Department of Molecular Cell Biology and Immunology, VU University Medical Center, Amsterdam, Netherlands, as part of the EuTRiPD project. Mouse parietal peritoneal biopsies were collected by ESR Evelina Ferranteli from the opposite side from the catheter installation. Model biopsies included mice undergoing PD with and without 5/6 nephrectomy (Nx) and uraemic controls and were fixed in Bouin's solution and embedded in paraffin. Paraffin samples were sent to Cardiff where they were sectioned (5 µm) and H&E stained by Mr. Dilwyn Havard at the Histopathology Department, University Hospital of Wales. Biopsy tissue was placed in the middle third of an uncharged, uncoated glass slide (VFM White coat slides CellPath Ltd). Peritoneal membrane thickness was determined using Arcturus Pixcell IIe infrared laser enabled LCM system (Applied Biosystems) and camera. Thickness measurement was performed using Image J software. Six independent measures were taken from different membrane areas and average was used for statistical analysis.

Peritoneal mesothelial and submesothelial compact zone were dissected using Arcturus Pixcell IIe infrared laser enabled LCM system (Applied Biosystems). Biopsy

tissue was laser selected and bound to a polymer membrane located on a cap (Arcturus ® Capsure ® Macro LCM caps, Applied Biosystems) that is on a slide and holds the selected tissue when lifted after the process. These experiments were carried out after Dr Christopher Carrington guidance at the Institute of Nephrology, Cardiff University. These experiments were possible thanks to ESR Evelina Ferrantelli and Prof R.H.J. Beelen collaboration who are partners of the EuTRiPD project that founded this research.

2.2. Cell Culture: Primary HPMCs and HeLa cell line

2.2.1. Cell culture conditions

Human peritoneal mesothelial cells (HPMCs) were obtained from omental donors undergoing abdominal surgery, with ethical approval and informed consent for the use of their omentum for research purposes (Stylianou et al, 1990; Yung et al, 2006). Peritoneal dialysis effluent (PDE) derived HPMCs were obtained from random stable PD patients by dialysis fluid centrifugation as described in Yáñez-Mo et al., 2003. These samples were kindly provided by Dr Manuel Lopez-Cabrera who is a partner of the EuTRiPD project. Omentum derived HPMCs extraction has been previously carefully characterized by a panel of markers described in Yáñez-Mo et al, 2003 and showed to be little or non-contamination from different cellular contents other than fibroblasts. Omentum derived cultures with fibroblasts contamination are easy to identify under the microscope and were in all cases disqualified for following studies. After trypsin digestion of the tissue, PDE isolation or vial thaw, cells were cultured in Earle's M199 medium (Life Technologies) supplemented with 10% fetal calf serum, 2 mM L-Glutamine, 100 U/ml penicillin, 100 µg/ml Streptomycin, 5 µg/ml Transferrin, 5 µg/ml Insulin and 0.4 µg/ml hydrocortisone from Sigma-Aldrich. HeLa cell line was kindly provided by MSc Hung-Chang Chen and were cultured in RPMI 1640 medium (Invitrogen) supplemented with 10% fetal calf serum, 50 mg/ml penicillin/streptomycin, 2 mM L-Glutamine, 1% sodium pyruvate and 100 µM non-essential amino (NEAA) from Sigma-Aldrich. Cells were grown at 37°C in a humidified incubator with 5% CO_2. The medium was changed every 2-3 days and cells were passaged at $\geq$ 90% confluence by regular trypsinization. All experiments were performed on second passage cells for HPMCs and passage < 15 for HeLa cell line at 80 - 90% confluence.

2.2.2. Cell viability

AlamarBlue assay was used for examination of relative cell number and/or viability. This method employs a non-toxic, cell permeable, blue and non-fluorescent dye, *resazurin*, converted to the pink and fluorescent dye *resorufin* in response to metabolic activity of cultured cells. The fluorescent and colorimetric signal is proportional to the number of living cells in the sample. To perform the assay, cells were incubated new culture medium without FBS at 37°C and 10% (v/v) solution of AlamarBlue reagent. After 1 hour of incubation the medium was transferred to a black 96 well plate (100 µl/well) and the fluorescenct signal was monitored using 544 nm excitation wavelength and 590 nm emission wavelength. Medium with 10% (v/v) AlamarBlue reagent was kept in the incubator for one hour before the measurement to use as a blank.

2.2.3. Cell stimulations

HPMCs were treated for different time periods and concentrations of human-recombinant TGF-β1 (R&D Systems) as specified in text and figure legends, and were growth arrested for 24 h prior to experimentation. In all cases, control cells were treated with growth-arrested medium (medium without FBS) for the indicated time period. Of note, TGF-β1 is used here as a simple and unique stimulus for mesothelial cells as a simplification of the multiple external and autocrine stimulus integrated by HPMCs in real disease context.

HPMCs treatment with different PD solutions was optimized prior experiment. 1:2 and 1:4 PD solution or phosphate buffered saline (PBS) solution in medium with no FBS was used for HPMC treatment over times to 48 h. In preliminary experiments, using dilutions of medium with PBS solution (as control) and PD solutions under study, compromised cell viability and made difficult to draw any conclusions on PD solution differences. 1% FBS supplementation of the medium prevented this compromise of viability, and was adopted for these experiments.

2.2.4. Transfections

Two kinds of plasmids have been used for this study: plasmids for the expression of 3'UTR reporter genes and plasmids for the expression of miRNA precursors (pre-miRNAs) (Figure 2.1). Plasmids containing specific 3'UTR sequences downstream the firefly luciferase coding sequence were generated using *pMIR-REPORT* Luciferase vector (Applied Biosystems, AM5795) (Figure 2.1A) to study miRNA mediated post-transcriptional regulation. *Renilla* luciferase encoding plasmid (pRL, Promega) under a strong, constitutive promoter (Simian Virus 40, SV40) was co-transfected with firefly luciferase reporter as a transfection efficiency control for reporter assays (ratio 5:50). Plasmids to express pre-miRNA sequences were generated using *psiSTRIKE* vector (Promega, 4397MA11_3A) (Figure 2.1B) with insertion downstream of the human U6 promoter, which is recognized by the RNA polymerase III.

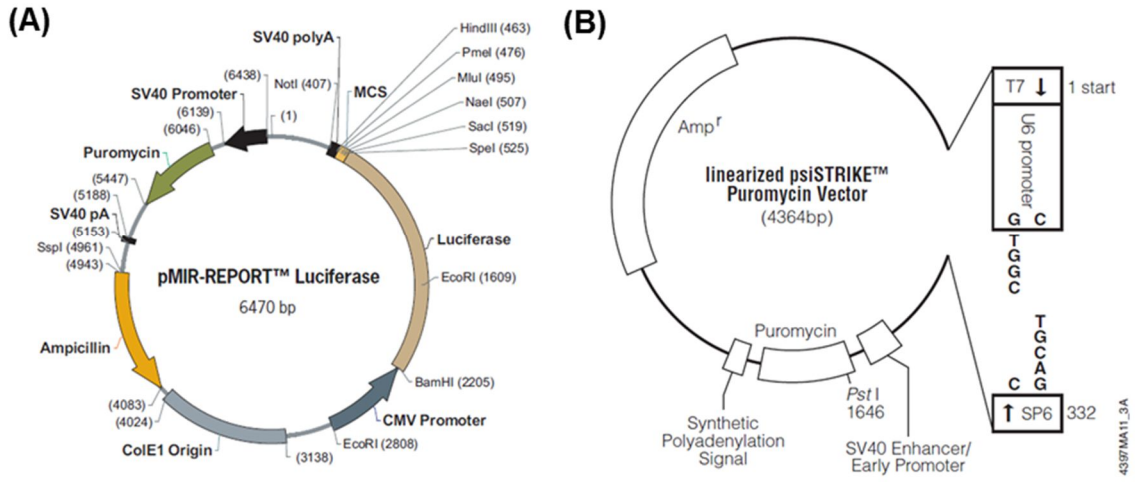

Figure 2.1. Vector circle map and sequence reference points. (A) pMIR-REPORT Luciferase vector. CMV Promoter (2210–2813), Firefly luciferase (540–2210), MCS (467–539), SV40 Poly(A) (404–467), SV40 Promoter (6139–6438), Puromycin (5447–6046), SV40 pA signal (5153–5188), Ampicillin (4083–4943), ColE1 Origin (3138–4024). **(B)** psiSTRIKE Puromycin Vector. T7 RNA polymerase transcription initiation site (1), U6 promoter (16-275), U6 transcription initiation site (276), SP6 RNA polymerase promoter (330-349), SP6 RNA polymerase transcription initiation site (332), Binding site of pUC/M13 Reverse Sequencing Primer (367-388), SV40 enhancer and early promoter (601-1019), SV40 minimum origin of replication (917-982), Puromycin-N-acetyltransferase coding region (1042-1641), Synthetic polyadenylation signal (1686-1734), β-lactamase (Ampr) coding region (2686-3546), Binding site of pUC/M13 Forward Sequencing Primer (4298-4321), T7 RNA polymerase promoter (4348-3).

miRNA reporter construction (pMIR-REPORT based plasmid)

PDZD2 3'UTR has a total length of 2875 pb. The average length of 3'UTR in vertebrates is variable but in humans is ~ 800 pb (Mignone et al, 2002). In addition, long sequences may have non-desired effects on reporter plasmid performance. Thus, a full *PDZD2* 3'UTR reporter (2545 pb) as well as three extra *PDZD2* 3'UTR reporters containing ~ 800 pb each (Figure 2.2) were generated. Other 3'UTR reporters generated included *FGF-18* (814 pb), *S100A10* (245 pb) and *MATN2* (1004 pb).

3'UTR amplification

Specific primers for *PDZD2, FGF-18, S100A10*, and *MATN2* 3'UTRs were designed (Table 2.1) according to In-Fusion HD Cloning Kit User Manual recommendations. PCR specific primers for sequences of interest contained 20 – 23 pb for the specific 3'UTRs sequence (black) followed at the 5' end by a *MluI* enzyme target sequence (green), 10 pb extensions complementary to *pMIR-REPORT* vector (red) and an extra CC (blue) to avoid start-synthesis complications (Table 2.1). 3'UTRs of interest were amplified using CloneAmp HiFi PCR Premix (Clontech, Cat. No. 639298) following protocol recommendations. 4 µl of diluted cDNA (10 ng of RT-RNA) from control HPMCs were mixed with 0.25 µM of designed primers, 12.5 µl of CloneAmp HiFi PCR premix and water in a total reaction volume of 25 µl. PCR amplification conditions were product-optimized and used as following detailed: *PDZD2* 1st 3'UTR (2 min at 98.0°C, 40 cycles of 15 sec at 98.0°C, 30 sec at 54.5°C and 1 min at 72.0°C, followed by an extension step of 5 min at 72.0°C and a cooling step at 4°C); *PDZD2* 2nd and 3rd 3'UTR (2 min at 98.0°C, 40 cycles of 15 sec at 98.0°C, 30 sec at 54.0°C and 1 min at 72.0°C, followed by an extension step of 5 min at 72.0°C and a cooling step at 4°C) and *PDZD2* Full 3'UTR (2 min at 98.0°C, 40 cycles of 15 sec at 98.0°C, 30 sec at 55.0°C and 3 min 30 sec at 72.0°C, followed by an extension step of 5 min at 72.0°C and a cooling step at 4°C). Primers designed for *FGF-18, S100A10* and *MATN2* full 3'UTR amplification owned very different melting temperatures, therefore, touchdown PCR amplification protocols were used to overcome this issue. Touchdown PCR amplification used for *FGF-18* 3'UTR was (2 min at 98.0°C; 41 cycles of 82.0 to 41.0°C for 15 sec with 1°C decrement per cycle and 30 sec at 72.0°C; 25 cycles of 15 sec at 98.0°C, 30 sec at 41.0°C and 30 sec at 72.0°C; followed by an extension step of 5 min at 72.0°C and cooling step at 4°C); and *S100A10* and *MATN2*

3'UTRs were (2 min at 98.0°C; 27 cycles of 64.0 to 37.0°C for 15 sec with 1°C decrement per cycle and 30 sec at 72.0°C; 25 cycles of 15 sec at 98.0°C, 30 sec at 37.0°C and 30 sec at 72.0°C; followed by an extension step of 5 min at 72.0°C and cooling step at 4°C). Similar reaction as described above but using water instead of cDNA was used as a Control Negative (CN). PCR amplification was verified using conventional agarose gel electrophoresis in 1% (w/v) agarose gel containing Ethidium bromide for DNA band visualization and was run in 1x TAE buffer.

Electrophoretic DNA mobility depends on fragment size and is slightly modified by DNA conformation, agarose type and concentration, applied voltage and electrophoresis buffer. Specific PCR product was cut from the agarose gel and spin-column purified using QIAquick gel extraction kit (Quiagen, Cat. No. 28706). Briefly, gel slice was weighted, mixed with 3 volumes of Buffer QG and incubated at 50°C for 10 min while constant vortexing the tube every 2 – 3 min. Subsequently, 1 volume of isopropanol was added and the mixture was passed through a QIAquick spin column by 1 min centrifuge at maximum speed. Column was successively washed by 500 µl Buffer QG, 750 µl Buffer PE, extra centrifuged with no wash buffer to remove residual fluid and DNA eluted in 50 µl of water.

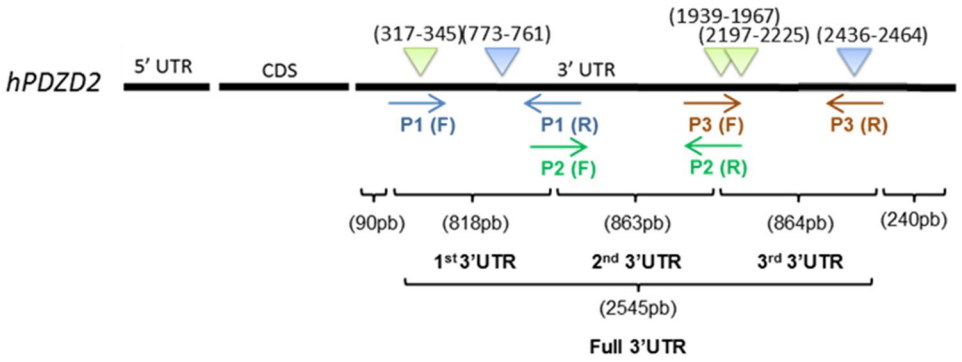

Figure 2.2. *PDZD2* 3'UTR luciferase reporter generation using *pMIR-REPORT* Luciferase vector. Reporter constructs diagram. The 3'UTR of *PDZD2* (~ 2.88 kb) was cloned downstream *firefly* in the *pMIR-REPORT* Luciferase vector generating four different reporter constructs: 1st 3'UTR, 818pb, containing one putative binding site for miR-21 and one for miR-31; 2nd 3'UTR, 863pb, containing no putative binding sites; 3rd 3'UTR, 864pb, containing one putative binding sites for miR-21 and two for miR-31; and Full 3'UTR, 2545pb, containing the whole three sequences described above. miR-21 binding site – blue arrow, miR-31 binding site – Green arrow.

Plasmid generation	Inserts or PCR-primers (5' – 3')
miRNA reporter construction (*pMIR-REPORT* based plasmid)	
***pMIR-hPDZD2* 1st**	**F:** CCGATATCACGCACGCGTACACTGGTACAGACACGGAC **R:** CCGCCGGCATAGACGCGTTGTCTGCTCTTGGACTGACC
***pMIR-hPDZD2* 2nd**	**F:** CCGATATCACGCACGCGTGGTCAGTCCAAGAGCAGACA **R:** CCGCCGGCATAGACGCGTACCTCTCTAGGCCGACTTCA
***pMIR-hPDZD2* 3rd**	**F:** CCGATATCACGCACGCGTTGAAGTCGGCCTAGAGAGGT **R:** CCGCCGGCATAGACGCGTAGATGGAAATGAAACCCAGCCT
pMIR-hFGF-18	**F:** CCGATATCACGCACGCGTGCCACCCCGCCGCGGCCCCT **R:** CCGCCGGCATAGACGCGTTTAAATAATTTGTCTGTTGT
pMIR-hS100A10	**F:** CCGATATCACGCACGCGTGCAGAAATGAGCAGTTCGCT **R:** CCGCCGGCATAGACGCGTGGAACTAAAAAAGAACTTTA
pMIR-hMATN2	**F:** CCGATATCACGCACGCGTAGATTAGAAATCGCGACACA **R:** CCGCCGGCATAGACGCGTGAGTTTGACCATTTATTTGT
***pMIR FGF-18* Mut-m21**	**F:** TATATTTCGTATTTATTTCACCTCTCTGTAT **R:** AAATACGAAATATATATATAATATATATAATATAGCTGGTTTTT
***pMIR S100A10* Mut-m21**	**F:** CAGATTTCGTTTTGATTTTT **R:** CAAAACGAAATCTGGTATTT
Pre-miRNA plasmid construction (*psiSTRIKE* U6 based plasmids)	
***psiSTRIKE* pre-miR-CN**	**A:** ACCGCGTATCGTAAGCAGTACTAAGTTCTCTAGTACTGCTTACGATACGCTTTTTC; **B:** TGCAGAAAAAGCGTATCGTAAGCAGTACTAGAGAACTTAGTACTGCTTACGATACG
***psiSTRIKE* pre-miR-21**	**A:** ACCGTGTCGGGTAGCTTATCAGACTGATGTTGACTGTTGAATCTCATGGCAACACC AGTCGATGGGCTGTCTGACATTTTTC; **B:** TGCAGAAAAATGTCAGACAGCCCATCGA CTGGTGTTGCCATGAGATTCAACAGTCAACATCAGTCTGATAAGCTACCCGACA
***psiSTRIKE* pre-miR-31**	**A:** ACCGGGAGAGGAGGCAAGATGCTGGCATAGCTGTTGAACTGGGAACCTGCTATGC CAACATATTGCCATCTTTCCTTTTTC; **B:** TGCAGAAAAAGGAAAGATGGCAATATGTTG GCATAGCAGGTTCCCAGTTCAACAGCTATGCCAGCATCTTGCCTCCTCTCC

Table 2.1. Plasmids generated for this study and oligonucleotide sequences used for cloning. Bold F and R indicate PCR primer sequences while A and B indicate inserts.

pMIR-REPORT vector digestion

1 µg of *pMIR-REPORT* vector was digested using 1 µl of *MluI* enzyme (New England BioLabs, R01985) and 1 µl of Buffer 3.1 in a total volume of 10 µl at 37°C overnight. A similar reaction using water instead of vector was used as a CN. Digested plasmid and CN sample were mixed with 2 µl of loading buffer (GelPilot DNA Loading Dye, 5x, QUIAGEN, Cat. No. 239901) and loaded into 1% electrophoresis gel. 1Kb ladder (New England BioLabs, N0552G) was also loaded into the gel and run at 90 V during 60 min. A single band containing the linear plasmid was cut and plasmid was purified using QIAquick gel extraction kit as previously described above.

In-Fusion Cloning reaction

In-Fusion protocol was followed for cloning reaction with minor modifications. In brief, 25 ng of PCR purified fragment was mixed with 25 ng of linearized vector, 1 µl of In-fusion HD enzyme premix and water in a total volume of 5 µl.

Escherichia coli Transformation

Stellar competent *Escherichia coli* (*E. coli*) were thawed on ice and 25 µl of bacteria suspension were incubated with 1.25 µl of In-Fusion reaction previously described for transformation during 30 min in 12 ml polypropylene tube. The suspension was placed at 42°C for 45 sec and chilled on ice for 2 min. 500 µl of 37°C pre-warmed SOC medium were subsequently added to the bacteria suspension and incubated for 1 hour at 37°C with shaking. 25 µl of transformed bacteria were seed on YTx2 agar plate (Appendix) containing 100 µg/ml ampicillin and growth at 37°C overnight.

E. coli purification

Single colony was transferred to a new 12 ml polypropylene tube containing 5 ml YTx2 broth (Appendix) with 100 µg/ml ampicillin and incubated overnight at 37°C with shaking. Plasmid purification was performed using GenElute HP Plasmid MiniPrep Kit (Sigma-Aldrich, NA0160), following manufacturer's recommendations. 4 ml bacterial culture was centrifuged for 3 min at ≥ 12,000 x *g* and room temperature (RT). Bacterial pellet was re-suspended in 200 µl of Resuspension Solution, and 200 µl of Lysis Buffer were added and mixed by inversion. After 5 min at RT, 350 µl of cold, Neutralization Buffer were added, mixed by inversion and centrifuged for 10 min at ≥ 12,000 x *g* and RT. Miniprep Binding Columns were washed with 500 µl of Column Preparation Solution

prior cleared bacterial lysate load, and passed through the column by centrifugations for 1 min at ≥ 12,000 x *g* at RT. The column was further washed with 500 µl of Wash Solution 1 (41% ethanol) and 750 µl of Wash Solution 2 (44% ethanol) followed by 1 min at ≥ 12,000 x *g* at RT with no wash buffer to remove residual fluid and plasmid DNA eluted in 50 µl of water. 800 µl of bacterial culture were mixed with 200 µ of glycerol and stored frozen at - 80°C.

pMIR-REPORT Plasmid Verification

pMIR-REPORT containing 3'UTR inserts of interest included two *MluI* sites flanking the insert. *MluI* digestion of plasmids containing the expected insert will produce two products (~ 0.8 or 2.5 Kb and 6.47 Kb). Thus, plasmid concentration was quantified using NanoDrop 2000 UV spectrophotometer. NanoDrop uses absorbance wavelength 260 nm (A_{260nm}) measures to calculate nucleic acid concentration using the following equation:

[Total DNA µg/ml] = A_{260nm} x 50 x dilution factor.

1 µg of plasmid DNA was digested with 1 µ of *MluI* (New England Biolabs, R0140S) and 1 µl of NEBuffer 3.1 in a total volume of 10 µl and run in 1% (w/v) agarose gel together with samples processed without enzyme (Figure 2.3). Plasmid positive sequences were confirmed by sequencing (Eurofins Genomics, Prepaid Barcodes, 3098-000PPB).

pMIR-REPORT plasmid mutation

Specific primers for *FGF-18* and *S100A10* seed miRNA sequence mutation were designed (Table 2.1) according to In-Fusion HD Cloning Kit User Manual recommendations. Primers were designed to overlap with each other 15 pb (purple and orange) at their 5' end and incorporate the desired substitution (orange). As previously described (Clovis et al, 2012), four nucleotides (corresponding to seed sequence positions 2^{nd} – 5^{th}) were mutated to the same miRNA nucleotide found in miRNA seed sequence to maximize repulsive effect. *pMIR-REPORT* containing *FGF-18* and *S100A10* 3'UTR were amplified using CloneAmp HiFi polymerase following protocol recommendations. 5 ng of pMIR-R plasmid were mixed with 0.25 µM of designed primers, 12.5 µl of CloneAmp HiFi PCR premix and water in a total reaction volume of 25

µl. PCR amplification conditions were product-optimized: 2 min at 98.0°C, 40 cycles of 15 sec at 98.0°C, 30 sec at 55.0°C and 1 min at 72.0°C, followed by a cooling step at 4°C. PCR amplification was verified on 1% (w/v) agarose gel and specific PCR product was cut from the gel and spin-column purified as detailed above. 25 ng of linear construction containing the desired mutation was incubated with 0.5 µl of In-Fusion enzyme in a total volume of 5 µl at 50°C for 15 min. 25 µl of competent cells were transformed using 1.25 µl of the above reaction as previously described (see 2.2.3.).

Pre-miRNA plasmid construction (psiSTRIKE U6 based plasmids)

miR-21, miR-31 and miR-CN pre-miRNA plasmids were generated by ligation of annealed DNA oligonucleotides A and B (Table 2.1) into the *psiSTRIKE* U6 vector following manufacturer's recommendations.

Oligonucleotide design

Oligonucleotide (A) contained pre-miRNA sequences described in miRBase release 21 (Kozomara & Griffiths-Jones, 2014) for miR-21 and miR-31 followed by the U6 termination sequence (TTTTT, green) and an additional C residue (orange). This last residue will create a new *PstI* restriction site upon insert ligation that will allow positive plasmid discrimination. Oligonucleotide (B) includes TGCAG overhang sequence (red), which is complementary to *siSTRIKE U6* sticky end, and an oligonucleotide (A, blue) complementary sequence excluding the last four nucleotides. Pre-miR-CN sequences were previously designed by Krupa 2010 based on miR-CN sequences used by Life Technologies and recommended loop sequence AAGTTCTCT (Krupa, 2010) (Table 2.1).

Oligonucleotide annealing

Oligonucleotide A-B annealing was performed by incubation at 90°C for 3 min followed by a second incubation at 37°C for 15 min in the Oligo Annealing Buffer (Promega) at 40 ng/µl final concentration each. The resulting, double-stranded DNA, owns *psiSTRIKE U6* complementary 5' overhangs to enable effective directional ligation.

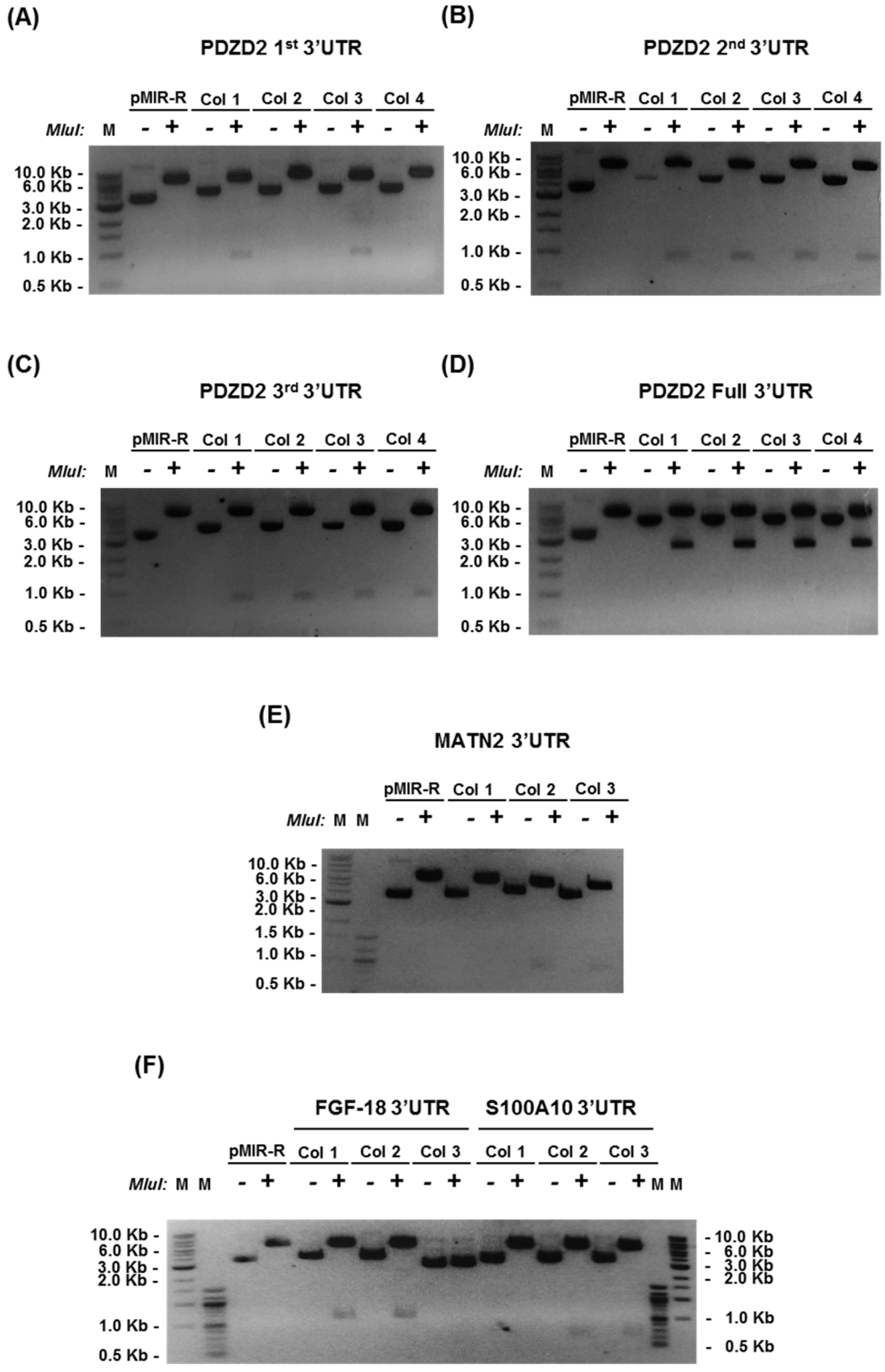

Figure 2.3. Potential positive E. Coli colonies selection for each specific 3'UTR luciferase reporter generated prior sequencing confirmation. (A) E. Coli colonies potentially containing *pMIR-REPORTER PDZD2* 1st 3'UTR insert of interest *MluI* digested. **(B)** E. Coli colonies potentially containing *pMIR-REPORTER PDZD2* 2nd 3'UTR insert of interest *MluI* digested. **(C)** E. Coli colonies potentially containing *pMIR-REPORTER PDZD2* 3rd 3'UTR insert of interest *MluI* digested. **(D)** E. Coli colonies potentially containing *pMIR-REPORTER PDZD2* full 3'UTR insert of interest *MluI* digested. (**E)** E. Coli colonies potentially containing *pMIR-REPORTER MATN2* 3'UTR insert of interest *MluI* digested. **(F)** E. Coli colonies potentially containing *pMIR-REPORTER FGF-18* and *S100A10* 3'UTR insert of interest *MluI* digested.

psiSTRIKE U6 vector digestion

1 µg of *psiSTRIKE U6* vector were digested using 1 µl of *BbsI* enzyme (New England BioLabs, R0539S) and 1 µl of NEBuffer 2.1 in a total volume of 10 µl at 37°C overnight. Digested plasmid was mixed with 2 µl of loading buffer, loaded into 1% electrophoresis gel and run at 90 V during 60 min as previously described (see 2.2.3.). Single band containing amplified linear plasmid was cut and purified as described above (see 2.2.3.).

Annealed oligonucleotide-psiSTRIKE U6 ligation and subsequent cloning steps

4 ng of annealed oligonucleotide were mixed with 50 ng of linear *psiSTRIKE U6* vector and 1 µl of quick T4 DNA ligase (New England Biolabs, M2200S) in 5 µl of quick ligation buffer and a total volume of 10 µl. Ligation was carried out for one hour at RT. Competent *E. coli* transformation was performed as described above (see 2.2.3.) with minor changes including the use of 50 µl of bacteria suspension together with 2.5 µl of ligation reaction previously described for transformation. 50 µl of transformed bacteria were seed this time on YTx2 agar plate (Appendix) containing 100 µg/ml ampicillin and growth at 37°C overnight. *E. coli* plasmid purification was performed as described above (see 2.2.3.).

Plasmid Verification

siSTRIKE U6 plasmid contains one *PstI* site prior ligation and a second one is created as a successful ligation result. Therefore, *PstI* digestion of plasmids containing the expected insert will produce two products (~3.0 and 1.4 Kb). Similarly as described above (see 2.2.3.), 1 µg of plasmid DNA were digested with 1 µ of *PstI* (New England Biolabs, R0140S) and 1 µl of NEBuffer 3.1 in a total volume of 10 µl. Digested samples were separated in 1% (w/v) agarose gel as described in detail in (see 2.2.3.). Samples without the enzyme were processed and run into the same gel. In adition, plasmid sequences were confirmed by sequencing by (Eurofins Genomics, Prepaid Barcodes, 3098-000PPB).

Transient HPMCs transfections: Protocol optimization.

Human primary MCs are very delicate to culture *in vitro* and not easy to transfect. No previous protocol had been established in this laboratory to successfully transfect HPMCs with small RNAs and/or plasmids before this study. Therefore, the use of different transfection reagents before to set up a protocol for the project was tested. Details of the transfection reagents and protocols tested are summarized in Table 2.2. 24-well plates were seed and transfected by 80% confluence following described protocols (Table 2.2). After drop-wise transfection-mixture addition to HPMCs, plates were mixed gently by agitation, pipetting when indicated, and placed into the incubator. In all cases, medium was replaced 4 h after transfection by serum-free medium and miRNAs were measured 48 h after transfection. Transfection reagents were tested by using *psiSTRIKE-miR-CN* (Control) and *psiSTRIKE-miR-31* as miR-31 was less expressed than miR-21 in HPMCs and differences would be easier to measure. Lipofectamine LTX & PLUS (Thermo Fisher Scientific, 15338100) reagent showed the greatest miR-31 induction when cells were transfected with *psiSTRIKE-miR-31* compared to *psiSTRIKE-miR-CN* plasmid (Figure 2.4). Nevertheless, subsequent experiments showed significant HPMCs morphological changes associated with *psiSTRIKE-miR-CN* plasmid overexpression which threshold was difficult to determine as they were highly dependent on donor. No morphological differences were observed when HPMCs were transfected with *pMIR-REPORT* and *Renilla* luciferase encoding plasmids.

Transient transfections with DNA plasmids and small RNAs

Four kinds of small RNAs have been used for this study including *mir*Vana miRNA mimic (Thermo Fisher Scientific), *Silencer Select* siRNA (Thermo Fisher Scientific), *miRCURY LNA* miRNA inhibitor (Exiqon) and *mir*Vana miRNA inhibitor (Thermo Fisher Scientific) (Table 2.3). *mirVana miRNA mimics* are small, chemically modified double-stranded RNAs that mimic endogenous miRNAs and enable miRNA functional analysis by up-regulation of miRNA activity using cell machinery mechanisms. *Silencer Select* are annealed siRNA duplexes, algorithm designed, off-target effect predicted and functionally confirmed. *miRCURY LNA* miRNA inhibitors are antisense oligonucleotides with perfect target sequence complementary that when introduced into cells sequester their target miRNA in highly stable hetero-duplexes preventing miRNA regulation of its

normal cellular mRNA targets. *mirVana miRNA inhibitors* are small, chemically modified single-stranded RNA molecules that bind and inhibit specific miRNAs allowing functional analysis by miRNA activity down-regulation.

Product (Manufacturer)	***Delivery***	***Requirements***	***Brief Protocol***
K2 Transfection system (Biontex Laboratories GmbH, T060)	Cationic lipid (liposome) delivery combined with decreased cell ability to detect nucleic acids	Suitable complete growth medium containing antibiotics and FBS	Add 9.5 µl of K2 Multiplier to each well 2 h prior transfection. Mix by gently pipetting Solution A containing 28.5 µl serum-free medium and 0.25 µg DNA with Solution B comprising 28.5 µl serum-free medium and 2.3 µl K2 Transfection Reagent. Incubate the mixture 15 - 20 min at RT and add immediately after to the cells.
Viromer Yellow (Lipocalix, VY-01LB-01)	Alkyl moieties combined with long chain fatty acids that switch conformation facilitating membrane crossing during endocytosis due to acidic environment.	Suitable complete growth medium containing antibiotics and FBS Recommended for cells known as 'non-transfectable'.	Dilute DNA to 9 ng/µl using Buffer E and mix separately 4 µl Viromer Yellow with 96 µl Buffer E following the indicated order. Place 15 µl of pre-diluted Viromer in a sterile tube and add 85 µl of DNA solution in Buffer E. Mix by gentle pipetting and allow complexation for 15 min prior transferring 33 µl of the complexes to the cells.
FuGENE HD (Promega, E2311)	A mixture of lipids and other components in 80% ethanol	No antibiotics in the transfection medium Suitable with FBS	Dilute 0.25 µg of DNA using 100 µl Opti-MEM Reduced Serum Medium and add 1-5 µl of FuGENE HD Transfection Reagent to the mixture immediately. Incubate the mixture 5 - 15 min at RT and add 25 µl of the FuGENE HD Transfection Reagent/DNA mixture per well while mixing by pipetting during 30 sec.
Lipofectamine LTX & PLUS Reagent (Thermo Fisher Scientific, 15338100)	Cationic lipid formulation	No antibiotics in the transfection medium Suitable with FBS	Dilute 0.25 µg of DNA using 100 µl Opti-MEM Reduced Serum Medium and mix gently prior and after adding 0.5 µl of PLUS Reagent. Incubate the mixture for 5 min at RT and add 1.25 µl of Lipofectamine LTX Reagent to the mix and incubate for 30 min at RT prior transferring 100 µl of the complexes to the cells.
jetPRIME Transfection Reagent (Polyplus transfection, Cat. No. 114-07)	Polymer formulation	Suitable complete growth medium containing antibiotics and FBS	Dilute 0.25 µg of DNA using 50 µl jetPRIME Buffer, mix by vortexing and add 1 µl of jetPRIME Reagent, mix and incubate for 10 min at RT. Add 50 µl of transfection mix onto the cells.

Table 2.2. Table summarizing transfection systems used for this study. Quantities described above are adapted for experiment size equivalent to 24-well plate.

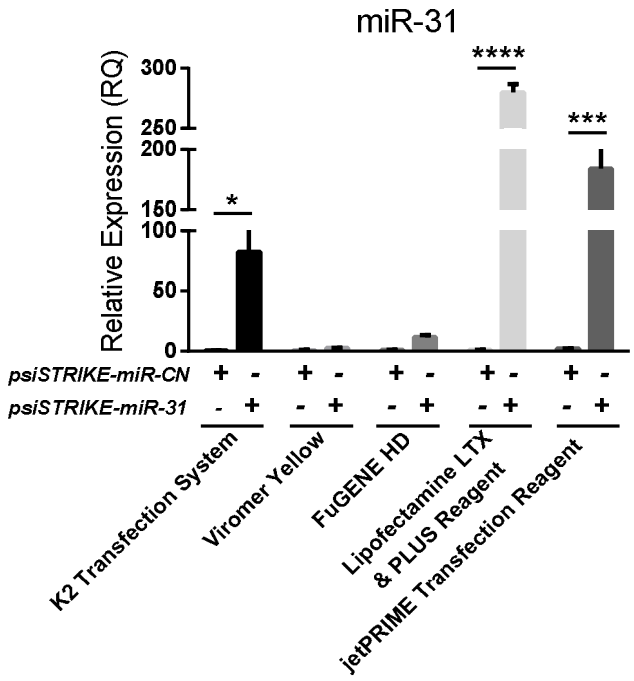

Figure 2.4. HPMCs transfection system optimization. 24-well plates were seed and transfected by 80% confluence following described protocols for K2 transfection system, Viromer Yellow, FuGENE HD, Lipofectamine LTX & PLUS Reagent and jetPRIME Transfection Reagent together with psiSTRIKE-miR-CN and psiSTRIKE-miR-31 as detailed in Table 2.1. Relative miR-31 expression was measured 48 h after cell transfection by RT-qPCR and normalized to miR-191 expression. Data were analyzed by two-way ANOVA for matched samples by both factors followed by post-hoc Holm-Sidak's test within each each transfection method mean compared with control mean. Data represent the mean S.E.M. from three independent donor experiments. *p < 0.05; ***p < 0.005; ****p < 0.001.

Small RNA	Catalog Number
mirVana miRNA mimic hsa-miR-31-5p	Cat. No. 4464066 MC11465
mirVana miRNA mimic hsa-miR-21-5p	Cat. No. 4464066 MC10206
mirVana miRNA Mimic Negative Control #1	Cat. No. 4464058
Silencer Select FGF18 siRNA	Cat. No. 4392420 S17213
Silencer Select S100A10 siRNA	Cat. No. 4392420 S12429
Silencer Select MATN2 siRNA	Cat. No. 4392420 S8533
Silencer Select PDZD2 siRNA	Cat. No. 4392420 S22889
Silencer Select Negative Control No.1 siRNA	Cat. No. 4390843
miRCURY LNA microRNA inhibitor hsa-miR-21-5p	Cat. No. 4102261-001
miRCURY LNA microRNA inhibitor hsa-miR-31-5p	Cat. No. 4100872-001
miRCURY LNA microRNA inhibitor Negative Control A	Cat. No. 199006-001
mirVana miRNA inhibitor hsa-miR-21-5p	Cat. No. MH10206
mirVana miRNA inhibitor hsa-miR-31-5p	Cat. No. MH11465
mirVana miRNA Inhibitor Negative Control #1	Cat. No. 4464078

Table 2.3. Small RNAs used in this study.

mirVana miRNA mimic were used at concentrations of 5 pM, 10 pM and 20 pM for target mRNA measurements (48 h after transfection) to prove treatment consistency.5 pM concentrations were used for protein quantification (72 h after transfection). No morphological differences were observed when HPMCs were transfected with different concentrations of miRNA mimic-CN neither when compared with mimic-21 or mimic-31 at concentrations described for experiment. *Silencer Select* siRNA was tested for transfection in HPMCs at different concentrations including 10 nM, 20 nM, 30 nM and 40 nM. 30 nM was the concentration that showed higher target transcript down-regulation after 48 h of transfection for *PDZD2* while 40 nM showed greater target mRNA down-regulation for *FGF-18, S100A10* and *MATN2* and were, therefore, chosen for subsequent analysis (Figure 2.5). Finally, *miRCURY LNA* inhibitors performance can be measured by de-repression of endogenous miRNA targets (validated or predicted) and can be measured at mRNA level. miRNA RT-qPCR, sometimes reported in literature, is not a reliable method for measuring miRNA knock-down as these inhibitors do not degrade their targets but form stable complexes that cause miRNA accumulation. In addition, LNA oligonucleotides have been described to interfere with miRNA PCR primers rising aberrant results. Thus, *miRCURY LNA* inhibitors were tested at 25 pM, 50 pM, 1 nM, 25 nM, 50 nM, 75 nM, 100 nM and 200 nM; mRNA targets (*PDCD4, SPRY1, PTEN* for LNA-miR-21 and *LATS2, STK40* for LNA-miR-31) were measured 24, 48 and 72 h after transfection and possible differences by transfection methods were chased by comparing Lipofectamine LTX & PLUS Reagent with Lipofectamine RNAiMAX Reagent (Thermo Fisher Scientific, Cat. No. 13778030). Additionally, HPMCs were transfected twice with *miRCURY LNA* inhibitors using 25 pM, 50 pM, 25 nM, 50 nM and 12 h of difference between transfections. No differences in mRNA target expression were measured under all conditions described above. Exiqon specialists were contacted to share this outcome and found no clear explanation for the results obtained. Literature describes final use concentrations of *miRCURY LNA* inhibitors much higher than those described by Exiqon standard protocol *in vitro* which indicates potent activity at final concentrations of 1 - 50 nM, although pointing out that a more extensive range of 1 - 100 nM can be analyzed in optimization experiments. *miRCURY LNA* inhibitor concentration required may be even higher for this specific research as miR-21 and miR-31 were two of the highest miRNAs expressed in HPMCs.

Longer research time to develop this part of the project would have allow to test higher *miRCURY LNA* inhibitor concentrations and target protein levels with the concentrations and methods already described. Nevertheless, there are other miRNA inhibitors currently available at the market including *mir*Vana miRNA inhibitor. Indeed, these miRNA inhibitors were used at concentrations of 5 pM, 10 pM and 20 pM for target mRNA measurements (48 h after transfection) and showed significant and consistent complementary results to those displayed by *mir*Vana miRNA mimics for already described miR-21 and miR-31 targets.

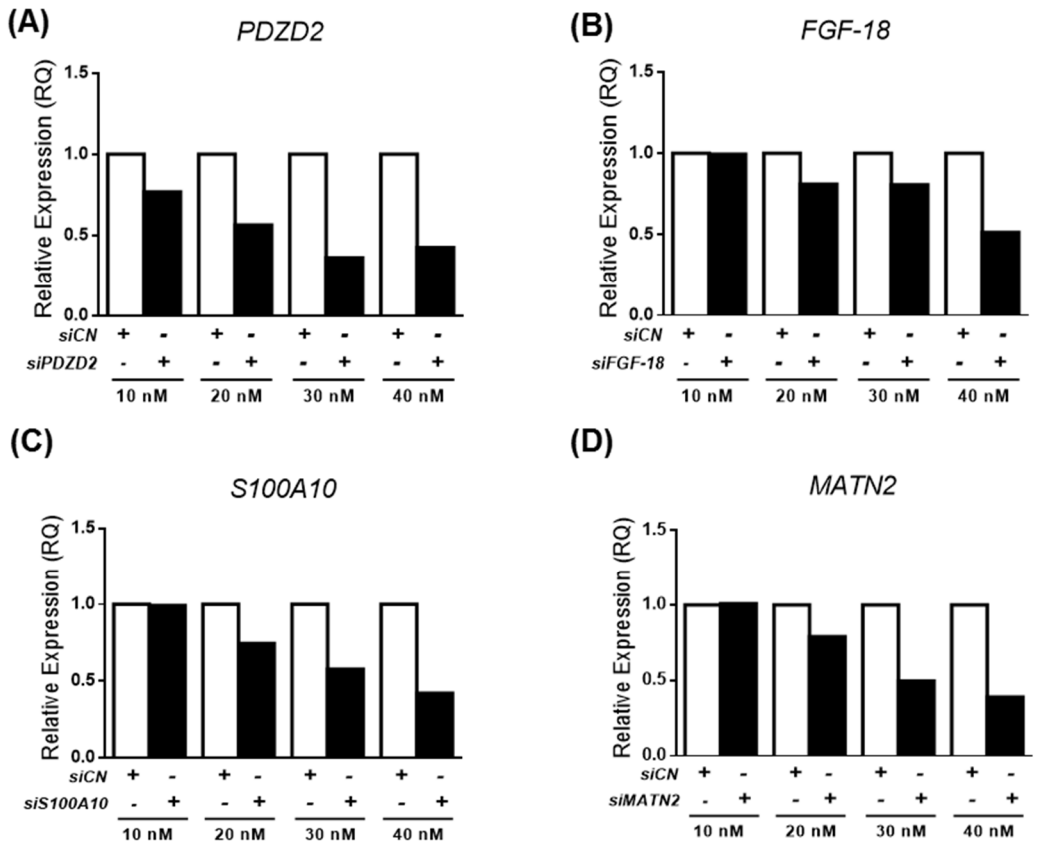

Figure 2.5. siRNA transfection optimization for *PDZD2, FGF-18, S100A10* and *MATN2*. 24-well plates were seed and transfected by 80% confluence following described protocol for Lipofectamine LTX & PLUS Reagent together and different siRNA concentrations. *PDZD2, FGF-18, S100A10 and MATN2* relative expression was measured 48 h after cell transfection.

2.3. RNA analysis

2.3.1. RNA isolation

2.3.1.1. RNA extraction from PD samples

When this project was initiated there was no published and validated protocol for miRNA extraction from PD effluent. Initial experiments using isolation protocol for urine samples previously developed at the department by Dr Beltrami (Beltrami, 2014) was compared with newly reported protocols for highly diluted samples (Burgos et al, 2013). Two commercially accessible kits for RNA and/or miRNA extraction from fluid samples were used: the *Qiagen miRNA-easy* mini kit (QIAGEN, Cat. No 217004) was used with minor modifications recommended by Dr Beltrami (Beltrami, 2014), while the *mirVana PARIS* kit (Thermo Fisher Scientific, Cat. AM1556) was used with progressive addition of minor modifications recommended by Burgos et *al*. 2013 (Burgos et al, 2013). Full protocol optimization for RNA extraction from 4h PDE from patients is developed in Chapter 4 (see 4.2.1-6) and included the use of (i) *mirVana PARIS* kit, (ii) 1/3 volume ethanol to the aqueous phase, (iii) no use of MS2 RNA carrier, and (iv) cold Speed-Vac for 40 min.

For RNA isolation using *mirVana PARIS kit*, PD effluent samples from PD patients were handled consistent with manufacturer's recommendation with the following modifications. 600 µl of PDE sample were centrifuged for 20 min at 400 *x g* at 4°C. 500 µl of sample were transferred to a new eppendorf to which 500 µl of denaturing solution and 0.5 pM of spike in *Caenorhabditis elegans* (cel-miR-39) (Ambion, Cat. No 4464066, Part No. MC10956) were subsequently added. Of note, order of reagent addition was important in this step as previous cel-miR-39 spiked into the PDE could trigger RNAse mediated cel-miR-39 degradation. Subsequently, samples were processed according to manufacturer's protocol. After recovering 900 µl of aqueous phase (E1) the remaining organic layer was re-hydrated with 900 µl of water and an extra 1000 µl of aqueous phase (E2) were re-isolated (Figure 4.3A). Following sample processing was performed according to manufacturer's guidelines, with the entire aqueous phase from each

sample loaded onto a single affinity column. RNA extracts were eluted in 100 µl of water previously warmed at 95°C in a silicon coated eppendorf and cold Speed-Vac during 40 min. Final RNA concentrated extracts were stored at -80°C before experiment.

2.3.1.2. RNA extraction from tissue samples (LCM and manual microdissection)

Formalin-fixed, paraffin-embedded (FFPE) samples were processed immediately after sectioning using RecoverAll™ Total Nucleic Acid Isolation kit (Thermo Fisher Scientific; AM1975) according to the manufacturer's recommendations. Membrane polymer situated upon LCM caps was carefully removed from the caps and miRNAs were extracted with minute protocol modifications. Variants introduced include (i) deparaffinization step was required and performed before LCM and (ii) 1 µg of RNA carrier MS2 (Roche; Cat. No. 10165988001) was added during the nucleic acid isolation stage to improve RNA recovery.

Briefly, 400 µl of Digestion Buffer and 4 µl of Protease were combined into eppendrofs containing LCM membrane polymers and incubated at 50°C for 15 min and at 80°C for 15 min. 120 µl of Isolation Additive together with 275 µl of 100% ethanol and 1.25 µl of MS2 RNA carrier were added to each sample. 700 µl of mixture was placed into a filter cartridge and centrifuged during 30 sec at 10,000 x *g*. Nucleic acids bind to the cartridge filter while the remaining substances pass through and are discarded. Filters are subsequently washed using wash 1 buffer and wash 2/3 buffer. DNA was degraded by incubating the filter with 60 µl of DNA mix containing 6 µl 10 x DNase Buffer, 4 µl DNase and 50 µl water for 30 min at RT. Cartridge filters were newly washed using wash 1 buffer and wash 2/3 buffer. Clean RNA was eluted with pre-heated water 95°C (60 µl). RNA was stored in all cases at -80°C prior experiment.

2.3.1.3. RNA extraction from HPMCs

HPMCs were lysed in TRI reagent (Termo Fisher Scientific; Cat. No. 15596-026), and RNA was extracted as recommended by the manufacturer. TRI reagent combines phenol and guanidine thiocyanate in a single phase to quickly inhibit RNase activity. 6-well plated cells were lysed in 1 ml TRI Reagent solution and incubated at room temperature for 5 min to favor total dissociation of nucleoprotein complexes. 200 µl of

chloroform (Sigma) were added to the homogenate, vortexed vigorously, incubated 5 min at room temperature and centrifuged at 12,000 *x g* for 15 min at 4°C to separate aqueous and organic phases. RNA stays at the upper (aqueous phase) while DNA and proteins displace to the interphase or organic phase respectively. Aqueous phase was isolated and RNA precipitated by adding 500 µl of isopropanol (Sigma) and centrifuging at 12,000 *x g* for 10 min at 4°C. RNA precipitates were washed 3 times with 1 ml of 75% ethanol (Sigma) and centrifuged 12,000 *x g* for 5 min at 4°C. Clean RNA pellet was air-dried for 15 min and rehydrated in 10 µl of nuclease-free water. Sample purity and RNA concentration was measured using 1 µl of sample by NanoDrop 2000 spectrophotometer (Thermo Scientific). RNA was stored in all cases at -80°C prior experiment.

2.3.1.4. RNA quantification and quality control

RNA concentration was measured using NanoDrop 2000 UV spectrophotometer. NanoDrop uses absorbance wavelength 260 nm (A_{260nm}) measures to calculate nucleic acid concentration using the following equation:

[Total RNA µg/ml] = A_{260nm} x 40 x dilution factor.

NanoDrop also measures absorbance wavelength 280 nm (A_{280nm}) to provide a contamination parameter. A_{260nm}/A_{280nm} ratio of ~2.0 is accepted as *'pure'* RNA while lower ratios indicate sample contamination by other molecules that may include protein, phenol or other contaminants that absorb strongly at or near 280 nm. A_{260nm}/A_{230nm} ratio was also used as a second indicator of nucleic acid sample purity. A_{260nm}/A_{230nm} ratio of ~2.0 – 2.2 is accepted as *'pure'* RNA while lower ratios indicate sample contaminants that absorb near 230 nm. EDTA, carbohydrates (plant extractions) and phenol absorb near 230 nm while TRI Reagent (phenolic solution) absorbs at 230 nm and ~270 nm. RNA chemical contamination may result in concentration overestimation and/or affect downstream analysis. Only samples with a ratio above 1.5 were used for further analysis.

Total RNA/miRNA extracted, mean A_{260}/A_{280} and A_{260}/A_{230} purity ratios from PDE samples were low and inaccurately read using NanoDrop 2000c. NanoDrop 2000c uses

1-2 µl of sample to measure absorbance of UV-visible light to quantify nucleic acid concentration and has a usable range between 0.4 - 15,000 ng/µl. Sample pH and ionic strength changes cause Absorbance variation (Wilfinger et al, 1997). Further RNA quality and concentration assessment were performed using 1.5 µl of sample and Agilent 2100 Bioanalyzer in conjunction with RNA 6000 Pico assay which has a usable range between 50 – 5000 pg/µl. Samples were run by the Central Biotechnology Service (CBS) of Cardiff University. Although the ladder ran properly something interfered with the run of the PDE samples suggesting a cofounding factor in the lavage solution that was causing the effects (Figure 2.6). This possibility was reported and confirmed by Dr Krystyna Nahlik, genomics support scientist from Agilent Technologies. Dr Krystyna Nahlik indicated that Pico kit was very sensitive to increased salt concentration in the samples which can greatly reduce the overall signal. Therefore, it was not possible to accurately estimate RNA yield and purity using the above *mirVana PARIS* optimized protocol for PDE samples. Following the results obtained from this first study (Figure 4.1-3) the *mirVana* protocol was employed for further research.

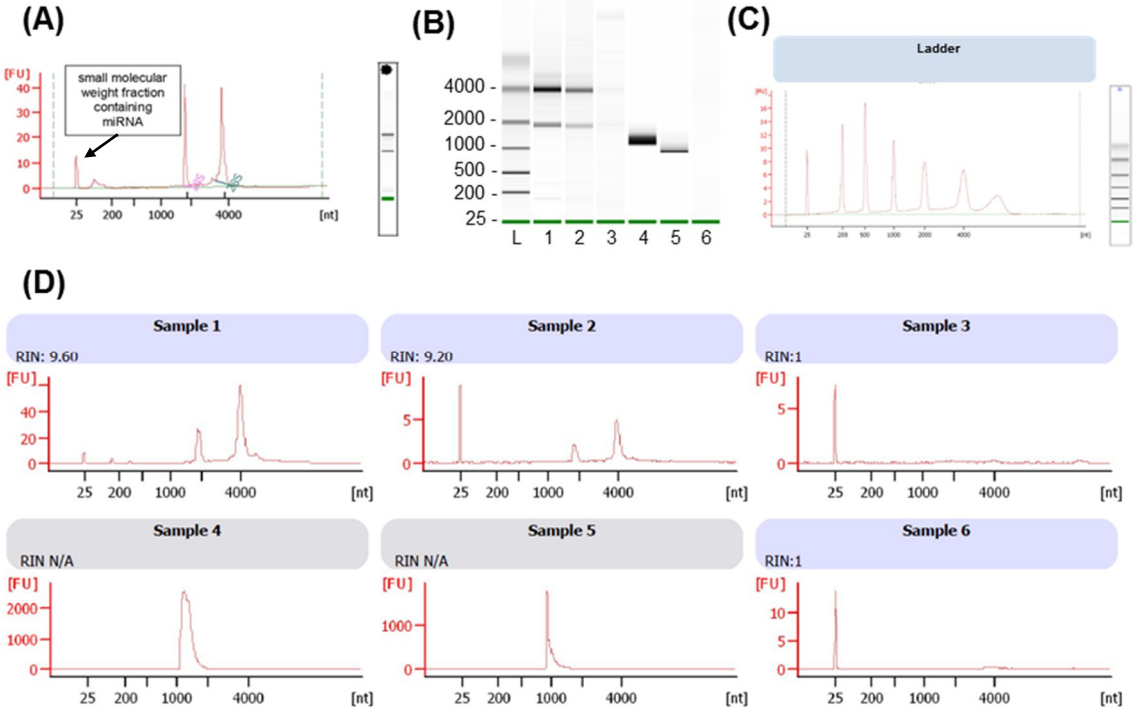

Figure 2.6. PD Effluent miRNA purity and quantification. (A) Example of total RNA sample analyzed by electropherogram and displaying miRNA and small RNAs region. **(B)** Capilar electrophoresis of six independent RNA extracted PDE samples. **(C)** Ladder. **(D)** RNA extracted PDE independent electropherograms (n=6).

2.3.2. miRNA detection

miRNAs can be detected by different methods including northern blot, solution hybridization and RT-PCR-based methods. RT-PCR-based methods are more sensitive, accurate, do not use radiolabeled reagents and can be quantitative, therefore, were chosen as a first option for this project.

miRNA size (~ 22 nt) does not allow common RT-PCR reaction used for mRNA. Two short RNA quantitative RT-PCR systems were described a decade ago based on stem-loop RT-qPCR (Applied Biosystems TaqMan miRNA assays; now Thermo Fisher Scientific) and polyadenylation-based RT-qPCR (Invitrogen NCode miRNA Detection System) (Chen et al, 2005; Shi & Chiang, 2005) (Figure 2.7). miRNA detection using stem-loop system (Thermo Fisher Scientific) involved two-steps quantitative reverse transcription – polymerase chain reaction (RT-qPCR) (Chen et al, 2005) (Figure 2.7A). RT step uses a miRNA specific RT primer that contains few nucleotides complementary to the mature miRNA 3' end and a long extra-sequence. This unrelated sequence forms a stem-loop structure that cannot interact with non-specific molecules in the RT reaction including pre- and pri-miRNA, increasing assay specificity. Assay PCR primers are identical to the mature miRNA 5' end and a sequence into the long stem-loop RT primer. TaqMan probes provide fluorescence signal needed for quantitative detection and bind between the miRNA and RT-primer. Thermo Fisher Scientific TaqMan miRNA assays are tested and amplification efficiency values range from 100% (±10%). Invitrogen NCode miRNA Detection System employs a polyadenylation reaction and a subsequent RT transcription of the resulting tailed miRNA (Shi & Chiang, 2005) (Figure 2.7B). Nevertheless, this system was previously analyzed at the department and showed poor sensitivity and reliability (Krupa, 2010). Of note, Thermo Fisher Scientific recently released TaqMan Advanced miRNA cDNA Synthesis Kit (Thermo Fisher Scientific, A28007) which provides a universal RT approach for all TaqMan Advanced miRNA Assays (Figure 2.7C). This new method uses 3' poly-A tailing and 5' ligation of an adaptor sequence to extend the miRNA prior RT while cDNA is universally amplified using miRNA specific primers. Nevertheless, TaqMan Advanced technology was not available when

this project started and miRNA detection using two-step stem-loop system (Thermo Fisher Scientific) was used during this thesis.

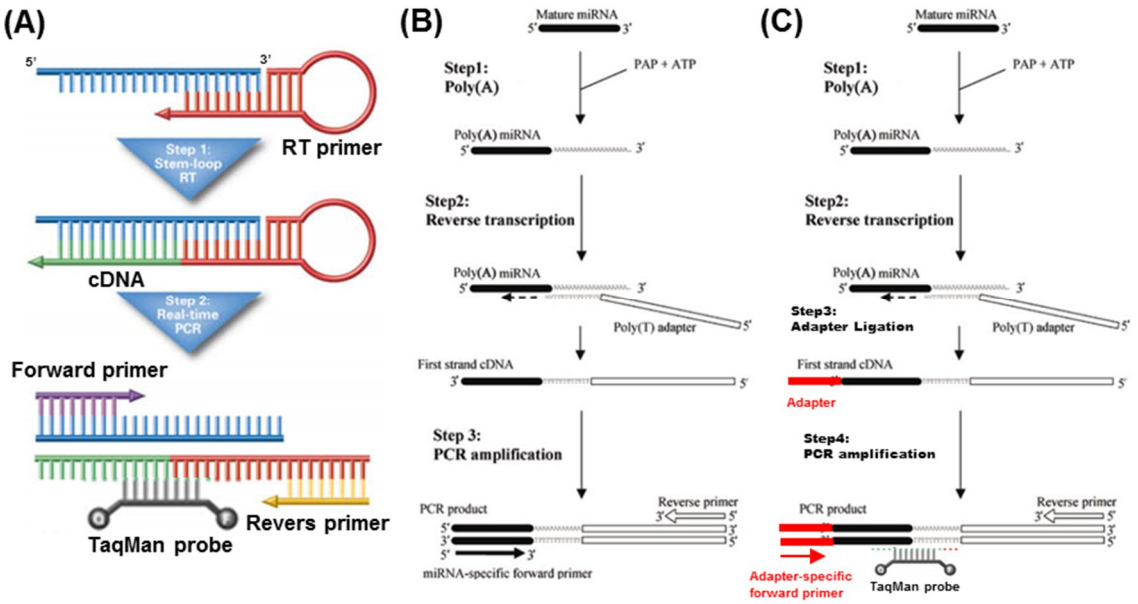

Figure 2.7. Schematic overview of RT-qPCR miRNA detection systems. (A) Stem-loop RT-qPCR miRNA detection system. miRNA quantification using this technology entails two consecutive steps. Firstly, RT reaction combines a long stem-loop specific miRNA primer containing few nucleotides complementary with a particular miRNA 3' end. Secondly, quantitative PCR with a specific miRNA forward primer, a reverse primer localized into the long stem-loop RT-primer sequence and TaqMan probes as a fluorescence source binding to the region between the two PCR primers (Chen *et al.* 2005). **(B)** Polyadenylation-based RT-qPCR miRNA detection system. miRNA quantification using this technology entails three consecutive steps. Firstly, total RNA is polyadenylated (poly(A)). Secondly, poly(A) miRNAs are RT using poly(T) adapter. Finally, quantitative PCR with a specific forward primer, reverse primer complementary to poly(T) adapter and SYBR green fluorescent DNA binding dye which binds all double - stranded DNA, is performed (Shi & Chiang 2005). **(C)** TaqMan advanced RT-qPCR miRNA detection system. miRNA quantification using this technology entails four consecutive steps. Firstly, total RNA is polyadenylated (poly(A)). Secondly, poly(A) miRNAs are RT using poly(T) adapter. Thirdly, oligonucleotide adapter is ligated to the miRNA 5' end. Finally, quantitative PCR with a specific adapter forward primer, reverse primer complementary to poly(T) adapter and TaqMan probes as a fluorescence source binding to the region between the two PCR primers.

2.3.2.1. Reverse Transcription

miRNA Reverse transcription (RT) was performed using the High-Capacity cDNA Reverse Transcription Kit (Thermo Fisher Scientific, Cat. No. 4372814). RT master mix contained: 4.25 µl water, 1.5 µl 10 x Reverse Transcription Buffer, 0.15 µl 100 mM dNTPs, 0.1 µl 40 U/µl RNase Inhibitor (New England BioLabs® Inc, Cat. No. M0307S), 1 µl 50 U/µl MultiScribe Reverse Transcriptase and 3 µl 5x miRNA RT-primer specific (Table 2.4). 10 µl of RT master mix were added to 5 µl of cell extracted RNA (10 ng) or 5µl of tissue isolated RNA. Alternatively, 5.75 µl of RT master mix lacking water was added to

9.25 µl of PDE extracted RNA. RT non-template control (RT-NTC) or negative control reaction contained an equal volume of water instead of diluted RNA. Thermal cycling conditions used were: 30 min at 16°C, 30 min at 42°C, 5 min at 85°C, followed by a cooling step at 4°C. Generated cDNA was diluted with water 1:3 prior use in qPCR reaction which will be detail in the next section (see 2.3.2.2.).

2.3.2.2. Quantitative Polymerase Chain Reaction

miRNA quantitative polymerase chain reaction (qPCR) was performed combining 1 µl of miRNA specific PCR primers and TaqMan probe (designed and supplied by Thermo Fisher Scientific, Table 2.4), 5 µl of water and 10 µl of Universal PCR Master Mix with No AmpErase UNG consisting of an optimized and thermostable solution of DNA polymerase, deoxynucleotides, and passive reference dye ROX (Thermo Fisher Scientific, Cat. No. 4440047). 16 µl of miRNA specific master mix and 4 µl of (1:3) diluted cDNA, diluted (RT-NTC) and water (qPCR-NTC) were added to wells into Optical 96-Well Fast Plate (Thermo Fisher Scientific, Cat. No. 4346906). MicroAmp Optical Adhesive Film (Thermo Fisher Scientific, Cat. No. 4311971) was used to seal the plate previous reaction performance on ViiA7 Real-Time PCR System (Thermo Fisher Scientific, Cat. No. 4453534) according to manufacturer's cycling parameter recommendations: 10 min at 95°C, 40 cycles of 15 secs at 95°C and 1 min at 60°C.

miRNA assay	Catalog Number
cel-miR-39	Part. Number 4427975 Assay ID 000200
has-miR-21-5p	Part Number 4440887 Assay ID 000397
hsa-miR-31-5p	Part Number 4440887 Assay ID 002279
hsa-miR-191-5p	Part Number 4440887 Assay ID 002299
mmu-miR-31-5p	Part Number 4427975 Assay ID 000185

Table 2.4. TaqMan RT-qPCR assays used in this study.

2.3.2.3. miRNA microarrays

Microarray assays were performed on HPMCs derived from four independent donors. miRNA expression was measured in control samples and after 1 ng/ml of TGF-β1 treatment for 48 h. TGF-β1-driven MMT was confirmed in all samples by analysis of the eight molecular markers previously described. RNA was extracted using TRI reagent with minimal changes to the manufacturer's recommendations (see 2.3.1.3.). A total of 1 µg in a volume of ≤2 µl of total RNA from each sample was subsequently used for *Toray* microarray analysis, performed by Central Biotechnology Services at Cardiff University as described previously (Jenkins et al, 2014).

RNA quality and concentration assessment were performed using 1 µl of sample (< 500 ng/µl) Agilent 2100 Bioanalyzer. A final 500 ng of total RNA from each sample was labeled with Cy5 using the Label IT miRNA labeling kit. 3D-Gene antisense-miRNA oligo chips were hybridized with the resulting labeled miRNAs. The chips were rigorously washed prior fluorescent signal scanner by ScanArray Lite Scanner and analyzed using GenePix Pro software (see 2.6.1.).

2.3.3. mRNA detection

mRNAs were measured in whole samples by two-step quantitative reverse transcription – polymerase chain reaction (RT-qPCR).

2.3.3.1. Reverse Transcription

mRNA Reverse transcription (RT) and consequent cDNA generation was performed using High-Capacity cDNA Reverse Transcription Kit (Thermo Fisher Scientific, Cat. No. 4372814). RT master mix contained: 4.1 µl nuclease-free water, 2 µl 10 x RT Buffer, 0.8 µl 100 mM dNTPs, 0.1 µl 40 U/µl RNase Inhibitor (New England BioLabs® Inc, Cat. No. M0307S), 1 µl 50 U/µl MultiScribe Reverse Transcriptase and 2 µl 10 x RT random primers. 10 µl of RT master mix were added to 10 µl of cell extracted RNA containing 1 µg of RNA. RT non-template control (RT-NTC) or negative control reaction contained an equal volume of water instead of diluted RNA. Thermal cycling conditions used were: 10 min at 25°C, 2 h at 37°C and 5 secs at 85°C, followed by a

cooling step at 4°C. Generated cDNA was diluted by adding 60 µl of water prior use in qPCR reaction which will be detail in the next section (see 2.3.3.2.).

2.3.3.2. Quantitative Polymerase Chain Reaction

mRNA quantitative polymerase chain reaction (qPCR) was performed combining 0.6 µl of mRNA specific PCR primers (300 nM, forward and reverse, Table 2.5), 10 µl of Power SYBR® Green PCR Master Mix (Thermo Fisher Scientific, Cat. No. 4367659) and 4.8 µl of water. 16 µl of mRNA specific master mix and 4 µl of diluted cDNA, diluted (RT-NTC) and water (qPCR-NTC) were added to wells into Optical 96-Well Fast Plate (Thermo Fisher Scientific, Cat. No. 4346906). MicroAmp Optical Adhesive Film (Thermo Fisher Scientific, Cat. No. 4311971) was used to seal the plate previous reaction performance on ViiA7 Real-Time PCR System (Thermo Fisher Scientific, Cat. No. 4453534) according to manufacturer's cycling parameter recommendations: 10 min at 95°C, 40 cycles of 15 secs at 95°C and 1 min at 60°C. Single PCR product amplification was confirmed by melting curve analysis.

Specific mRNA primers were designed using Primer-BLAST and NCBI sequence database, to amplify all known splice-variants. To elude genomic DNA amplification, primers were in different exons or bound to exon-exon junctions for design. PCR product length was, ideally, between 75 – 150 bp.

2.3.4. RT-qPCR data analysis

For qPCR data analaysis, Viia7 software and GraphPad Software version 6 were used. Relative expression was calculated using the $2^{-\Delta\Delta CT}$ method (Livak & Schmittgen, 2001). Threshold cycle (C_t), indicates the number of PCR cycles needed to detect fluorescence during specific PCR product amplification. Thus, 100% efficiency denotes double number of product copies with every PCR cycle. Single cycle difference ($\Delta C_t = 1$) between two samples indicates 2-fold change in gene expression between samples. Two cycles difference ($\Delta C_t = 2$) indicates 4-fold (2^2) change in gene expression, $\Delta C_t = 3$ indicates 8-fold (2^3) change, etcetera. miR-191 and GAPDH have been used here as endogenous housekeeping genes for data analysis. Other miRNAs and mRNA controls were evaluated including miR-16, 18S rRNA and U6 snRNA but showed poorer performance.

Symbol	Reverse and Forward Primers (5'-3')	Primer design
E-CADHERIN	F: TCCCAATACATCTCCCTTCACA R: ACCCACCTCTAAGGCCATCTTT	By T.Bodenham
ZO-1	F: GGAGAGGTGTTCCGTGTTGT R: GGCTAGCTGCTCAGCTCTGT	By D.D.Luo
OCCLUDIN	F: TAAATCCACGCCGGTTCCTGAAGT R: AGGTGTCTCAAAGTTACCACCGCT	Subramanyam et al., 2011
CLAUDIN-1	F: CGGGTTGCTTGCAATGTGC R: CCGGCGACAACATCGTGAC	Kaarteenaho et al., 2010
FIBRONECTIN	F: CCGAGGTTTTAACTGCGAGA R: TCACCCACTCGGTAAGTGTTC	By T.Bodenham
COLLAGEN1A1	F: CATGTTCAGCTTTGTGGACCTC R: TTGGTGGGATGTCTTCGTCT	By T.Bodenham
SNAIL	F: TTTACCTTCCAGCAGCCCTA R: GGACAGAGTCCCAGATGAGC	By D.D.Luo
α-SMA	F: AACTGGGACGACATGGAAA R: AGGGTGGGATGCTCTTCAG	By T.Bodenham
GAPDH	F: CCTCTGACTTCAACAGCGACAC R: TGTCATACCAGGAAATGAGCTTGA	By A.Krupa
NPPB	F: CTTTCCTGGGAGGTCGTTCC R: GTTGCGCTGCTCCTGTAAC	By M. Lopez-Anton
S100A10	F: TCGCTGGGGATAAAGGCTAC R: GCCAGAGGGTCTTTTTGATTTTCC	By M. Lopez-Anton
SASH1	F: CCTGGAAGTGGAGAAACCCG R: GCCAAGCGACTCTTCGATCT	By M. Lopez-Anton
TIMP3	F: TGCAACTTCGTGGAGAGGTG R: AGCAGGACTTGATCTTGCAGT	By M. Lopez-Anton
AIM1L	F: CAGACTGTGAGTAGAGGGAGC R: CAACCTGTCTGGAGGTGTCC	By M. Lopez-Anton
CASKIN1	F: GAGGGCAAGAGCTCTGAGG R: TGATGAAGTTGGGGGCGTAG	By M. Lopez-Anton
DUSP8	F: GAGCGAGGTCCAGCACCAT R: GGTGACCCCTGAAGTGAGGA	By M. Lopez-Anton
FGF18	F: GACGATGTGAGCCGTAAGCA R: GAGCTGGGCATACTTGTCCC	By M. Lopez-Anton
MATN2	F: CGGTGCAAGAAATGCACTGA R: CCAGTGACAAACTGCTTCACG	By M. Lopez-Anton
NELL2	F: GCACATGCCTGAATGGAACC R: AGTGGGCAGTCAGGATTTGG	By M. Lopez-Anton
RHOB	F: TTGCAACTGACTTGGGGAGG R: GACAGGCACAAAGTTCGCTT	By M. Lopez-Anton
PDCD4	F: TGGATTAACTGTGCCAACCA R: TCTCAAATGCCCTTTCATCC	By M. Lopez-Anton
SPRY1	F: AGATGCATGCCAGGTTTCCA R: TAACGAACTGCCACTGCCAT	By M. Lopez-Anton
PDZD2	F: CCTGGCATTGGGAGAAGTGT R: CATCCAGACTCAGTCCCAGC	By M. Lopez-Anton
LATS2	F: CAGATTCAGACCTCTCCCGT R: CTTAAAGGCGTATGGCGAGT	By M. Lopez-Anton
STK40	F: CCAGTGCCCTTGCCTCATAA R: AATCTCGGCTCAAAAGGGCA	By M. Lopez-Anton

Table 2.5. Quantitative PCR SYBER Green primers designed and used in this study.

Differences between sample starting RNA concentration, or subsequent process inaccuracies, were normalized to the expression of a non-experimentally influenced gene/miRNA called *endogenous* control. $2^{-\Delta\Delta CT}$ method, calculates sample specific C_t differences between *target* gene/miRNA and *endogenous* control ($\Delta C_t = C_t^{TARGET} - C_t^{ENDOGENOUS\ CONTROL}$). $2^{-\Delta\Delta CT}$ method expresses quantity relative to a selected base sample, called *calibrator*, (e.g. untreated control) in a way that *calibrator expression* = 1 and all other quantities are expressed as an n-fold difference relative to the *calibrator* ($\Delta\Delta C_t = . \Delta C_t - \Delta C_t^{CALIBRATOR}$). Final sample specific $2^{-\Delta\Delta CT}$ calculation proportionate target gene/miRNA expression that is endogenous control normalized and calibrator relative, called relative expression (RQ). Alternatively, 40-C_t was used when adequate.

2.4. Protein analysis

2.4.1. Western blot

Detection of already described miRNA targets by Western blot was used to evaluate miRNA manipulation of specific targets of study.

Cell lysis

Whole cell samples were collected using RIPA Lysis Buffer (Santa Cruz Biotechnology, sc-24988). Cells were previously washed 3 times with cold PBS. Immediately prior use 10 µl PMSF, 10 µl sodium orthovanadate and 10 µl protease inhibitor cocktail solution per 1X ml of RIPA Lysis Buffer, containing Tris-HCl, NP-40, Na-deoxycholate, SDS, NaCl, EDTA and NaF, were prepared and 200 µl/well of complete RIPA were added on experimental 6 well-plates. Cells were incubated on ice during 5 min and lysate was collected with a cell scraper help into an Eppendorf to centrifuge for 10 min and 16,000 *xg* at 4°C. Cell supernatant was collected, aliquoted and - 80°C stored until needed.

Bradford Assay protein quantification

BioRad Protein Assay (BioRad, 5000001) is based on the Bradford method and consists on a dye-binding assay in which a dye color changes in response to protein concentration (Bradford, 1976). Coomassie Brilliant Blue G-250 dye maximal absorbance

shifts from 465 nm to 595 nm when protein binding occurs. Standard Bovine Serum Albumin (BSA) curve was prepared by 2 - fold serial dilutions (1000 – 15.6 ng/µl range) and protein cell lysates were diluted 4 - fold. Bradford reagent 5x was diluted with water 1:5 and 200 µl/well were added into 96 well-plate wells containing 5 µl of BSA standards, samples or water (blank) in triplicate. Absorbance at 595 nm was measured after 5 min using a FLUOstar OPTIMS plate reader.

SDS-PAGE

Sodium dodecyl sulfate-polyacrylamide gel electrophoresis (SDS-PAGE) was performed by the method of Laemmli (Laemmli, 1970). Protein samples were thawed on ice and 15 µg or 30 µg of sample were mixed with 3x Reducing Loading Buffer (see Appendix) and heated at 95°C for five minutes. Samples were ice cooled and gel loaded for electrophoresis (Table 2.6). Additionally, 5 µl of ladder were loaded in one of the wells. Gel electrophoresis was performed using BioRad Mini Protein II devices, in Running Buffer (see Appendix), at 100 V for 20 min and 150 V for considered time.

Components	Resolving gel 7.5% (w/v)	Stacking gel
Water	7.275 ml	6.1
Buffer	1.5 M Tris-HCl pH 8.8 3.75 ml	0.5 M Tris-HCl pH 6.8 2.5 ml
10% (w/v) SDS	150 µl	100 µl
Acrylamide 29.2% (w/v)/ Bisacrylamide 0.8% (w/v)	3.75 ml	1.3 ml
10% Ammonium Persulphate (0.05 g in 500 µl water)	75 µl	75 µl
TEMED	7.5 µl	10 µl

Table 2.6. Sodium dodecyl sulfate-polyacrylamide gels for electrophoresis (SDS-PAGE)

Protein transfer to nitrocellulose membrane

Nitrocellulose membrane (GE Healthcare, Life Sciences) transfer of gel electrophoresis separated proteins was performed using BioRad Mini Blot II devices. Membrane, filter paper and pads were pre-soaked in cold Transfer Buffer (see Appendix). Transfer cassette was assembled following the negative charge by a pad, paper, gel, membrane, two papers, pad and positive charge. The cassette was installed into the holder and the device was filled with pre-chilled Transfer buffer, an ice pack and stirring bar. Transfer was performed for 1 hour at 100 V.

Antibodies Incubation

Nitrocellulose membrane was blocked to prevent non-specific antibody binding for 1 hour with 5 % BSA (w/v) in Phosphate-Buffered Saline (PBS) solution containing 0.1 % (v/v) Tween-20. Membrane was washed with 0.5 % (v/v) Tween-20 in PBS for 10 min and subsequently incubated overnight at 4°C with primary antibodies in PBS with 0.1 % (w/v) BSA and 0.1 % (v/v) Tween-20. Membranes were washed 3x with 0.5 % (v/v) Tween-20 in PBS for 10 min each and subsequently incubated overnight at 4°C with appropriated secondary antibody. Primary and secondary antibodies were PDCD4 (1:1000; #9535 D29C6; Cell Signalling Technology), GAPDH (1:2000; ab9885; Abcam), goat anti-rabbit IgG-HRP (1:10000; sc-2004; Santa Cruz Biotechnology) and goat anti-mouse IgG-HRP (1:10000; sc-2005; Santa Cruz Biotechnology. Following, secondary antibody incubation membrane was washed with 0.5 % (v/v) Tween-20 in PBS for 10 min, excess of solution was removed while keeping the membrane wheat and ladder was underlined using a (WesternSure™ Pen, LI-COR) pen. Membrane was homogenously sprayed using WesternBright ECL Spray (Advansta, K-12049-D50) and incubated at room temperature for 1 min, protein detected images were captured *via* C-DiGit Chemiluminescent Western Blot Scanner and densitometry analysis was conducted using Image Studio Version 5.2 Software.

Membrane stripping and re-probing

Membrane stripping was performed by incubation in Stripping Buffer (Re-Blot™ Plus-Strong, Merck Millipore), at room temperature for 30 min. Subsequently, membranes were washed 3x with 0.5 % (v/v) Tween-20 in PBS for 10 min each and process adequacy was confirmed by lack of membrane signal after HRP substrate incubation. Membranes were then washed and re-probed as described previously.

2.4.2. Immunohistochemistry

Immunohistochemical staining of peritoneal membrane study samples was performed on 5 µm sections mounted on glass slides as previously described (Heller et al, 2007). After deparaffinization and rehydration the sections were incubated in 3% hydrogen peroxide to block endogenous peroxidases. Heat-induced antigen retrieval was performed in a microwave oven, using 0.005 M citrate buffer (pH 6). Polyclonal rabbit anti p-SMAD2/3 (Santa Cruz; sc-11769) was incubated for 1 h at room temperature (1:100). Monoclonal rabbit anti PDCD4 (Cell signalling, D29C6) was incubated overnight at 4°C (1:200). Incubation with biotinylated secondary reagents (Vector) for 30 min was followed addition of ABC reagent (Vector) and detection carried out using 3'-Diaminobenzidine (DAB, Sigma, Taufkirchen, Germany). Cell nuclei were counterstained with hematoxylin. Isotype control antibody in PBS was used as a negative control.

Aperio Analysis

Immunohistochemical images were captured and evaluated using Aperio Precision Image Analysis Software (USA). The Positive Pixel Count Algorithm (version 9) output was used to calculate total p-SMAD2/3 and PDCD4 staining. The algorithm quantifies the positive pixels in a scanned virtual slide. Input algorithm parameters are specific color ranges in the HSI colorspace (Hue value 0.1; Hue width 0.5) and intensity ranges to differentiate between weak, medium, strong and negative staining. Intensity thresholds (upper/lower limit): weak 220/175, medium (175/100), strong (100/0) and negative (255/220). Thresholds were optimized and validated specifically for p-SMAD2/3 and PDCD4. Positivity was calculated as total number of positive pixels divided by total number of pixels: $(N_{total}-N_n)/(N_{total})$.

2.4.3. Luciferase activity

Firefly (*Photinus pyralis*) luciferase coding DNA sequence (CDS) was used for all reporter plasmids created in this study and was routinely co-transfected with a control plasmid coding for *Renilla* (*Renilla reniformis*) luciferase. Firefly and Renilla luciferases have different origin, structures and substrate requirements allowing bioluminescent

reaction discrimination. Dual-Luciferase Reporter Assay System (Promega, E1910), both luciferase activities can be measured sequentially in a single sample.

Briefly, transfected cells were washed 3x with PBS and 50 µl of Passive Lysis Buffer (1:5 diluted in water) was added per well (48 well-plate). Experimental cells were incubated with gentle rocking during 15 min at room temperature and cell lysates were subsequently transferred to Eppendorfs. 20 µl of aliquoted sample was transferred into white 96-well-plate wells and 50 µl of Luciferase Assay Reagent II (firefly luciferase substrate) was added prior luminescence measurement on FLUOstar OPTIMA plate reader. 50 µl of Stop & Glo Reagent (*Renilla* luciferase substrate and previous reaction quencher) were added to 96-well-plate wells prior *Renilla* luminescence measurement. Untransfected cell lysates were used to determine background. Results express relative ratio of experimental firefly vector to control *Renilla* vector luciferase activity introduced in HeLa and HPMCs.

2.5. Bioinformatics

2.5.1. microRNA target prediction

miRNA target prediction programs are routinely used to find miRNAs that may regulate genes of interest and/or to identify possible targets of specific miRNAs. Diana (Paraskevopoulou et al, 2013; Reczko et al, 2012), miRanda - mirSVR (Betel et al, 2010; Betel et al, 2008), miRDB (Wang & El Naqa, 2008; Wong & Wang, 2015) and TargetScan (Agarwal et al, 2015; Nam et al, 2014) are between the algorithms most commonly used for predictions and were chosen to identify possible new targets of the miRNAs of interest. An actualized summary Table 2.7 based on Peterson et *al.* 2014 is displayed below to compare these tools (Agarwal et al, 2015; Peterson et al, 2014; Wong & Wang, 2015). The threshold used for each one of these algorithms and comparison on Figure 5.6 was Diana = 0.7, miRanda – mirSVR = - 0.95, miRDB = all targets and TargetScan = -0.24. The use of these tools as well as their quality and reliability will be further discussed in Chapters 5 and 6.

Tool Name	Seed match	Cons.	Free energy	Site access.	Target-site abundance	Machine learning	References
Diana	X	X	X	X	X	X	(Paraskevopoulou et al, 2013; Reczko et al, 2012)
miRanda-mirSVR	X	X	X	X		X	(Betel et al, 2010; Betel et al, 2008)
miRBD	X	X	X	X	No*	X	(Wang & El Naqa, 2008; Wong & Wang, 2015)
TargetScan	X	X	X*	X*	X*	No*	(Agarwal et al, 2015; Nam et al, 2014)

Table 2.7. Summary of in silico miRNA target prediction methods used for this study. Acess. (accessibility), Cons (Conservation). Table displayed is based on Peterson et *al.* 2014 summary table and *actualized with references that were not available for Petersons et *al*. 2014 review.

2.5.2. miRNA conservation and mRNA – miRNA hybrid prediction

mRNA 3'UTR target site conservation for identified genes of interest was analyzed across different animals including human, chimpanzee, rhesus, rabbit, mouse, rat, cow, horse, dog and elephant. Target sequences were acquired using TargetScan and alignment was performed with mega 6. mRNA-miRNA hybrid was predicted using Diana v5.0 (Paraskevopoulou et al, 2013; Reczko et al, 2012).

2.6. Statistical analysis

Differences between two individual experimental groups of normally distributed values were compared by matched or non-matched two-tailed *t* test. In the case of multiple comparisons, one- or two-way analysis of variance (ANOVA) followed by post hoc Holm-Sidak's test was used.

For the clinical data, Pearson's correlations were used for normally distributed variables, transformed as necessary, and Spearman's for other variables, with no correction for multiple testing in an exploratory analysis. Multivariable linear regression with backwards stepwise variable selection was used for natural log transformed miR-21 and square root transformed miR-31 variables, and to avoid problems with suppressor effects dialysate cytokine values were entered as a block.

2.6.1. miRNA microarrays

GenePix Pro software considers a valid spot any probe hybridization which signal intensity is greater than the mean intensity of the background signal plus 2 standard deviations. A normalization step for each specific miRNA adjusted median value is subsequently performed. This will identify and remove sources of systematic variation within arrays correcting for spatial and dye bias. The relative miRNAs expression level is determined by comparing the mean signal intensity of the real hybridizated spots with their average value across the microarray experiment. To reliably compare data from multiple chips a quantile-normalization was applied to the values. This last normalization minimizes non-biological differences between arrays giving to disparate datasets the same histogram distribution by transforming the quantiles to obtain the same value.

Chapter 3 – Identification of miRNAs involved in Peritoneal Mesothelial MMT

3.1 Introduction

PD therapy leads to a complex microenvironment that drives peritoneal membrane damage *via* altered expression of a broad spectrum of cytokines and factors. TGF-β1 is a pro-fibrotic cytokine, the up-regulation of which has been associated with poor PD results, and is assumed to be a key molecule in peritoneal deterioration (Gangji et al, 2009; Lai et al, 2000; Yao et al, 2008). The importance of TGF-β1 in peritoneal decline has also been indicated by (i) rodent studies (Margetts et al, 2005; Margetts et al, 2001; Patel et al, 2010a), (ii) overexpression of TGF-β1 antagonist molecules including Smad7 and BMP-7 (Guo et al, 2007; Loureiro et al, 2010; Nie et al, 2007; Yu et al, 2009), and (iii) TGF-β1-blockade *via* synthetic peptides (Loureiro et al, 2011). TGF-β1 is a well characterized molecule triggering EMT in different tissues and organs (Gui et al, 2012; Xu et al, 2009), and an essential molecule for mesothelial cell MMT conversion during PD treatment (Aguilera et al, 2005; Loureiro et al, 2011; Yang et al, 2003; Zhu et al, 2010). TGF-β1-driven phenotypic change in primary mesothelial cells was, therefore, the primary model chosen to study mechanisms of peritoneal MMT progression associated with PD therapy (Selgas et al, 2006), although this model was also supplemented in subsequent experiments by additional *in vitro*, *ex vivo* and *in vivo* approaches.

Limited research has studied miRNAs implications in the regulation of key molecular pathways driving peritoneal membrane alterations leading to PD failure (see 1.6.3). *In vitro* models, although more simplistic, may be critical to understand the specific pattern of miRNA expression in response to a known stimulus in a specific cell type where mechanistic research can be pursued. The study of miRNA profile associated to TGF-β1-driven MMT process in mesothelial cells was found to suit this research in four ways. miRNAs are (i) variable, (ii) specific, (iii) highly stable, and (iv) regulate gene expression. On the other hand *in vitro* mesothelial cells TGF-β1-driven MMT model is (i) simple, unique stimulus; and (ii) cell specific. miRNA characteristics (i) and (ii) associated to the models of study would be developed during this chapter while (iii) and (iv) would be further deepened and characterized in Chapters 4 and 5 respectively.

Consequently, the research pursued in this chapter (i) characterized mesothelial miRNA profile and responses to TGF-β1 *in vitro*, which identified miR-21 and miR-31 for further study, (ii) found increased miR-21 and miR-31 in mesothelial cells and supernatant after treatment with different PD fluids *in vitro*, (iii) identified miR-21 and miR-31 up-regulation in PD effluent (PDE) derived mesothelial cells exhibiting a mesenchymal phenotype when cultured *ex-vivo*, (iv) determined elevated miR-21 and miR-31 expression in peritoneal membrane biopsies from PD patients, (v) evaluated peritoneal membrane thickness and miRNA pattern of expression in an uraemic PD mouse model, and (vi) assessed miRNA miR-21 and miR-31 expression in supernatant from TGF-β1-treated mesothelial cells.

3.2. Results

3.2.1. TGF-β1 induces Phenotypic Changes in Human Peritoneal Mesothelial Cells *in vitro*

Before profiling mesothelial miRNA expression, a careful characterization of *in vitro* mesothelial-to-mesenchymal transition (MMT) was performed using primary cultures of mesothelial cells with replicate experimental cells from different omental donors. Converting a mesothelial cell to a mesenchymal cell is a complicated and organized series of processes that entails cellular structural and functional changes, including a deep molecular rearrangement and distinct changes in gene expression regulation. The MMT process begins with the detachment of inter-mesothelial adhesions and the down-regulation of adhesion molecules including E-cadherin, ZO-1, Claudins and Occludins. Here, TGF-β1 down-regulated mRNA expression of epithelial markers E-cadherin, ZO-1, Occludin and Claudin-1 at 48 h (Figure 3.1A). This effect was TGF-β1-concentration dependent and showed a threshold for statistical significance at 1 ng/ml for all the markers of study (Figure 3.1A).

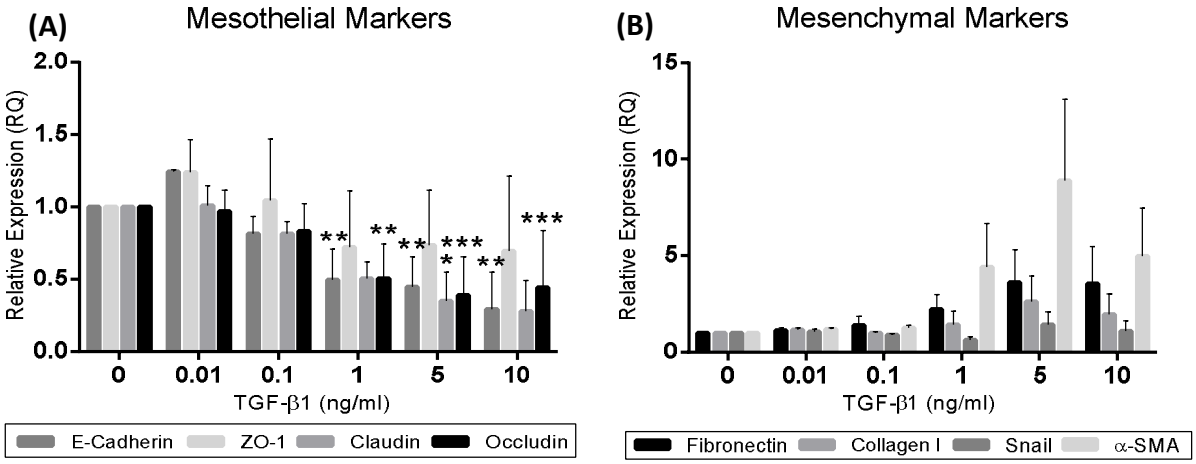

Figure 3.1. TGF-β1 represses epithelial and induces mesenchymal markers in mesothelial cells in a concentration dependent fashion. Omentum-derived mesothelial cells were treated with TGF-β1 at the indicated concentrations during 48 h. **(A)** Epithelial markers: E-Cadherin, ZO-1, Occludin and Claudin-1. **(B)** Mesenchymal markers: Fibronectin, Collagen I, Snail and α-SMA. mRNA expression of all markers was analyzed by RT-qPCR and normalized to GAPDH mRNA expression. Data were analyzed by one-way ANOVA for matched samples followed by post-hoc Holm-Sidak's test comparing each concentration mean with the control mean. Data represent the mean S.E.M. from three independent donor experiments. *p < 0.05; **p < 0.01; ***p < 0.005.

Snail1 is a key early transcription factor up-regulated during peritoneal TGF-β1-mediated MMT and known to repress E-cadherin expression. Consequently, mesothelial cells lose their apical-basal polarity and assume a front-back organization *via* cytoskeleton rearrangement, α-SMA expression acquisition and enhanced migratory capabilities. Ultimately, cells develop the ability to degrade the basal membrane up-regulating matrix metalloproteinases (MMPs) expression and invading the submesothelial compartment. Throughout the course of the MMT, mesothelial cells acquire greater competences to synthesize extracellular matrix (ECM) components including Fibronectin and Collagen I (Aroeira et al, 2005). Here, TGF-β1 up-regulated mRNA expression of mesenchymal markers Fibronectin, Collagen I, and α-SMA at 48 h (Figure 3.1B). Nevertheless, only α-SMA transcript showed a threshold for statistical significance at 1 ng/ml and Snail mRNA expression did not vary in mesothelial cells incubated with different doses of TGF-β1 after 48 h of treatment (Figure 3.1B).

Loss of epithelial morphology and acquisition of fibroblast-like form was evident when mesothelial cells were incubated with 5 and 10 ng/ml of TGF-β1 after 48 h of treatment (Figure 3.2). Nevertheless, most of the mesothelial and mesenchymal markers studied showed a threshold for statistical significance at 1 ng/ml. Importantly,

MMT reversibility has been shown to be feasible during, at least, the initial-phases of the process. Consequently, the identification of early MMT stages in PD patients together with the determination of molecules that revert MMT promoting mesenchymal-to-mesothelial transition (rMMT) must be a priority in the PD field. Along these lines, this research focused in key early changes during mesothelial cells conversion that would lead the MMT process associated to the treatment. The minimum concentration of TGF-β1 able to induce MCs molecular expression reprogramming was, consequently, chosen for subsequent time-course characterization.

Time-course experiments were then carried out to investigate temporal variation downstream TGF-β1 gene regulation. Down-regulation of epithelial mRNA markers was observed from 48 h onwards (Figure 3.1A; Figure 3.3, A-D). The mRNA expression of epithelial markers ZO-1, Claudin and Occludin was affected by cell confluence and was most evident after 72 h of treatment (Figure 3.3, A-D). By contrast, Fibronectin, α-SMA and Collagen I mesenchymal transcript markers were induced by 12-24 h, with Snail mRNA expression peaking at 2 h (Figure 3.3, E-H). Snail has been described to be involved in the alterations of intercellular adhesion during the MMT process, and its early activity here may contribute to the latter changes observed in epithelial markers (Figure 3.1A).

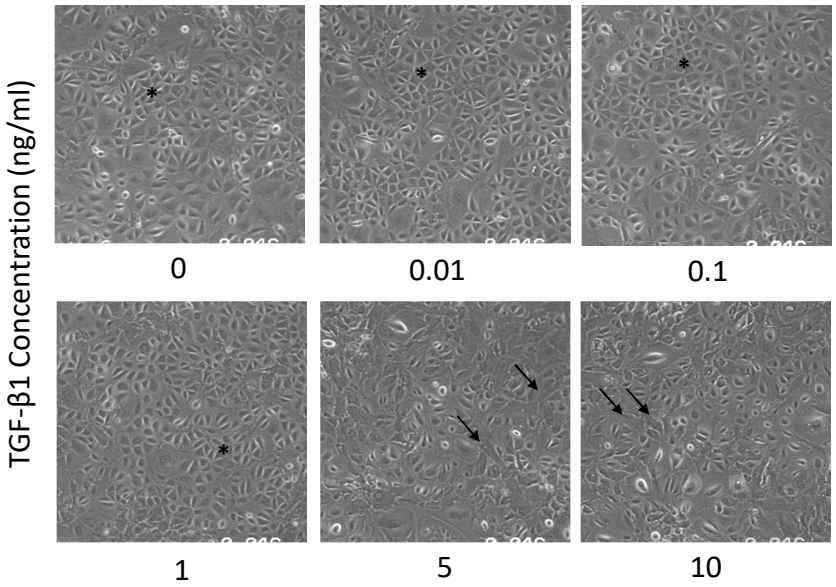

Figure 3.2. Phenotypic time-course changes of HPMCs in culture after TGF-β1 treatment. Omentum-derived mesothelial cells were treated with 0, 0.01, 0.1, 1, 5 and 10 ng/ml of TGF-β1 during 48 h. (0-1 ng/ml of TGF-β1) Characteristic epithelial morphology of polygonal shape cells from a confluent monolayer, star indicated. (5 and 10 ng/ml of TGF-β1) Loss of epithelial morphology and acquisition of fibroblast-like form, arrow indicated. One representative experiment of three is shown. Zeiss Axiovert 135 microscope. Magnification: 200x.

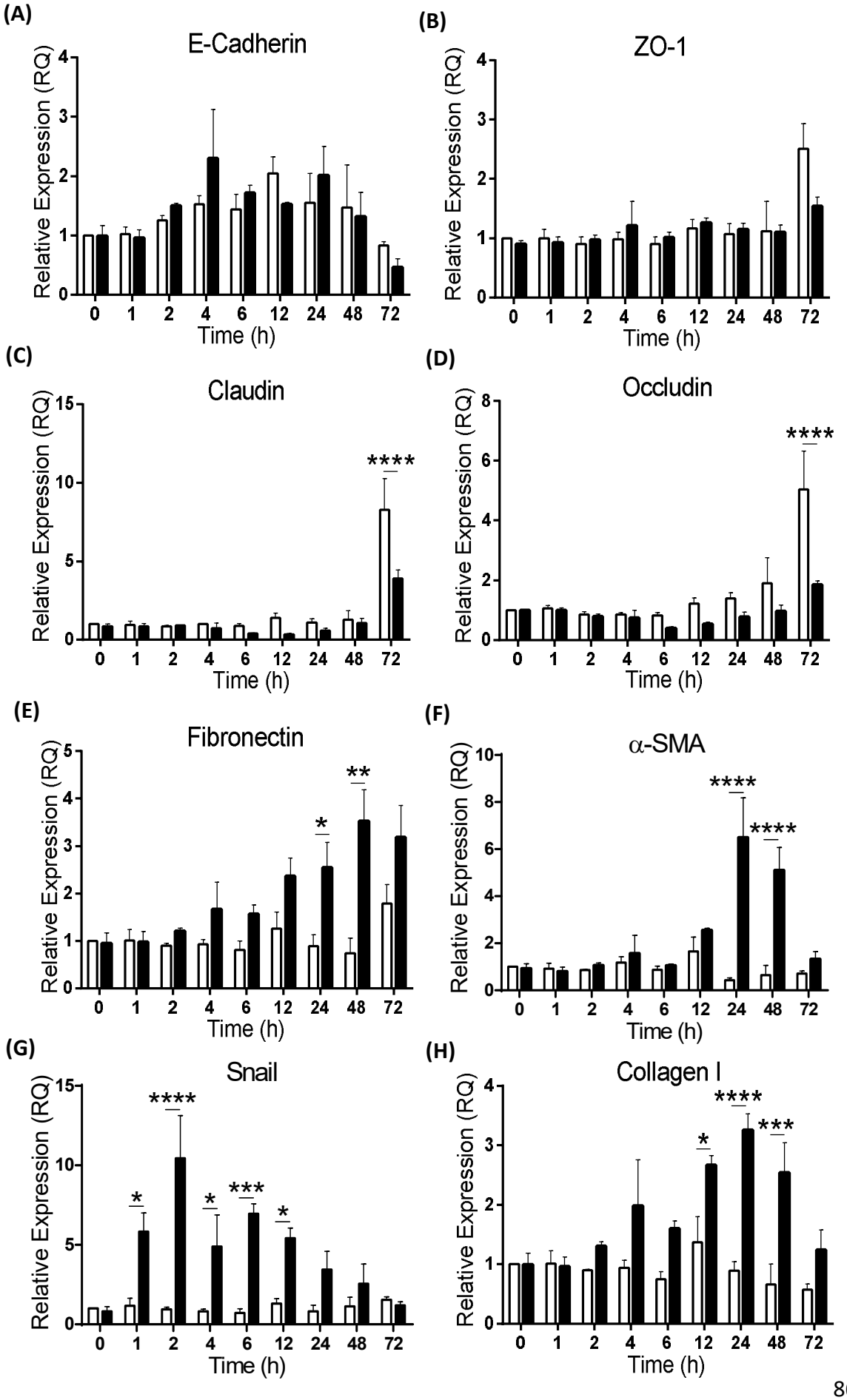
(A)
E-Cadherin
Relative Expression (RQ)
Time (h)
(B)
ZO-1
(C)
Claudin
(D)
Occludin
(E)
Fibronectin
(F)
α-SMA
(G)
Snail
(H)
Collagen I
0 1 2 4 6 12 24 48 72

Figure 3.3. TGF-β1 represses epithelial and induces mesenchymal markers in mesothelial cells in a time dependent fashion. Omentum-derived mesothelial cells were treated with TGF-β1 at the indicated times. Control - white bars, TGF-β1 (1ng/ml) - black bars. **(A)** E-Cadherin. **(B)** ZO-1. **(C)** Occludin 1. **(D)** Claudin-1. **(E)** Fibronectin. **(F)** Collagen I. **(G)** Snail. **(H)** α-SMA. mRNA expression of all markers was analyzed by RT-qPCR and normalized to GAPDH mRNA expression. Data were analyzed by two-way ANOVA for matched samples by both factors followed by post-hoc Holm-Sidak's test between treatments at each time point. Data represent the mean S.E.M. from three independent donor experiments. *p < 0.05; **p < 0.01; ***p < 0.005; ****p < 0.001. (See above page)

Phenotypic changes were not seen before 24 h. Fibroblast-like architecture was visible around 48 h, and these changes were most evident after 72 h (Figure 3.4). In summary, these results demonstrated that in primary HPMCs from multiple donors, 1 ng/ml of TGF-β1 induced changes consistent with an MMT process after 48 h. This study was consequently focused in early key changes in miRNA expression during mesothelial cells conversion that would lead the MMT process associated to the treatment.

3.2.2. Mesothelial miRNA profile is altered by TGF-β1

To elucidate the influence of TGF-β1 treatment on mesothelial cells miRNA expression profiles, cells isolated from four different donors incubated with TGF-β1, 1 ng/ml for 48 h and control non-treated cells were compared. Global miRNA expression was quantified by hybridization array. Independent biological replicates displayed high consistency (Figure 3.5B). A total of 699 miRNAs were detected in at least three samples and were included in subsequent analysis.

miRNAs were analyzed on the basis of baseline level of expression, fold change in response to TGF-β1, and statistical significance of the observed change (Figure 3.5A). 95 of 699 miRNAs were differentially regulated by a fold change greater than 1.5 x. Of these, miR-21 and miR-31 were among the most highly expressed in HPMCs, and were induced by TGF-β1 treatment (Figure 3.5A). Additional miRNAs previously associated with peritoneal membrane transport change and fibrosis were detected at low signal intensity in this profile and did not change significantly in response to TGF-β1 (includes miRs -15a, -17, -30, -192, -377, -589). Therefore, subsequent analysis focused on miR-21 and miR-31.

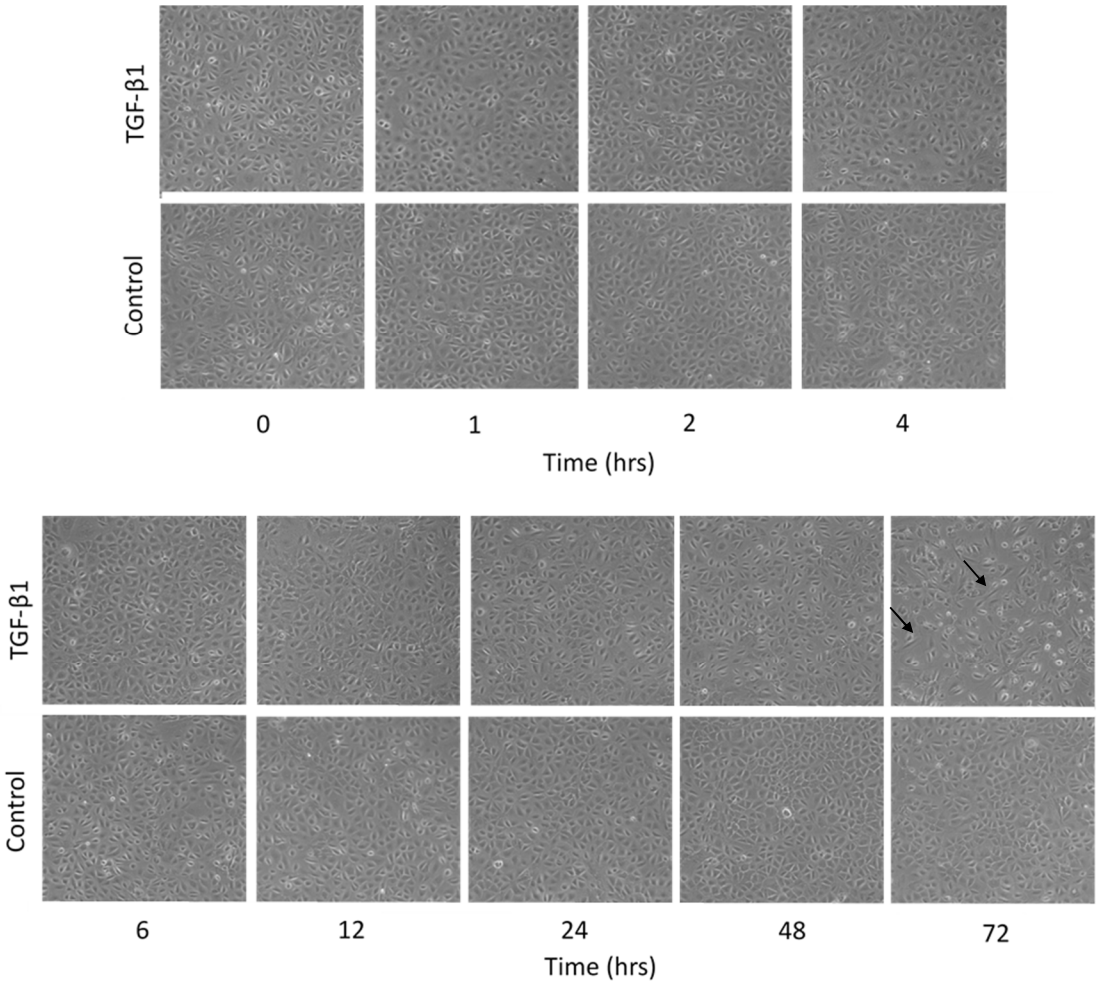

Figure 3.4. Phenotypic time-course changes of HPMCs in culture after TGF-β1 treatment. Omentum-derived mesothelial cells were treated for 0, 1, 2, 4, 6, 12, 24, 48 and 72 h with TGF-β1 (1 ng/ml). (0-24 h) Characteristic epithelial morphology of polygonal shape cells from a confluent monolayer. (48 h) Loss of epithelial morphology and acquisition of fibroblast-like form. (72 h) Loss of epithelial morphology and acquisition of fibroblast-like phenotype with disruption of intercellular junctions characteristic of a migratory phenotype. One representative experiment of three is shown. Zeiss Axiovert 135 microscope. Magnification: 200x.

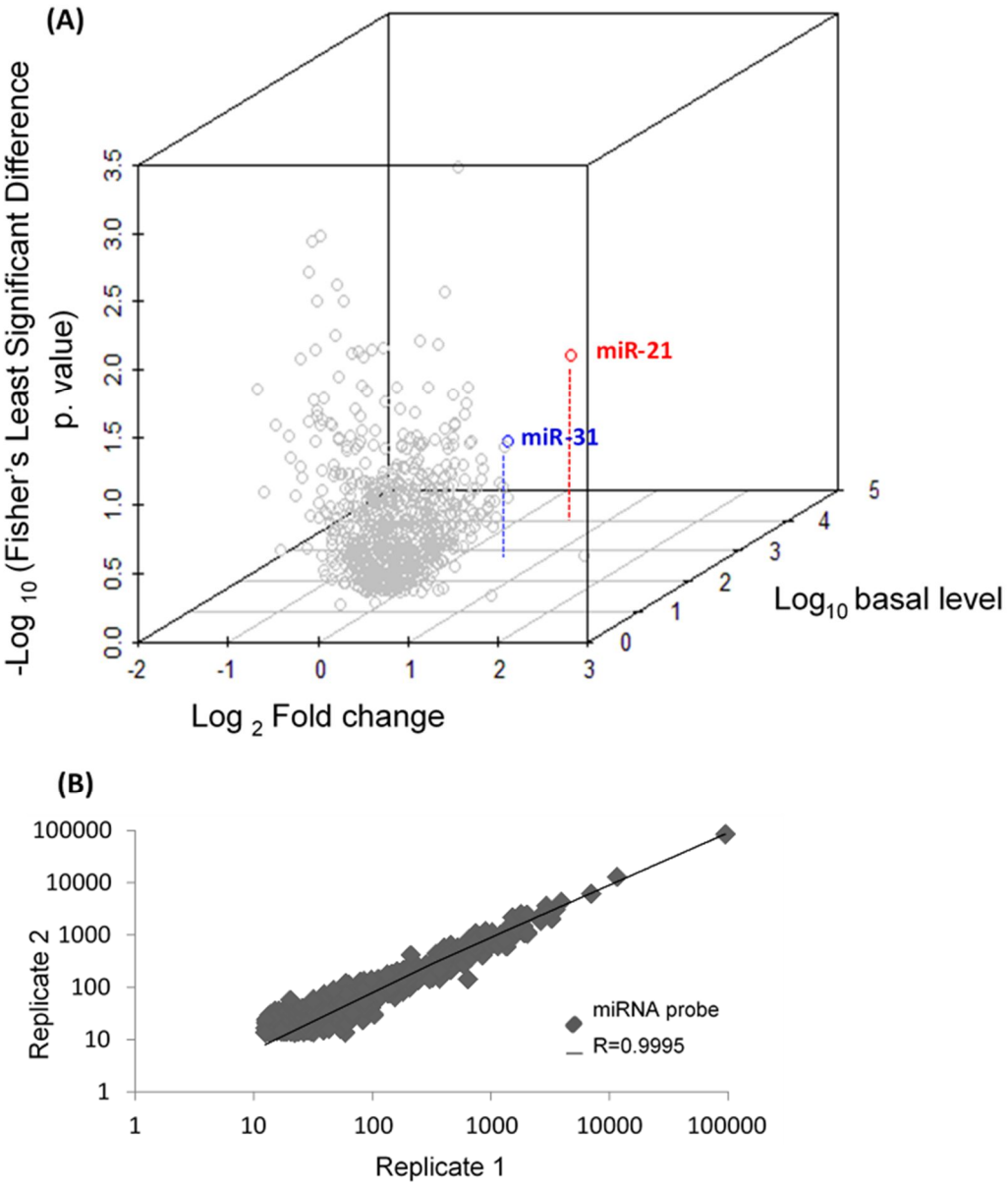

Figure 3.5. miRNA profiling in TGF-β1-stimulated HPMCs. (A) Three-dimensional scatter plot of miRNA expression following 1ng/ml of TGF-β1-treatment for 48 h (x axis: $\log_2$ fold change of the normalized miRNA signal (mean of at least three replicates); y axis: $-\log_{10}$ p value obtained from one-way ANOVA followed by Fisher's least significant difference (LSD) post hoc analysis; z axis: $\log_{10}$ of the level of baseline expression in mesothelial cells). miR-21 (red), miR-31 (blue). **(B)** Scatterplot of 2 technical replicates showing correlation for all miRNA probes.

Up-regulation of miR-21 and miR-31 in primary HPMCs was then validated using miRNA-specific Taqman RT-qPCR assays (fold change: miR-21, 1.8 x, p=0.012; miR-31, 1.7 x, p=0.004) (Figure 3.6A). Induction of expression of these miRNAs was further confirmed by TGF-β1 dose-response analysis (Figure 3.6, B-C).

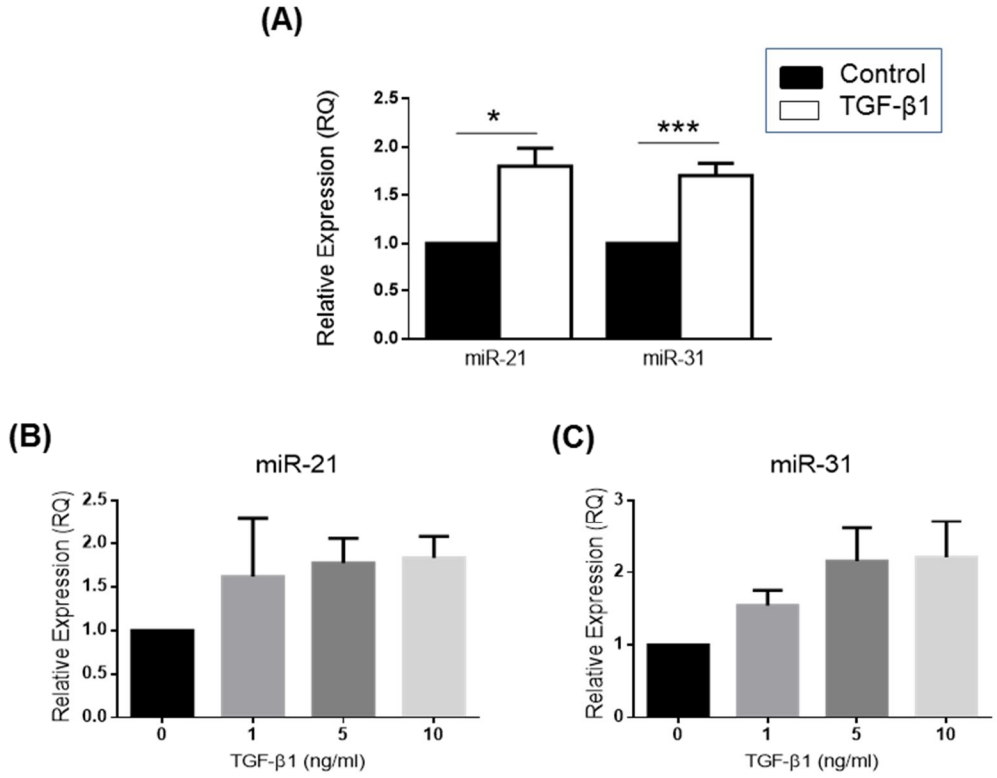

Figure 3.6. TGF-β1 significantly induces miR-21 and miR-31 expression in HPMCs after 48 hours of treatment. Omentum-derived mesothelial cells were treated with 1 ng/ml of TGF-β1 **(A)** or 0, 1, 5 and 10 ng/ml of TGF-β1 **(B-C)** for 48h. Expression of miR-21 and miR-31 was analyzed by RT-qPCR and normalized to miR-191 expression. Data were analyzed by paired, two tail, *t* test or one-way ANOVA for matched samples followed by post-hoc Holm-Sidak's test comparing each condition mean with the control omentum-derived mean. Data represent the mean S.E.M. from five **(A)** or three **(B-C)** independent donor experiments. *$p < 0.05$; ***$p < 0.005$.

3.2.3. PDF-treated MCs display morphological changes and supernatant miRNA release

Previous research has linked HPMCs exposure to different PD fluid compounds with mesothelial cells MMT, sterile peritoneal inflammation and peritoneal membrane mesothelial cell loss. Therefore, whether HPMCs treated with different PD fluids could alter their phenotype and, most importantly, up-regulate the miRNAs of study at both, cellular and supernatant levels was analyzed.

The characteristics of the PD solutions used for this study are summarized in Table 3.1. After treatment optimization (see 2.2.2.) HPMCs where incubated with 50% PDF in 1% FBS medium or control HPMCs medium for 48 h. Loss of epithelial MCs monolayer and different extent of morphological changes and acquisition of fibroblast-like phenotype was observed when control and PBS conditions where compared with glucose 2.3% and different PD fluid conditions (Figure 3.7A). Due to the high number of different conditions compared and the variability between donors significant differences in miRNA expression at cellular or supernatant level could not be identified (Figure 3.8). Nevertheless, miR-21 showed a trend to increase with PDF treatment and PBS dilution at cellular level while being differentially released into the supernatant only with PDF exposure (Figure 3.8, A-B). On the other hand, miR-31 showed a trend to increase with PDF treatment at both cellular and supernatant level (Figure 3.8, C-D). The PDF inducing the highest miR-21 release to the supernatant were BicaVera 2.3% = 2.818 (-3.331 to 8.968), Physioneal 2.27% = 2.514 (-2.368 to 7.396), Balance = 1.632 (0.2114 to 3.053) and Nutrinil = 1.584 (-1.123 to 4.290) while for miR-31 these were BicaVera 1.5% = 2.299 (-1.812 to 6.409), Physioneal 2.27% = 1.935 (-0.1909 to 4.060), Extraneal = 1.673 (-0.348 to 3.695) and Nutrinil = 1.597 (-0.268 to 3.462) (95% confidence interval). Three of the four PD solutions that induced higher miR-21 release to the supernatant contain also the highest glucose percentages (BicaVera 2.3%, Physioneal 2.27% and Balance 2.3%); nevertheless CAPD4 also holds 2.3% of glucose and was between the fluids that less induced miR-21. Surprisingly, three of the four PD solutions that better increased miR-21 also own the higher pH (BicaVera 7.4, Physioneal 7.4 and Balance 7.0) while no trend was detected between the buffer of use and higher miR-21 release in

HPMCs. No pattern was found between miR-31 up-regulation in MCs supernatant and PD fluid composition. In common, PD fluid exposure resulted in a decrease in cell viability to a higher extent than medium dilution and/or glucose 2.3% incubation (Figure 8E). Higher levels of compromised cell viability were found with Extraneal = 49.98% (9.226% to 90.74%), Physioneal 2.27% = 59.62% (31.05% to 88.18%), Nutrineal = 63.85% (37.30% to 90.40%) and BicaVera 2.3% = 64.92% (44.42% to 85.42%) (95% confidence interval). Three of the four PD solutions that induced lower cell viability also showed higher miR-21 and miR-31 levels at the supernatant but no trend was detected within viability and PD solution composition. These results demonstrate that HPMCs treated with PDF can differentially release miRNAs to the supernatant and encouraged the study of further models of peritoneal membrane deterioration and MMT associated to PD therapy.

The characteristics	pH	Chambers	Osmotic agent	Buffer	GDPs	Disadvantages
Nutrineal® (Baxter)	5.5	Single	1.1% Amino Acids	Lactate 40 mmol/L	No	Contains lactate; low pH; single daily exchange
Balance® (Frasenius)	7.0	Double	2.3% Glucose	Lactate 35 mmol/L	Low	Contains lactate and glucose; no-neutral pH
CAPD4® (Frasenius)	5.5	Single	2.3% Glucose	Lactate 35 mmol/L	Medium	Contains lactate and glucose; low pH
Extraneal® (Baxter)	5.6	Single	7.5% Icodextrin	Lactate 40 mmol/L	Low	Contains lactate; low pH; single daily exchange
BicaVera® (Frasenius)	7.4	Double	1.5% Glucose	Bicarbonate 34 mmol/L	Low	Contains glucose
			2.3% Glucose			
Physioneal® (Baxter)	7.4	Double	1.36% Glucose	Lactate 10 mmol/L and Bicarbonate 25 mmol/L	Low	Contains glucose; low lactate exposure
			2.27% Glucose			

Table 3.1. Peritoneal dialysis solutions selected for study. Data summarized from package product information and García-López et al. 2012.

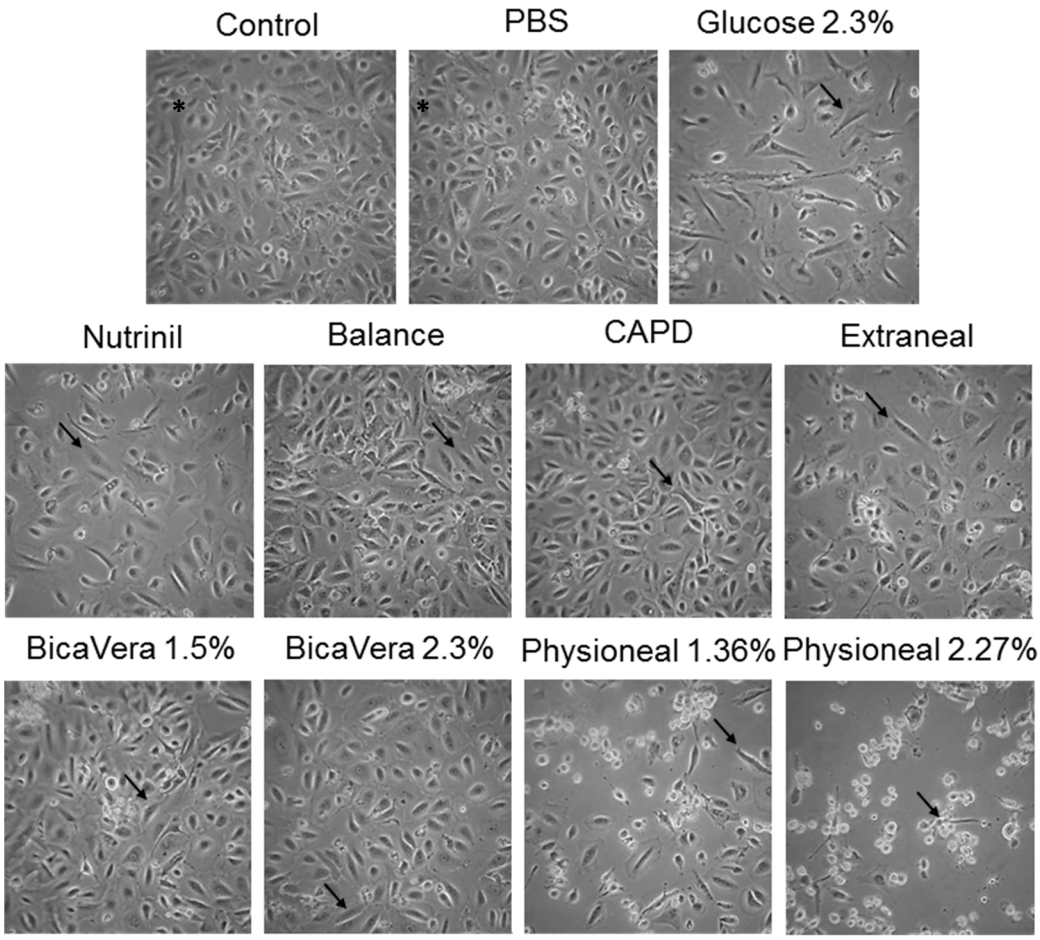

Figure 3.7. Phenotypic changes of cultured HPMCs after treatment with different PD fluids. Omentum-derived mesothelial cells were treated for 48 h with 50% of the specified PD fluids. (Control and PBS) Characteristic epithelial morphology of polygonal shape cells from a confluent monolayer, star indicated. (Glucose 2.3% and PD fluids) Loss of epithelial MCs monolayer and different extent of morphological changes and acquisition of fibroblast-like phenotype, arrow indicated. One representative experiment of four is shown. Zeiss Axiovert 135 microscope. Magnification: 200x.

Figure 3.8. miR-21 and miR-31 profiling in HPMCs and cellular supernatant after treatment with different PD fluids. Omentum-derived mesothelial cells were treated for 48 h with 50% of the specified PD fluids or control HPMCs medium. **(A)** cellular miR-21. **(B)** supernatant miR-21. **(C)** cellular miR-31. **(D)** supernatant miR-31. **(E)** AlamarBlue cell viability assay over a period of 48 h. Expression of miR-21 and miR-31 was analyzed by RT-qPCR and normalized to miR-191 expression. Data were analyzed by one-way ANOVA for matched samples followed by post-hoc Holm-Sidak's test comparing each condition mean with the control omentum-derived mean. Data represent the mean S.E.M. from four independent donor experiments. (See following page).

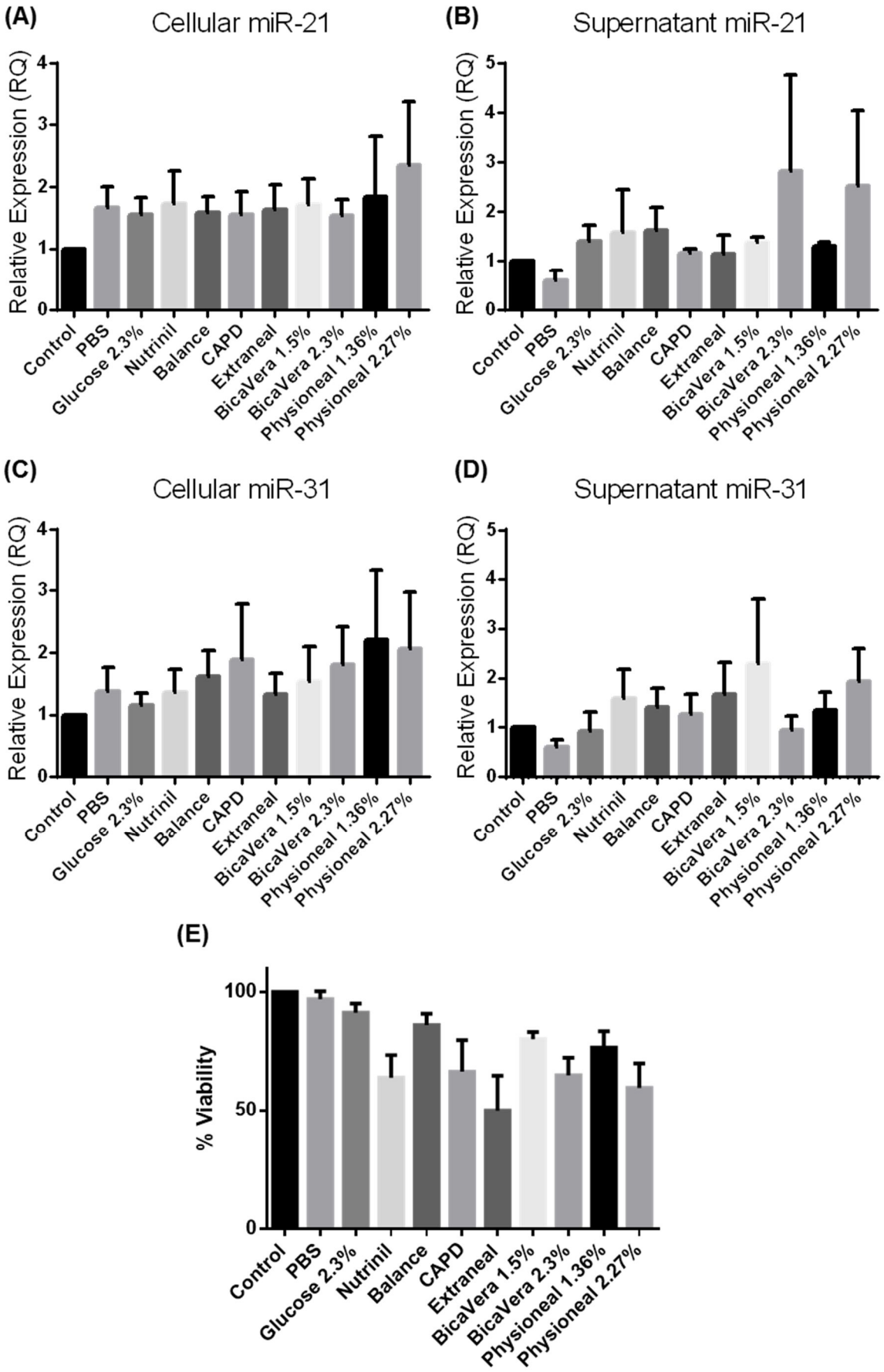
(A)
Cellular miR-21
Relative Expression (RQ)
0
1
2
3
4
Control
PBS
Glucose 2.3%
Nutrinil
Balance
CAPD
Extraneal
BicaVera 1.5%
BicaVera 2.3%
Physioneal 1.36%
Physioneal 2.27%
(B)
Supernatant miR-21
Relative Expression (RQ)
0
1
2
3
4
5
Control
PBS
Glucose 2.3%
Nutrinil
Balance
CAPD
Extraneal
BicaVera 1.5%
BicaVera 2.3%
Physioneal 1.36%
Physioneal 2.27%
(C)
Cellular miR-31
Relative Expression (RQ)
0
1
2
3
4
Control
PBS
Glucose 2.3%
Nutrinil
Balance
CAPD
Extraneal
BicaVera 1.5%
BicaVera 2.3%
Physioneal 1.36%
Physioneal 2.27%
(D)
Supernatant miR-31
Relative Expression (RQ)
0
1
2
3
4
5
Control
PBS
Glucose 2.3%
Nutrinil
Balance
CAPD
Extraneal
BicaVera 1.5%
BicaVera 2.3%
Physioneal 1.36%
Physioneal 2.27%
(E)
% Viability
0
50
100
Control
PBS
Glucose 2.3%
Nutrinil
Balance
CAPD
Extraneal
BicaVera 1.5%
BicaVera 2.3%
Physioneal 1.36%
Physioneal 2.27%

3.2.4. PDE-derived MCs have increased levels of miR-21 and miR-31

Ex vivo MCs cultured from PDE from PD patients have a diverse range of morphologies, ranging from cuboidal form, comparable to those observed from omentum-derived MCs, to fibroblast-shaped cells. Yáñez-Mó et al. 2003, characterized this PDE-derived MCs model by the study of cellular morphology and expression of key molecular markers that suggested an MMT process (Yáñez-Mó et al, 2003). Therefore, miR-21 and miR-31 were evaluated in PDE-derived HPMCs cultured *ex vivo*, divided as previously described (Yáñez-Mó et al, 2003) into those exhibiting phenotypic changes consistent with early MMT (E: epithelial phenotype) or late MMT (NE: non-epithelial phenotype) (Figure 3.9A). RNA from this model was kindly provided by Dr Manuel Lopez-Cabrera and used for analysis. Non-epithelial PDE-derived cells showed increased miR-21 and miR-31 expression compared with control omentum-derived HPMCs (Figure 3.9, B-C). These data support the potential of miR-21 and miR-31 to act as sentinels for PD-induced peritoneal membrane deterioration in PD patients.

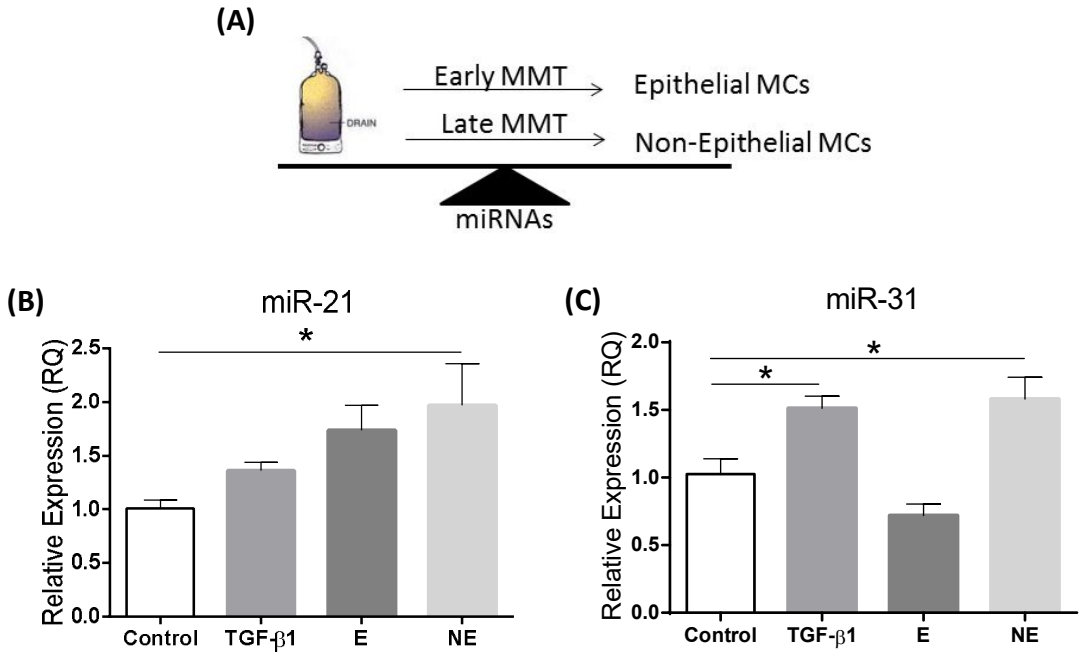

Figure 3.9. miR-21 and miR-31 profiling in a model of progressive peritoneal membrane deterioration. (A) Peritoneal effluent derived (PDE) cells diagram, a model of progressive peritoneal membrane deterioration. Relative expression of miR-21 and miR-31 in control omentum-derived mesothelial cells (HPMCs), TGF-β1 treated (1ng/ml, 48h) and cultured peritoneal effluent derived (PDE) cells with epithelial (E) and non-epithelial (NE) phenotype. **(B)** miR-21 expression. **(C)** miR-31 expression. Expression of miR-21 and miR-31 was analyzed by RT-qPCR and normalized to miR-191 expression. Data were analyzed by one-way ANOVA followed by post-hoc Holm-Sidak's test comparing each condition mean with the control omentum-derived mean. Data represent the mean S.E.M. from five independent donor experiments. *$p < 0.05$.

3.2.5. PM thickness and miR-21 follow the same pattern of expression in a uraemic PD mouse model

A uraemic PD mouse model was next analyzed to elucidate whether changes in PM thickness were associated with differential miRNA expression *in vivo*. In order to evaluate the effects of PD therapy in a clinically relevant model, a newly designed mouse model by ESR Evelina Ferrantelli combining long-term PD exposure and uraemia was chosen. Peritoneal membrane from mice undergoing PD with and without 5/6 nephrectomy (Nx) were kindly provided by ESR Evelina Ferranteli and examined, and compared with uraemic controls (n=7 per group, 12-14 weeks + 10 weeks of experiment) (Figure 3.10A). 5/6 Nx PDF treated group showed a significant increase in PM thickness compared to the 5/6 Nx control group (mean thickness 21.970 (7.053 to 36.890) vs 9.115 (4.779 to 13.450); 95% confident interval; $p<0.05$) (Figure 3.10C). The mesothelial and submesothelial compact zone of H&E FFPE samples were LCM micro-dissected for miRNA analysis (Figure 3.10B). Similarly, the examination of PM miRNA expression showed a trend to up-regulate PM miR-21 in the 5/6 Nx PDF treated group compared to the 5/6 Nx control group (Figure 3.10D). Nevertheless, this trend was not reproduced when miR-31 was analyzed (Figure 3.10E). Of note, although miR-31 seed sequence is conserved between human and mouse the full miRNA sequence is not exactly the same. The implications of this will be further discussed below. The results shown here demonstrate that PD treatment causes a peritoneal membrane thickening that is aggravated by the uraemic condition, and that miR-21 may be a miRNA especially suited to monitor peritoneal membrane changes in PD patients.

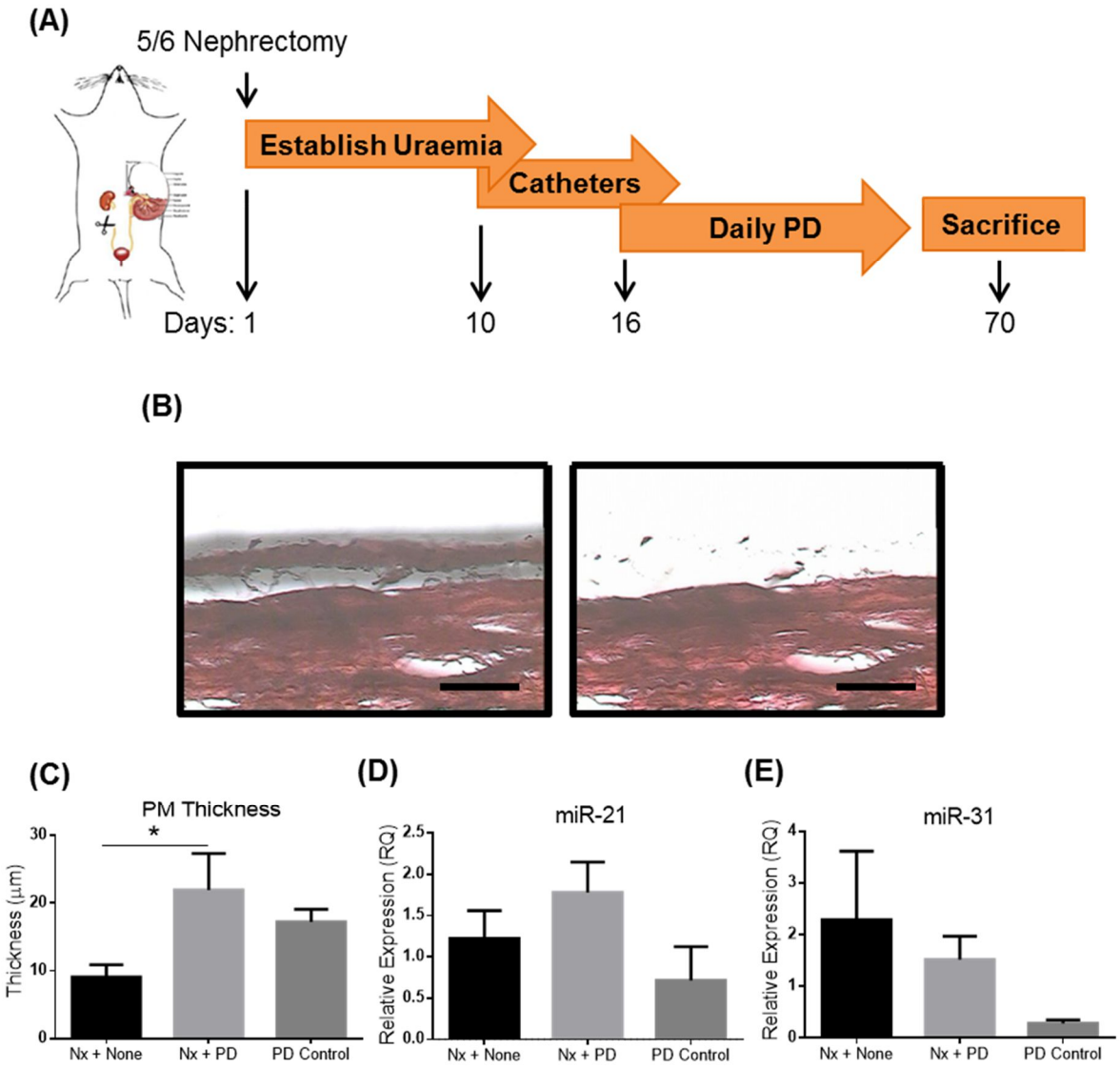

Figure 3.10. miR-21 and miR-31 profiling in an uraemic PD mouse model. (A) Uraemic PD mouse model diagram. **(B)** Formalin-fixed paraffin embedded (FFPE) samples were H&E stained and LCM micro-dissected to measure relative miRNA expression. Mesothelial and submesothelial compact zone was specifically micro-dissected by LCM selection (left panel) and specific removed are (right panel). Scale bar, 50 µm. **(C-E)** PD mouse model study in which the following groups where comapared 5/6 nephrectomy (Nx + none), 5/6 nephrectomy + daily PD treatment during 56 days (Nx + PD) and PD treatment during 56 days (PD control). **(C)** Peritoneal membrane thickness. **(D)** miR-21 expression. **(E)** miR-31 expression. Expression of miR-21 and miR-31 was analyzed by RT-qPCR and normalized to miR-191 expression. Data were analyzed by one-way ANOVA followed by post-hoc Holm-Sidak's test comparing all condition means. Data represent the mean S.E.M. from seven independent samples. *p < 0.05.

3.2.5. Supernatant from TGF-β1-treated MCs have increased levels of miR-21 and miR-31

To assess the potential of miR-21 and miR-31 as biomarkers to monitor peritoneal mesothelial MMT and the maintenance of the structural integrity of the peritoneal membrane in PD patients, miRNA expression was analyzed in supernatant from TGF-β1-treated MCs *in vitro*. For this aim, HPMCs where carefully washed 3 x with PBS before serum starvation and TGF-β1 incubation, in order to avoid possible contamination with FBS miRNAs (Figure 3.11A). Both miRNAs showed a trend to increase in HPMC supernatant after 72 h of TGF-β1 stimulation (Figure 3.11, B-C). These results demonstrated that in a well characterized *in vitro* model of TGF-β1-induced MMT in HPMCs, miR-21 and miR-31 up-regulation can not only be monitored at cellular level but also at the supernatant.

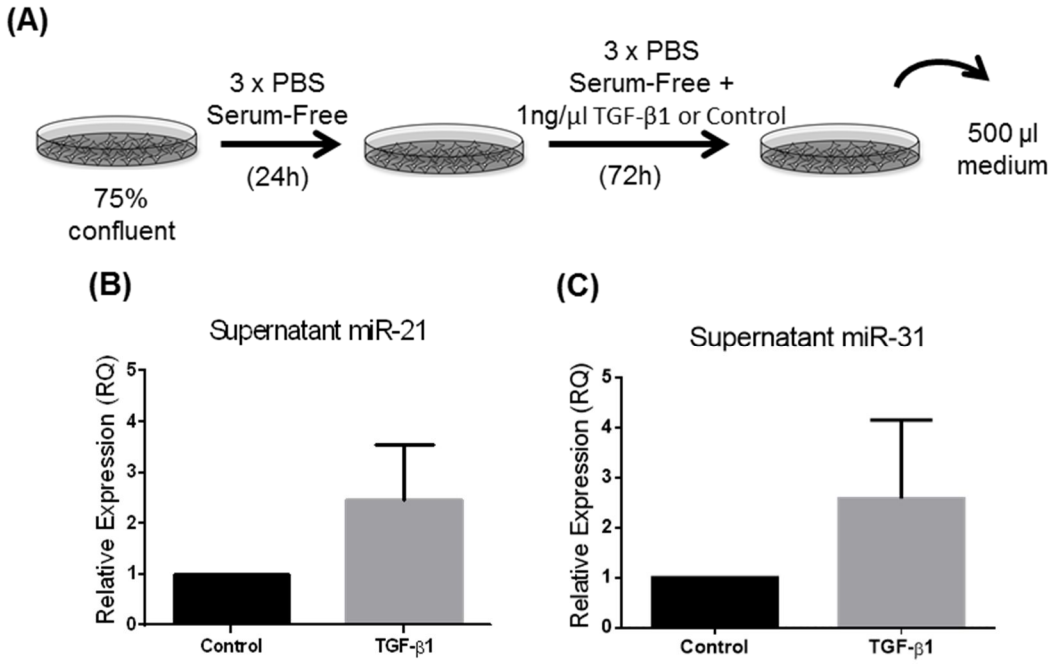

Figure 3.11. miR-21 and miR-31 profile in supernatant of HPMCs after TGF-β1 treatment. Omentum-derived mesothelial cells were treated with 1 ng/ml of TGF-β1 for 72 h. **(A)** Experimental model diagram. **(B)** Supernatant miR-21. **(C)** Supernatant miR-31. Expression of miR-21 and miR-31 was analyzed by RT-qPCR and normalized to miR-191 expression. Data were analyzed by paired, two tail, *t* test. Data represent the mean S.E.M. from three independent donor experiments.

3.3. Discussion

The peritoneal membrane has a complex structure, and includes cells of multiple lineages. The mesothelial cell layer forms the interface between dialysate and membrane, and plays an important role in determining changes associated with PD therapy failure (Selgas et al, 2006). Of the wide range of cytokines and factors that are deregulated during the complex process of PD treatment-driven membrane alterations, TGF-β1 plays a pivotal role (Loureiro et al, 2011). Indeed, PD patients have a high basal inflammatory state at the peritoneal cavity that includes increased TGF-β1 levels. This cytokine induces early changes (Snail expression, Figure 3.3G) that could partially explain a future peritoneal MCs MMT process (mesothelial markers down-regulation after 48 h, Figure 3.1A; and mesenchymal markers up-regulation between 24-72 h, Figure 3.3, E-F and H) and, ultimately, lead to fibrosis and ultrafiltration failure.

This research focused on the minimum TGF-β1 concentration and time able to induce mesothelial and mesenchymal changes during characterization analysis for following studies (1 ng/ml, 48 h). Of note, gross phenotypical changes were not observed under the TGF-β1 concentration and time selected, and were only apparent with higher concentrations or longer time-exposures (Figure 3.2 and 3.3). These decisions were based on the aims and background of the research including (i) evidence of MMT reversibility has been shown only during the early-MMT stages; (ii) miRNAs could be used as diagnostic tools to indicate the initial-phases of the MMT process; and (iii) early-MMT miRNA changes may be direct therapy targets. However, it is important to consider that higher doses of TGF-β1 and, particularly, coordinated effects of TGF-β1 together with other important inflammatory and pro-fibrotic stimuli, may have additional effects important to the processes underlying peritoneal fibro-genesis, and that miRNAs are likely also to play important roles in these processes.

Since the start of this project in September 2012, there has been a large increase in published findings describing miRNAs in many contexts, reflecting the wide current interest in this class of regulator molecules. Papers addressing miRNAs in the context of PD remain more limited. Those that were published during my studies are tabulated in

the general discussion (Table 6.1) and provide some additional evidence for miRNAs as regulators of key molecular pathways driving peritoneal membrane alterations leading to PD failure. Nevertheless, most PD-related miRNA studies have taken a literature-based approach to identify candidate miRNAs for further analysis (Table 6.1) (Bao et al, 2015; Chen et al, 2012a; Yu et al, 2014; Zhang et al, 2013). Thus, miRNAs implicated in epithelial-to-mesenchymal transition (EMT) in other contexts have been associated with mesothelial cells MMT during PD therapy in the last years (Yu et al, 2014; Zhou et al, 2013). However, it is commonly recognized that EMT processes may greatly differ depending on specific cell population and context. Therefore, extrapolation of miRNAs related to the EMT process in different research areas into the peritoneal fibrosis field is suboptimal, and miRNA expression profiling techniques are a better approach.

Animal models offer a useful approach to study PD therapy, but models that come close to mimicking the processes occurring in patients are necessarily complex (González-Mateo et al, 2009; Lameire et al, 1998). The use of intraperitoneal injection of dialysate as PD model has many advantages including low cost, high practicality and low infection risk (Lin et al, 2015; Liu et al, 2014; Liu et al, 2015; Morishita et al, 2016; Yu et al, 2014; Zhou et al, 2013). Nevertheless better PD models, in which a catheter is permanently inserted into the peritoneal cavity of the animals, have been described (González-Mateo et al, 2009). It is also important to remember that miRNA sequences are not always conserved between humans and animals (Kozomara & Griffiths-Jones, 2014), and analyzing their relevance in humans is, therefore, highly important (Table 6.1) (Lin et al, 2015; Liu et al, 2014; Liu et al, 2015; Morishita et al, 2016).

Several articles published during the development of this research have based their miRNA microarray analysis on total peritoneal RNA samples (Table 6.1) (Lin et al, 2015; Liu et al, 2014; Liu et al, 2015; Morishita et al, 2016; Zhou et al, 2013). Nevertheless, it is well accepted that PD treatment induces several structural and functional changes at the peritoneal cavity including changes in the percentages of constituent cell types and phenotype (Fernandez de Castro et al, 1994). miRNA expression profiles will change with each defined cell phenotype and context. Therefore, the study of miRNAs from total peritoneal samples has important associated challenges

defining the specific cell-type contribution and validating the changes in different, cell-specific models.

Indeed, CAPD patient PDE cell populations have been previously described as composed principally of macrophages (78%), followed by lymphocytes (12.3%), neutrophils (4.9%), eosinophils (2.6%), mesothelial cells (1.9%) and mast cells (0.3%) (Bos et al, 1991). Therefore, although the study patients would be free of peritonitis, macrophages will still have an important contribution to the miRNA profile measured by total PDE-derived cells miRNA array. Consequently, miRNA arrays based on all PDE-derived cells and/or full membrane digests (Lin et al, 2015; Liu et al, 2014; Liu et al, 2015; Morishita et al, 2016; Zhou et al, 2013) may not be a good model for mesothelial cell changes associated to PD therapy as suggested by some of the published articles in the field. Similarly, when the studied miRNAs are selected from the existing literature, the choice of an appropriate model of study remains essential (Bao et al, 2015; Chen et al, 2012a; Yu et al, 2014).

In vitro models, although more simplistic, may be critical to understand the specific pattern of miRNA expression in response to a known stimulus in a specific cell-type where mechanistic research can be pursued. Therefore, in this research, primary human mesothelial miRNA expression and responses to TGF-β1 were defined. This approach was chosen not only to identify candidate miRNAs that may act as biomarkers and/or important contributors during the early MMT process but also a cellular model in which consequent mechanistic effects could be subsequently investigated (Figure 6.1C, Table 6.1). miRNA data was examined here considering three important parameters for research (i) baseline level of expression, (ii) fold change in response to TGF-β1, and (iii) statistical significance of the observed change (Figure 3.5A). Hybridization array data is often presented purely on the basis of fold change and significance level. However, this approach may lead to focus on less abundant transcripts, potentially a problem for future biologically relevant research given that miRNAs' function as negative regulators of mRNAs is sensitive to the stoichiometry of miRNA:mRNA (Ebert & Sharp, 2012; Hansen et al, 2013; Salmena et al, 2011). Two abundant miRNAs, miR-21 and miR-31, the expression of which was increased when MCs were incubated with TGF-β1, were selected for subsequent study. Nevertheless,

alternative approaches including the study of miRNAs that where not present at baseline level but up-regulated following TGF-β1 exposure could have been taken.

Ongoing efforts are being made to improve PD biocompatibility, but controversy remains regarding downstream effects of PD fluids on mesothelial cell MMT and long-term benefits of biocompatible solutions (Blake et al, 2013; Johnson et al, 2012). Recent improvements introduced in PD solutions include (i) glucose degradation product reduction *via* physical glucose (low pH) separation from the buffer during sterilization and storage, (ii) partial replacement of glucose by icodextrin, or (iii) amino acids, and (iv) lactate buffer replacement by bicarbonate (see 1.3.2). PD fluids used in this chapter for research varied regarding osmotic and buffer compounds, pH and glucose degradation products (GDPs) (Table 3.1). Global phenotypic changes in MCs and levels of miRNAs of interest in both cells and cell supernatant were assessed after PDF treatment (solution: medium 1% FBS supplemented, 1:1) for 48 h. Although a general pattern of miRNA up-regulation induced by PDF treatment could be observed at the cellular level, miRNA measurement seemed more likely to be solution-dependent when measured in cell supernatant (Figure 3.8). miRNAs have been recently shown to better correlate on supernatant rather than at the cellular component in other models and contexts. For instance, Hansen et al. 2014 showed that miR-888, let-7c and miR-200b correlated with disease status more closely with the supernatant from prostatic secretions in urine rather than using the pellet fraction (Hansen et al, 2013). Nevertheless, due to the high variability observed between primary MCs from different donors and the amount of PD solutions selected for study no significant changes could be identified. Therefore, future study is necessary for conclusive results regarding the differential levels of miRNAs measured in HPMCs and cell supernatant after exposure to PD fluids. It would also be interesting to study TGF-β1 expression as well as the epithelial and mesenchymal markers used in this chapter to characterize HPMCs MMT process driven by PD solutions *in vitro* and possible autocrine TGF-β1 response. Finally, it would be especially interesting, using a higher experimental number, to compare miRNA expression with the expression of other molecules that are used as markers for MCs damage, for example CA-125 and IL-6 (Lopez-Anton et al, 2015).

Of note, although miRNAs can be actively released from cells (Chen et al, 2012b; Schwarzenbach et al, 2014), supernatant miRNA measured here may only be indicative of cell injury and death due to treatment (Figure 3.7 and 3.8E). This raises two important questions regarding (i) the need to reconsider the term *biocompatible* for PD solutions which may be too hopeful and induce patient misconception by other terms like *less non-biocompatible* or *more-biocompatible*, and (ii) regarding miRNA stability and/or protection of the cell-free miRNAs measured in this context, which would be further discussed during the following Chapters 4 and 6.

Although a general pattern was difficult to observe in supernatant miRNA expression of HPMCs treated with different PD fluids, there was an observable trend indicating that solutions with higher glucose concentrations induced higher miR-21 expression (Figure 8B). Different studies have described a raise in PMCs TGF-β1 expression after PD solution exposure and, especially, after glucose-containing fluid exposure, which would explain subsequent increase in miR-21 expression. Mizuri and co-workers detected an increase in TGF-β1 expression in rat PMCs exposed to glucose-containing PDF (Mizuiri et al, 2009). Indeed, HPMCs incubation with glucose and sodium lactate, either alone or in combination, enhanced TGF-β1 mRNA expression and protein secretion (Wong et al, 2003). Ha et al. 2001 compared the effect of Dianeal (1.5% and 4.25% glucose and 40 mmol/L lactate buffer) with Physioneal (1.5% and 4.25% glucose, 15 mmol/L lactate and 25 mmol/L biocarbonate buffers) and Extraneal (7.5% icodextrin and 40 mmol/L lactate buffer) 1:2 diluted in serum-free media for 48 h (Ha et al, 2002). They observed TGF-β1 secretion was significantly increased by Dianeal 4.25% and Extraneal; with icodextrin increasing TGF-β1 secretion in a dose-dependent manner (Ha et al, 2002). This last interesting observation regarding icodextrin would be further discussed during next chapter.

PDE-derived MCs used in this chapter were previously characterized by Dr Manuel López-Cabrera group following established protocols (López-Cabrera et al, 2006; Yáñez-Mó et al, 2003). PDE proliferative MCs displayed high ICAM-1 and CA-125 expression, which is negative in omentum-derived fibroblasts and suggests a mesothelial MMT origin of non-epithelioid MCs (López-Cabrera et al, 2006; Yáñez-Mó et al, 2003). Cytokeratins and E-cadherin are epithelial markers highly expressed in

omentum-derived MCs and gradually decreased in epithelioid and non-epithelioid PDE-derived MCs. Although, only a minor non-epithelioid population remained cytokeratin and E-cadherin positive, omentum-derived fibroblasts did not express these markers (López-Cabrera et al, 2006; Yáñez-Mó et al, 2003). The study of particular mesenchymal markers including Snail, N-cadherin, Fibronectin, Collagen I, α-SMA, and fibroblast specific protein-1 (FSP-1), which were progressively increased in epithelioid and non-epithelioid PDE-derived MCs confirmed PD-induced MCs MMT changes in this model (López-Cabrera et al, 2006; Yáñez-Mó et al, 2003). Further experiments found increased miR-21 and miR-31 in PDE-derived mesothelial cells with mesenchymal characteristics. These results associate miR-21 and miR-31 to a progressive peritoneal mesothelial cell deterioration during PD treatment that was previously shown *ex vivo* to define an adverse response to PD (Yáñez-Mó et al, 2003).

Different PD animal models have been established during recent years. Among them, the thickening and miRNA expression in the mesothelial and sub-mesothelial compact zone from a uraemic PD mouse model was specifically studied. Precise peritoneal mesothelial and sub-mesothelial compact zone micro-dissection was possible via LCM and histopathology expert guidance. Peritoneal membrane thickening increased with PD therapy and followed the same pattern as miR-21 expression (Figure 3.10, C-D). Nevertheless, miR-31 did not follow the expected pattern of expression. Of note, both miRNAs are highly conserved in mammals and miR-31 has been studied successfully in other mouse models of human disease. miR-21 and miR-31 are independently transcribed and will, therefore, be regulated by different factors that may not be fully conserved between species. Further research would be needed to clarify these possible alternatives. Of note, here Dianeal was used to treat uraemic mice, which is a PD solution that was not included between the analyzed *in vitro* fluids shown above (Figure 3.7 and 8, Table 3.1). Dianeal® (Baxter) uses glucose 3.86% as osmotic agent and lactate 40 mmol/L as a buffer in a single chamber under low pH 5.2 and contains, therefore, a high amount of GDPs being poorly-biocompatible but adequate for the model of study (García-López et al, 2012). The trend of use of this solution will probably be reduced during the following years and therefore was not considered for these *in vitro* study of PD fluids. Instead, CAPD4, which also uses glucose 2.3% and lactate 35

mmol/L in a single bag and at a low pH 5.5, was used as a medium-GPDs solution for study. Nevertheless, it would be interesting to know miRNA regulation in HPMCs following Dianeal exposure. Additionally, to include a control non-uraemic non-PD animal group to know the basal thickness of the PM as well as the basal levels of miRNA expression would add valuable information to this model highlighting any effects due to uraemia.

Finally, the fact that this research was able to measure both miRNAs in the supernatant from TGF-β1-treated MCs where they displayed, in both cases, a trend to increase, suggested that they could be used as MMT biomarkers for PD therapy. It is important to note that although both miRNAs are up-regulated by TGF-β1 in most of the models developed during the chapter, they will probably have different specific roles during the MMT process (see Chapter 5). A given miRNA can regulate the expression of hundreds of mRNAs. Moreover, target mRNAs are likely to be simultaneously controlled by multiple miRNAs rather than by the action of a single miRNA alone. Alternatively, miRNAs may be actively synthesized and secreted not only to modulate intra-cellular pathways but also to influence the behavior of neighboring cells in a paracrine fashion (Chen et al, 2012b). This creates a complex network in which several miRNA-regulated pathways cooperate to promote profound and specific effects in MCs phenotype and function but also potentially modulating the whole peritoneal cavity during the progression of PD therapy.

miRNAs have been shown to be promising as biomarkers in patients with kidney disease (Beltrami et al, 2012; Bowen et al, 2013) but there has been limited study to date in PD patients. During this chapter miR-21 and miR-31 level of expression was shown to be increased in different, well-established models associated with structural and functional alterations of the peritoneal membrane during peritoneal dialysis. These MMT models included (i) *in vitro* MCs TGF-β1 stimulated, (ii) MCs treated with different PD solutions *in vitro*, (iii) *ex vivo* MCs with epithelial and non-epithelial phenotype, and (iv) *in vivo* uraemic PD mouse model. Therefore, these results suggested to consider the possibility of measuring miR-21 and miR-31 in PDE from PD patients and to correlate their levels of expression with different clinical parameters associated with peritoneal membrane deterioration and worse PD outcome (see Chapter 4).

Chapter 4 – Evaluation of miRNAs as biomarkers in PD effluent from patients

4.1. Introduction

Continuous dialysis fluid exchange allows easy access to monitor peritoneal cells and miRNA expression in PD effluent (PDE). This presents the enticing possibility of monitoring peritoneal cavity homeostasis during PD treatment. Nevertheless, no PDE-derived biomarker is currently used in clinical routine to monitor the homeostatic maintenance of the peritoneal cavity. miRNAs have shown a sound potential as biomarkers in several fields. Thus, PDE-derived miRNAs may be particularly suitable as biomarkers due to their specific pattern of expression, easy detection, stability, and reliability in other contexts (Akat et al, 2014; Di Leva et al, 2014; Liang et al, 2007; Lorenzen et al, 2012). Although, PD-miRNA research is in an early stage there is a particular interest regarding miRNA as biomarkers to help individualizing PD treatment. However, until now, no one has examined PDE extracellular miRNAs and their utility as PDE biomarkers remains to be established.

To date, research on miRNA expression associated with PD therapy has been limited in scale and has primarily chosen a literature-based miRNA-candidate methodology or had other significant design weaknesses (See 1.6.3 and Chapter 6). In this chapter, the potential of miRNAs as MMT biomarkers during PD therapy was investigated. This research (i) developed a new method for miRNA extraction and RT-qPCR measurement in 4 h PDE samples, (ii) evaluated the correlation of miR-21 and miR-31 in PDE with clinical parameters associated with peritoneal membrane MMT and treatment stability, in a cohort of 230 patients taken from the Global Fluid Study; and (iii) measured miR-21 and miR-31 expression as well as TGF-β1 pathway activation in peritoneal membrane biopsies from PD patients.

4.2. Results

4.2.1. Stability of PDE miRNAs at room temperature

Before studying samples from the Global Fluid Study (GFS), a careful analysis of PDE miRNA stability was performed. The GFS is an international, multicenter, prospective, observational cohort study of 959 patients (Lambie et al, 2013). Sample collection and storage methodology was standard but variability between sample processing times cannot be completely dismissed, due to the different handling of subjects and to possible complications. PDE from the GFS was, in all cases, spun and kept at -80ºC within the following 6 h after withdrawal from the peritoneal cavity. PDE miRNA stability was studied during incubation at room temperature at time points up to 24 h, to evaluate sample adequacy for this research within a reasonable processing timescale. Samples for this work were obtained from the Wales Kidney Tissue Bank (WKTB).

Fresh overnight PDE samples from three different control patients were collected for the study. PDE was aliquoted into two 50 ml falcon tubes. One tube was spun during 20 min at 400 *x g* and room temperature (RT), while the other was kept at RT. 1 ml aliquots from each sample were collected after 0, 4, 8 and 24 h, and spun during 20 min at 400 *x g* and RT (Figure 4.1A). 500 µl of PDE supernatant were taken, RNA extracted and RT-qPCR analyzed. Results were analyzed by two-way ANOVA with matched values for both factors (method and time). Multiple comparisons were performed by post-HOC Holm-Sidack's test comparing each time mean with the control (0 h) mean. Samples were stable at room temperature for the miRNAs of study independently if they were spun/not spun when collected (Figure 4.1, B-D). miRNAs were stable within a reasonable time-scale (less than 8 h) and differences in their expression compared with control-time (0 h) were only observed for miR-21 after 24 h of room temperature (Figure 4.1, B-D). The miRNAs of study (miR-21, -31 and -191) and, likely, other miRNAs, are stable in PD fluid without need of a special handling within a reasonable time-scale (less than 8 h). Therefore, PDE samples from this biobank are adequate for the measurement and study of selected miRNAs.

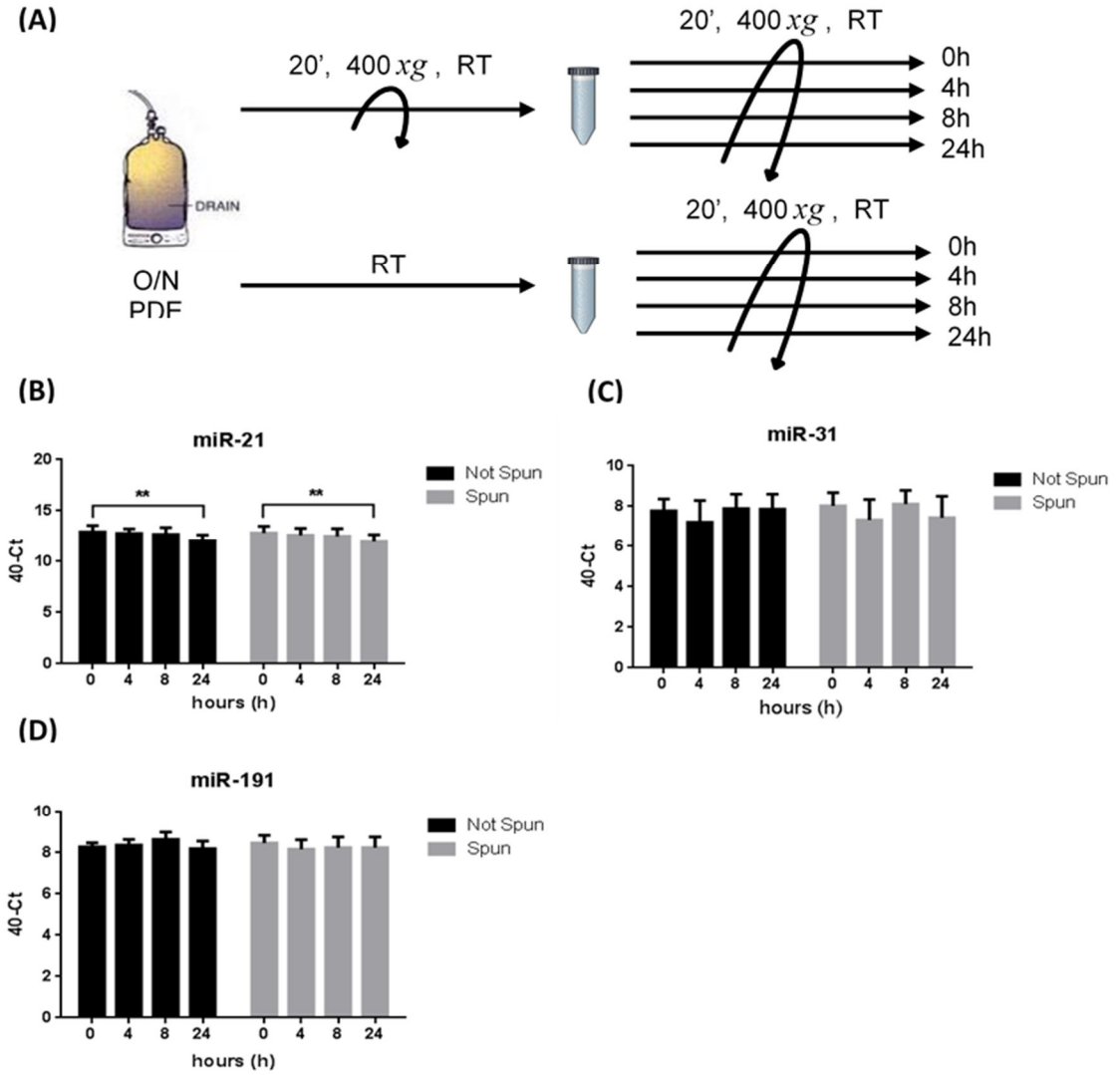

Figure 4.1. Stability of PDE miRNAs at room temperature. (A) Experiment diagram. Fresh overnight PDE samples were aliquoted into two 50 ml falcon tubes. One tube was spun during 20 min at 400 *x g* and RT while the other was kept on RT. 1 ml aliquots from each sample were collected after 0, 4, 8 and 24 h, and spun during 20 min at 400 *x g* and RT. 500 µl of PDE supernatant were taken for experiment. **(B-D)** Expression of all miRNAs was analyzed by RT-qPCR and expressed as 40-Ct. **(B)** miR-21. **(C)** miR-31. **(D)** miR-191. Data were analyzed by two-way ANOVA for repeated measures by both factors, followed by post-hoc Holm-Sidak's test comparing each time mean with the control (0 h) mean. Data represent the mean S.E.M. from four independent donor experiments. **p < 0.01.

4.2.2. Optimization of extraction of overnight PDE miRNAs

Overnight PDE from patients was suitable for miRNA measurement with mean Ct values lower than 35, which is the established limit of qPCR detection. Mean (minimum-maximum) Ct values were miR-21, 27.16 (26.01-28.90); miR-31, 31.97 (30.56-33.28) and miR-191, 31.54 (30.41-32.11) (Figure 4.2, A-B). GFS dialysate sampling was from a 4 h peritoneal equilibration test (PET) and no amplification plot was detected following this protocol in a first, preliminary measurement. There were two possible manners of improving the RT-qPCR miRNA measurement from PDE of the GFS: (1) to optimize the RNA isolation process and/or (2) to optimize the RT and qPCR reaction.

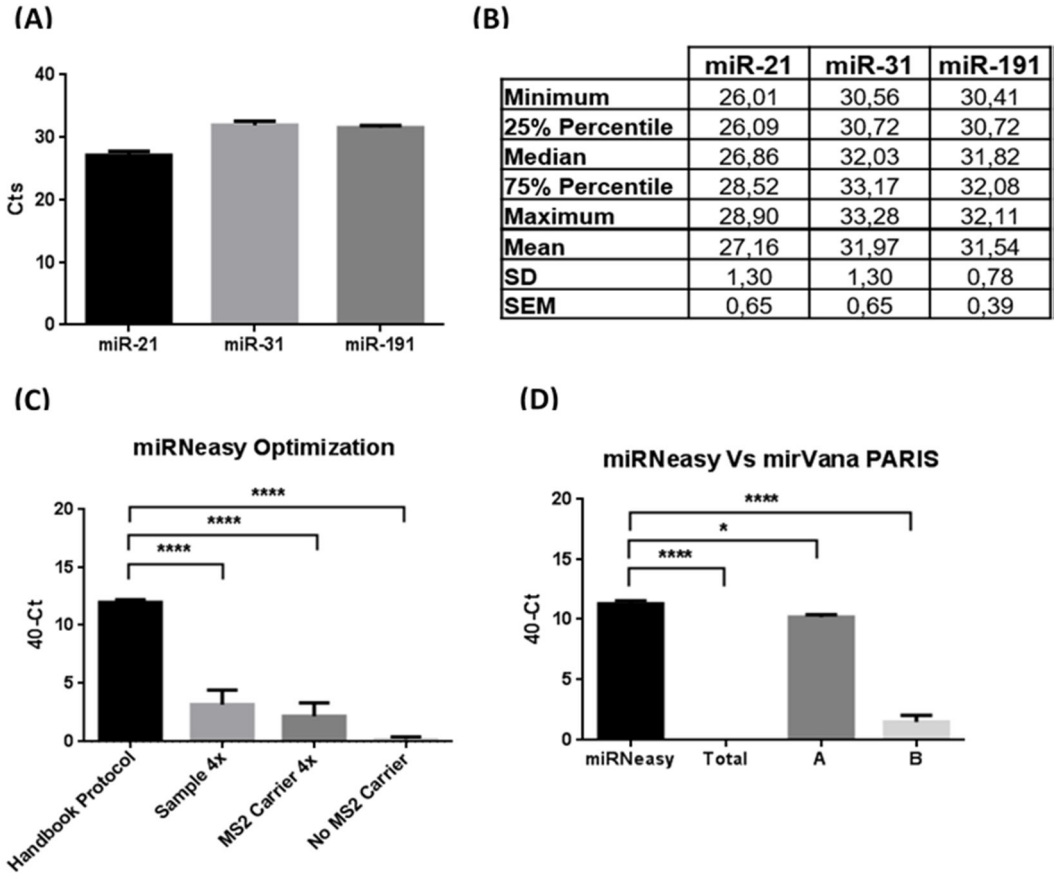

	miR-21	miR-31	miR-191
Minimum	26,01	30,56	30,41
25% Percentile	26,09	30,72	30,72
Median	26,86	32,03	31,82
75% Percentile	28,52	33,17	32,08
Maximum	28,90	33,28	32,11
Mean	27,16	31,97	31,54
SD	1,30	1,30	0,78
SEM	0,65	0,65	0,39

Figure 4.2. Peritoneal dialysis effluent (PDE) RNA extraction optimization. (A) Overnight PDE miRNA expression using *miRNAeasy Mini* Kit. **(B)** Overnight PDE miRNA expression statistics. **(C)** *miRNAeasy Mini* Kit PDE-RNA isolation optimization using handbook protocol, increased sample (4x), increased MS2 carrier (4x) or no MS2 carrier. **(D)** PDE-RNA isolation comparison between *miRNAeasy Mini* and *mirVana PARIS* kit using the three different protocols detailed by the kit (see Figure 4.3). Data were analyzed by one-way ANOVA for matched samples followed by post-hoc Holm-Sidak's test comparing each protocol mean with the control mean. Data represent the mean S.E.M from three independent donor experiments. *$p < 0.05$; ****$p < 0.001$.

4.2.3. PDE miRNA isolation optimization

To improve the miRNA isolation step, this research attempted to enhance miRNA quantity obtained with the *miRNeasy Mini* kit (QIAGEN). *Handbook protocol*, previously used for overnight PDE, was compared with extractions including increased sample 4 x, increased MS2 RNA carrier 4 x and no MS2 RNA carrier used. miR-21 measurement by RT-qPCR was performed for evaluation. None of the modifications introduced to the protocol increased the efficiency of the original extraction protocol (Figure 4.2C). Burgos et al. 2013, recently evaluated different RNA isolation kits for very diluted samples of cerebrospinal fluid and indicated high isolation efficiency with *mirVana PARIS* kit (Burgos et al, 2013). The *mirVana PARIS* handbook protocol offers two isolation alternatives: Total RNA (1.25 volumes of ethanol and a single column) and using two consecutive columns: first column (A) recommended for large RNAs, >200 nt (1/3 volume of ethanol), which effluent is filtered by a second column (B) suggested for small RNAs <200 nt (2/3 volume of ethanol) (Figure 4.3A). RNA from overnight PDE was extracted using Handbook protocol for *miRNeasy Mini* kit and the three isolation alternatives of *mirVana PARIS* kit. miR-21 was measured in all samples by RT-qPCR for evaluation. *miRNeasy Mini* kit performance was similar to *mirVana PARIS* kit (A) while (Total) and (B) extraction were less efficient (Figure 4.2D). *mirVana PARIS* RNA elution volume recommended by Handbook protocol is double the amount of that suggested by *miRNeasy Mini* kit. Therefore, total RNA eluted from *mirVana PARIS* (A) was estimated to contain an amount of miRNAs near twice of that eluted by *miRNeasy,* and was selected for future optimization.

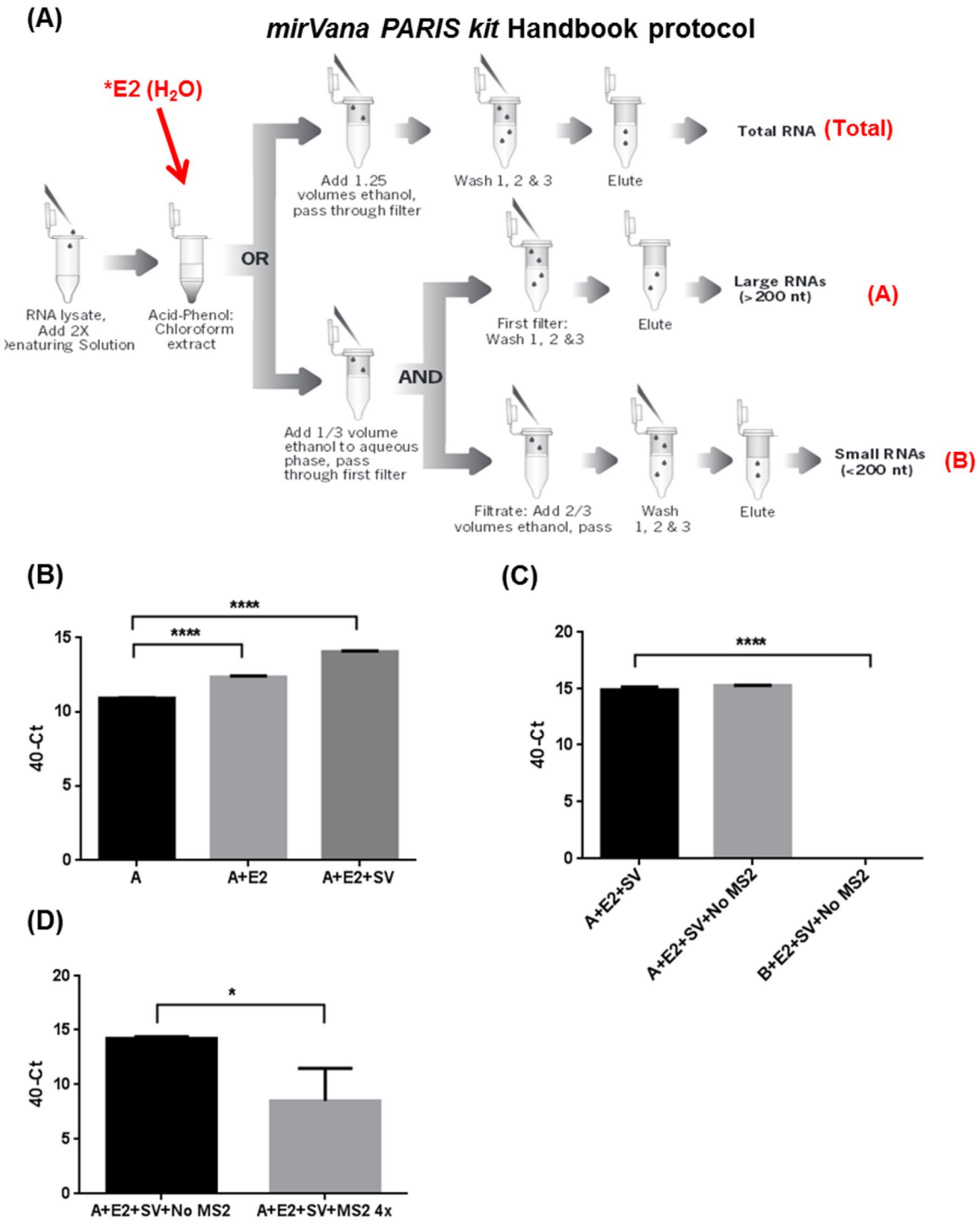

Figure 4.3. PDE miRNA isolation optimization. (A) *mirVana PARIS* handbook protocol diagram for RNA isolation alternatives. *mirVana PARIS* handbook protocol recommends three isolation alternatives including total RNA, large RNAs, >200 nt and small RNAs <200 nt. Second extraction (E2) step in which the remaining interphase and organic layer were re-hydrated and re-isolated with water is labeled and further described at the text. **(B-D)** *mirVana PARIS* PDE miRNA isolation optimization. **(B)** Isolation optimization: second extraction with water (E2), Speed-Vac step (SV). **(C-D)** Isolation optimization: MS2 RNA carrier is not necessary for the extraction. Data were analyzed by paired, two tail, t-test or one-way ANOVA for matched samples followed by post-hoc Holm-Sidak's test comparing each protocol mean with the control mean. Data represent the mean S.E.M. from three independent donor experiments. *p < 0.05; ****p < 0.001.

The organic phase division for nucleic acid extraction entails the upper aqueous layer, confining the RNA, being prudently taken, avoiding contamination from the interphase and the organic phase below. With the intention of isolating the aqueous phase with the smallest volume of impurities from the matter below, part of the RNA-comprising aqueous layer is left behind. To increase RNA recovery, *mirVana PARIS* handbook protocol for isolation (A) was subsequently improved by adding a second extraction (E2) step in which the remaining interphase and organic layer were re-hydrated and re-isolated with water (Figure 4.3A). An equal volume of 'removed-aqueous phase' of water was added to the acid-phenol chloroform extract, vortexed for 30 - 60 sec to mix and centrifuged for 5 min at maximum speed (10,000 *x g*) at room temperature to separate again the aqueous and organic phases. The aqueous phase was carefully removed and processed with the previously extracted aqueous phase. Finally, a 40 min, cold, Speed-Vac (SV) step was introduced to concentrate the final eluted samples in silicone coated eppendorfs. E2 increased the final eluted RNA concentration by 1.44 Cts while the addition of E2+SV enhanced the measurement by 3.14 Cts (Figure 4.3B). Addition of MS2 carrier RNA did not improve miRNA isolation using either *mirVana PARIS* kit (A) and (B) handbook isolation protocol neither greating increasing MS2 by four times (Figure 4.3, C-D). In short, after PDE miRNA isolation optimization, miRNA concentration was increased by 3.144 Cts. Given that 1 Ct difference approximates to a doubling of miRNA signal, this represents a substantial optimization in signal. Subsequently, this research was focused on the optimization of the RT and qPCR reaction.

4.2.4. Reverse Transcription Chemistry Evaluation

To improve miRNA RT the possibility of eliminating the water of this reaction and subsequently adding the remaining extra volume as additional isolated RNA was investigated. TaqMan miRNA RT assays are tested and amplification efficiency values range from 100% (±10%) when measured samples are free of PCR inhibitors. PCR performance may be affected by different substances. miRNAs have never been previously extracted from 4 h PDE and it is important to consider the possibility of carrying different inhibitors from the PD fluid. Sample dynamic range testing is based on

serial dilution and was limited due to the high dilution of the initial sample. To overcome this issue 1 µl of 10 ng RNA from HPMC cells was spiked into each of the testing samples. 3, 6 and 9 µl of PDE-RNA were miR-21 reverse transcribed using the same total volume and 4 µl of serial RT dilutions were used to evaluate the RT performance by qPCR (Figure 4.4D).

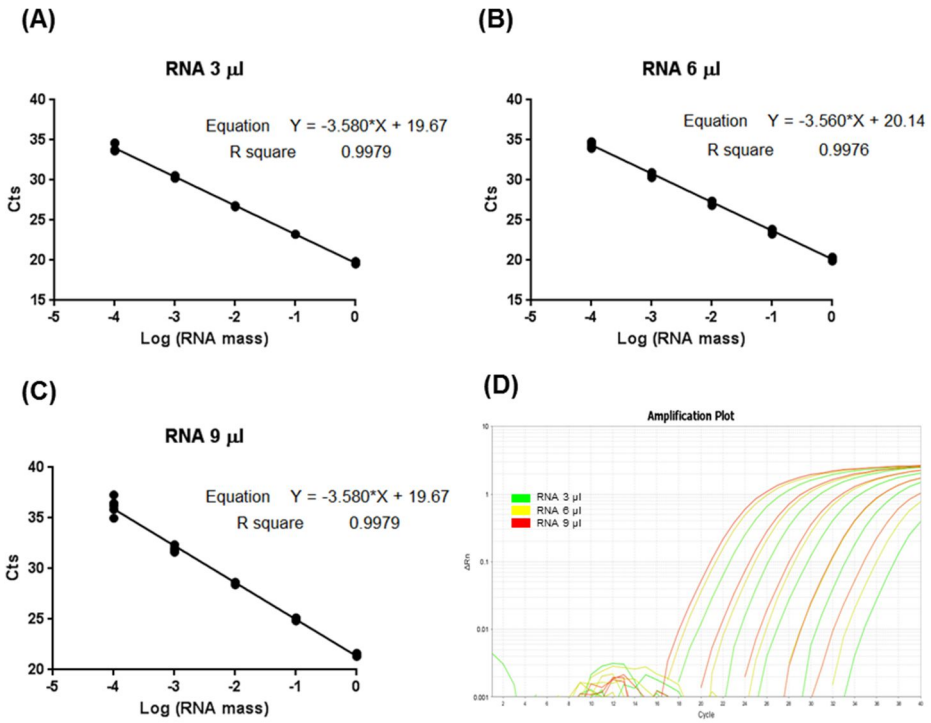

Figure 4.4. Reverse Transcription Chemistry Evaluation. (A-C) Serial dilutions from RT product standards of 3, 6 and 9 µl of PDE isolated RNA were qPCR independently evaluated for miR-21. **(A)** miR-21 expression for 3 µl PDE isolated RNA. **(B)** miR-21 expression for 6 µl PDE isolated RNA. **(C)** miR-21 expression for 9 µl PDE isolated RNA. **(D)** miR-21 qPCR amplification plot comparing serial dilutions of RT product from 3, 6 and 9 µl of PDE isolated RNA from a single donor. Data were RNA mass log transformed and analyzed by linear regression. Data represent serial dilutions from five independent donor experiments.

Exceeding the capacity of the reaction was not an issue, as the analyzed samples were highly diluted. Nevertheless, the linearity of the reaction, with a potential increase in sample volume and, a subsequent potential increase in inhibitors from the PDE, was important. The linearity of the reverse transcription is called efficiency (E) and can be calculated as: $E = (10^{-1/Slope}-1) \times 100$

The efficiency of 3, 6 and 9 µl of reverse transcribed PDE-RNA was in all cases 90.25, and, therefore, within the values range guaranteed by the supplier (Figure 4.4, A-C). R^2=0.9979 and 0.9976 indicated there were no potential precision issues that could drastically affect low-fold change variations in target expression (Figure 4.4, A-C). PCR inhibition due to potential chemical contaminants isolated from the PDE together with

the RNA was also a matter of interest. PCR efficiency greater than 100% and low R^2 values are characteristics of a plot demonstrating PCR inhibition. These characteristics were absent, and, therefore inhibition was not a matter of concern for these samples and experimental conditions. Finally, RT protocol modifications by introducing a higher concentration of sample at the RT step was a good optimization approach, as this was not affecting the efficiency of the measurements.

4.2.5. qPCR Chemistry Evaluation

Similarly, to improve miRNA qPCR the possibility of eliminating the water of this reaction and adding the remaining extra volume with isolated RNA was investigated. TaqMan miRNA qPCR assays are also tested and amplification efficiency values range from 100% (±10%) when measured samples are free of PCR inhibitors. Nevertheless, a careful evaluation of this optimization process was needed for the reasons named above. 9 µl of 4 h PDE-RNA were reverse transcribed with 1 µl of 10 ng RNA from HPMC cells spiked-into each of the testing samples and 3, 6 or 9 µl of serial RT dilutions were used to evaluate the qPCR performance using the same total volume (Figure 4.5D).

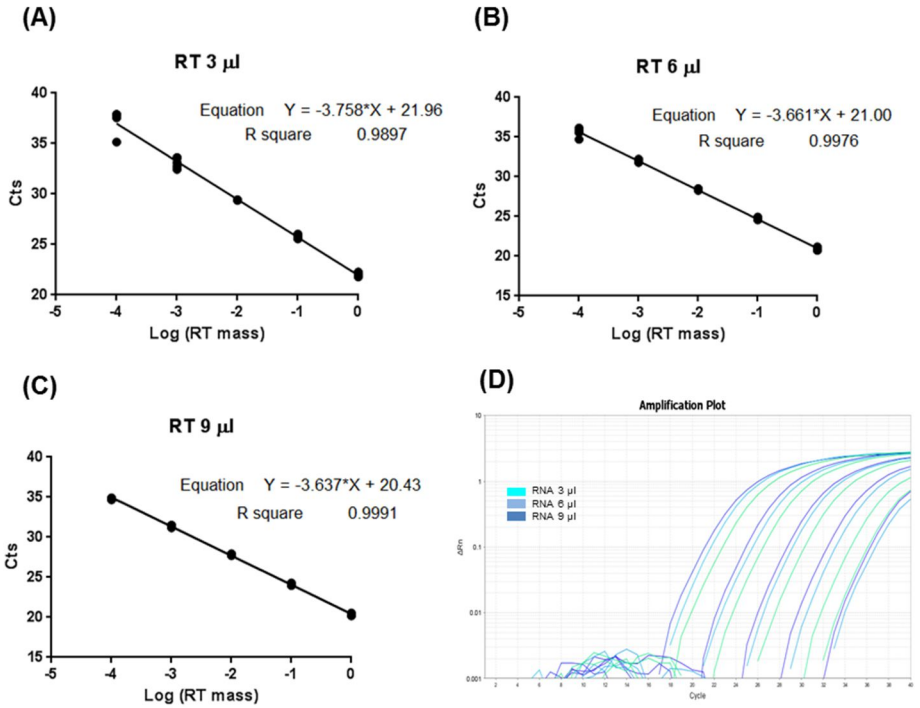

Figure 4.5. qPCR Chemistry Evaluation. (A-C) Serial dilutions from 9 µl of PDE isolated RNA RT product were qPCR independently evaluated using 3, 6 and 9 µl of diluted RT product for miR-21. **(A)** miR-21 expression for 3 µl of RT product. **(B)** miR-21 expression for 6 µl of RT product. **(C)** miR-21 expression for 9 µl of RT product. **(D)** qPCR amplification plot comparing serial dilutions of 9 µl of PDE isolated RNA RT product independently qPCR evaluated using 3, 6 and 9 µl of diluted RT product for miR-21 from a single donor. Data were RNA mass log transformed and analyzed by linear regression. Data represent serial dilutions from five independent donor experiments.

Newly, exceeding the capacity of the reaction was not an issue. Nonetheless, the linearity of the reaction with a potential increase in RT mass was important. The efficiency of 3, 6 and 9 µl of PCR PDE-RT was 84.54, 87.56 and 88.34 and, therefore, similar to the values ranges guaranteed by the supplier in standard conditions (Figure 4.5, A-C). R^2=0.9897, 0.9976 and 0.9988 indicated there were no potential precision issues that could drastically affect low-fold change variations in target expression (Figure 4.5, A-C). Indeed, higher volumes gave us better efficiency due to the high dilution of the samples reaching the RT-qPCR limit of detection. PCR inhibition caused by potential chemical contaminants isolated from the PDE, together with the RT mass, was also a matter of interest in this case. PCR efficiency was not greater than 100% and R^2 values were high. Therefore, PCR inhibition should, thus, not be an issue for these samples. Finally, PCR protocol modification performed by introducing a higher concentration of RT sample at the PCR step, was a good optimization approach, as greater concentrations of PDE-RT product represented a tighter and greater efficiency. This was neither inhibiting the PCR reaction nor affecting the accuracy of the measurement.

4.2.6. RT and qPCR reaction optimization, PDE GLOBAL samples

To improve miRNA RT and qPCR step, the possibility of eliminating the water of both reactions and adding the remaining extra volume with isolated RNA (+RT) or diluted RT (+PCR) product respectively was investigated. +RT showed that 4 h PDE met the cycle threshold for RT-qPCR detection earlier for miR-21 mean ± SD, (1.33 ± 0.5555 Ct earlier detection); miR-31, 2.039 ± 1.4918 Cts and miR-191, 1.919 ± 0.3745 Cts while the addition of +RT+PCR enhanced the measurement for miR-21, 2.75 ± 0.5632 Cts; miR-31, 3.81 ± 1.4758 Cts and miR-191, 2.961 ± 0.5387 Cts compared with the control sample following RT and qPCR handbook protocol (Figure 4.6, A-C). Subsequently, miR-21 was measured for three independent overnight and 4h PDE samples from GLOBAL using the optimization approaches for RNA extraction, RT and qPCR already established. As expected, 4h PDE had less miR-21 content compared with overnight PDE samples, consistent with the difficulty of measuring miRNAs in these samples without protocol optimization (Figure 4.6, D). Average 4h PDE miRNA measurement of miR-21, miR-31, miR-191 and a spiked in cel-miR-39 were in all cases lower than 35 Cts: miR-21, 32.18 ±

0.4290 Cts; miR-31, 34.64 ± 1.035 Cts; miR-191, 34.46 ± 0.2940 and cel-miR-39, 32.95 ± 0.4476 (Figure 4.7, A-B). cel-miR-39 was spiked into these samples in order to study the final consistency and uniformity of the results obtained between samples. The coefficient of variation (CV) is the standard deviation of a sample divided by the mean and is used as a measure of sample variability. CV (cel-miR-39) = 0.02, and therefore, the consistency of the process was considered to be sufficient to continue with the study (Hellemans et al, 2007). miR-31 and miR-191 were close to the 35 Ct limit of reliable qPCR detection due to high level of Ct variation when target quantities approach a single copy (Poisson distribution). Nevertheless, protocol optimization was adequate to measure miRNAs in a large study of GLOBAL samples (4h PDE exchange) in which samples reaching 35-40 Ct values would be eliminated from the analysis. Before further research was undertaken, optimization suitability of this protocol was confirmed by Dr Wim Reidt, an expert from ThermoFisher Scientific technical support.

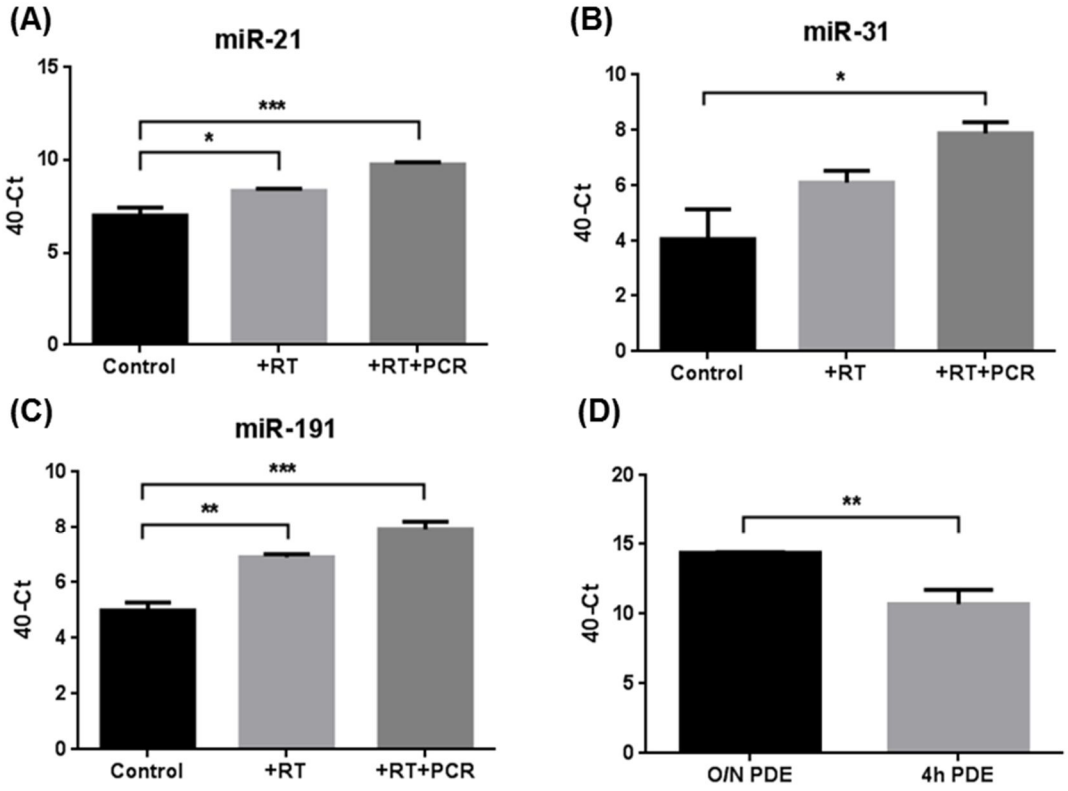

Figure 4.6. Final 4 h PDE-RNA extraction, RT and qPCR reaction optimization, GLOBAL PDE samples. (A-C) miRNA quantification using manufactures adapted protocol developed in figures 1-3 (Control), with additional diluted RNA added at the RT (+RT) and with additional diluted RT added at the PCR (+PCR) respectively. **(A)** miR-21. **(B)** miR-31. **(C)** miR-191. **(D)** GLOBAL, 4h exchange PDE miRNA expression after extraction, RT and qPCR reaction optimization compared with O/N PDE for miR-21. Data were analyzed by unpaired, two-tail, *t*-test or one-way ANOVA for matched samples followed by post-hoc Holm-Sidak's test comparing each protocol mean with the control mean. Data represent the mean S.E.M. from three independent donor experiments. *$p < 0.05$; **$p < 0.01$; ***$p < 0.005$.

(A)

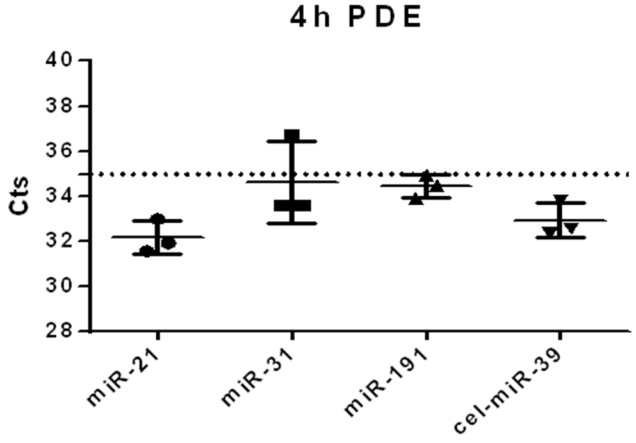

(B)

	miR-21	miR-31	miR-191	cel-miR-39
Minimum	31,59	33,60	33,94	32.40
25% Percentile	31,59	33,60	33,94	32.40
Median	31,94	33,61	34,49	32.60
75% Percentile	33,02	36,71	34,96	33.84
Maximum	33,02	36,71	34,96	33.84
Mean	32,18	34,64	34,46	32.95
SD	0,743	1,79	0,509	0.775
SEM	0,429	1,03	0,294	0.447

Figure 4.7. miRNA measurements in GLOBAL PDE, 4h exchange. GLOBAL, 4h PDE exchange miRNA expression after extraction, RT and qPCR reaction optimization. **(A)** miRNAs -21, -31, -191 and cel-miR39 quantification using manufactures adapted protocol developed in Figures 1-6. Threshold limit for RT-qPCR detection Ct=35 (dot line). **(B)** Statistical description of miRNAs selected for study. Data represent mean S.E.M. from three independent donor experiments.

4.2.7. miR-21 and miR-31 expression correlate with clinically important parameters

To assess the potential of miR-21 and miR-31 as biomarkers to monitor the maintenance of the structural integrity of the peritoneal membrane, miRNA expression was analyzed in samples from a cohort of 230 patients from the GFS. A gene maximization approach was used to design the plate layout for experiment and, therefore, the amount of samples/plate was limited by the amount of miRNAs measured. Due to the relatively high sample size of the experiment, inter-run calibrators (IRCs) were used to quantify differences between qPCR plates (Derveaux et al, 2010; Hellemans et al, 2007). IRCs comprised three independent RT-PDE samples, pre-aliquoted at the start of the analysis and present in each of the qPCR plates run in this

study. A non-template control (NTC) was also present in all plates for all miRNAs of this study. 0.5 pM of a synthetic exogenous small RNA *Caenorhabditis elegans* (cel-miR-39) was spiked into each sample (after denaturing solution addition to avoid degradation by PDE RNAses (Mitchell et al, 2008). cel-miR-39 provided an internal positive control for RNA isolation, cDNA synthesis and PCR amplification. miR-191 CV across the study was determined to show its stability and, therefore, its suitability as a reference miRNA (Hellemans et al, 2007). The goal for any reference gene is to have the smallest CV possible and, generally, a variability of less than 10-15% is acceptable. CV (miR-191) = 0.0534 (0.0539 before IRC correction) and is, therefore, a suitable reference miRNA for this study.

Table 4.1 displays baseline clinical characteristics of the patients whose samples are included in this analysis. When measured in effluent of prevalent PD patients, or more than 9 months under therapy, detection of miR-21 and miR-31 was significantly higher in comparison with incident cases (fold difference: miR-21, 3.26 x, p=0.0015; miR-31, 1.84 x, p=0.0007) (Figure 4.8, A-B). The study of expression of both miRNA according to different semesters showed a significant increase between 12-18 months of therapy compared with control, 0-6 months and a trend to increase with time (fold change: miR-21, 4.35 x, p<0.0001; miR-31, 0.93 x, p=0.0005) (Figure 4.8, C-D).

To investigate the potential relationship between miR-21 and miR-31 with parameters associated with poor PD outcome, an exploratory correlation analysis was performed (Table 4.2).This analysis was undertaken by Dr Mark Lambie and showed that both miRNAs correlated with each other *R*=0.26, although miR-21 better correlated with parameters associated with an inflammatory condition. Notably, miR-21 was found to correlate with IL-6 *R*=0.28, icodextrin use *R*=0.28, miR-31 *R*=0.26, peritonitis count *R*=0.25, urine volume *R*=-0.19, 4 hour D/P creatinine *R*=0.16, BMI *R*=0.15 and PD duration *R*=0.13. miR-31 better correlated with urine volume *R*=-0.24, dialysate glucose concentration *R*=0.22, PD duration *R*=0.19, peritonitis count *R*=0.18, and BMI *R*=0.16.

Characteristic	Patients (n=230)
Age (yr)	54.3±16.2
Body mass index (kg/m^2)	26.5±5.3
Average Dialysate glucose concentration (%)	1.56±0.38
4-hour D/P creatinine	0.75±0.15
Duration of PD (month)	2.85 (1.23, 16.19)
Albumin (g/L)	34.9±4.9
Dialysate IL-6 (pg/mL)	3.57 (0.94, 10.44)
Dialysate IFN-γ (pg/mL)	0.97 (0, 4.49)
Dialysate IL-1β (pg/mL)	0 (0, 0.072)
Dialysate TNF-α (pg/mL)	0 (0, 0.20)
Plasma IL-6 (pg/mL)	1.25 (0.67, 2.49)
Urine volume (mL)	904 (292, 1595)
Comorbidity score	1 (0, 1)
Icodextrin use (%)	36.30
Biocompatible solution use (%)	7.30
Men (%)	54.30
APD use (%)	31.20
Peritonitis count	0 (0, 0)

Table 4.1. Descriptive characteristics of 230 patients selected as a study population are summarized at the table above. Patients were selected from a single center (Stoke PD fluid) part of the GLOBAL fluid registry. Center selection was done based on better patient information registry. Data are presented as the mean ± SD, median (interquartile range), or as percentage. Data prepared by Dr Mark Lambie, responsible of Stoke PD fluid data registry.

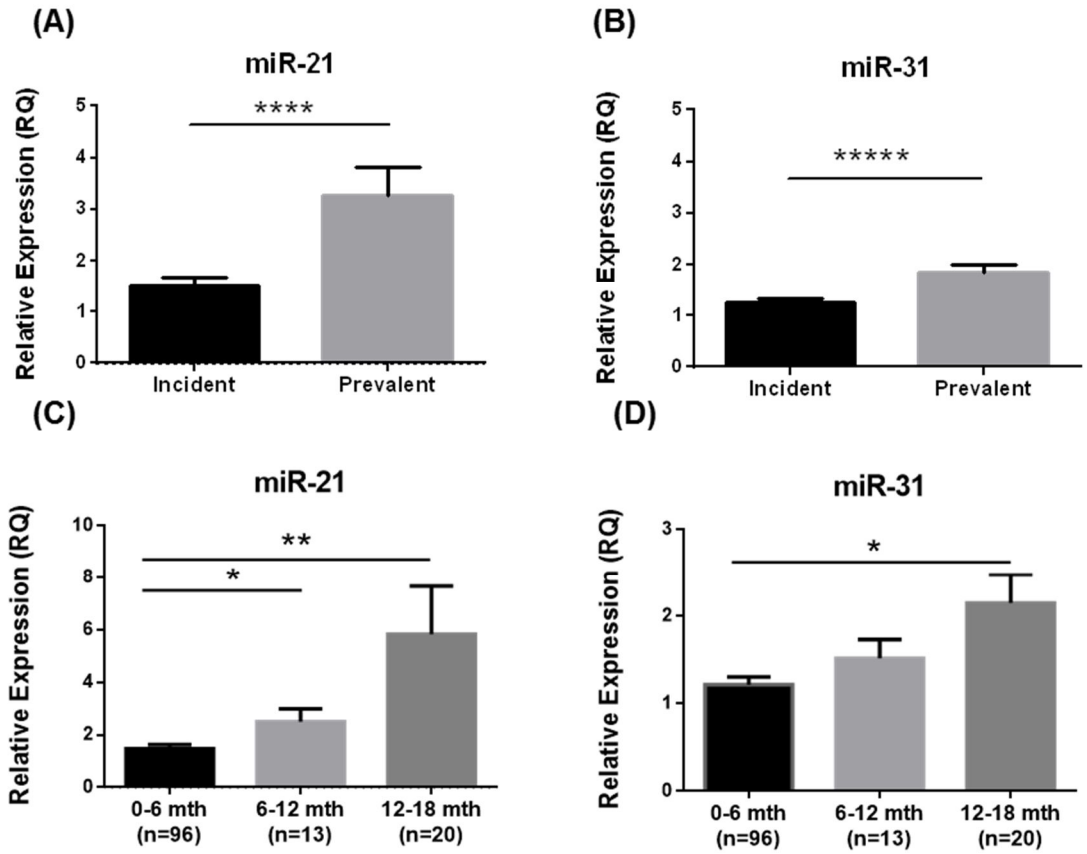

Figure 4.8. Up-regulation of miR-21 and miR-31 expression in peritoneal dialysis effluent (PDE) from PD patients (n=230). RNA from 230 PDE samples was isolated and RT-qPCR analyzed. Relative expression of miR-21 and miR-31 was normalized to miR-191 expression. **(A-B)** Prevalent PD compared with incident cases (n=230). **(A)** miR-21 up-regulation versus incident patients. **(B)** miR-31 up-regulation versus incident patients. **(C-D)** Variation in miR-21 and miR-31 expression according to different time in PD. **(C)** miR-21 expression versus 0-6 months. **(D)** miR-31 expression versus 0-6 months. Data were analyzed by unpaired, Mann-Whitney test and Kruskal-Wallis non-parametric test followed by post-hoc Dunn's test comparing the mean of each column with the mean of a control '0-6 mth' column. Data represent the mean S.E.M. from detailed n samples. *$p < 0.05$; **$p < 0.01$; ****$p < 0.001$; and *****$p < 0.0001$.

In order to understand the relevance of these variables for the described up-regulation of miR-21 and miR-31, Dr Mark Lambie performed a multivariable linear regression with backwards stepwise variable selection for all parameters included in Table 4.2 and each miRNA (Table 4.3 and 4.4). Consequently, stepwise variable selection determined a group of tighter risk factors that associated with each miRNA in predicting PD outcome. miR-21 better associated with dialysate icodextrin usage *R*=0.52, (95% confidence intervals 0.20, 0.84), peritonitis count *R*=0.16, (0.03, 0.29), miR-31 *R*=0.52 (0.15, 0.90) and dialysate cytokines (Table 3). On the other hand, miR-31 showed little associations with biocompatible solution use *R*=0.18 (-0.04, 0.40), use of CAPD vs APD *R*=0.14 (0.02, 0.25), miR-21 *R*=0.087 (0.038, 0.136), peritonitis count *R*=0.052 (0.006,

0.098), plasma albumin *R*=0.0096 (-0.001, 0.020) and urine volume *R*=-0.0001 (-0.00017, -0.00003 (Table 4.4). These results indicate that both miRNAs correlate with clinical parameters that have been described to be important in triggering the MMT process associated with PD therapy.

Variable	miR-31	miR-21
miR-21	0.26[c]	
Age	0.05	0.03
Body mass index	0.16[a]	0.15[a]
Dialysate glucose concentration	0.22[b]	0.04
4-hour D/P creatinine	0.13	0.16[a]
Duration of PD	0.19[b]	0.13[a]
Albumin	0.03	-0.10
Dialysate IL-6	0.04	0.28[c]
Dialysate IFN-γ	0.09	-0.10
Dialysate IL-1β	0.00	0.006
Dialysate TNF-α	0.05	0.04
Plasma IL-6	0.00	0.11
Urine volume	-0.24[c]	-0.19[b]
Comorbidity	0.03	0.02
Icodextrin use	0.00	0.28[c]
Biocompatible solution use	0.08	0.10
Gender	0.09	-0.02
Type of PD	0.06	-0.10
Peritonitis count	0.18[b]	0.25[c]

Table 4.2. PDE miR-21 and miR-31 correlation with clinically important parameters (n=230). Preliminar exploratory correlation analysis. Both miRNAs correlate with each other, although miR-21 seemed to better correlate with parameters associated with an inflammatory condition which encouraged us to perform a deeper statistical analysis. Statistical analysis was conducted by Dr Mark Lambie, responsible of Stoke PD fluid data registry. [a]$p<0.05$, [b]$p<0.01$, [c]$p<0.001$.

Variable	Coefficient (95% Confidence Interval)	p value
Icodextrin Usage	0.52 (0.20, 0.84)	0.002
Peritonitis Count	0.16 (0.03, 0.29)	0.015
Dialysate IL-6	0.28 (-0.02, 0.58)	0.065
Dialysate TNF-α	0.86 (-0.61, 2.34)	0.25
Dialysate IFN-γ	-0.77 (-1.21, -0.33)	0.001
Dialysate IL-1β	0.69 (-0.89, 2.27)	0.39
miR-31	0.52 (0.15, 0.90)	0.006
Body Mass Index	0.027 (-0.0004, 0.054)	0.053

Table 4.3. Multivariable Regression of miR-21 (n=230). To understand the relevance of all parameters included in Table 2 for the described up-regulation of miR-21 multivariable linear regression with backwards stepwise variable selection was performed. Stepwise variable selection determined a group of tighter risk factors that associated with miR-21 in predicting PD outcome that are detailed at the table above. The predicted variable, miR-21, was log transformed. Statistical analysis was conducted by Dr Mark Lambie, responsible of Stoke PD fluid data registry.

Variable	Coefficient (95% Confidence Interval)	p value
Peritonitis Count	0.052 (0.006, 0.098)	0.028
miR-21	0.087 (0.038, 0.136)	0.001
Biocompatible solution usage	0.18 (-0.04, 0.40)	0.114
Plasma Albumin	0.0096 (-0.001, 0.020)	0.077
Urine volume	-0.00010 (-0.00017, -0.00003)	0.003
Use of CAPD vs APD	0.14 (0.02, 0.25)	0.023

Table 4.4. Multivariable Regression of miR-31 (n=230). To understand the relevance of all parameters included in Table 2 for the described up-regulation of miR-31 multivariable linear regression with backwards stepwise variable selection was performed. Stepwise variable selection determined a group of tighter risk factors that associated with miR-31 in predicting PD outcome that are detailed at the table above.The predicted variable, miR-31, was square root transformed. Statistical analysis was conducted by Dr Mark Lambie, responsible of Stoke PD fluid data registry

4.2.8. TGF-β1 signalling is activated, and miR-21 and miR-31 expression is increased, in PD patient peritoneal membrane biopsies

Next, whether changes in activation of TGF-β1 signalling and miR-21 and miR-31 expression could be observed in the mesothelial cell layer of patients undergoing PD was analyzed. In order to evaluate the effects of the therapy, distinct from associated vascular pathology or other comorbidity that may be present in biopsies from adult patients, samples from the International Pediatric Membrane Biopsy Registry were kindly selected by ESR Maria Bartosova and studied in collaboration with her. Children undergoing PD with conventional and with biocompatible fluids were examined, and compared with uraemic and non-uraemic controls (n=11 per group, mean age at biopsy: PD conventional 9.1 years, PD biocompatible 8.9 years, control uraemic 9.6 years, control non-uraemic 8.0 years; mean duration of PD: PD conventional 30 months, PD biocompatible 31 months). SMAD2 and SMAD3 phosphorylation was determined, as a measure of TGF-β1 activity. Phospho-SMAD2/3 staining of formalin-fixed paraffin embedded (FFPE) samples were measured using Aperio Precision Image Analysis Software and a count algorithm for positive pixel detection (Figure 4.9A). The mesothelial and submesothelial compact zone of PD patients displayed enhanced TGF-β1 pathway activation compared with controls and uraemic (Figure 4.9, A-B). Significant p-SMAD2/3 enhanced expression was observed in the mesothelium of PD patients under conventional PD fluid treatment compared with healthy controls (Figure 4.9B). miRNA analysis of manually micro-dissected FFPE samples also showed an increase in miR-21 expression at the mesothelium of PD patients compared with healthy and uraemic controls (Figure 4.9C). Due to a high variability between samples in the control group, no difference was seen between healthy controls and PD patients in miR-31 peritoneal membrane expression. However, a trend of up-regulation in miR-31 expression was observed between uraemic controls and PD patients (Figure 4.9D). These results demonstrate that PD therapy is associated with TGF-β1 signalling pathway activation, as well as the expression of miR-21 and miR-31, in the peritoneal membranes of PD patients.

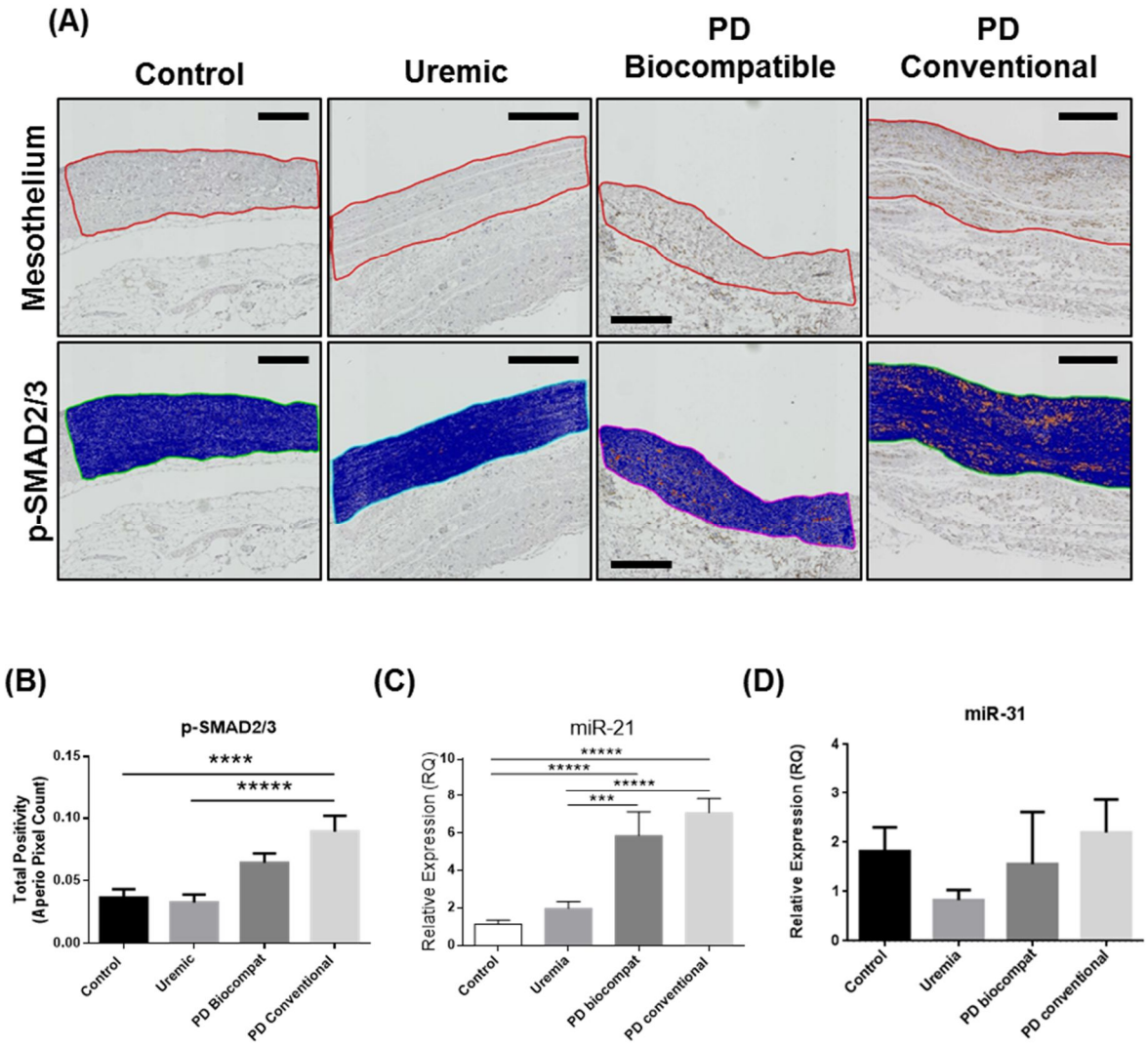

Figure 4.9. Expression of p-SMAD2/3, miR-21 and miR-31 in 44 biopsies from the International Pediatric Membrane Biopsy Registry. Formalin-fixed paraffin embedded (FFPE) samples were p-SMAD2/3 stained and manually macro-dissected to measure relative miRNA expression. miR-21 and miR-31 expression was analyzed by RT-qPCR and normalized to miR-191 expression. Histological image analysis using Aperio Precision Image Analysis Software. **(A)** Mesothelial and submesothelial compact zone selection (upper panel) and p-SMAD2/3 detection of the area of interest by the Aperio positive pixel count algorithm (lower panel). Negative background is showed in blue and positive p-SMAD2/3 detection is showed in yellow-orange. Scale bar, 300 µm. **(B)** Level of p-SMAD2/3 staining was defined using a count algorithm for positive pixel detection. Conventional PD P-SMAD2/3 was up-regulated versus healthy controls and uraemic controls. **(C)** Conventional and biocompatible PD miR-21 was up-regulated when compared with control and uraemic patients. **(D)** miR-31 up-regulation was ns. Data were analyzed by one- way ANOVA followed by post-hoc Holm-Sidak's test. Data represent mean S.E.M. from eleven age-matched samples and equal average PD duration between PD groups. ***p<0.005; ****p<0.001 and *****p<0.0001.

4.3. Discussion

PD is an effective form of renal replacement therapy. Unfortunately, it is often limited by deterioration in the structural and functional characteristics of the peritoneal membrane. New biomarkers are needed, to help individualize PD therapy, to serve as appropriate surrogates in clinical trials, and to guide the development of innovations in the therapy. These data showed that miR-21 and miR-31 level of expression are increased in different, well-established models associated with structural and functional alterations of the peritoneal membrane during peritoneal dialysis (see Chapter 3). Moreover, both miRNAs can be measured in the peritoneal dialysis effluent from PD patients where they correlate with valuable clinical parameters indicating poor PD outcome.

An important challenge of measuring miRNAs by RT-qPCR from PDE was the high dilution of the miRNA contained in the sample. The first research objective approached was, therefore, to develop an optimal approach for RNA purification to maximise the recovered miRNA fraction. An approach based on use of the *mirVana* PARIS kit for miRNAs purification, using four steps of optimisation was established and included (i) total RNA eluted from *mirVana* PARIS kit (column A) which contained a miRNA amount nearly twice of that eluted by *miRNeasy*, (ii) interphase/organic-phase re-hydration and phenol-chloroform re-extraction of the sample which increased the eluted miRNA concentration by 1.44 Cts, (iii) a 40 min, cold, Speed-Vac (SV) step which enlarged the miRNA fraction by 1.7 Cts; while (iv) addition of MS2 RNA carrier RNA did not further improve the yield. Surprisingly, the highest miRNA eluted from *mirVana* PARIS kit was found in column A, which according to the handbook protocol is better at recovering large RNAs (>200 nt) rather than in column B, which is meant to collect small RNAs (<200 nt) (Figure 4.2D and 4.3A). This issue was discussed with Dr Wim Reidt, a technical support specialist from ThermoFisher scientific, who explained that this result was probably due to the pH and the nature of the samples used for experiment. This theory could be validated performing a re-extraction of the samples using the two columns' protocol recommended by the manufacturer, and would expect to find higher miRNA

levels at the column B. Nevertheless, this question was finally considered to be beyond the purposes of this thesis and that line of investigation did not continue.

An additional limitation of optimizing *Qiagen miRNeasy* for miRNA purification is its size exclusion of miRNA species lower than 18 nt. This restriction would not affect the study developed in this thesis as miRNA species of interest are: miR-21 (22 nt), miR-31 (21 nt) and; miR-191 (23 nt). Nevertheless, an examination of human miRNAs described demonstrated that ~ 68 human miRNAs are smaller than 18 nt, constituting ~ 3% of all mature miRNA catalogued until now (miRBase; October 2012). Current research held at the department uses the PD effluent RNA extraction method developed in this chapter to address new experimental questions (see Chapter 6). Future research may include the measurement of miRNA species lower than 18 nt and, therefore, optimizing *Qiagen miRNeasy* was discarded as alternative.

Further protocol optimizations were introduced at the RT and qPCR step by eliminating the water and adding the remaining extra volume with isolated diluted RNA and diluted RT respectively. TaqMan miRNA assays were evaluated for amplification efficiency performance after adding an extra volume of isolated RNA and an extra volume of PDE-RNA transcribed to the PCR step. The changes introduced showed not to inhibit the PCR reaction neither to affect the accuracy of the measurements. Indeed, PCR efficiency was found to be better when higher volumes of RT product were added to the PCR reaction (88.34% PCR efficiency with 9 µl while 84.54% with 3 µl). This was due to better chemistry performance when samples are farther from the limit of RT-qPCR detection (Figure 4.5). After protocol optimization 4 h PDE miRNA measurement were in all cases lower than 35 Cts and, therefore, adequate to measure miRNAs in a large study comprising GLOBAL samples. The possibility of studying PDE miRNA expression in an animal model of the disease in which 5/6 nephrectomy was combined with PD in mice has also drawn attention during this project (see Chapter 2 and 3). Nevertheless, PDE samples are further limited when acquired from mice models. PDE obtained from the last PD exchange was, in all cases about 100 µl in the mice model and, unfortunately, did not allow us to get a reliable miRNA measure below the limit of qPCR detection.

PDE samples from the GFS were frozen down and conserved at -80° C (see Chapter 2). The GFS kept no record regarding the number of thawing-refreezing cycles the samples suffered. This issue has been reported to the manager of the study and it is now recorded and considered to be an important factor. For this study, the highest filled aliquots were chosen for each of the PDE samples needed. An estimation of 2-3% of the samples used for the study had probably been defrosted before. Extracellular miRNAs have been shown to be very stable along numerous thawing-refreezing cycles in different body fluids and, together with the small numbers that these samples represented, this factor was not considered a major limitation for this study (Mitchell et al, 2008). Nevertheless, fresh frozen PDE from different patients has been collected, frozen down and conserved at -80° C. This was done in case future studies using PDE samples from the GFS require an analysis of the specific effect of different thawing-refreezing cycles on these samples. Considering that the aim of this study was to evaluate the possibility of using PDE derived miRNAs to monitor peritoneal membrane MMT during PD therapy, a more clinically relevant parameter to analyse was PDE miRNA stability at room temperature. Newly, extracellular miRNAs have already been proven to be very stable at room temperature, for up to 24 h, in different body fluids (Mitchell et al, 2008). This analysis was important for us for two reasons: (i) to confirm that PDE from the GFS was collected within a reasonable processing timescale for miRNA detection and; (ii) to validate the bedside feasibility of the technique. The miRNAs of study and, likely, other miRNAs, were stable in PDE without need of a special handling within a reasonable time-scale of < 8 h.

The population under study presented here was designated with Dr Mark Lambie, and the sample size analyzed was the maximum feasible by the chosen registry (n=230). The samples analyzed were in all cases the first sample collected from each patient and a single institute was used to exclude centre effects. Van de Luijtgaarden et al. 2011 analyzed PD population characteristics in seven European renal registries (van de Luijtgaarden et al, 2011). PD population baseline characteristics reported (BCR) by van de Luijtgaarden et al. 2011 recalculated from their paper and compared with the population of study (PS) here are: age, mean ± SD (BCR, 58±16; PS, 54.3±16.2); males, % (BCR, 63; PS, 54.30) and comorbidity count, median (interquartile range) (BCR: 1 (0,1);

PS, 1 (0,1). In general, PS population was 4 years younger and had 8.7% less males while comorbidity score remained the same than BCR. Education, clinical guidelines and transplant activity may be factors explaining these divergences, which were considered minor for this study. Of note, excluding Sweden, the remaining European countries studied by van de Luijtgaarden et al. 2011 were less prone to choose PD as a therapy compared to the UK (van de Luijtgaarden et al, 2011).

An important robustness of this research is that it is founded on an extensive PD population combining both, incident and prevalent patients, from a deep-seated, high quality cohort. There were, nevertheless, some limitations. A randomized clinical study reporting the outcomes of PD therapy is not only unfeasible but also unethical (Korevaar et al, 2003). Despite this, randomized trials are the only system to elude confounding by prescription, which happens when specialists choose patients for a single therapy due to particular arguments. In this investigation, additional data potentially relevant for us like TGF-β1 dialysate cytokine levels was lacking. The dialysate cytokine levels used for the correlations reported here were those previously measured in Lambie et al. 2013 by electrochemiluminescence and did not include TGF-β1 (Lambie et al, 2013). Of note, active TGF-β1 dialysate cytokine levels may highly differ from those read by HPMCs due to multiple variables including (i) level of TGF-β1 expression, (ii) ligand trapping molecules that control the formation of molecule gradients, (iii) mediators of ligand traps release, (iv) antagonistic ligands, (v) ligand-receptor TGF-β1 presentation via accessory proteins, and (vi) the combination of expressed signalling receptor molecules. Indeed, there have been few attempts to measure TGF-β1 from PD effluent samples from patients (Gangji et al, 2009; Jones et al, 2001; Kinashi et al, 2013; Lai et al, 1999; Zweers et al, 1999). Overall, the number of patients included in these studies are low and TGF-β1 concentrations reported are not consistent between groups. Nevertheless, TGF-β1 levels are, in all cases, increased in long term PD patients. Instead, mesothelial and submesothelial TGF-β1 pathway activation in an independently matched cohort of peritoneal biopsies from the International Pediatric Membrane Biopsy Registry was studied, and TGF-β1 pathway activation was associated with miRNA expression (Figure 4.9B). Of note, peritoneal mesothelial and sub-mesothelial pSMAD2/3 was not measured here in combination of further HPMCs markers and may indicate TGF-β1

pathway activation in cells from different origin including activated fibroblasts and macrophages.

The existence of extracellular miRNAs in 4 h PDE samples and miRNA correlations with important clinical parameters associated to the progression of the MMT process may represent a golden goose of non-invasive biomarkers in PD therapy. Considering that miRNA deregulation is an early episode in the MMT associated to PD (Figure 3.9), the determination of PDE miRNA levels may be valuable in unmasking peritoneal MMT, which can help to individualize PD therapy. This research showed for the first time that miR-21 and miR-31 expression was up-regulated in PDE from prevalent compared to incident PD patients (Figure 4.8, A-B). When miRNA expression was plotted by semesters the results were consistent with those previously described by Del Peso et al. 2008 reporting an increase in prevalence of submesothelial fibrosis and MMT according to different semesters (Del Peso et al, 2008). It is noteworthy that the fourth semester, in which MMT was remarkable higher in Del Peso et al. 2008 studies, has not been included here due to low sample size (n=2).

Multivariable linear regression with backwards stepwise variable selection for all parameters included in Table 4.2 and each miRNA was performed to understand the relevance of miRNA correlations with parameters associated to the MMT process. Both miRNAs showed to correlate with each other. miR-21 expression was associated with peritonitis count and dialysate IFN-γ, as well as with IL-6, TNF-α and IL-1β. IFN-γ has been shown to regulate the secretion of IL-6 by mesothelial cells (McLoughlin et al, 2003), which are the major producers of IL-6 within the peritoneal cavity (Topley et al, 1993; Witowski et al, 1996). It is also known that TNF-α or IL-1β stimulation of HPMCs results in a time and dose dependent increase in IL-6 production (Topley et al, 1993). IL-1β stimulation of HPMCs can also be synergistically enhanced by the simultaneous presence of IFN-γ (McLoughlin et al, 2003). *In vivo*, although IFN-γ alone had no significant effect on intraperitoneal IL-6 secretion, co-administration with IL-1β resulted in synergistic increase of intraperitoneal IL-6 levels (McLoughlin et al, 2003). IL-6-type cytokines endeavor their response *via* gp130, which is their universal signal-transducing receptor subunit (Ernst & Jenkins, 2004; Heinrich et al, 2003). HPMCs lack expression of IL-6 receptor (IL-6R) and require soluble IL-6R (sIL-6R) to trigger IL-6 response, inducing

gp130 activation and selectively regulating STAT3 which is a transcription factor critical for transformation (McLoughlin et al, 2004). miR-21 is controlled by an upstream enhancer containing two, evolutionary conserved, STAT3 binding sites (Löffler et al, 2007). Indeed, miR-21 induction by IL-6 has been reported to be strictly dependent on STAT3 in a broad range of models including multiple myeloma, mammary epithelium, hepatocellular carcinoma (HCC), oral squamous cell carcinoma and keratinocytes (Chen et al, 2015; Iliopoulos et al, 2010; Lu et al, 2015; Löffler et al, 2007; Zhou et al, 2014). STAT3 is, therefore, not merely an IL-6 effector, but combined with miR-21 and its multiple downstream tumour suppressor targets, is an important element linking inflammation to epigenetic changes and cell transformation.

Ongoing efforts are being made to improve PD biocompatibility. Nevertheless, the long-term benefits of biocompatible solutions remain controversial (Blake et al, 2013; Johnson et al, 2012). Icodextrin is a high molecular weight glucose polymer created as a substitute for dextrose as an osmotic agent during PD. Icodextrin levels of advanced glycation end products (AGEs) resulting from glucose degradation products (GDPs) are low compared with standard PDF. AGEs induce TGF-β1 expression among other cytokines *via* the receptor for advanced glycation end products (RAGE) and promote MMT transformation. Indeed, anti-RAGE blocked TGF-β1 up-regulation and submesothelial fibrosis in rat peritoneum (De Vriese et al, 2003). This research show that miR-21 expression in PDE correlates with icodextrin use and that TGF-β1 and miR-21 expression are up-regulated in peritoneal biopsies from PD patients. This is also the case when using biocompatible PD solutions (Figure 4.9, A-C) indicating the necessity to further improve the solutions in use. Interestingly, this study have also shown a low correlation between miR-21 and BMI. miR-21 has also been involved in the regulation of adipogenic differentiation, is highly expressed in adipose tissue and positively correlates with BMI (Keller et al, 2011). Conversely, long-term inhibition of miR-21 has led to a reduction of obesity in db/db mice (Seeger et al, 2014).

miR-31 also associates with biocompatible solution usage and peritonitis count. miR-31 is up-regulated in psoriasis and esophageal squamous cell carcinoma, two inflammatory associated diseases where regulates cytokine/chemokine expression by targeting *STK40*, a negative regulator of NF-κB signalling (Taccioli et al, 2015; Xu et al,

2013). It has been reported that APD has various advantages compared with CAPD comprising peritonitis incidence, greater solute clearance and lower hernia incidence (Rabindranath et al, 2007). In this regard, this study showed a correlation between miR-31 expression and the use of CAPD versus APD. Rabindranath et al. 2007 described three randomized controlled trials (RTCs) comparing continuous ambulatory peritoneal dialysis (CAPD) with all forms of automated peritoneal dialysis (APD) (Rabindranath et al, 2007). APD showed significantly lower peritonitis rates compared to CAPD (two trials, 107 patients, rate ratio 0.54 95% CI 0.35-0.83) and hospitalization rate (one trial, 82 patients, rate ratio 0.60, 96% CI 0.39-0.93). In a more recent study comparing CAPD and APD outcomes; patient survival appeared to be higher in the latter group although this could not be explained by differences in infections episodes (Cnossen et al, 2011). Nevertheless, more studies are needed to address the controversy associated to the possibility of considering peritoneal modality itself as a risk factor for inflammation, peritonitis and technique survival.

Different groups demonstrated that uraemic conditions lead to mesothelial thickening and moderate vasculopathy suggesting that uraemia causes inflammation and peritoneal membrane remodeling (Fusshoeller, 2008; Williams et al, 2002). Due to a high variability between samples, no difference was observed between healthy controls and uraemic patients when miR-31 peritoneal membrane expression was studied while miR-21 showed an expected trend to increase with uraemia (Figure 4.9, C-D). Both miRNAs displayed a trend of up-regulation in peritoneal membrane biopsies when uraemic and PD patients where compared (Figure 4.9, C-D). Although both miRNAs negatively correlated with urine volume in an exploratory correlation analysis, multivariable linear regression showed that miR-31 better correlated with urine volume when analyzed in PDE from patients. Vascular endothelial growth factor (VEGF) and inflammatory cytokines including interleukin (IL)-1β and tumor necrosis factor-alpha (TNF-α) are significantly up-regulated in uraemic patients and may cooperate deregulating local inflammatory microenvironment and leading to mesothelial thickening during PD.

Fibro-proliferative changes have been determined in the peritoneal membrane of PD patients, together with minor changes in uraemic (pre-dialysis) patients

(Fusshoeller, 2008; Williams et al, 2002). Peritoneal vascular changes are also frequently evident in adult patients, which may make it difficult to separate therapy-induced alterations from those related to the propensity of individuals with CKD to accelerated cardiovascular disease. At the time of PD onset the pediatric peritoneal tissue is devoid of vascular alterations. In order to determine the 'pure' effects of the therapy, pediatric biopsy samples were examined, from the International Pediatric Peritoneal Biopsy Registry. TGF-β1 signalling was clearly evident in biopsies from PD patients compared to controls, and was associated with increased miR-21 and miR-31 in the mesothelial and submesothelial zones. Given recent fate mapping studies, which have delineated an important contribution of submesothelial fibroblasts to peritoneal fibrosis in mouse models (Chen et al, 2014), understanding the potential role of miRNAs including miR-21 and miR-31 to submesothelial fibroblast phenotype may also be an important future area of study.

It is important to note that although both miRNAs are up-regulated by TGF-β1 in this context, they may have different specific roles during the MMT process. A given miRNA can regulate the expression of hundreds of mRNAs. Moreover, target mRNAs may be simultaneously controlled by multiple miRNAs rather than by the action of a single miRNA alone. This creates a complex network in which several miRNA-regulated pathways cooperate to promote profound and specific effects in cell phenotype and function during the progression of the disease. In this research, the miRNAs under study correlated with different parameters associated with patient outcome during PD therapy (Table 4.3 and 4.4). It is likely that underlying this is a distinct regulatory contribution from each miRNA, and further study developed in Chapter 5 will help to define specific targets and pathways regulated by miRNAs in this context that may be important for the MMT process.

Recently it was shown that exosomes participate in different biological functions including angiogenesis, cell proliferation, tumour cell invasion or immune response to neighboring or distant cells. It has also been shown that in diverse biological functions, protein, mRNA and miRNAs are transferred between cells in a selective way and functionally active extracellular miRNAs can be taken up and affect gene expression in the recipient cells. Interestingly, it was shown that the exosome RNA profile is different

from the RNA profile of the parental cells, suggesting that this packing is selective. Urine exosomal miRNAs have been previously studied at this laboratory by Dr Cristina Beltrami, nevertheless, due to time limitations during the development of this thesis exosomal miRNAs were not evaluated in PDE neither in urine from PD patients.

There are no other PD-related miRNA studies up to date that had analyzed miRNAs at PD effluent supernatant although some authors measured miRNAs in total PDE or cells from patients (Chen et al, 2012a; Xiao et al, 2015; Zhang et al, 2012). In this study, miR-21 and miR-31 correlated with each other and with different clinically important parameters including residual renal function, icodextrin usage, dialysate cytokine levels, peritonitis count preceding sample collection and therapy modality. In conclusion, these data identify miR-21 and miR-31 as potential biomarkers to monitor the peritoneal membrane of patients undergoing PD therapy.

Chapter 5 – Determination of miRNAs function in peritoneal mesothelial MMT

5.1. Introduction

The role of a given miRNA is determined through the mRNAs that targets as well as by its regulatory influence on their expression. Bioinfomatic target prediction algorithms are used to identify mRNAs containing miRNA-specific regulatory binding sites, but present techniques yield many putative targets, and lack precision. *In silico* putative target prediction approaches used for this study combine several characteristics to determine whether a miRNA can regulate certain mRNAs and are summarized in Table 2.7. Briefly, miRNA target algorithm features include (i) miRNA 5' seed region (bases 2 – 8) sequence complementarity with mRNA target gene 3'UTR, (ii) sequence conservation, (iii) mRNA/miRNA thermal stability, (vi) site accessibility, and (v) number of target sites. Additional characteristics are contemplated by different algorithms and distinct weight may be attributed to similar parameters, meaning that different algorithms yield overlapping but distinct pools of predicted targets, and that combined analysis employing several algorithms may be effective.

Accordingly, genuine knowledge on miRNA and gene sequence may be enough to predict a large number of targets. However, these approaches originate lists of candidate targets that contain a relatively high amount of false-positives, false-negatives and indirect targets while missing some real targets. Additionally, miRNA target expression regulation is dependent on several further factors comprising (i) miRNA:target pool ratio (Bosson et al, 2014), (ii) miRNA:target site affinity pool ratio (Bosson et al, 2014), (iii) cell type specific UTR binding co-factors, and (vi) regulatory site elimination due to alternative cleavage and/or polyadenylation (Sandberg et al, 2008). Thus, the pure existence of a miRNA binding site is not enough for expecting mRNA regulation and determining mRNA targets to define specific miRNAs function is, undoubtedly, one of the most challenging parts of miRNA research.

Consequently, the research developed in this chapter firstly studied (i) the possibility of involving previously characterized miR-21 and miR-31 targets as contributors in peritoneal mesothelial cells MMT process. Secondly the study performed here used (ii) putative target predictions in order to identify new targets for the identified miRNAs and context of interest. Finally, once miRNA:target interplays were selected for subsequent study, different methods were used to confirm *in silico* target predictions including (iii) miRNA:target measurement

and inverse correlation, (iv) miRNA:target deep sequence analysis, (v) use of miRNA mimic and inhibitor molecules, and (vi) differential 3'UTR reporter gene analysis for candidate sequences.

5.2. Results

5.2.1. miR-21 may contribute to the MMT process by targeting *PDCD4, SPRY1* and/or *PTEN* while miR-31 may participate by targeting *LATS2* and *STK40* in HPMCs

TGF-β1 promotes EMT while up-regulating miR-21 in a wide spectrum of cell types. miR-31 may also be involved in this process. To understand the biological mechanism by which miR-21 and miR-31 up-regulation may lead to MMT and fibrosis in HPMCs the expression of putative target genes previously reported in the literature was studied. miR-21 has been shown to down-regulate numerous targets in different contexts including (i) programmed cell death protein 4 (*PDCD4*) (Asangani et al, 2008; Brønnum et al, 2013; Yao et al, 2011), (ii) Sprouty homologue 1 (*SPRY1*) (Brønnum et al, 2013; Thum et al, 2008), (iii) phosphatase and tensin homolog (*PTEN*) (Dey et al, 2012; Meng et al, 2007) contributing to mesenchymal phenotype and stimulating cell motility, migration and invasion. On the other hand, it has been demonstrated that miR-31 can directly regulate (i) large tumour suppressor kinase 2 (*LATS2*) (Mitamura et al, 2014), and (ii) serine/threonine kinase 40 (*STK40*) (Xu et al, 2013) stimulating transformation and invasion while up-regulating the production of inflammatory mediators. Bioinformatics prediction showed that the 3'UTRs of *PDCD4*, *SPRY1* and *PTEN* have a conserved target site for miR-21 while the 3'UTRs of *LATS2* and *STK40* perfectly matched with the seed region of miR-31 (Figure 5.1). In addition, 3'UTR reporter activity has also been used in different cell lines for these genes *PDCD4* (Asangani et al, 2008; Brønnum et al, 2013; Yao et al, 2011), *SPRY1* (Brønnum et al, 2013; Thum et al, 2008), *PTEN* (Dey et al, 2012; Meng et al, 2007), *LATS2 (Mitamura et al, 2014)* and *STK40* (Xu et al, 2013).

(A)

```
                 *  * **   ********* **   **
Human            GAAUAUUCUAAUAAGCUACCUUUUGUAA
Chimpanzee       GAAUAUUCUAAUAAGCUACCUUUUGUAA
Rhesus           GAAUAUUCUAAUAAGCUACCUUUUGUAA
Rabbit           GAAUAUUCCAAUAAGCUACCUUUUGUAA
Mouse            GG-UGUUCUGAUAAGCUACUUUC--UAA
Rat              GGGUGUUCUGAUAAGCUACUUUC--UAA
Cow              GGAUAUUCUCAUAAGCUACCUUUUGUAA
Horse            GAAUAUUCUCAUAAGCUACCUUUUGUAA
Dog              GAAUAUUCUCAUAAGCUACCUUUUGUAA
Elephant         GAAUAUUAUAAUAAGCUACCUUUUGUAA
```

(A')

(*PDCD4*,Target Position 220-248)

```
     5'  G           A        3'
          AAUAU   UCU AUAAGCUA
          ||.||   ||| ||||||||
          UUGUA   AGA UAUUCGAU
     3' AG     GUC   C        5'
```

(miR-21)

(B)

```
                  *****  ********* *  * ****
Human            UUGCUU--AAAUAAGCUAUG-UAUUAAA
Chimpanzee       UUGCUU--AAAUAAGCUAUG-UAUUAAA
Rhesus           UUGCUU--AAAUAAGCUAUG-UAUUAAC
Rabbit           UUGCUUUUAAAUAAGCUAUG-UGUUAAA
Mouse            GUGCUU--AAAUAAGCUAUA-UAUUAA-
Rat              GUGCUU--AAAUAAGCUAUA-UAUUAA-
Cow              UUGCUU--AAAUAAGCUAUA-UAUUAAA
Horse            UUGCUU--AAAUAAGCUGUG-UAUUAAG
Dog              UUGCUU--AAAUAAGCUAUGGUAUUAAG
Elephant         UUGCUU--AAAUAAGCUAUG-UAUUAAA
```

(B')

(*SPRY1*,Target Position 393-421)

```
5' AG    U   UAA   CUUAA         3'
     CAAC GUU   UUG     AUAAGCUA
     |||| .|.   .||     ||||||||
     GUUG UAG   GAC     UAUUCGAU
3'  A        UCA                5'
```

(miR-21)

(C)

```
                 *   *  *   *    *  *    **
Human            C--UGGUUGUUAAGCUAGGUAUUUUGA
Chimpanzee       C--UGGUUGUUAAGCUAGGUAUUUUGA
Rhesus           C--UGGUUCUUAAGCUAGAUAUUUUGA
Rabbit           C--UGGUUCUUAGGUGAGCUAUUUUGA
Mouse            C--UGACUCUAAAUGUAGUUGCUCUGU
Rat              C--UGGCUAUUAAUUUAGUUGCUCUGC
Cow              CUUUGGUUUUUAAGUUAGCUAUGUUGA
Horse            CUUUGGUUCUUAAGUUACCUAUUUUGA
Dog              CAUUGGUUCUUAAGUUAGCUGU-UUGA
Elephant         CUUCGGGUCCUAAGUUAGCUAUUUUGA
```

(C')

(*PTEN*,Target Position 1599-1607)

```
    5' A    UACUA    UA       3'
        CAAC      UUG  AAGCUA
        ||||      .||  ||||||
        GUUG      GAC  UUCGAU
    3' A    UAGUCA   UA       5'
```

(miR-21)

(D)

```
                   * *** * ******************
Human            -AUUACCAUAUCUUGCCAUUCACAGCAG
Chimpanzee       -AUUACCAUAUCUUGCCAUUCACAGCAG
Rhesus           -AUUACCGUAUCUUGCCAUUCACAGCAG
Rabbit           -AUCACCGUAUCUUGCCAUUCACAGCAG
Mouse            -AU-ACCGUAUCUUGCCAUUCACAGCAG
Rat              -GUUACCGUAUCUUGCCAUUCACAGCAG
Cow              CGUGACCGUGUCUUGCCAUUCACAGCAG
Horse            -AUUACCAUAUCUUGCCAUUCACAGCAG
Dog              -AUUACCAUAUCUUGCCAUUCACAGCAG
Elephant         -AUUACCGUAUCUUGCCAUUCACAGCAG
```

(D')

(*LATS2*,Target Position 668-696)

```
      5' UA            A 3'
          CCA UAUCUUGCC
          ||| .||||||||
          GGU GUAGAACGG
      3'  C   C        A 5'
```

(miR-31)

(E)

```
                                  ******************
Human            UGGAUGCCCGUCUUGCCAG.UGGGGCCACCUCUUGCCAG
Chimpanzee       UGGAUGCCCGUCUUGCCAG.UGGGGCCACCUCUUGCCAG
Rhesus           UGGAUGCCCGUCUUGCCAG.UGGGGCCACCUCUUGCCAG
Rabbit           -------------------.UGGGGCCACCUCUUGCCAG
Mouse            UGGAUGCCCGUCUUGCCAG.UGGGGCCACCUCUUGCCAG
Rat              UGGAUGCCCGUCUUGCCAG.UGGGGCCACCUCUUGCCAG
Cow              UGGAUGCCCGUCUUGCCAG.UGGGGCCACCUCUUGCCAG
Horse            UGGAUGCCUGUCUUGCCAG.UGGGGCCACCUCUUGCCAG
Dog              UGGAUGCCGGUCUUGCCAG.UGGGGCCACCUCUUGCCAG
Elephant         UGGAUGCCCGUCUUGCCAG.UGGGGCCACCUCUUGCCAG
```

(E')

(*STK40*,Target Position 2574-2602)

```
5' A   GG                A 3'
    AGU  AUGCC  CGUCUUGCC
    ||.  |||||  |.|||||||
    UCG  UACGG  GUAGAACGG
3'     A      UC         A 5'
```

(*STK40*,Target Position 2897-2925)

```
    5' G    C         A 3'
        GCCA C UCUUGCC
        |||| | |||||||
        CGGU G AGAACGG
    3' A    C U       A 5'
```

(miR-31)

Figure 5.1. miR-21 and miR-31 3'UTR target site conservation for *PDCD4, SPRY1, PTEN* and *LATS2, STK40* respectively across different animals. (A-E) Target sequences were acquired using TargetScan and alignment was performed with mega 6. Human complementary nucleotide sequences and 10 nucleotides up- and down-stream are presented. Conserved human complementary nucleotides at the seed binding area are displayed in red and whole nucleotide conservation is indicated with stars. **(A'-E')** mRNA-miRNA hybrid was predicted using Diana v5.0. Seed binding area is displayed in red while remaining nearby nucleotides are shown in black (mRNA) and blue (miR-21 and miR-31). **(A, A')** *PDCD4*. **(B, B')** *SPRY1*. **(C, C')** *PTEN*. **(D, D')** *LATS2.* **(E, E')** *STK40.*

We first determined mRNA expression levels of *PDCD4*, *SPRY1*, *PTEN, LATS2 and STK40* in control HPMCs, TGF-β1 treated and PDE derived cells with epithelial (early-MMT) and non-epithelial (late-MMT) (Figure 5.2, A-E) phenotype. In all cases, greater MMT conditions (late-MMT), previously characterized by increased miR-21 and miR-31 expression (Figure 3.9, B-C), displayed decreased expression of these genes compared with control HPMCs (Figure 5.2, A-E). Intermediate MMT conditions (TGF-β1 and early-MMT models); with lower miR-21, also showed transitional levels of *PDCD4*, *SPRY1* and *PTEN* compared with the late-MMT model (Figure 5.2, A-C). Interestingly, miR-31 exhibited a greater expression when HPMCs were treated with TGF-β1 than in PDE derived cells with epithelial phenotype (Figure 3.9C) and the inverse pattern of expression was shown by *LATS2* and *STK40* targets (Figure 5.2, D-E).

We further examined the association between miR-21, miR-31 and the specific targets of study across all patients and MMT conditions previously described (Figure 5.2, A'-E'). A significant negative association between miR-21 and *PDCD4* (Figure 5.2A', r=-0.464, P=0.039) and miR-31 with *LATS2* (Figure 5.2D', r=-0.443, P=0.050) and *STK40* (Figure 5.2E', r=-0.607, P=0.004) was found. Nevertheless, miR-21 correlation with *SPRY1* and *PTEN* were not significant (Figure 5.2B', r=-0.431, P=0.058; Figure 5.2C', r=-0.266, P=0.258). These initial experiments suggested that miR-21 might negatively regulate *PDCD4* while miR-31 might negatively regulate *LATS2* and *STK40* in HPMCs at post-transcriptional level. The weaker, not significant, association between miR-21 and *SPRY1*/*PTEN* may indicate that although their regulation is important during the MMT process in HPMCs this may not be only mediated by miR-21 but part of a more complex regulation.

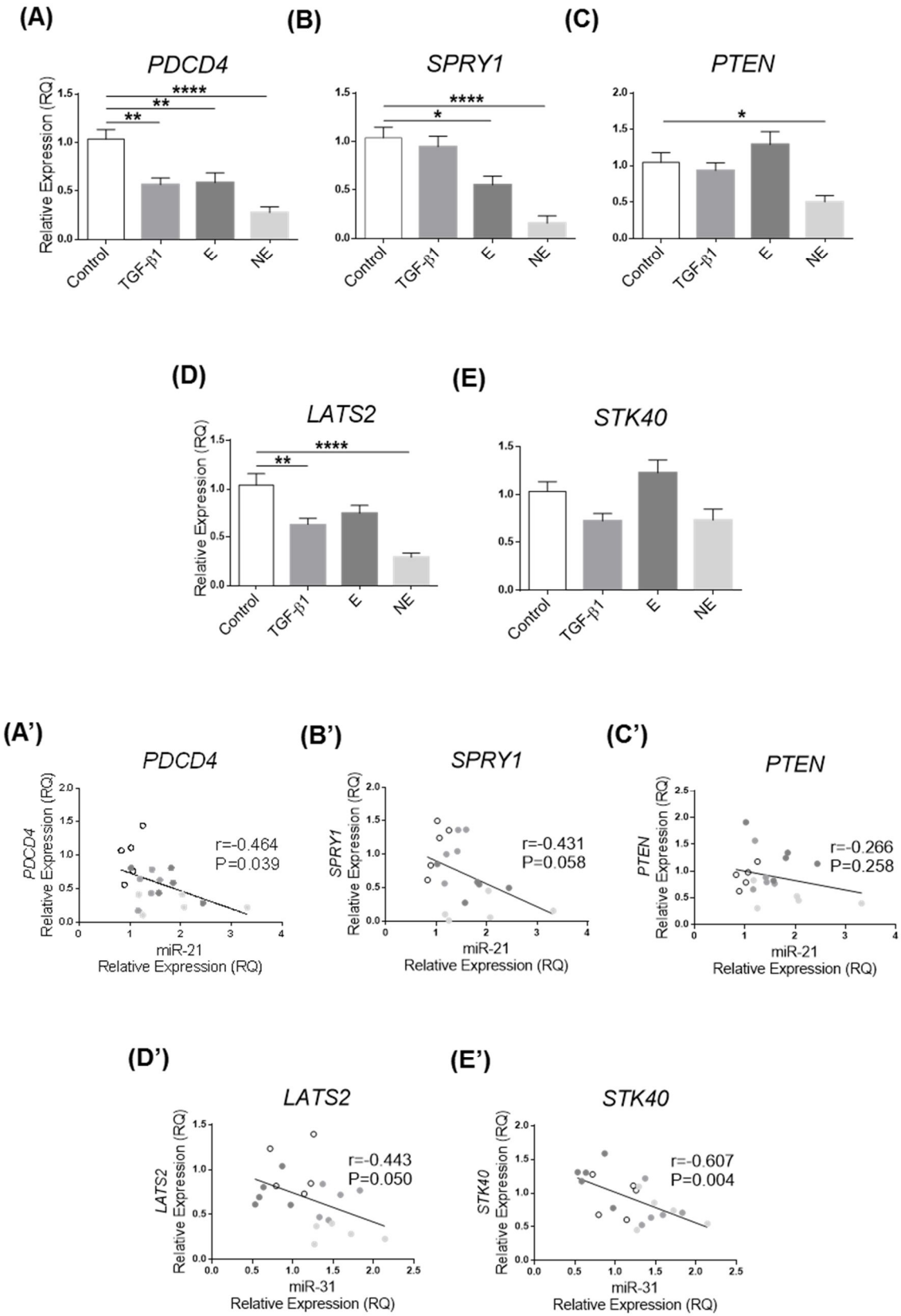
(A)
PDCD4
Relative Expression (RQ)
Control
TGF-β1
E
NE
(B)
SPRY1
(C)
PTEN
(D)
LATS2
(E)
STK40
(A')
PDCD4
r=-0.464
P=0.039
miR-21
Relative Expression (RQ)
(B')
SPRY1
r=-0.431
P=0.058
(C')
PTEN
r=-0.266
P=0.258
(D')
LATS2
r=-0.443
P=0.050
miR-31
(E')
STK40
r=-0.607
P=0.004

Figure 5.2. miR-21 and miR-31 contribute to the MMT process by targeting *PDCD4, SPRY1, PTEN* and *LATS2, STK40* respectively in different models and may contribute to HPMCs MMT process. (A-E) Relative mRNA expression in control omentum-derived mesothelial cells (HPMCs), TGF-β1 treated (1ng/ml, 48h) and cultured peritoneal effluent derived (PDE) cells with epithelial (E) and non-epithelial (NE) phenotype (n=5 for each group). **(A)** *PDCD4*. **(B)** *SPRY1*. **(C)** *PTEN*. **(D)** *LATS2.* **(E)** *STK40.* **(A'-E')** Scatter plot showing correlation of miR-21 and miR-31 with their respective target mRNA levels in HPMCs – black circle, TGF-β1 treated – light grey, and PDE cells with E – dark grey, and NE – pale grey, phenotype.**(A')** *PDCD4*. **(B')** *SPRY1*. **(C')** *PTEN*. **(D')** *LATS2.* **(E')** *STK40.* Target gene and miR-21 expression was analyzed by RT-qPCR and normalized to *GAPDH* and miR-191 expression respectively. Data were analyzed by one-way ANOVA followed by post-hoc Holm-Sidak's test. Pearson's correlation test was used for association (n=20). Data represent the mean S.E.M. from five independent donor experiments. *p < 0.05; **p < 0.01; ****p < 0.001.

To test whether miR-21 and miR-31 indeed could regulate the levels of candidate target mRNAs in disease relevant cells, primary HPMCs were transfected with different concentrations of miR-21 and miR-31 mimic and inhibitor molecules. miR-21 manipulation selectively regulated *PDCD4* but not *SPRY1* and *PTEN* mRNA levels (Figure 5.3 and 5.4, A-C) while miR-31 regulated both, *LATS2* and *STK40* mRNAs in primary HPMCs (Figure 5.3 and 5.4, D-E). Taken together, these data demonstrated that knockdown of *PDCD4* by miR-21 as well as *LATS2* and *STK40* by miR-31 may contribute to MMT, alteration of cellular adhesions and promotion of fibrosis in HPMCs.

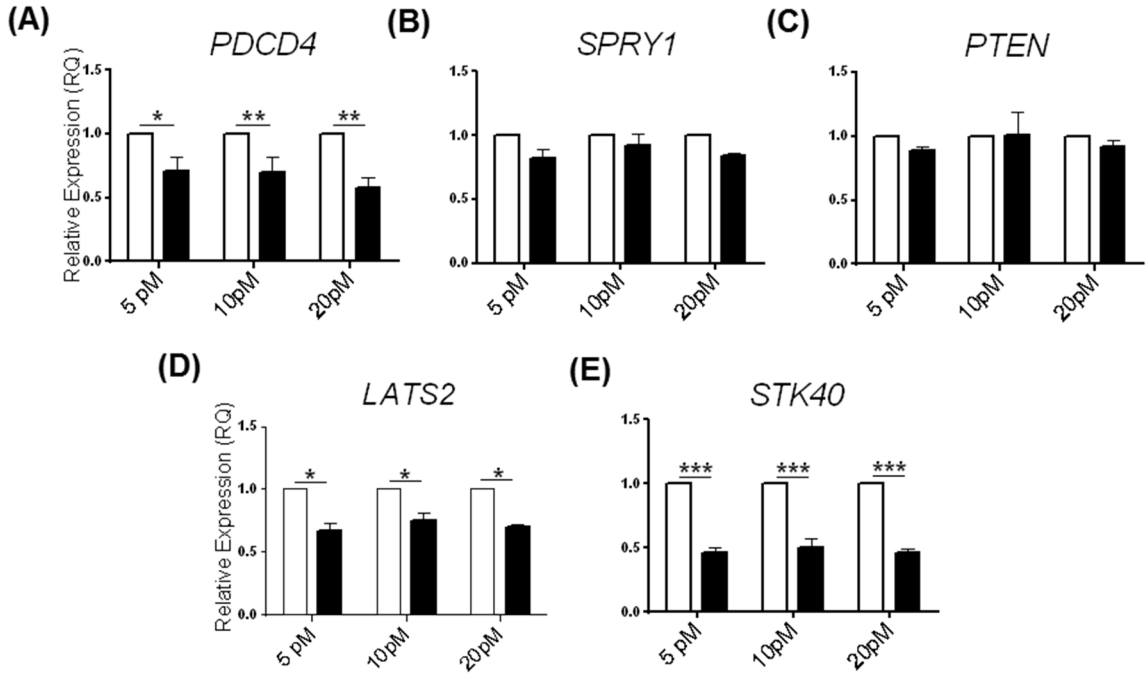

Figure 5.3. miR-21 and miR-31 target mRNA expression after miRNA mimic delivery in HPMCs (A-E) Target mRNA expression after 48h of miRNA mimic delivery (5pM, 10pM and 20pM) in HPMCs. miR-control – white bars, miR-21-mimic and miR-31-mimic – black bars and three independent donor experiments.**(A)** *PDCD4*. **(B)** *SPRY1*. **(C)** *PTEN.* **(D)** *LATS2.* **(E)** *STK40*. Target gene expression was analyzed by RT-qPCR and normalized to *GAPDH* expression respectively. Data were analyzed by matched factor two-way ANOVA followed by post-hoc Holm-Sidak's test. Data represent the mean S.E.M. from three independent donor experiments. *p < 0.05; **p < 0.01; ***p < 0.005.

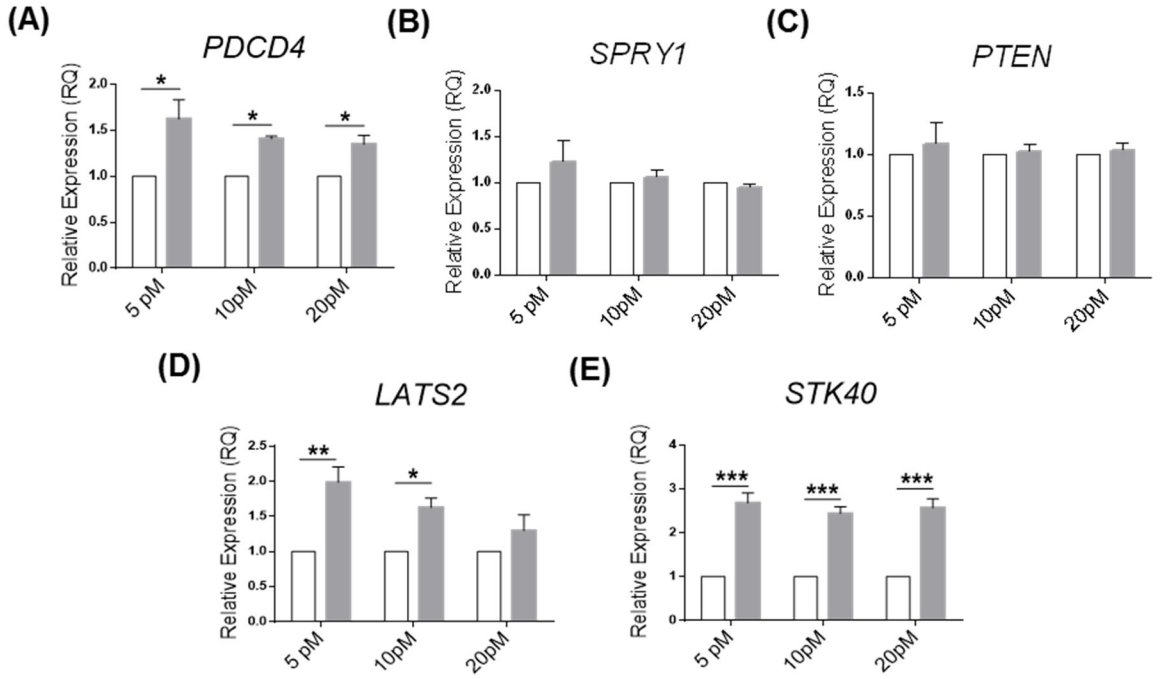

Figure 5.4. miR-21 and miR-31 target mRNA expression after miRNA inhibitor delivery in HPMCs (A-E) Target mRNA expression after 48h of miRNA inhibitor delivery (5pM, 10pM and 20pM) in HPMCs. miR-control – white bars, anti-miR-21 and anti-miR-31 – grey bars and three independent donor experiments.**(A)** *PDCD4*. **(B)** *SPRY1*. **(C)** *PTEN.* **(D)** *LATS2.* **(E)** *STK40*. Target gene expression was analyzed by RT-qPCR and normalized to *GAPDH* expression respectively. Data were analyzed by matched factor two-way ANOVA followed by post-hoc Holm-Sidak's test. Data represent the mean S.E.M. from three independent donor experiments. *p < 0.05; **p < 0.01; ***p < 0.005.

5.2.2. miR-21 contributes to the MMT process by targeting *PDCD4* in HPMCs

Previous data shown in Chapter 4 indicated that miR-21 better correlated with clinical parameters including icodextrin usage, peritonitis count and dialysate cytokines which are deregulated during the complex process of PD treatment-driving membrane alterations. Thus, this research was further focused on miR-21 contribution to the MMT process by targeting *PDCD4* in HPMCs. miR-21 over-expression significantly decreased PDCD4 protein in primary HPMCs after 72h of transfection (Figure 5.5A). Peritoneal membrane biopsies showed a significant down-regulation in PDCD4 expression at the mesothelial and submesothelial compact zone of PD patients using both, biocompatible and non-biocompatible solutions, compared with healthy controls (Figure 5.5, B-C). Previous literature has shown that PDCD4 down-regulation triggers an increase in Snail protein and a consequent decrease in E-cadherin expression which in turn, stimulates β-catenin/TCF dependent transcription (Figure 5.5D) (Asangani et al, 2008; Brønnum et al, 2013; Yao et al, 2011). Thus,

miR-21 down-regulation of PDCD4 in HPMCs may not only contribute to the detachment of inter-mesothelial adhesions but also to the acquisition of a new molecular program dictating a distinct expression regulation characteristic of an MMT process (Figure 5.5D).

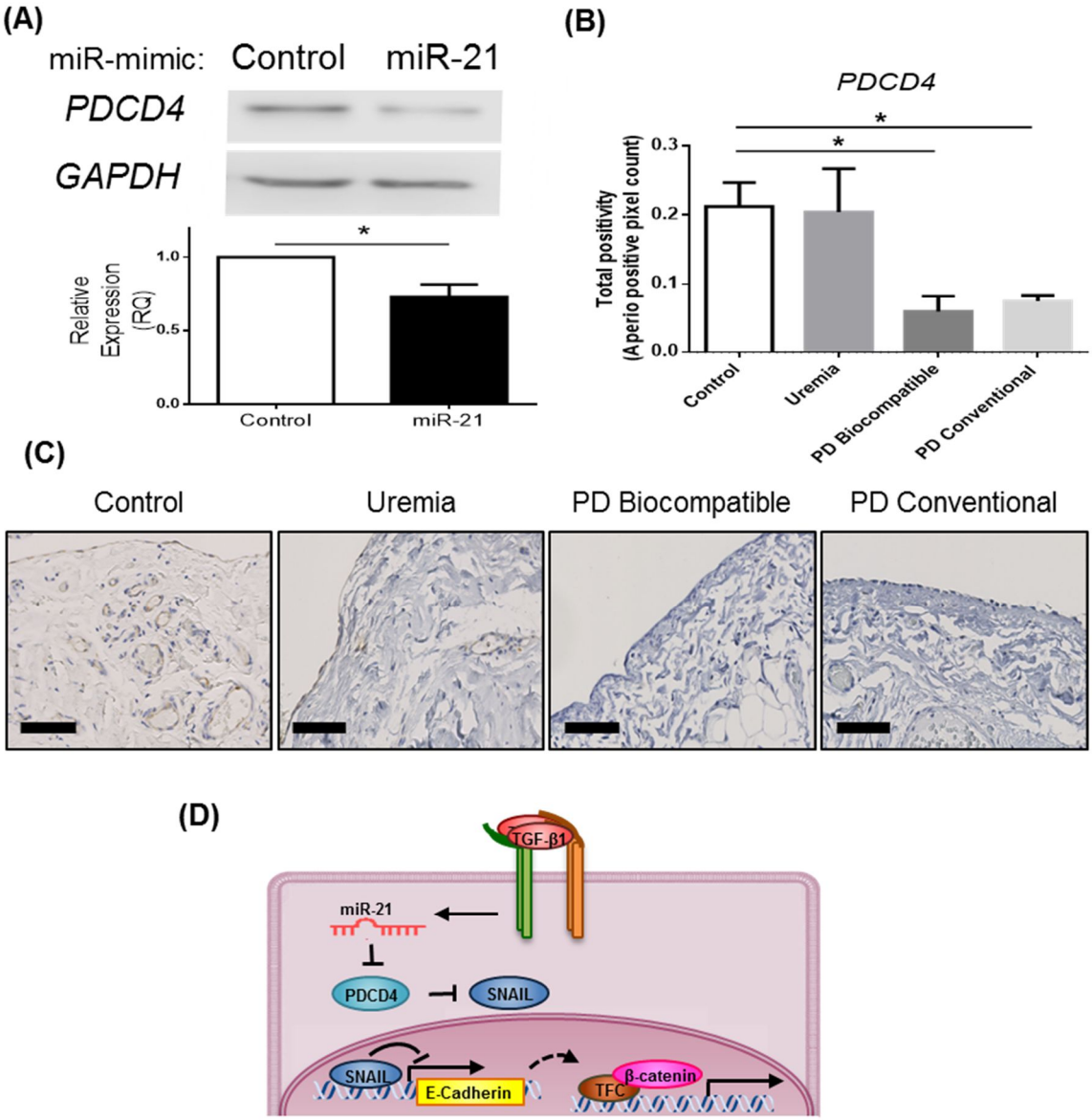

Figure 5.5. miR-21 may contribute to the MMT process by targeting PDCD4 in HPMCs. (A) PDCD4 protein expression and quantification after 72h of 5 pM miRNA mimic delivery in HPMCs analyzed by western blot (n=6). **(B-C)** Formalin-fixed paraffin embedded (FFPE) samples were PDCD4 stained. **(B)** Histological image analysis using Aperio Precision Image Analysis Software. Mesothelial and submesothelial compact zone was selected as area of interest and PDCD4 staining was quantified by the aperio positive pixel count algorithm. **(C)** Positive PDCD4 detection (brown). Scale bar, 80 µm. **(D)** Schematic representation of TGF-β1 triggered MMT regulation via miR-21 up-regulation in HPMCs. TGF-β1 is up-regulated in PD patients and induce the expression of miR-21 in HPMCs. miR-21 directly targets PDCD4, up-regulating Snail protein and decreasing E-cadherin expression which, in turn, stimulates β-catenin/TCF dependent transcription. Data were analyzed by paired t test or one- way ANOVA followed by post-hoc Holm-Sidak's test. Data represent the mean S.E.M. from eleven age-matched samples and equal average PD duration between PD groups. *$p < 0.05$.

5.2.3. miR-21 and miR-31 *in silico* target prediction may identify new direct targets that contribute to the MMT process in HPMCs

Initial algorithm target prediction was performed prior identification of miR-21 and miR-31 associations with clinical parameters from the GFS. Thus, in this analysis similar importance was given to both miRNAs (Figure 5.6, A-B). Independent target prediction using Diana (Paraskevopoulou et al, 2013; Reczko et al, 2012) (blue), miRDB (Wang & El Naqa, 2008; Wong & Wang, 2015) (brown), miRanda (Betel et al, 2010; Betel et al, 2008) (green) and TargetScan (Agarwal et al, 2015; Nam et al, 2014) (red) *in silico* algorithms for miR-21 (dark color) and miR-31 (light color) were performed (Table 2.7; Figure 5.6A). Venn diagrams were used to identify common target predictions for both miRNAs and each one of the above mentioned algorithms (Figure 5.6A). Diana algorithm identified 481 likely targets for miR-21 and 574 for miR-31; 29 of these targets were commonly predicted for both miRNAs. Similarly, miRanda detected 492 possible targets for miR-21 and 306 for miR-31; 15 of which were joint plausible targets for these two miRNAs. miRDB distinguished 240 potential targets for miR-21 and 407 targets for miR-31; 8 of which were found to be shared by both miRNAs. Finally, TargetScan recognized 307 feasible targets for miR-21 and 425 for miR-31; 23 of these were also coincident targets for these two miRNAs. miR-21 and miR-31 common targets predicted and identified in Figure 5.6A (Diana=29, miRanda=15, miRBD=8, and TargetScan=23) where further inter-crossed using Venn diagram to identify targets that were predicted by three or more algorithms (Figure 5.6B). Three different targets for both miRNAs were identified by three or more prediction tools including Zinc Finger SWIM-Type Containing 6 (*ZSWIM6*), PDZ domain-containing protein 2 (*PDZD2*) and Mitogen-Activated Protein Kinase Kinase Kinase 1 (*MAP3K1*) (Figure 5.6B).

This research was conducted synchronously with data analysis shown in Chapter 4 and indicating miR-21 associated most clearly with factors implicated in peritoneal membrane alterations driven by PD therapy. Therefore, a second *in silico* target prediction approach focusing on miR-21 was performed. This second time, only miR-21 target predictions using Diana (blue), miRDB (brown), miRanda (green) and TargetScan (red) displayed in Figure 5.6A (dark color) were inter-crossed using Venn diagram to identify targets that were predicted by

three or more algorithms (Figure 5.6C). A total of 147 candidate targets were identified by three or more prediction tools and used to generate a list called *'miRNA#'* (blue) (Figure 5.6C).

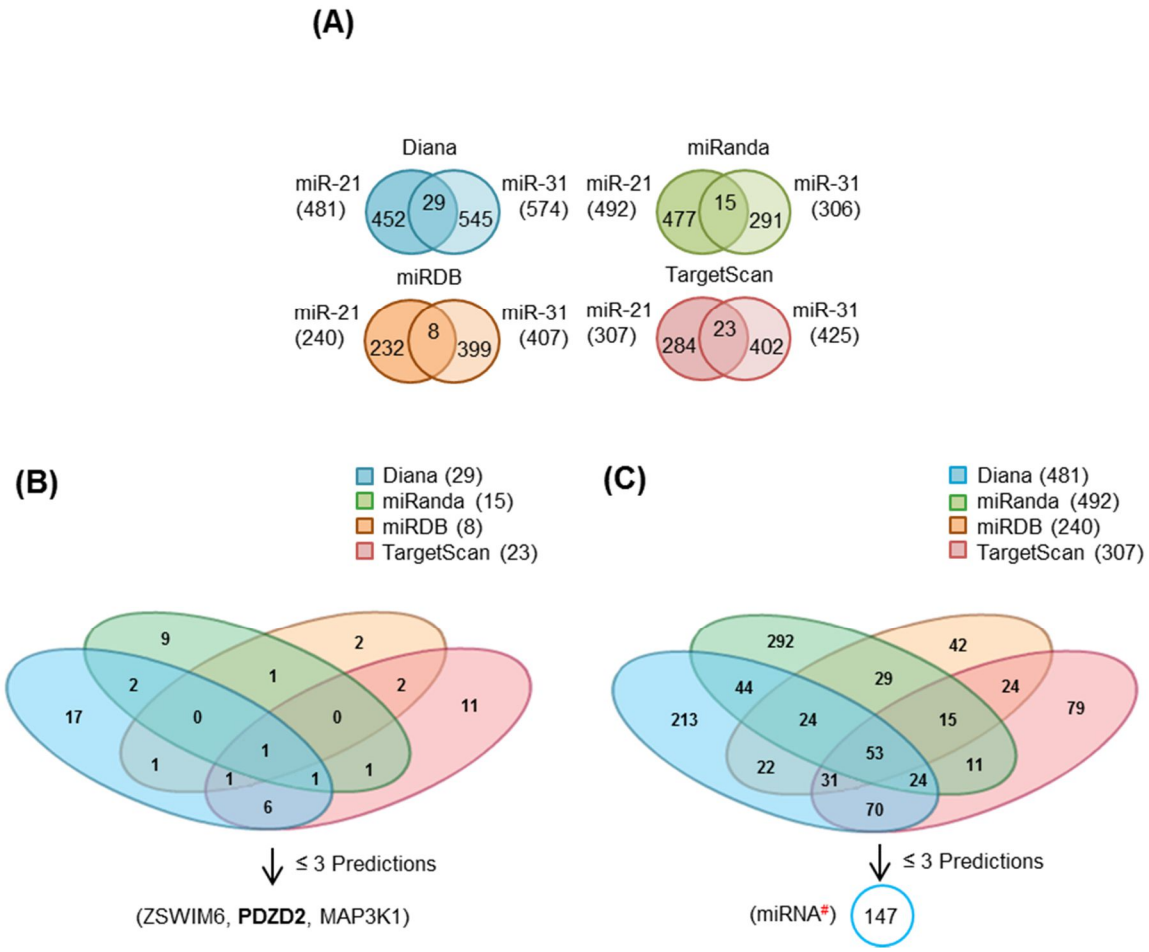

Figure 5.6. *In silico* target prediction to identify new miR-21 and miR-31 targets that may contribute to the MMT process in HPMCs. (A) Target prediction using Diana (blue), miRDB (brown), miRanda (green) and TargetScan (red) *in silico* algorithms for miR-21 (dark color) and miR-31 (light color). Venn diagram were used to identify common target predictions for both miRNAs. **(B)** miR-21 and miR-31 common target predicted and identified in (A) were further inter-crossed using Venn diagram to identify targets that were predicted by three or more algorithms. **(C)** Prediction of miR-21 targets alone was also analyzed using Diana (blue), miRDB (brown), miRanda (green) and TargetScan (red) inter-crossed using Venn diagram to identify targets that were predicted by three or more algorithms.

In order to evaluate the feasibility of these predictions mRNA array data from an *ex vivo* model of mesothelial cell MMT associated to PD therapy was used. mRNA array data were kindly provided by Dr Manuel Lopez-Cabrera displaying results from control omentum HPMCs, PDE derived MCs with epithelial phenotype (early-MMT) and PDE derived MCs with non-epithelial phenotype (late-MMT). mRNA array changes were analyzed comparing (i) control omentum HPMCs and PDE derived MCs with epithelial phenotype (early-MMT, green), (ii) PDE derived MCs with epithelial phenotype and non-epithelial phenotype (late-MMT, yellow), and (iii) control omentum HPMCs and PDE derived MCs with non-epithelial phenotype (whole-MMT, red) to generate three independent lists of mRNA changes under the conditions of study (Figure 5.7A). These array results showed that 274 transcripts were down-regulated in the early-MMT model (green) while 298 transcripts were less expressed during the late phase of the process (yellow) (Figure 5.7A). Overall, 774 genes were differentially down-regulated when comparing extreme phenotypes as a whole-MMT process model (red) (Figure 5.7A). Subsequently, *ZSWIM6, PDZD2* and *MAP3K1* were sought in the three lists of gene changes generated from the *ex vivo* model previously described. From these, *PDZD2* mRNA was identified by the array data to be differentially down-regulated during both early and late MMT. Nevertheless, no changes were identified in *ZSWIM6* and *MAP3K1* gene transcription displayed by the array.

Similarly, miR-21 targets predicted in Figure 5.6C (miRNA[#], blue) were further inter-crossed using Venn diagram with the mRNA array list changes identified in figure 5.7A (lists: green, yellow, red) (Figure 5.7B). Five miR-21 predicted targets were identified to be differentially down-regulated during early-MMT (Figure 5.7B'), two in the late-MMT course (Figure 5.7B'') and ten when the whole-MMT was compared (Figure 5.7B'''). miR-21 possible targets identified included Natriuretic Peptide B (*NPPB*), *PDZD2*, S100 calcium-binding protein A10 (*S100A10*), SAM And SH3 Domain Containing 1 (*SASH1*) and Metalloproteinase inhibitor 3 (*TIMP3*) for early-MMT (Figure 5.7B'); *PDZD2* and *SASH1* for late-MMT (Figure 5.7B''); and Absent In Melanoma 1-Like (*AIM1L*), CASK Interacting Protein 1 (*CASKIN1*), Dual Specificity Phosphatase 8 (*DUSP8*), Fibroblast Growth Factor 18 (*FGF-18*), Matrilin 2 (*MATN2*), Neural EGFL Like 2 (*NELL2*), *PDZD2*, (Ras Homolog Family Member B (*RHOB*), *SASH1* and Sprouty RTK Signalling Antagonist 1 (*SPRY1*) for whole-MMT (Figure 5.7B'''). Thirteen different possible

miR-21 direct targets identified above and likely to be important in the MMT process associated to PD treatment were selected for subsequent study.

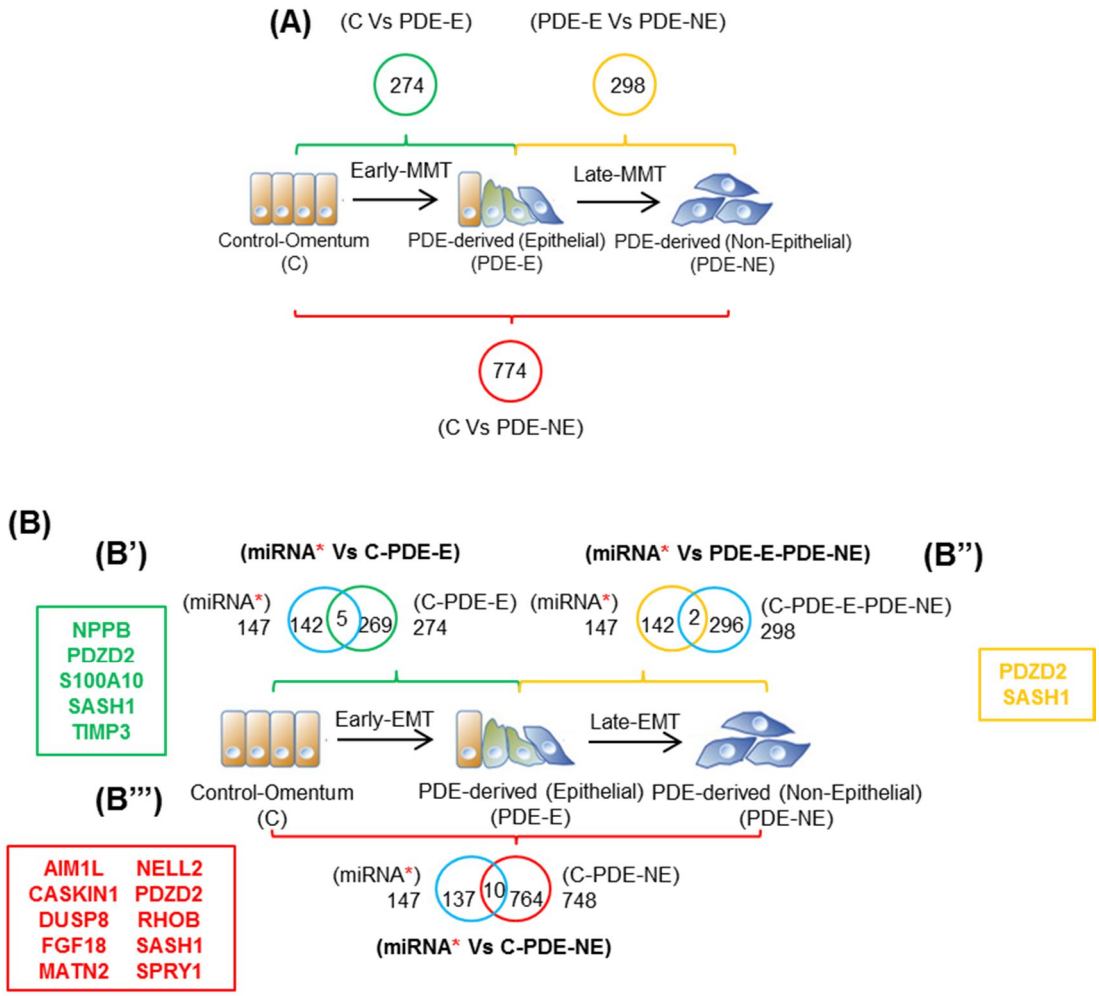

Figure 5.7. mRNA array changes for early, late and whole MMT process associated to PD therapy in HPMCs. **(A)** Diagram displaying mRNA array changes comparing control omentum HPMCs and PDE derived MCs with epithelial phenotype (early-MMT, green), PDE derived MCs with epithelial phenotype and non-epithelial phenotype (late-MMT, yellow), and control omentum HPMCs and PDE derived MCs with non-epithelial phenotype (whole-MMT, red). **(B)** Diagram displaying miR-21 targets predicted and identified in Figure 5.6C (blue) further inter-crossed using Venn diagram with the mRNA array changes identified in (**A**; green, yellow, red). Common targets identified by Figure 5.6C and **(A)** inter-crossed lists are shown into squares with the respective MMT color (**B'**, early-MMT; **B''**, late-MMT; **B'''**, whole-MMT).

5.2.4. Target prediction screening in HPMCs under MMT conditions

Predicted miR-21 targets were screened in a model of progressive peritoneal membrane deterioration in which mRNA expression was measured in control omentum-derived HPMCs, TGF-β1 treated and peritoneal effluent derived (PDE) cells with epithelial (E) and non-epithelial (NE) phenotype. Potential miR-21 target expression for each of the model conditions described above as well as association between miR-21 and specific potential targets of study across MMT conditions are shown in Figure 5.8. *SPRY1* expression and association with miR-21 has been previously described and discussed in Figure 5.2B, B'. Eleven of thirteen possible miR-21 targets identified *in silico* followed a pattern of mRNA expression consistent with a direct and/or indirect regulation by miR-21 in a model of progressive peritoneal membrane deterioration (Figure 5.8). Plausible miR-21 regulated transcripts included *PDZD2, S100A10, SASH1, AIM1L, CASKIN1, DUSP8, FGF-18, MATN2, NELL2* and *SPRY1* (Figure 5.8, B-D, B'-D', F-M and F'-M'). Significant inverse association between miR-21 and four of these targets was found including *S100A10* (Figure 5.8C', r=-0.555, P=0.011), *CASKIN* (Figure 5.8G', r=-0.468, P=0.038), *DUSP8* (Figure 5.8H', r=0.468, P=0.029) and *NELL2* (Figure 5.8K', r=-0.463, P=0.040). *NPPB, TIMP3* and *RHOB* were the only targets that did not follow the expected tendency in mRNA expression reduction in the model of study (Figure 5.8A, A', E, E', L and L'). Indeed, a significant positive association between miR-21 and *NPPB* (Figure 5.8A', r=0.763, P<0.0001) was found while positive association trends were identified between miR-21 with *TIMP3* (Figure 5.8E', r=0.173, P=0.465) and a mild association with *RHOB* (Figure 5.8L', r=0.107, P=0.653). Of note, *SPRY1* has previously been identified and confirmed to be miR-21 specific targets (Thum et al, 2008) and was, therefore, not considered for future research (Figure 5.8B, B'). Thus, target prediction screening in HPMCs under MMT conditions decreased the initial target selection to nine potentially miR-21 regulated transcripts including *PDZD2, S100A10, SASH1, AIM1L, CASKIN1, DUSP8, FGF-18, MATN2* and *NELL2*.

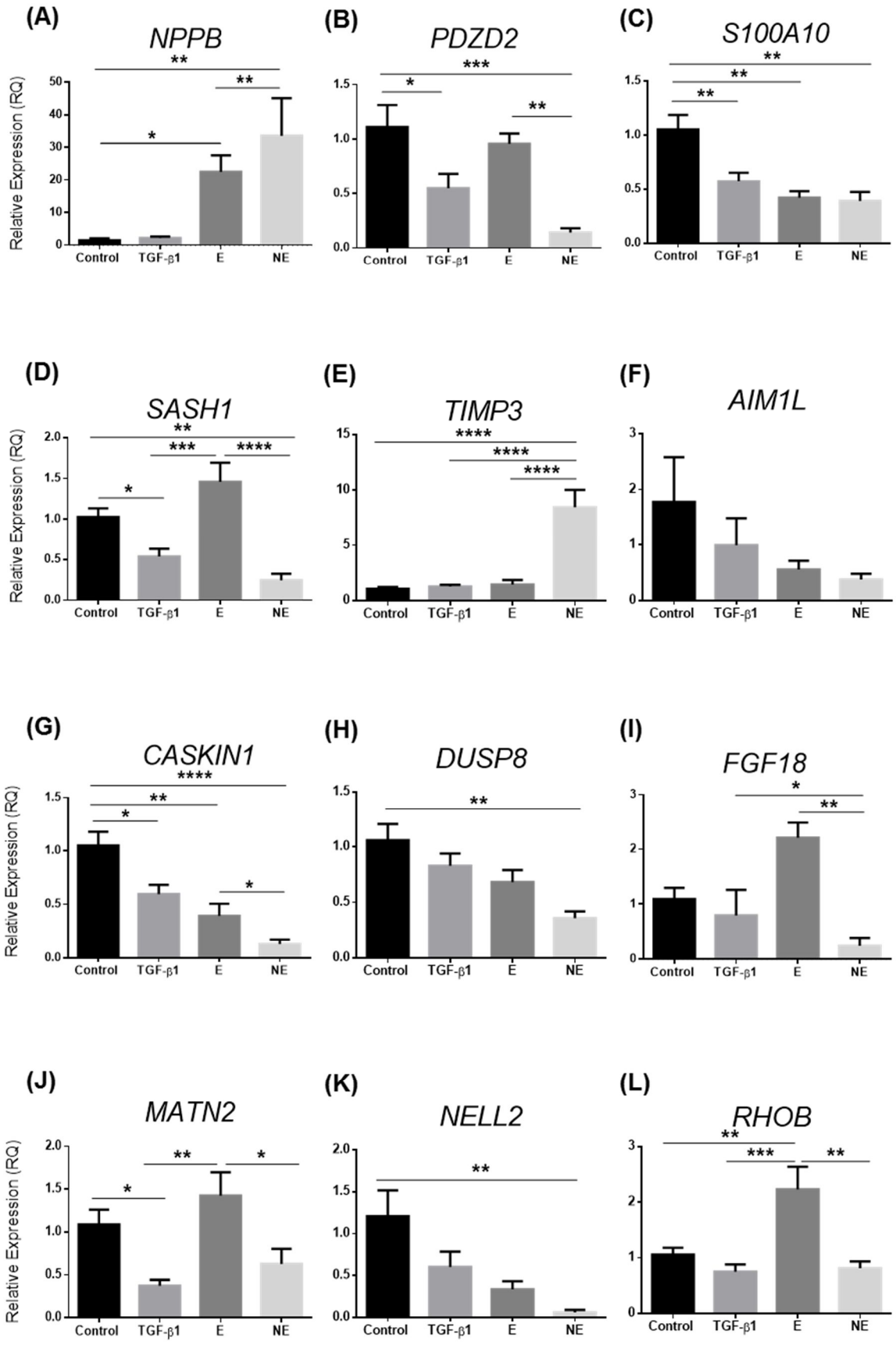
(A)
NPPB
Relative Expression (RQ)
Control
TGF-β1
E
NE
(B)
PDZD2
(C)
S100A10
(D)
SASH1
(E)
TIMP3
(F)
AIM1L
(G)
CASKIN1
(H)
DUSP8
(I)
FGF18
(J)
MATN2
(K)
NELL2
(L)
RHOB

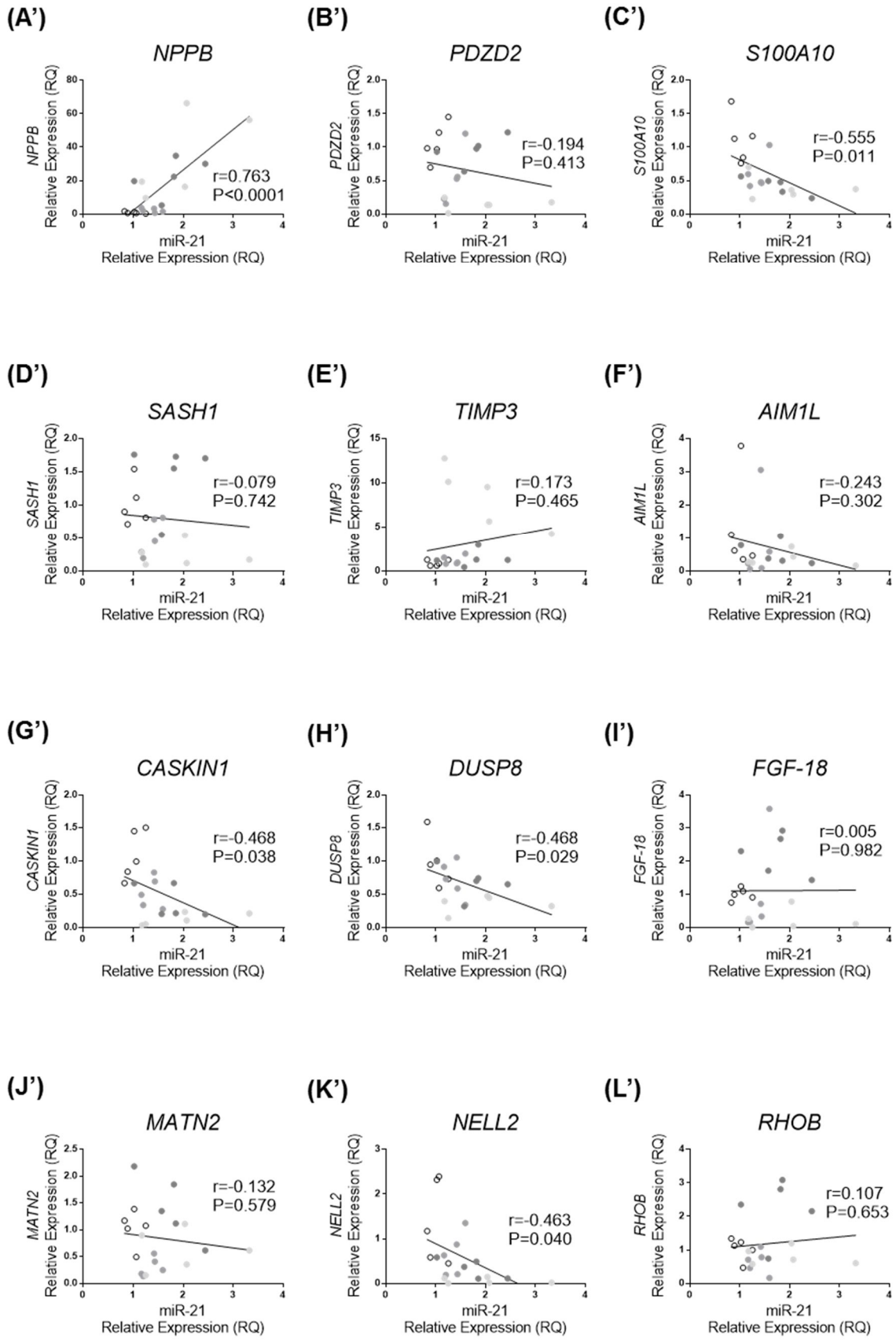
(A')
NPPB
NPPB Relative Expression (RQ)
r=0.763
P<0.0001
miR-21 Relative Expression (RQ)
(B')
PDZD2
PDZD2 Relative Expression (RQ)
r=-0.194
P=0.413
miR-21 Relative Expression (RQ)
(C')
S100A10
S100A10 Relative Expression (RQ)
r=-0.555
P=0.011
miR-21 Relative Expression (RQ)
(D')
SASH1
SASH1 Relative Expression (RQ)
r=-0.079
P=0.742
miR-21 Relative Expression (RQ)
(E')
TIMP3
TIMP3 Relative Expression (RQ)
r=0.173
P=0.465
miR-21 Relative Expression (RQ)
(F')
AIM1L
AIM1L Relative Expression (RQ)
r=-0.243
P=0.302
miR-21 Relative Expression (RQ)
(G')
CASKIN1
CASKIN1 Relative Expression (RQ)
r=-0.468
P=0.038
miR-21 Relative Expression (RQ)
(H')
DUSP8
DUSP8 Relative Expression (RQ)
r=-0.468
P=0.029
miR-21 Relative Expression (RQ)
(I')
FGF-18
FGF-18 Relative Expression (RQ)
r=0.005
P=0.982
miR-21 Relative Expression (RQ)
(J')
MATN2
MATN2 Relative Expression (RQ)
r=-0.132
P=0.579
miR-21 Relative Expression (RQ)
(K')
NELL2
NELL2 Relative Expression (RQ)
r=-0.463
P=0.040
miR-21 Relative Expression (RQ)
(L')
RHOB
RHOB Relative Expression (RQ)
r=0.107
P=0.653
miR-21 Relative Expression (RQ)

Figure 5.8. Predicted miR-21 target profiling in a model of progressive peritoneal membrane deterioration. **(A-L)** Relative mRNA expression in control omentum-derived mesothelial cells (HPMCs), TGF-β1 treated (1ng/ml, 48h) and cultured peritoneal effluent derived (PDE) cells with epithelial (E) and non-epithelial (NE) phenotype (n=5 for each group). **(A)** *NPPB*. **(B)** *PDZD2*. **(C)** *S100A10.* **(D)** *SASH1.* **(E)** *TIMP3.* **(F)** *AIM1L*. **(G)** *CASKIN1*. **(H)** *DUSP8.* **(I)** *FGF18*. **(J)** *MATN2*. **(K)** *NELL2*. **(L)** *RHOB*. **(A'-L')** Scatter plot showing correlation of miR-21 and potential mRNA targets in HPMCs – black circle, TGF-β1 treated – light grey, and PDE cells with E – dark grey, and NE – pale grey, phenotype. **(A')** *NPPB*. **(B')** *PDZD2*. **(C')** *S100A10*. **(D')** *SASH1*. **(E')** *TIMP3*. **(F')** *AIM1L.* **(G')** *CASKIN1.* **(H')** *DUSP8.* **(I')** *FGF18.* **(J')** *MATN2*. **(K')** *NELL2.* **(L')** *RHOB*. Target gene expression was analyzed by RT-qPCR and normalized to GAPDH. Data were analyzed by no matched one-way ANOVA followed by post-hoc Holm-Sidak's test. Data represent the mean S.E.M. from five independent donor experiments. *p < 0.05; **p < 0.01; ***p < 0.005 ****p < 0.001.

miR-21 mimic delivery in HPMCs was used to further screening *in silico* target predictions of the nine remaining targets identified. Three different miR-21 and miR-control mimic concentrations (5 pM, 10 pM and 20 pM) were used for this study (Figure 5.9). Four of the nine targets studied were significantly down-regulated by miR-21 mimic delivery including *PDZD2*, *S100A10*, *FGF-18* and *MATN2* (Figure 5.9A, B, G and H). miR-21 inhibitor was also transfected in HPMCs to additionally screen the feasibility of the nine targets determined *in silico*. Three different miR-21 and miR-control inhibitor concentrations (5 pM, 10 pM and 20 pM) were utilized for this purpose (Figure 5.10). Seven of the nine targets analyzed were significantly up-regulated by miR-21 inhibition comprising *PDZD2*, *S100A10*, *CASKIN, DUSP8, FGF-18*, *MATN2* and *NELL2* (Figure 5.10A, B, E, F, G, H and I). Targets that showed to be commonly regulated by miR-21 gain- and loss-of-function experiments were selected for further research including *PDZD2*, *S100A10*, *FGF-18* and *MATN2* (Figure 5.9 and 5.10A, B, G and H).

Deep analysis on 3'UTR target site types and conservation for *PDZD2, S100A10, FGF-18*, *MATN2* and miR-21 and miR-31 across different animals is shown in Figure 5.11. *PDZD2* 3'UTR showed to contain five different seed regions, two for miR-21 and three for miR-31, while the rest of the targets identified enclosed a single miR-21 seed region (Figure 5.10). Successful miRNA-target seed-matched site ranking, although variable, has been averaged as 8mer (miRNA seed match + A at position 1 (A1) and match at position 8 (m8)) >> 7mer-m8 (miRNA seed match + m8) > 7mer-A1 (miRNA seed match + A1) >> 6mer > no site; in which the last pair barely differs (Bartel, 2009). Thus, target sequence analysis for *PDZD2* showed to display a miR-31 8mer site (Figure 5.11B'), miR-21 7mer-m8 site (Figure 5.11C'), miR-31 7mer-8m site (Figure 5.11D'), miR-31 8mer site with a potential 3' supplementary site which is characterized by 1-5 nt loop and supplementary pairing of ≥ 3-4 pairs (Figure 5.11E') (Bartel,

2009), and miR-21 8mer site (Figure 5.11F') while *S100A10* exhibited a 7mer-m8 site (Figure 5.11G'), and *FGF-18* and *MATN2* 8mer each (Figure 5.11, H' and I'). Interestingly, multiple miRNA-binding sites for miR-21 and miR-31 in *PDZD2* 3'UTR may be especially effective for repression (Bartel, 2009). Nevertheless, *PDZD2* miRNA target site conservation was found to be considerably poor (0-50%) while *S100A10* was 75%, *FGF-18* was 100% and *MATN2* was 75% (Figure 5.11, B-I). Overall, all miRNA-target seed-matched sites considered for future research belonged to the two site types of miRNA-target with higher relative efficiency (Bartel, 2009) and with *FGF-18*, *S100A10* and *MATN2* target sites being ≥ 75% conserved.

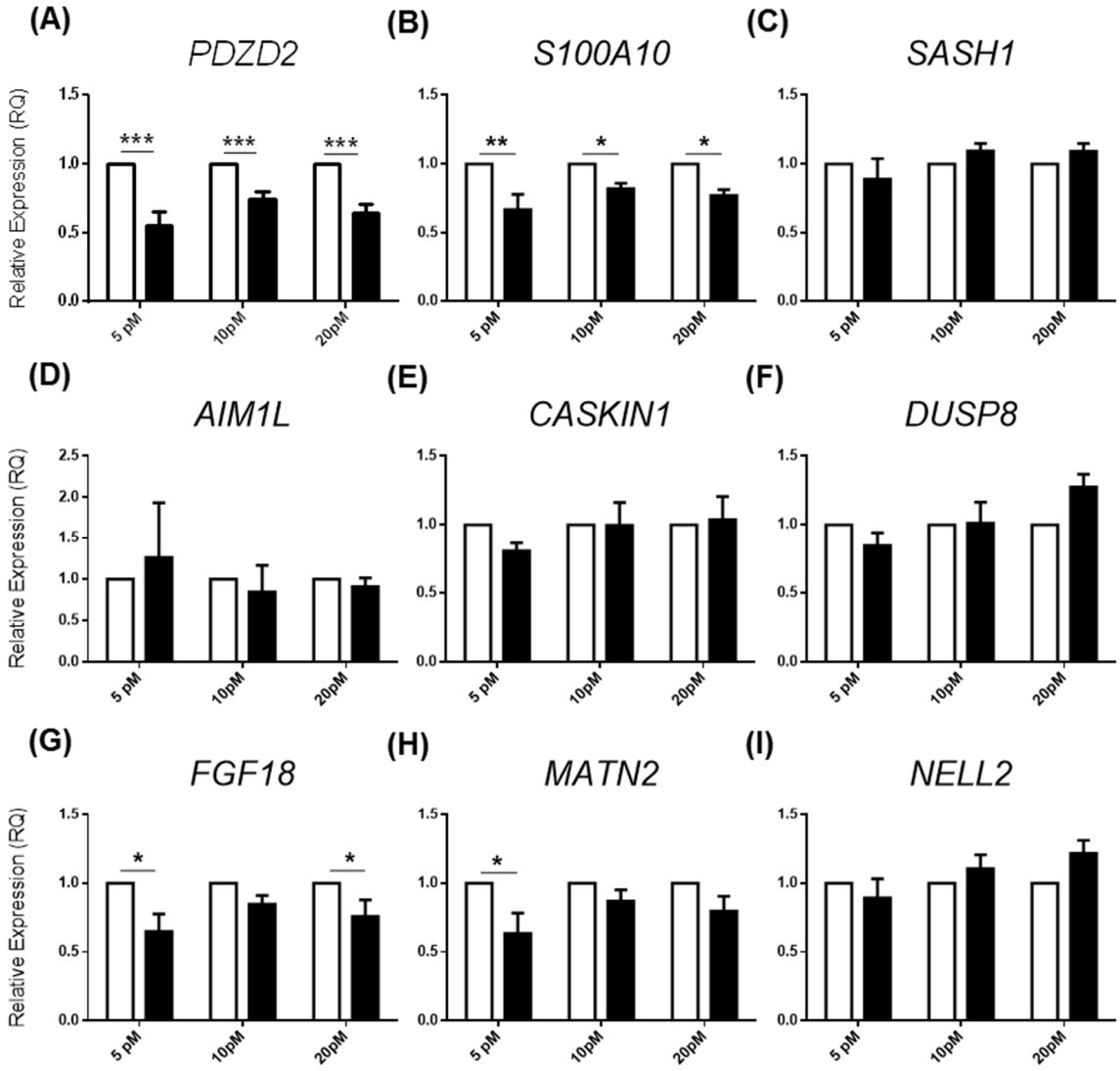

Figure 5.9. miR-21 target mRNA expression after miRNA mimic delivery in HPMCs (A-I) Target mRNA expression after 48h of miRNA mimic delivery (5pM, 10pM and 20pM) in HPMCs. miR-control – white bars, miR-21 – black bars and three independent donor experiments. **(A)** *PDZD2*. **(B)** *S100A10*. **(C)** *SASH1.* **(D)** *AIM1L.* **(E)** *CASKIN1*. **(F)** *DUSP8*. **(G)** *FGF18*. **(H)** *MATN2.* **(I)** *NELL2.* Target gene expression was analyzed by RT-qPCR and normalized to *GAPDH* expression respectively. Data were analyzed by matched factor two-way ANOVA followed by post-hoc Holm-Sidak's test. Data represent the mean S.E.M. from three independent donor experiments. *$p < 0.05$; **$p < 0.01$; ***$p < 0.005$.

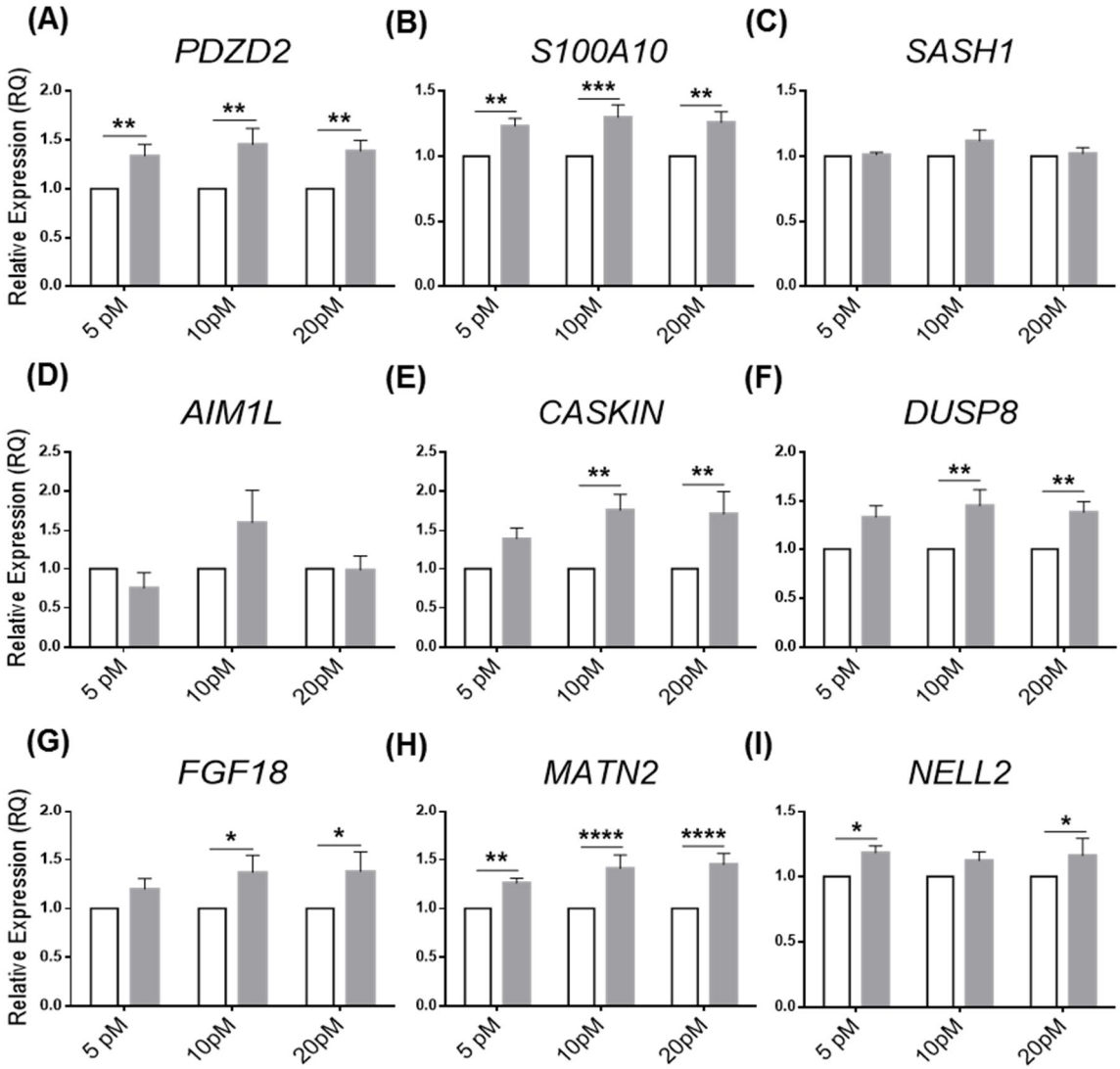

Figure 5.10. miR-21 target mRNA expression after miRNA inhibitor delivery in HPMCs (A-I) Target mRNA expression after 48h of miRNA inhibitor delivery (5pM, 10pM and 20pM) in HPMCs. miR-control – white bars, miR-21 inhibitor – grey bars and six independent donor experiments. **(A)** *PDZD2*. **(B)** *S100A10*. **(C)** *SASH1*. **(D)** *AIM1L.* **(E)** *CASKIN1*. **(F)** *DUSP8*. **(G)** *FGF18*. **(H)** *MATN2.* **(I)** *NELL2.* Target gene expression was analyzed by RT-qPCR and normalized to *GAPDH* expression respectively. Data were analyzed by matched factor two-way ANOVA followed by post-hoc Holm-Sidak's test. Data represent the mean S.E.M. from six independent donor experiments. *$p < 0.05$; **$p < 0.01$; ***$p < 0.005$ and ****$p>0.001$.

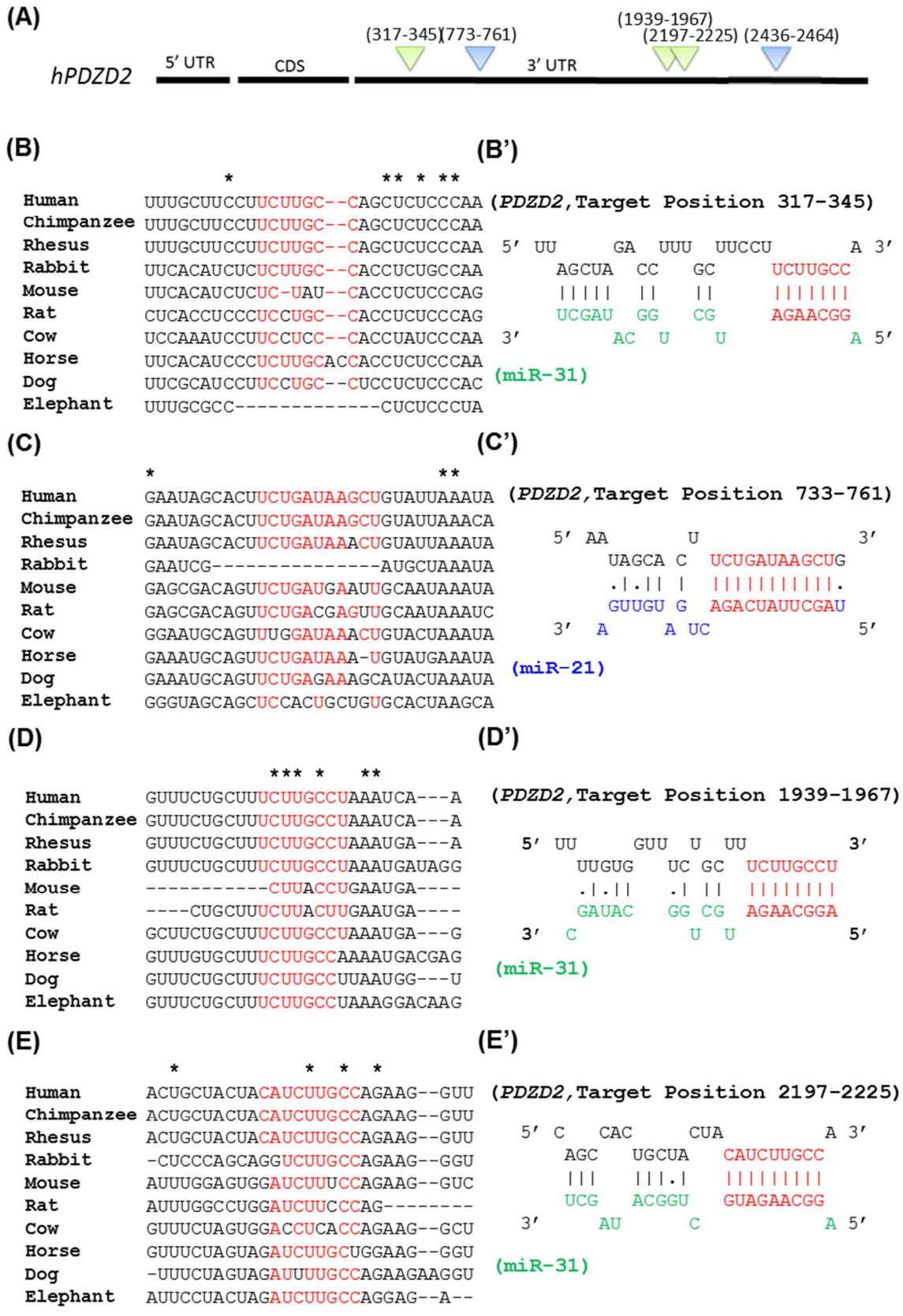
(A)
hPDZD2
5′ UTR
CDS
3′ UTR
(317-345)
(773-761)
(1939-1967)
(2197-2225)
(2436-2464)
(B)
Human UUUGCUUCCUUCUUGC--CAGCUCUCCCAA
Chimpanzee UUUGCUUCCUUCUUGC--CAGCUCUCCCAA
Rhesus UUUGCUUCCUUCUUGC--CAGCUCUCCCAA
Rabbit UUCACAUCUCUCUUGC--CACCUCUGCCAA
Mouse UUCACAUCUCUC-UAU--CACCUCUCCCAG
Rat CUCACCUCCCUCCUGC--CACCUCUCCCAG
Cow UCCAAAUCCUUCCUCC--CACCUAUCCCAA
Horse UUCACAUCCCUCUUGCACCACCUCUCCCAA
Dog UUCGCAUCCUUCCUGC--CUCCUCUCCCAC
Elephant UUUGCGCC----------CUCUCCCUA
(B')
(PDZD2,Target Position 317-345)
5′ UU GA UUU UUCCU A 3′
AGCUA CC GC UCUUGCC
UCGAU GG CG AGAACGG
3′ AC U U A 5′
(miR-31)
(C)
Human GAAUAGCACUUCUGAUAAGCUGUAUUAAAUA
Chimpanzee GAAUAGCACUUCUGAUAAGCUGUAUUAAACA
Rhesus GAAUAGCACUUCUGAUAAACUGUAUUAAAUA
Rabbit GAAUCG----------AUGCUAAAUA
Mouse GAGCGACAGUUCUGAUGAAUUGCAAUAAAUA
Rat GAGCGACAGUUCUGACGAGUUGCAAUAAAUC
Cow GGAAUGCAGUUUGGAUAAACUGUACUAAAUA
Horse GAAAUGCAGUUCUGAUAAA-UGUAUGAAAUA
Dog GAAAUGCAGUUCUGAGAAAGCAUACUAAAUA
Elephant GGGUAGCAGCUCCACUGCUGUGCACUAAGCA
(C')
(PDZD2,Target Position 733-761)
5′ AA U 3′
UAGCA C UCUGAUAAGCUG
GUUGU G AGACUAUUCGAU
3′ A A UC 5′
(miR-21)
(D)
Human GUUUCUGCUUUCUUGCCUAAAUCA---A
Chimpanzee GUUUCUGCUUUCUUGCCUAAAUCA---A
Rhesus GUUUCUGCUUUCUUGCCUAAAUGA---A
Rabbit GUUUCUGCUUUCUUGCCUAAAUGAUAGG
Mouse ----------CUUACCUGAAUGA----
Rat ----CUGCUUUCUUACUUGAAUGA----
Cow GCUUCUGCUUUCUUGCCUAAAUGA---G
Horse GUUUGUGCUUUCUUGCCAAAAUGACGAG
Dog GUUUCUGCUUUCUUGCCUUAAUGG---U
Elephant GUUUCUGCUUUCUUGCCUAAAGGACAAG
(D')
(PDZD2,Target Position 1939-1967)
5′ UU GUU U UU 3′
UUGUG UC GC UCUUGCCU
GAUAC GG CG AGAACGGA
3′ C U U 5′
(miR-31)
(E)
Human ACUGCUACUACAUCUUGCCAGAAG--GUU
Chimpanzee ACUGCUACUACAUCUUGCCAGAAG--GUU
Rhesus ACUGCUACUACAUCUUGCCAGAAG--GUU
Rabbit -CUCCCAGCAGGUCUUGCCAGAAG--GGU
Mouse AUUUGGAGUGGAUCUUUCCAGAAG--GUC
Rat AUUUGGCCUGGAUCUUCCCAG--------
Cow GUUUCUAGUGGACCUCACCAGAAG--GCU
Horse GUUUCUAGUAGAUCUUGCUGGAAG--GGU
Dog -UUUCUAGUAGAUUUUGCCAGAAGAAGGU
Elephant AUUCCUACUAGAUCUUGCCAGGAG--A--
(E')
(PDZD2,Target Position 2197-2225)
5′ C CAC CUA A 3′
AGC UGCUA CAUCUUGCC
UCG ACGGU GUAGAACGG
3′ AU C A 5′
(miR-31)

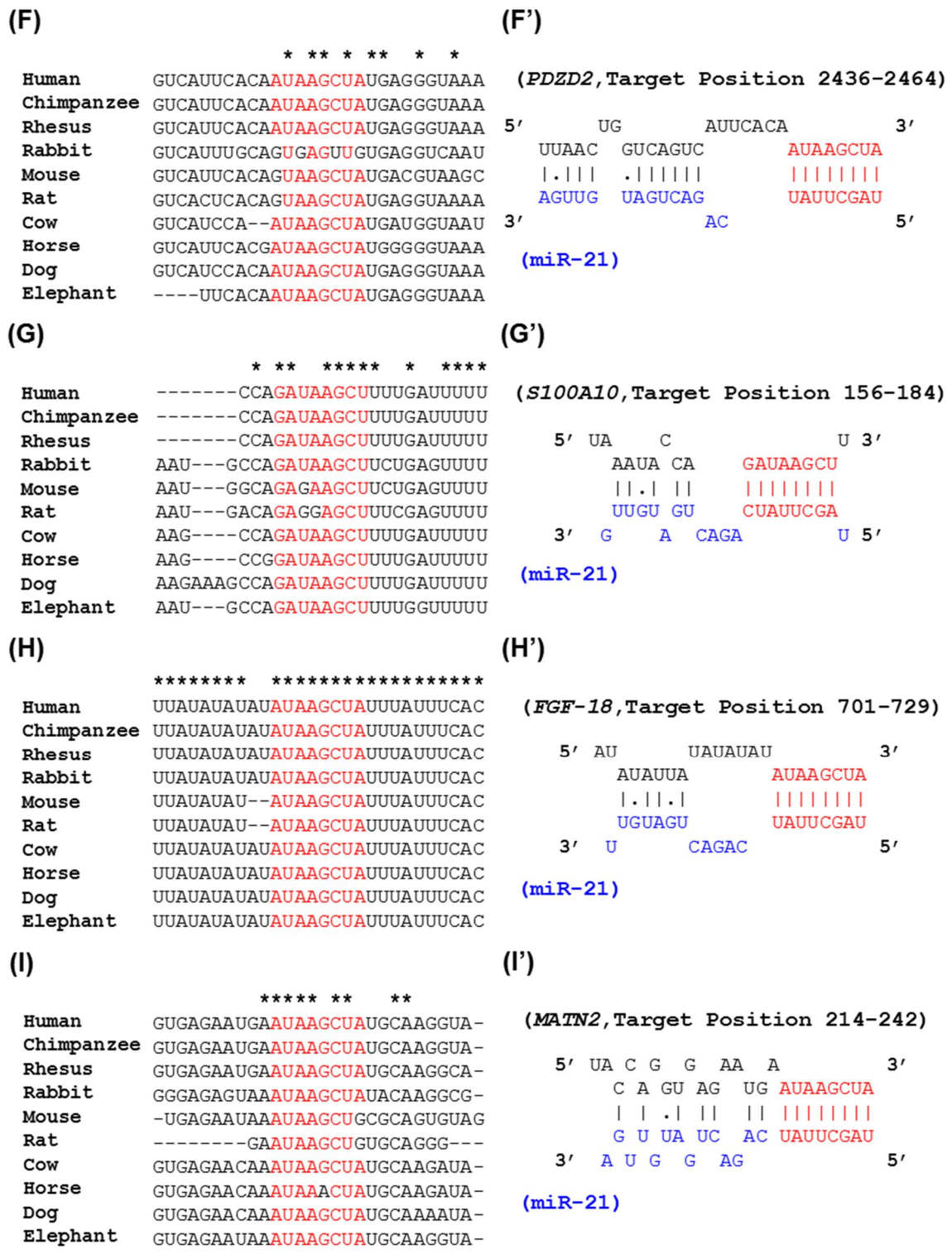

Figure 5.11. miR-21 and miR-31 3'UTR target site conservation for *PDZD2, S100A10, FGF10* and *MATN2* across different animals. (A-J) Target sequences were acquired using TargetScan and alignment was performed with mega 6. Human complementary nucleotide sequences and 10 nucleotides up- and down-stream are presented. Conserved human complementary nucleotides at the seed binding area are displayed in red and whole nucleotide conservation is indicated with stars. **(A'-J')** mRNA-miRNA hybrid was predicted using Diana v5.0. Seed binding area is displayed in red while remaining nearby nucleotides are shown in black (mRNA) and blue (miR-21) and green (miR-31). **(A)** Esquematic PDZD2 3'UTR displaying miR-21 and miR-31 target sequences **(B-G, B'-G')** *PDZD2*. **(H, H')** *S100A10*. **(I, I')** *FGF18*. **(J, J')** *MATN2*.

5.2.5. Luciferase 3'UTR analysis indicates that miR-21 may directly regulate *S100A10* and *FGF-18*

Specific luciferase reporter plasmids were designed and cloned using *pMIR-REPORT* plasmid for each one of the four targets of interest as detailed in Chapter 2. To avoid non-desired effects on reporter plasmid performance due to *PDZD2* 3'UTR sequence length (2875 pb) four different plasmids were generated including *PDZD2* 3'UTR initial sequence (818 pb), middle sequence (863 pb), terminal sequence (864 pb) and full sequence (2545 pb) (Figure 2.2A) while whole 3'UTR sequences were used for *FGF-18* (814 pb), *S100A10* (245 pb) and *MATN2* (1004 pb). The generated plasmids were co-transfected into HeLa cell line and primary HPMCs with *renilla luciferase* reporter plasmids together with miRNA mimic or inhibitor molecules (Figure 5.12). Relative luciferase expression was significantly reduced when *S100A10* 3'UTR plasmid was co-transfected with miR-21 mimic while showed a trend in increase when co-transfected with miR-21 inhibitor in HeLa cells (Figure 5.12B). Similar trends in *S100A10* 3'UTR driven luciferase expression were observed in two different HPMC donor samples (Figure 5.12B'). Although not significant, a trend in relative luciferase expression consistent with a direct miR-21 regulation of *FGF-18* 3'UTR was observed in both, HeLa and HPMCs (Figure 5.12, A-A'). No trend in luciferase expression was observed when *MATN2* and *PDZD2* reporters were analyzed in HeLa cells (Figure 5.12, C-H). Thus, although more research is needed to confirm these data (see Chapter 5.3), miR-21 may be a real direct regulator of *S100A10* and *FGF-18* in both, HeLa and HPMCs.

Figure 5.12. *FGF-18, S100A10, MATN2* and *PDZD2* 3'UTR luciferase reporter assay indicates that miR-21 may directly regulate *S100A10* and *FGF-18* sequence. Relative luciferase activity of target 3'UTR reporter plasmids generated and co-transfected with miR-21/miR-31 mimic or inhibitor molecules were compared with co-transfections using specific controls after 48 h. **(A, A')** *FGF18*. **(B, B')** *S100A10*. **(C)** *MATN2*. **(D)** *PDZD2* first 3'UTR sequence. **(E)** *PDZD2* central 3'UTR sequence. **(F)** *PDZD2* terminal 3'UTR sequence. **(G)** Full *PDZD2* sequence. **(A-G)** experiments were performed in HeLa cells while **(A'-B')** were performed in HPMCs. Firefly reporter was co-transfected with 5 pM of miRNA mimic or inhibitor and normalized to *Renilla* luciferase. Data represent the mean S.E.M. from four independent experiments done by duplicate for HeLa and two independent donor experiments done by duplicate for HPMCs. **p < 0.01.

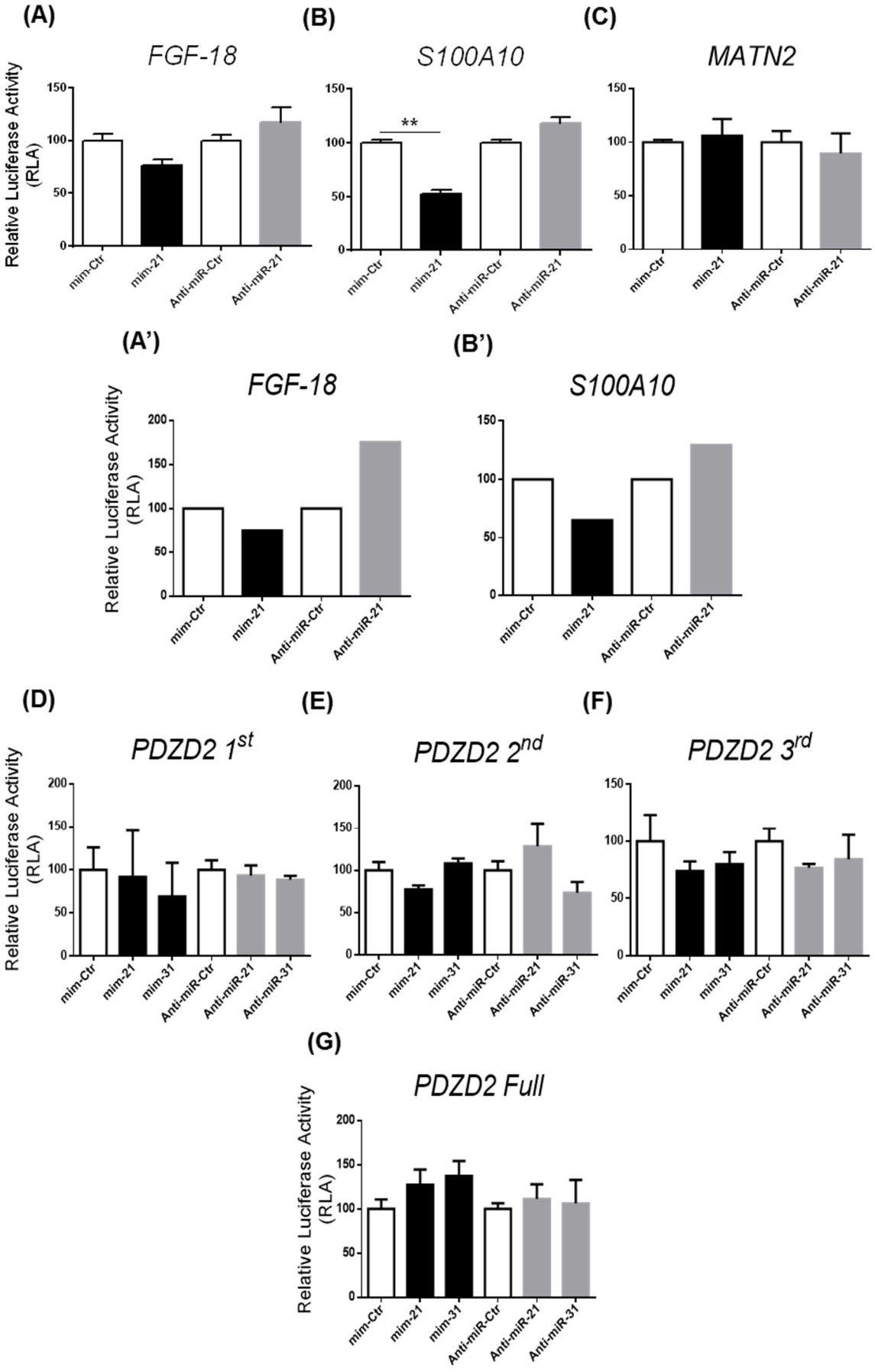
(A)
FGF-18
Relative Luciferase Activity (RLA)
150
100
50
0
mim-Ctr
mim-21
Anti-miR-Ctr
Anti-miR-21
(B)
S100A10
**
(C)
MATN2
(A')
FGF-18
200
(B')
S100A10
(D)
PDZD2 1st
mim-31
Anti-miR-31
(E)
PDZD2 2nd
(F)
PDZD2 3rd
(G)
PDZD2 Full

5.2.6. Target specific down-regulation and downstream contribution in HPMCs

Specific siRNA molecules were purchased for each one of the four targets of interest and were transfected for 48 h into HPMCs to study their broad contribution to the MMT process. No differences in mesothelial cell phenotype were observed under light microscopy after 48 h of specific siRNA delivery into primary HPMCs compared with controls. Additionally, all mesothelial and mesenchymal markers previously associated with TGF-β1 induced MMT process (Figure 3.1 and 3.3), were studied in this context. Target specific siRNA molecules were, in all cases, able to reduce mRNA expression of the particular target of study (Figure 5.13). No significant changes in the transcription of mesothelial nor mesenchymal markers were identified after *FGF-18* down-regulation (Figure 5.13, A-A''). Unexpectedly, *S100A10* down-regulation showed to increase Claudin mRNA expression in a significant fashion (Figure 5.13B'). Interestingly, *MATN2* up-regulated Snail transcription (Figure 5.13C'') and *PDZD2* showed to induce Snail mRNA expression in a non-significant manner while down-regulated E-cadherin, ZO-1 and Occludin transcriptional levels (Figure 5.13C' and C''). There have been no previous identification and/or characterization of either of these targets during the MMT process associated to peritoneal dialysis and therefore, little is known about their possible contribution in this context. Nevertheless, a detailed analysis of each target feasible contribution to the MMT process described in literature is discussed during the next section (see 5.3).

Figure 5.13. *PDZD2* may contribute to MMT process via mesothelial cell adhesion regulation in HPMCs. mRNA expression after 48h of siControl, siFGF-18, siS100A10 and siMATN2 (40 nM) and siPDZD2 (30 nM) delivery in HPMCs. siControl – white bars, siTarget – black bars and six independent donor experiments. Mesothelial mRNA markers studied include E-cadherin, ZO-1, Occludin and Claudin while Mesenchymal mRNA markers determined covered Fibronectin, Collagen I, Snail and α-SMA. **(A)** siFGF-18. **(B)** siS100A10. **(C)** siMATN2. **(D)** siPDZD2. Data were analyzed by paired *t* test or paired multiple *t* test corrected for multiple comparisons by Holm-Sidak. Data represent the mean S.E.M. from six independent donor experiments. *$p < 0.05$; **$p < 0.01$; ***$p < 0.005$.

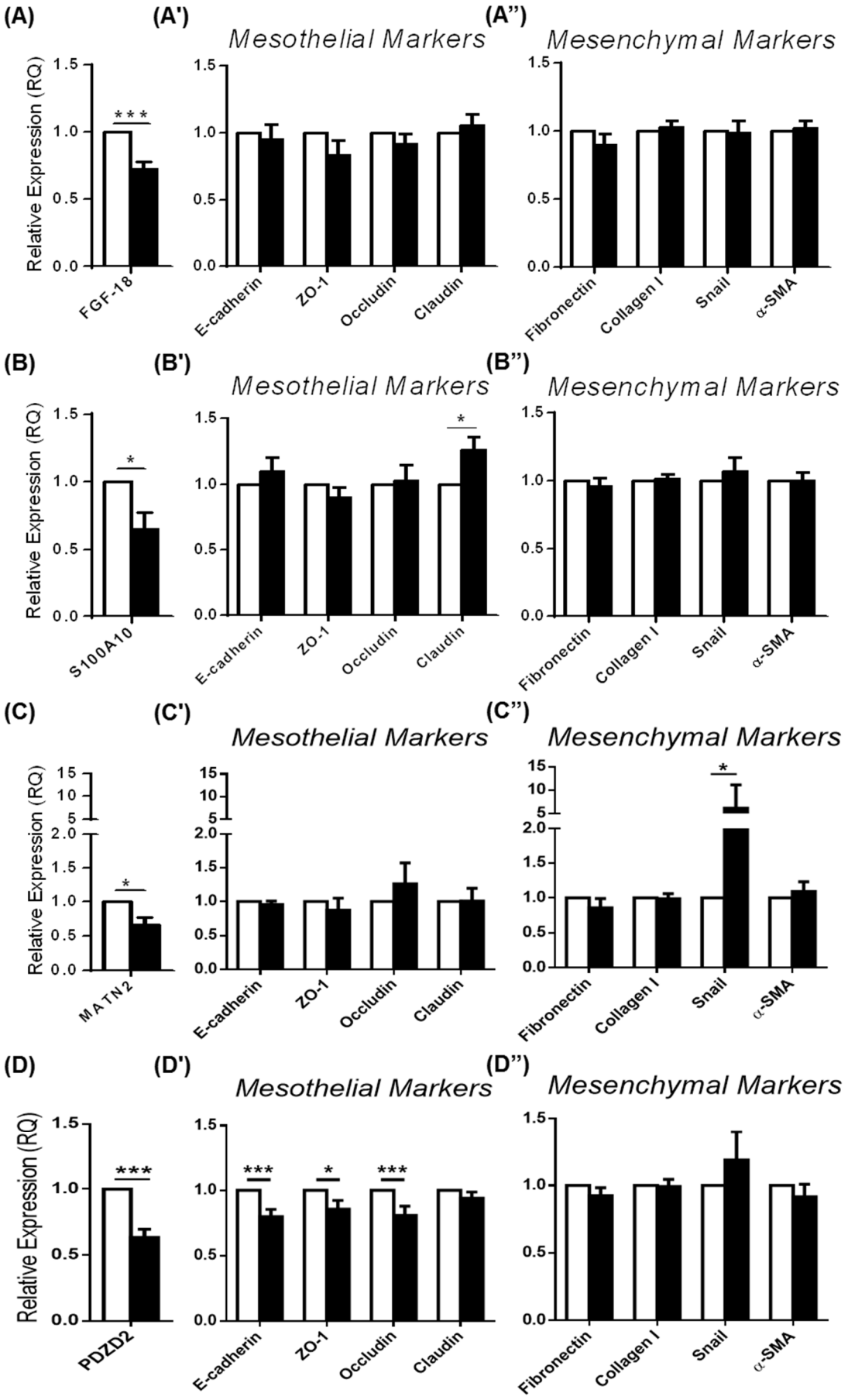
(A)
(A')
(A")
Mesothelial Markers
Mesenchymal Markers
Relative Expression (RQ)
FGF-18
E-cadherin
ZO-1
Occludin
Claudin
Fibronectin
Collagen I
Snail
α-SMA
(B)
(B')
(B")
S100A10
(C)
(C')
(C")
MATN2
(D)
(D')
(D")
PDZD2

5.3. Discussion

miRNA function is ultimately defined by the pool of mRNA that a specific miRNA may target and its regulatory effect on their expression in a defined context. Undoubtedly, the recognition and study of specific direct miRNA targets is one of the most difficult fields in miRNA research. It is important to acknowledge here that a lack of change in mRNA levels during a specific context and/or after miRNA mimic/inhibitor transfection does not exclude the possibility of studying a real target (Figure 5.3 and 5.4, B and C) (Pasquinelli, 2012). Indeed, metazoan miRNAs mediate translational repression, mRNA degradation, or a combination of both. The levels of mRNA destabilization by miRNAs has been a classic polemic topic in the field of miRNA research. Nevertheless, experimental re-evaluation of miRNAs described to down-regulate protein production in the absence of mRNA destabilization demonstrated broad transcriptomic imprint on seed-matched mRNAs (Guo et al, 2010).

Of note, miRNA mimic/inhibition transfection into cells may show and/or create interactions that do not happen at animal level. Additionally, luciferase 3'UTR reporters are an artificial tool to identify direct miRNA regulation *in vitro*. It is important to consider that different cell types will also express a different panel and levels of RNA-binding proteins, shaping intracellular 3'UTRs tertiary structures which may thus vary considerably from algorithm predictions. Additionally, gain and loss of function as well as reporter assays are performed here with miRNAs that are already expressed in large levels, which may also mask real target modulation due to the lack of profound, easily recognizable effects. These considerations may explain the fact that some miR-21 direct targets described in the literature were not found to be regulated in HPMCs when miRNA levels of expression were manipulated *in vitro*, including *SPRY1, PTEN* and *TIMP3* (Figure 5.3 and 5.4, B and C; Figure 5.8 E and E'). This may also be relevant to the lack of a trend in *MATN2* and *PDZD2* 3'UTR luciferase reporter expression when co-administrated with miRNA mimic/inhibitor molecules (Figure 5.12, C-H). Nevertheless, experiments based on gain and loss of miRNA function together with the study of the 3'UTR reporters of possible mRNA targets are broadly accepted and considered to be

the major bench techniques to demonstrate direct and/or indirect mRNA regulation by a specific miRNA.

To understand how miR-21 up-regulation may lead to MMT and fibrosis in the peritoneal membrane, the expression of already described miR-21 target genes was studied. Here, miR-21 mediated repression of PDCD4 in mesothelial cells, at both mRNA and protein levels (Figure 5.3A, 5.4A and 5.5, A-C). PDCD4 down-regulation has been shown to trigger an increase in Snail protein and a consequent decrease in E-cadherin expression, which in turn stimulates β-catenin/TCF dependent transcription (Asangani et al, 2008; Brønnum et al, 2013; Yao et al, 2011) (Figure 5.5D). Thus, miR-21 down-regulation of PDCD4 in HPMCs may not only contribute to the detachment of inter-mesothelial adhesions but also to the acquisition of a new molecular program, dictating a distinct expression regulation characteristic of an MMT process (Figure 5.5D). Additionally, further research to modulate PDCD4 protein levels using miR-21 inhibitor molecules would have been interesting, but this was finally not possible due to the limited time of this project.

Target-prediction tools have improved during recent years (Table 2.7). Nevertheless, there is still a substantial divergence in their predictions, as shown in Figure 5.6. Due to the experimental approach selected to conduct this research there was a large number of miRNA-target interactions initially selected for direct miRNA regulation inquiry (Figure 5.6), and analysing protein changes at the model of study as well as gain and loss of function assays would have been an arduous starting point. Therefore, mRNA expression changes were used to screen likely direct and indirect changes induced by miRNA in this context. It is possible that some direct miRNA-target interactions may have been masked by the selected approach of study due to non-destabilized mRNA expression and/or mediating translational repression (Figure 5.8 and 5.9). Nevertheless, this was a necessary choice due to the limited time of the project.

Although the relative importance of target site conservation is a matter of argument in the miRNA field, conserved sites exhibit greater real miRNA recognition than non-conserved sites with similar sequence context scores (Bartel, 2009). Doubtless, due to large specific favourable context selection of conserved sites while researchers

and currently available target prediction algorithms are still unaware of all features characterizing these contexts. For this reason, to further study target site conservation of the four targets selected for research including *FGF-18, S100A10, MATN2* and *PDZD2* (Figure 5.11) was decided.

Deep genome studies of miRNA target site conservation and efficacy showed that 7-8 nt target sites are more effective when located in non-middle regions of long 3'UTRs (Grimson et al, 2007). This may explain the apparent non-direct regulation of *PDZD2* by miR-21 and miR-31 even when several target sites were identified (Figure 5.11A). *PDZD2* 3'UTR total length was 2875 pb, which is much longer than human 3'UTR average ~ 800 pb (Mignone et al, 2002), and miRNA sites contained at the 3'UTR region may be blocked by side segment interactions. Nevertheless, the three fractions of *PDZD2* 3'UTR reporters analyzed contained ~ 800 pb in all cases and did not show luciferase regulatory trend in expression when co-transfected with miR-21 and miR-31 miRNA mimic/inhibitory molecules (Figure 5.12, D-H). Additionally, the lack of a trend in *MATN2* 3'UTR luciferase expression when administrated with miR-21 mimic/inhibitory molecules indicated that *MATN2* is unlikely to be a direct miR-21 target (Figure 5.12C).

FGF-18 3'UTR reporter was found to have a non-significant trend in luciferase expression regulation when co-transfected with miR-21 mimic/inhibitory molecules, in both HeLa and primary HPMCs (Figure 5.12 A and A'). *S100A10* 3'UTR reporter displayed a significant luciferase expression down-regulation when co-administrated with miR-21 in HeLa cells, while a trend in increase if delivered with miR-21 inhibitory molecules (Figure 5.12B). Additionally, *S100A10* 3'UTR showed similar luciferase expression trends when co-administrated with miR-21 mimic/inhibitory molecules in primary HPMCs (Figure 5.12B'). Although not definitive, these results indicate that miR-21 may regulate both targets in a direct manner. In order to definitively prove this possibility, 4 nt seed region site mutagenesis has been used to generate mutant versions of *FGF-18* and *S100A10* 3'UTR luciferase reporters (see Chapter 2). Due to the limited time of this project, to show the significance of wild-type *FGF-18* and *S100A10* 3'UTR luciferase reporter expression when co-administrated with miR-21 mimic/inhibitory molecules as well as its abrogation by the use of 3'UTR luciferase reporters containing miR-21 seed region site mutations was not possible. Thus, future research approaching the above

mentioned experimental conditions would be necessary to conclusively identify *FGF-18* and *S100A10* as miR-21 direct targets.

The research developed during this chapter identified two new indirect miR-21 targets, *MATN2* and *PDZD2*, as well as two direct and/or indirect miR-21 target genes comprising *FGF-18* and *S100A10* (Figure 5.12) all of which were down-regulated in a MMT model mRNA array and may be important during the MMT process associated to PD therapy. During this process, miR-21 may regulate the above mentioned targets to control cellular decisions pivotal in MMT progression and/or finely tune specific protein networks. Of note, no previous description of *MATN2* and *PDZD2* expression in mesothelial cells have been reported before this research was performed. Additionally, none of these genes have been characterized as downstream miR-21 targets, neither have they been linked to the process of mesothelial to mesenchymal transition during PD therapy. A summary of the possible implications of work in other fields for these newly identified miR-21 targets is presented below.

FGF-18

FGF-18 belongs to the FGF family of polypeptides, involved in cell growth, differentiation, morphogenesis, tissue remodelling, inflammation, angiogenesis, tumour growth and developmental processes (Haque et al, 2007). The FGF family includes 22 members in humans which signal *via* tyrosine phosphorylation mediated by FGF receptors (FGFR1-4 and FGFRL1) and auxiliary intermediate molecules (Haque et al, 2007). Although structurally related, FGFs display distinct functions, secretory and receptor-mediated machinery and, therefore, trigger different ultimate biological functions.

FGF-18 is expressed during embryonic development and throughout lifespan. Transgenic FGF-$18^{-/-}$ mice are viable during embryonic development but die soon after birth due to cyanosis (Liu et al, 2002). FGF-$18^{-/-}$ mice expressed a distinct phenotype characterized by skeletal abnormalities, incomplete development and 10-15% size reduction (Liu et al, 2002) and mice with conditional deletion of FGF-18 in the lung displayed thicker interstitial mesenchymal compartments, embedded capillaries and reduced cell proliferation (Usui et al, 2004). On the other hand, overexpression of FGF-

18 in transgenic mice induced epithelial and mesenchymal proliferation in numerous tissues demonstrating FGF-18 pleiotropic growth factor effects (Hu et al, 1998) later shown to be highly dependent on context. Indeed, FGF-18 function has been shown to be deeply dependent on its spatial and temporal expression as well as on the expression of its receptors and the presence of specific growth factors. FGF-18 binds with high affinity to FGFR3 and FGFR4 but modestly to FGFR2 (Haque et al, 2007; Zhang et al, 2006) acting in a paracrine and/or autocrine fashion. Mesothelial cells express FGFR1-4, sustaining higher levels of FGFR4 and FGFR1 (Schelch et al, 2014). Thus, FGF-18 may act in mesothelial cells in an autocrine manner *via* FGFR4 stimulation.

In control fibroblasts, FGF-18 inhibited cell growth and enhanced migration (Joannes et al, 2016). The authors observed a non-significant increase in MMP2 and MMP3 expression, two matrix metalloproteinases implicated in extracellular matrix degradation and cell migration which are often necessary to acquire a cell migratory phenotype (Joannes et al, 2016). FGF-18 induction also enhances the expression of Snail1/2 homologs in a lung-targeted FGF-18 mouse model (Franco-Montoya et al, 2011). Additionally, FGF-18 partially inhibited TGF-β1-induced fibroblast activation (Joannes et al, 2016) and down-regulated collagen I expression in chondrocytes (Yamaoka et al, 2010). Of note, FGF-18 over-expression in lung decreased extracellular matrix and connective tissue components including matrilin-2 (Franco-Montoya et al, 2011). Interestingly, FGF-18 transcript was increased here, in a model of early mesothelial to mesenchymal trans-differentiation while decreased during later stages of the process (Figure 5.7I), and may act fine-tuning MMT associated to PD therapy. Thus, initial mesothelial FGF-18 up-regulation may be important for mesothelial cell acquisition of migratory capabilities to colonize the peritoneal submesothelial compact zone while later FGF-18 down-regulation may be necessary in order to develop a secretory phenotype contributing to extracellular matrix deposition.

Of note, FGF-18 was up-regulated in de-differentiated chondrocytes and was suggested to be a marker of de-differentiation (Yamaoka et al, 2010). Conversely, TGF-β1 has also been shown to stimulate the expression of FGF-18 in chondrocytes (Mukherjee et al, 2005). Following these and Franco-Montoya et al. 2011 observations indicated above it would be especially interesting to study time courses of HPMC

incubated with TGF-β1 for FGF-18 and matrilin-2 expression, as well as HPMCs incubated with FGF-18 for genes associated with TGF-β1 signalling and MMT. Additionally, it would also be interesting to investigate MMP2, MMP3, Snail1 and Snail2 HPMCs time-profiles after exogenous FGF-18 stimulation and knockdown *via* siFGF-18.

S100A10

S100A10, also known as p11, belongs to the S100 gene family together with 19 additional small isoforms in humans which have been involved in transcription, secretion, contraction, motility, cell growth, differentiation and cell cycle progression (Madureira et al, 2012). S100A10 is ubiquitously expressed and its distinctiveness from S100 family members lies in its incapability to bind Ca^{2+} and its constitutively active structure (Réty et al, 1999). Although S100A10 can be found as a homodimer, the predominant form of S100A10 is in a heterotetrameric complex with annexin A2 (AIIt), consisting of two copies of annexin A2 and S100A10 homodimers (Bharadwaj et al, 2013; Madureira et al, 2012). Indeed, annexin A2 is essential for S100A10 extracellular transport *via* the exosomal pathway (Fang et al, 2012), AIIt anchorage to the plasma membrane in a Ca^{2+} dependent fashion (Deora et al, 2004; Filipenko et al, 2000), and S100A10 protection from ubiquitin-dependent degradation (Yang et al, 2011).

Between the multiple functions attributed to S100A10 probably the most physiologically remarkable is its extracellular function as a plasminogen receptor. Within the cell surface AIIt complex, S100A10 binds plasminogen and mediates its activation by plasminogen activators, stimulating plasminogen conversion to wide protease plasmin and promoting fibrinolysis (Surette et al, 2011). S100A10 depletion using small interfering RNA in a human microvascular endothelial cell line *in vitro* showed a significant impairment in plasminogen binding (50%) and plasmin generation (60%) compared with controls (Surette et al, 2011). S100A10-null mice, although viable, showed impaired fibrinolysis and increased tissue fibrin deposition including in lungs, liver, spleen and kidney compared to wild-type mice litter mates (Surette et al, 2011). Thus, reduced S100A10 expression in HPMCs associated to PD therapy may reduce their fibrinolytic activity contributing to the accumulation of fibrin in the peritoneal membrane.

In kidney cells, S100A10 is involved in the formation of E-cadherin-based adherens junctions (Yamada et al, 2005) and mediates annexin A2:AHNAK interaction at the plasma membrane regulating actin cytoskeleton organization and cell membrane cyto-architecture (Benaud et al, 2004). Indeed, actin confocal microscopy analysis showed more flattened cell morphology when S100A10 depleted cells were compared with controls (Benaud et al, 2004) and sub-membranous complex between AHNAK and AIIt physically interacting with the actin cytoskeleton has been proposed (Hohaus et al, 2002). In this regard, it would have been also especially interesting to further study the downstream effects of miR-21 driven S100A10 down-regulation in HPMCs cell-cell adhesions as well as actin cytoskeleton.

In PD therapy, peritoneal dialysis fluids may impair the function of macrophages affecting pathogen clearance. This hypothesis was suggested by Ogata et al. 2011 who raised the possibility that potential of mesothelial cells to recruit monocyte/macrophages would be affected in PD patients (Ogata et al, 2011). Indeed, intraperitoneal administration of PDF suppressed infiltration of mononuclear cells in the peritoneum of mice following lipopolysaccharide injection (Ogata et al, 2011). Cell surface plasmin production is required for leukocyte recruitment to areas of inflammation (Gong et al, 2008) and macrophage recruitment may be partially impaired during PD therapy due to lower S100A10 expression levels and therefore, lower plasmin production.

In cancer, S100A10 levels have been described to be generally up-regulated. Nevertheless, mass spectrometry used to identify S100 isoform expression in thyroid samples found a significant decrease in S100A10 and annexin A2 in follicular adenoma and carcinoma and lower expression in papillary carcinoma when compared with normal thyroid samples (Martínez-Aguilar et al, 2015). Serial analysis of gene expression also identified S100A10 down-regulation in breast cancer irrespective of pathological state (Carlsson et al, 2005). Immunohistochemistry of prostate cancer patients also indicated S100A10 reduction of expression in all patients and 65% of prostate intraepithelial neoplasia (prostate cancer precursor) (Yee et al, 2007). The mechanism by which S100A10 is expressed and post-transcriptionally regulated is largely known and appears to be cell-type-specific. The research developed during this thesis showed a possible

direct regulation of S100A10 by miR-21 in peritoneal membrane fibrosis associated to PD treatment but may also establish the basis to understand S100A10 post-transcriptional regulation in further contexts.

MATN2

Matrilin-2 is a protein encoded by MATN2 gene that belongs to a four-member family of multi-subunit extracellular matrix proteins which are intimately structurally related and have been involved in the development of fibrillary structures and to act as adaptors between matrix components (Klatt et al, 2011). Matrilin-2 is widely expressed in connective tissue cells, smooth muscle and epithelia in which is pericellularly deposited (Klatt et al, 2011). Matrilin-2 has been shown to directly bind collagen I and non-collagenous proteins such as fibrillin-2, fibronectin and laminin-1-nidogen-1 complexes (Piecha et al, 2002), as well as weakly binding to α1β1 integrin (Mann et al, 2007), contributing to extracellular matrix supra-molecular organization and homeostasis. Transgenic matrilin-$2^{-/-}$ mice is viable, fertile and histologically normal during different embryonic and postnatal stages (Mátés et al, 2004). The lack of a distinct matrilin-$2^{-/-}$ mice phenotype may be due to redundant matrilin functions, but still affect animal survival under natural conditions. Indeed, matrilin-$2^{-/-}$ mice developed inferior axonal growth recovery after injury (Jonas et al, 2014), was a key molecule during myogenic differentiation (Deák et al, 2014), grew sporadic microscopic tumour in the liver at 10 months age (Fullár et al, 2014) and cellular matrilin-2 knock-down induced serious defects in skin wound healing (Ichikawa et al, 2008).

Interestingly, matrilin-2 has been involved in the control of the early stages of myogenic differentiation (Deák et al, 2014). *In vitro* and *in vivo* models of muscle differentiation exhibited a transient but crucial increase in matrilin-2 mRNA and protein level during myoblast differentiation followed by a decline in its expression during myofiber maturation (Deák et al, 2014). Indeed, matrilin-2 showed to induced a switch of the core transcription machinery associated to myofibroblast differentiation (Deák et al, 2014). Additionally, Ichikawa et al. 2008 studies showed that matrilin-2 regulated wound healing in an *in vitro* model using human keratinocyte cells (Ichikawa et al, 2008). In this model, matrilin-2 reduction induced cell migration into wound without cell proliferation and in a temporal regulated fashion (Ichikawa et al, 2008). Throughout

wound healing, extracellular matrix surrounding the wound area is degraded to facilitate subsequent wound cell migration and cellular repopulation together with new extracellular matrix deposition into the area. Taking together, these research indicate that proper temporal regulation of matrilin-2 expression may be especially important in mesothelial cell acquisition of a mesenchymal phenotype and mediating inflammatory responses as well as a possible migration into the submesothelial compact zone. Similarly, matrilin-2 transcript was shown here to be increased in a model of early mesothelial to mesenchymal trans-differentiation while decreased during later stages of the process and after TGF-β1 stimulation (Figure 5.7J), and may act fine-tuning MMT associated to PD therapy.

Of note, TGF-β1 showed to decrease matrilin-2 expression in myoblasts (Deák et al, 2014) and keratinocytes (Ichikawa et al, 2008), and may mediate the adequate matrilin-2 expression timing during myoblast differentiation and keratinocyte migration. Matrilin-2 promoter contains seven putative Smad sites that may mediate TGF-β1 inhibitory effect (Deák et al, 2014; Ichikawa et al, 2008). Additionally, this study proposed that TGF-β1 mediated miR-21 up-regulation may indirectly contribute to regulate differentiation programs and cell migration *via* matrilin-2 mRNA regulation (Figure 5.7J, 5.8H, 5.9H and 5.11C).

Matrilins have been shown to weakly interact with integrins promoting mild cell attachment which downstream capability to activate signal transduction and induce gene expression is unknown (Mann et al, 2007). Here, transient matrilin-2 mRNA know-down in primary HPMCs greatly induced Snail transcription in a significant fashion (Figure 5.12D). Nevertheless, future research should be conducted to establish the possible significance of these results at both, mRNA and protein levels, as well as their contribution during the MMT process associated to PD therapy and fibrosis.

PDZD2

PDZD2 (also known as PAPIN, AIPC, PIN1 and PDZK3) is a 301 kDa protein encoded by PDZD2 gene. PDZD2 is a ubiquitously expressed six-PDZ (PSD95, Discs-large and ZO-1) domain protein which domains are conserved protein-protein interaction modules that recognize specific carboxy-terminal sequences acting as molecular

scaffolds to enable macromolecular complexes assembly (Yeung et al, 2003). PDZD2 shows homology with pro-interleukin-16, an atypical cytokine that has been shown to function as a growth and differentiation factor in various cell types (Richmond et al, 2014; Yeung et al, 2003). C-terminal PDZD2 has been shown to be cleaved in a caspase-3-dependent mechanism to generate secreted PDZD2 (sPDZD2, of 37 kDa) containing two PDZ domains which may also interact with extracellular proteins facilitating the formation of extracellular complexes (Yeung et al, 2003).

In rats, PDZD2 was shown to interact with the basic helix-loop-helix transcription factor E12. Rat tagged PDZD2 over-expression experiments showed endoplasmic reticulum and nuclear localization in COS-7 cells (kidney from African monkey) (Yeung et al, 2003). Nevertheless, previous reports have detected PDZD2 at cell-cell contacts in lung sections and rat kidney cells (Deguchi et al, 2000) and at cytoplasm in prostate section (Chaib et al, 2001). PDZD2 has also been shown to interact with p0071, a ubiquitous member of the p120 catenin family of proteins, and to co-localize with classical cadherins at cell-cell junctions in lung sections and rat kidney cells (Deguchi et al, 2000; Keil et al, 2013). Thus, reduced PDZD2 expression in HPMCs associated to PD therapy may lessen cellular scaffolding function contributing to the loss of epithelial junctions in the peritoneal membrane.

In vitro treatment with recombinant sPDZD2 has been shown to induce p53 mRNA and protein up-regulation in human prostate cancer (DU-145), breast adenocarcinoma (MCF-7) and liver cancer (Hep-G2) cell lines (Tam et al, 2008). Of note, p53 protein is a transcriptional trigger of cell cycle arrest, senescence, and apoptosis which gene (TP53) is frequently mutated in human cancer (Vousden & Lane, 2007). Termen et al. 2013 showed that a unique allele p53 mutated is enough to speed mammary cell response to TGF-β1 driven EMT compared with wild type p53 which inhibits EMT and mammosphere growth (Termén et al, 2013). Interestingly, the authors also indicated that TGF-β1 stimulation led to a significant down-regulation of total p53 protein levels (Termén et al, 2013) which was explained *via* Mdm2 as indicated by Araki *et al.* 2010 (Araki et al, 2010). Indeed, co-treatment with p53 siRNA and TGF-β1 showed quicker E-cadherin and ZO-1 down-regulation as well as actin cytoskeleton reorganization into stress fibers with N-cadherin and fibronectin induction in mammary

cells (Termén et al, 2013). Taken together, in HPMCs, TGF-β1 induced PDZD2 down-regulation may also decrease sPDZD2 driven autocrine stimulation reducing p53 cellular levels and leading a more robust MMT response. Of note, PDZD2 has also been found to be expressed at the nucleus (Yeung et al, 2003) and may, therefore, have a direct nuclear function during the MMT process. Here, PDZD2 down-regulation was able to induce Snail mRNA expression in a non-significant fashion while significantly down-regulated E-cadherin and Occludin transcriptional levels (Figure 5.11D).

FGF-18, S100A10, MATN2 and PDZD2: four miR-21 targets in context

miR-21 was one of the first members of the small non-coding miRNA family to be characterized (Cai et al, 2004). Human miR-21 is located on chromosome 17q23.3 (mice, chr.11), in an intronic region of transmembrane protein 49 (TMEM49) gene, a homolog of rat vacuole membrane protein (VMP1) involved in cell-to-cell adhesion. Different promoters and primary transcripts have been characterized within the terminal intronic regions of TMEM49 resulting in a complex, and not fully understood, regulation network of miR-21 encoding transcripts (Cai et al, 2004; Fujita et al, 2008; Ribas et al, 2012). Primary miR-21 (pri-miR-21) originates within the last TMEM49 introns and bypass TMEM49 polyadenylation signals to include miR-21 hairpin (Cai et al, 2004). Conversely, TMEM49 transcripts initiate ~ 130 kb upstream miR-21 and can splice and polyadenylate upstream miR-21 hairpin but also bypass these polyadenylation signals to include miR-21 transcript, TMEM49-miR-21-regulation(Ribas et al, 2012). Mature miR-21 and consensus promoter regions are highly conserved sequences among vertebrates which may indicate a highly conserved transcriptional regulatory mechanism. miR-21 promoter holds conserved conserved enhancer elements including binding sites for activation protein 1 (AP-1; Fos and Jun family nuclear oncogenes), Ets/PU.1,C/EBP-α (factors governing haematopoietic lineage differentiation), nuclear factor I (NFI), serum response factor (SRF), p53 and signal transducer and activator of transcription 3 (STAT3) (Krichevsky & Gabriely, 2009).

miR-21 is one of the most highly expressed miRNAs in mammalian cells and its expression is further enhanced in many disease states including solid tumors and inflamed tissue. In this context, miR-21 has been highly associated with glioma, breast, ovarian, colorectal, stomach, HCC, prostate, pancreas, lung, head, thyroid, cervical,

leukemia and B-cell cancers in which has been mainly involved in proliferation, invasion and metastasis. Nevertheless, for the majority of cancers pri-miR-21 does not change while there is an increase in mature miR-21. Indeed, it has been shown that different molecules including SMAD2/3 recruit pri-miR-21 in a complex with the RNA helicase p68, a component of the Drosha microprocessor complex leading to a quick (< 30 min). pri-miR-21 processing to pre-miR-21 and following miRNA maturation.

Phenotypic repercussions of transiently disturbing unique miRNA and/or miRNA-target interplay are predicted to be subtle. Transient specific miRNA modulation as well as independent target down-regulation using specific siRNA molecules in HPMCs did not display evident phenotypic differences compared with controls. Additionally, mesothelial and mesenchymal markers studied after specific target down-regulation were not affected in a drastic manner (Figure 5.13). Nevertheless, target siRNA downregulation was probably suboptimal and greater target downregulation may show more obvious phenotypic as well as mesothelial and mesenchymal markers effects. Single miRNA-target site interaction is expected to trigger an mRNA down-regulation of less than 50% (Bartel, 2009). Additionally, the majority of mRNAs that contain conserved target sites for a specific miRNA also own further conserved regions for independent miRNAs (Lewis et al, 2005) and, therefore, multiple miRNA may have to be modulated before dramatic effects are seen on some targets. Similarly, target genes may be able to exhibit a certain degree of mRNA and protein changes in the absence of measurable repercussions. Thus, cellular regulatory networks may be able to absorb here a defect and/or excess of a specific target and/or miRNA. In this context, several particular perturbations more likely mimicking context real situations may be needed in order to achieve detectable phenotypic effects. Finally, the level of miRNA and/or target gain and/or loss of function triggered by the experimental conditions may be only able to produce a relatively mild phenotype that may be accurately measured by comparative sequencing analysis. Due to study time limitations to perform further research on simultaneous multiple target perturbations in order to characterize a possible characteristic phenotype was not possible, but future research addressing this potential may be especially interesting.

In conclusion, this research demonstrated that miR-21 and miR-31 up-regulation may lead to MMT and fibrosis in the peritoneal membrane *via* previously described targets including, respectively, *PDCD4* and *LATS2/STK40* (Figure 5.1, 5.3 and 5.4). In particular, miR-21 *PDCD4* regulation may trigger an increase in Snail contributing not only to inter-mesothelial adhesions loss but also to the acquisition of a new transcriptional program characteristic of an MMT process (Figure 5.5). Additionally, miR-21 expression was shown in Chapter 3 to better correlate with peritoneal membrane deterioration and may be an especially important molecule driving MMT. miR-21 *in silico* target determination and mRNA array scrutiny of candidates identified thirteen novel putative targets for miR-21 that may be important for the MMT associated with PD therapy (Figure 5.6 and 5.7). From these, *PDZD2* was also predicted to be a common miR-21/miR-31 target (Figure 5.6 and 5.7). The mRNA expression of gene candidates was evaluated in a combined *in vitro* and *ex vivo* model of progressive MMT associated to PD treatment. Interestingly, only three predicted targets did not follow an inverse pattern of expression with miR-21, while three candidates had already been described as miR-21 targets in previous studies (Figure 5.8). miR-21 mimic and inhibitor molecules showed to modulate the expression of four remaining candidates *FGF-18, S100A10, MATN2* and *PDZD2* (Figure 5.9 and 5.10). From these, the research developed here identified two indirect miR-21 targets, *MATN2* and *PDZD2*, as well as two direct and/or indirect miR-21 target genes comprising *FGF-18* and *S100A10* (Figure 5.11 and 5.12). Interestingly, *MATN2* and *PDZD2* expression have not been reported before in mesothelial cells and none of these targets has been previously linked to the MMT process associated to PD therapy. Finally, this project showed for first time that *MATN2* and *PDZD2* down-regulation was able to induce an increase in Snail transcription in HPMCs, which was significant for *MATN2* down-regulation (Figure 5.13C'' and D''). Interestingly, *FGF-18* expression has been previously associated with Snail1/2 regulation (Franco-Montoya et al, 2011) and *S100A10* has been involved in the formation of E-cadherin-based adherent junctions (Yamada et al, 2005). Thus, the four miR-21 targets identified here may contribute to the acquisition of a transcriptional cell machinery able to induce MMT in mesothelial cells. Indeed, *PDZD2* down-regulation was shown to trigger a significant decrease in E-cadherin, ZO-1 and Occludin levels in HPMCs decreasing primary mesothelial cell characteristics *in vitro* (Figure 5.13D'). Thus, the

research developed in this chapter stablished the bases of novel pathways by which miR-21 may drive peritoneal mesothelial MMT *via FGF-18, S100A10, MATN2* and *PDZD2* down-regulation which may, in turn, increase Snail1 transcription triggering a new cellular transcription program.

Chapter 6 – General Discussion

Long-term PD therapy is characterized by the loss of the structural and functional integrity of the peritoneal membrane which leads to a progressive fibrosis, angiogenesis and ultrafiltration failure resulting in a discontinuation of the therapy and, ultimately, transition to hemodialysis (Aroeira et al, 2007; Davies et al, 1998; Williams et al, 2002). PET can provide therapy functional information, but continuous morphological biopsy analysis is impractical. In PD patients, continuous dialysis fluid exchanges allows easy access to monitor potential peritoneal biomarkers for structural and functional peritoneal membrane changes. PDE contains several intra-peritoneal and leukocyte-derived macromolecules, proteins and RNA species, which may serve as potential biomarkers.

The development of biomarkers in complex multifactorial disease, such as PD therapy, is especially challenging. Thus, peritoneal therapy may require multiple biomarkers to achieve the degree of accuracy needed and different biomarkers may be required to address distinct specific questions. My research conducted during this project has allowed to measure miRNAs in PDE-supernatant samples for first time in the field stabilising the methodology necessary for future investigation. Eventually, PDE-miRNAs used as biomarkers may contribute individualizing PD therapy by indicating the adequacy of switching therapy, interrogating and discriminating clinical trials competence and to guiding the development of therapy innovations.

There is an obvious growing interest on miRNA research in the PD field. A clear indication is that while only two studies had been published before my PhD research started, during the course of my experiments a considerable amount of investigations were published (Table 6.1). Up-to-date literature on miRNA regulation of peritoneal cavity homeostasis during PD therapy is summarized in Table 6.1 and has been mainly focused on reported miRNAs associated with EMT in other contexts (Lopez-Anton et al, 2015). Additionally, a compendium of literature on miRNA regulation during PD therapy showing particular evidences in HPMCs are displayed in Figure 6.1.

miRNA	Study Selection	Model (s)	Target(s)	Downstream Signaling	Ref.
Down-regulation: miR-31*, miR-93, miR-100, miR-152, miR-497*, miR-192, miR-198 and miR-200b* **Up-regulation:** miR-122	Microarray analysis (Rat PD model, 4 weeks, total peritoneal tissue)	Rat PD model (4 weeks, total peritoneal tissue)	No	No	(Morishita et al, 2016)
Down-regulation: miR-30a	Microarray analysis (Rat PD model, 4 weeks, total peritoneal tissue)	Rat PD model (4 weeks, total peritoneal tissue) HMrSV5 and primary rat PMCs TGF-β1 stimulated Total peritoneal tissue from PD patients miR-30a stable overexpression in HMrSV5	Snail1[&]	miR-30a acts as a negative regulator of TGF-β1 and induces Snail1-dependent EMT during peritoneal fibrosis	(Lin et al, 2015)
Down-regulation: miR-653*, miR-598* **Up-regulation:** miR-136, miR-703[#], miR-30b, miR-107	Microarray analysis (Rat PD model, MGO-induced MMT, 1-2 weeks, total peritoneal tissue)	Rat MGO-induced MMT PD model (1-2 weeks, total peritoneal tissue) Rat MGO-induced MMT PD model. with miR-30b-ASO *Ex vivo* rat PMCs cultured *in vitro*	BMP7 (miR-30b)	BMP-7 is down-regulated in rat MGO-induced EMT PD model, reverted by miR-30b-ASO and directly targeted by miR-30b, which could antagonize TGF-β1 effects.	(Zhou et al, 2013)
Down-regulation: miR-200a-3p **Up-regulated:** miR-182-5p*, miR-488-5p, miR-296-3p, miR-292-5p*	Microarray analysis (mouse PD model, 4 weeks, total peritoneal tissue)	Mouse PD model (4 weeks, total peritoneal tissue)	No	No	(Liu et al, 2014)
Down-regulation: miR-129-5p	Microarray analysis (PDE-derived HPMCs from PD patients)	PDE-derived HPMCs from PD patients HMrSV5 TGF-β1 stimulated miR-129-5p overexpression and SIP1/SOX4 knockdown in HMrSV5 TGF-β1 stimulated	SIP1 SOX4	miR-129-5p modulates E-cadherin and vimentin expression by targeting SIP1 and SOX4 genes or by modulating the promoter activity of E-cadherin and vimentin by the TGF-β1/SIP1 pathway. miR-125-5p protects MCs undergoing MMT TGF-β1-induced during PD and may exert protective effect targeting SIP1 and SOX4.	(Liu et al, 2015)

miRNA	Study Selection	Model (s)	Target(s)	Downstream Signaling	Ref.
Up-regulation: miR-142-3p, miR-21-5p, miR-221-3p, miR-223-3p, miR-34a-5p, miR-327[#]	Microarray analysis (Rat PD model, MGO-induced MMT, 5 days/week treatment during 3 weeks, total peritoneal tissue)	Rat MGO-induced MMT PD model (2 weeks, total peritoneal tissue) Mice MGO-induced MMT PD model with anti-miR-21-5p-LNA Total PDE from PD patients	PPAR-α[&]	No	(Xiao et al, 2015)
Up-regulation: miR-21-5p, miR-31-5p	Microarray analysis (omentum-derived HPMCs TGF-β1 induced MMT)	Omentum-derived HPMCs (TGF-β1 and PD solution stimulated, miRNA mimic/inhibitor) PDE-derived HPMCs from PD patients (E and NE phenotype) PD patients and uremic PD mouse model (mesothelial and sub-mesothelial, FFPE) PDE-supernatant from PD patients	PDCD4[&]	PDCD4 down-regulates SNAIL. E-cadherin down-regulation and β-catenin/TCF dependent transcription activation may be a mechanism by which miR-21 contributes to peritoneal fibrosis	Lopez-Anton et al.)
		Omentum-derived HPMCs (TGF-β1 stimulated, miRNA mimic/inhibitor) PDE-derived HPMCs from PD patients (E and NE phenotype)	FGF-18[$] S100A10[$]	No	(Lopez-Anton et al.)
Down-regulation: miR-589	Un-published (pre-experiment CAPD profile miRNAs)	PDE-derived HPMCs from PD patients PDE-derived HPMCs and HMrSV5 TGF-β1 stimulated miR-589 overexpression in HMrSV5	No	No	(Lopez-Anton et al)
Down-regulation: miR-29b	Literature based: studies on TGF-β1-mediated fibrosis	Mouse PD model with miR-29b overexpression (total omentum and peritoneal tissue)	SP1[&]	Blockade of the Sp1/ TGF-β1/Smad3 pathway may be a mechanism by which miR-29b inhibited peritoneal fibrosis.	(Yu et al, 2014)
Down-regulation: miRNA-200c	Literature based	PDE-derived HPMCs from PD patients	No	No	(Lopez-Anton et al)

miRNA	Study Selection	Model (s)	Target (s)	Downstream Signaling	Ref.
Up-regulation: miR-15, miR-21, miR-192 **No-changes:** miR-377, miR-30, miR-17 **No-detection:** miR-216a, miR-217	Literature-based: studies on potential EMT miRNAs	PDE-derived cells from PD patients	No	No	(Chen et al, 2012a)
Down-regulation: miR-15a, let-7e **Up-regulation:** miR-193a **No-changes:** miR-16, miR-21	Literature-based: studies related to kidney development and diseases	Cultured HPMCs stimulated by D-glucose (Time course, 48 h) as a EMT model	No	No	(Bao et al. 2015)

Table 6.1. miRNAs implicated in the regulation of Peritoneal Cavity Homeostasis during Peritoneal Dialysis Therapy. (Table modified from Lopez-Anton et al. 2015)
*miRNA sequence is not conserved between the model of study and human.
#miRNA sequence is not present in miRBase (v21, June 2014) for rat or human.
&Putative targets already described (Bao et al, 2015).
$Future research is needed for direct target confirmation.

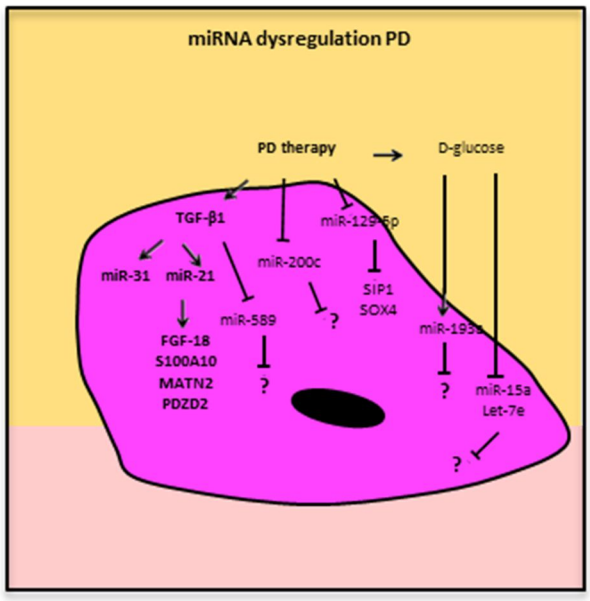

Figure 6.1: miRNA dysregulation in Peritoneal Dialysis. Up-to-date miRNAs for which specific evidence in HPMCs exists are shown. miRNAs and downstream targets studied during this thesis are shown in bold. (Figure modified from Lopez-Anton et al. 2015)

My thesis addressed the role of miRNAs in peritoneal fibrosis associated to PD therapy. Differently from the above mentioned research (Table 6.1 and Figure 6.1), I based my thesis on miRNA profiles of mesothelial cell expression in an *in vitro* model of TGF-β1 induced MMT. I found TGF-β1-driven MMT process in mesothelial cells comprised several research advantages including simplicity, unique stimulus, and cell specificity. These same characteristics can be also considered study limitations as a result of a lack of context. Therefore, I further confirmed the biological relevance of the

miRNAs identified by the validation of miRNA changes in different, well characterized *ex vivo* and *in vivo* models of peritoneal MMT associated to PD therapy. The described *in vitro* model allowed me the identification of miR-21 and miR-31 up-regulation during the MMT process. Consequently, I validated this increase in miRNA expression in different set of MMT models associated to PD therapy including (i) *in vitro* HPMCs treated with diverse PD solutions (cellular and supernatant study), (ii) *ex vivo* PD effluent derived HPMCs with epithelial and non-epithelial phenotype, (iii) peritoneal membrane from an *in vivo* uremic PD mouse model (mesothelial and sub-mesothelial compact zone), (iv) *ex vivo* PDE-supernatant from PD patients, and (v) peritoneal membrane from PD patients (mesothelial and sub-mesothelial compact zone) (see Chapter 3 and 4).

During this project I developed a solid methodology to use small PD effluent samples to quantify supernatant miRNA expression. This protocol optimization allowed me the association of miR-21 and miR-31 transcript levels with peritoneal membrane fibrosis and TGF-β1 pathway activation driving peritoneal MMT. Furthermore, miR-21 showed to specially correlate with different important parameters associated with poor membrane conditions and fibrosis and may contribute to peritoneal MMT in several manners (see Chapter 4). A significant strength of my research was the use of Global Fluid Study registry which is the largest cohort of stable PD patients available worldwide (Lambie et al, 2013). Assessing the comparability of my results with the outcomes obtained by different groups on the matter would be a future milestone. Nevertheless, the goal above mentioned will be especially challenging due to the limited studies published on the field and no-biobank availability.

An especially interesting future application of the technique that I developed here would be the detection of pathogen-specific miRNA signatures during acute peritoneal infection to discriminate individual micro-organisms and impact on treatment outcomes. Indeed, point-of-care tests are urgently sought to diagnose and specifically treat microbial infections to avoid multidrug resistance as recognized by the World Health Organization (WHO). Previous work developed at the Institute of Infection and Immunity in Cardiff University indicated that the host response evoked by distinct organisms is characteristic enough to identify pathogen-specific differences or 'immune fingerprints' before traditional culture results become available. These results combined

with my research developed here rises the idea of using miRNAs to allow the development of a pathogen-specific point-of-care diagnosis for patients with acute infections. MSc Amy Brook, who has just started her PhD in the laboratory, aims to use the technique that I have developed to study PD effluent miRNA content from bacterial infected patients to predict clinical outcome and/or the nature of infection.

Although miRNA point-of-care techniques are still in its infancy several analytical approaches have been developed for diagnostic purposes during the last twenty years including RT-qPCR, northern blot and luminescence tagging (Labib & Berezovski, 2015; Wang et al, 2013). Nevertheless, these techniques are not ideal and hold important disadvantages including high cost and long analysis course. Electrochemical biosensors are particular new promising tools for miRNA point-of care diagnostics due to their simplicity, speed, sensitivity and reasonable multiplexing feasibility. MSc Daniel Smith, who is based within the department in collaboration with the Chemistry department of Cardiff University and the industry, is interested in this line of investigation. Cardiff Institute of Nephrology has been traditionally interested in urine miRNA detection as biomarkers while my PhD was the first research developed at the center that addressed PD miRNAs. Thus, MSc Daniel Smith research is focussed on the development of an electrochemically active disposable 'dip-stick' to quantify urine miRNA concentration in a quick, non-specialist, non-invasive diagnostic test that will not require expensive equipment or highly specialised technicians to operate. Indeed, this biosensor has been tested and gave 6 fM sensitivity limit with synthetic urine while remaining specific within 1 mismatch. Although further research will be needed during the following years, these results indicate that future electrochemical 'dip-stick' technique adaptation to PD effluent miRNA detection may be doable within a reasonable time-scale.

My research identified PDCD4, an already described miR-21 target that down-regulates Snail while downstream controlling E-cadherin and β-catenin/TCF dependent transcription activation (see Chapter 5). Additionally, I performed *In silico* analysis combining 4 target prediction algorithms (Targetscan, miRanda, miRDB and Diana-microT) for miR-21 alone and in combination with miR-31. I integrated the resulting outcome with mRNA arrays comparing omentum vs PD effluent-derived HPMCs with epithealial (E) and non-epithelial (NE) phenotype. I identified 13 possible direct targets

for miR-21 and one for miR-31 during the MMT process associated to PD therapy and I model scrutinized them. I confirmed four of these miR-21 targets. Specifically, I identified two indirect miR-21 targets, *PDZD2* and *MATN2*, as well as two possible direct miR-21 targets *FGF-18* and *S100A10* (see Chapter 5). As detailed in Chapter 5 (see 5.3.), there are specific experimental approaches that I would be especially interested to perform in order to understand the particular pathways and contribution of each one of these targets to the peritoneal MMT process. Overall functional gene analysis indicated that selected targets may be modulators of Snail and cooperate driving MMT during peritoneal fibrosis (see 5.3.).

Additionally, the application of CRISPR/Cas9 technology for miR-21 gene manipulation combined with relevant *in vivo* mice PD therapy models would be especially interesting to consider for future research. Indeed, Dr Robert Jenkins, who is based in the department, is interested in exploring this option in a mice model of *Staphylococcus epidermidis cell-free supernatant* (SES)-induced peritoneal inflammation. In particular, his research aims to define *in vivo* miRNA regulation of tissue resident and inflammatory macrophage phenotype in the above mentioned *murine* model of peritoneal fibrosis. Thus, macrophage specific CRISPR/Cas9 driven miRNA gene manipulation will allow him to study macrophage population differences and associate those with tissue-specific functions during PD associated fibrosis. Similarly, the establishment of this methodology at the department will allow future technique adaptation for miR-21 manipulation in HPMCs to study changes in MMT associated to PD therapy within a reasonable time-scale.

Of note, miR-21 up-regulation has been synchronously identified in the field by Morishita et al. 2016, who studied total PDE samples from 33 patients and found no correlations with PD duration and PET results (D/P-Cr and D/D0 glucose) (Morishita et al, 2016). Nevertheless, the lack of association between miR-21 and PD duration as well as PET results in Morishita *et al*. 2016 studies may be merely due to limitations in the numbers of patients for study. Indeed, anti-miR-21-LNA intraperitoneally injected with MGO showed to significantly decrease peritoneal membrane thickening and MMT (Morishita et al, 2016) undoubtedly demonstrating miR-21 importance during the fibrosis process associated to PD therapy *in vivo* .

miR-21 therapeutic potential has built high interest between the pharmaceutical industries. Regulus therapeutics, *Inc* is a biopharmaceutical company leading miRNA therapies towards clinical development in fibrosis, hepatitis C, immune-inflammatory diseases, metabolic diseases and oncology. The above company owns miR-21 patient rights including miR-21 sequence and complement, chemically modified anti-miR-21 oligonucleotides and methods of anti-miR-21 use for the treatment of fibrosis. Similar patents owned by different research centers and universities can be found for promoter driven targeted therapy as well as for broad diagnostic, prognostic and treatment applications (For additional information of these patents see: Bhat; Balkrishen, Marcusson; Eric, microRNA compounds and methods for modulating miR-21 activity, citing patient US9267137, filing date January 15, 2015, and publication date February 23, 2016, Patent URL: http://patft.uspto.gov/netacgi/nph-Parser?Sect1=PTO2&Sect2=HITOFF&p=1&u=%2Fnetahtml%2FPTO%2Fsearch-bool.html&r=1&f=G&l=50&co1=AND&d=PTXT&s1=miR-21.TI.&OS=TTL/miR-21&RS=TTL/miR-21).

Taken together, my data provide a detailed characterisation of mesothelial miRNA expression and responses to TGF-β1, and identified miR-21 and miR-31 as promising biomarkers for peritoneal fibrosis associated to PD therapy. Additionally, my research identified new miR-21 targets that may be interesting downstream contributors for the MMT process. These targets possess unknown therapeutic potential not only in the MMT process associated to PD therapy but also in other contexts in which miR-21 up-regulation has been characterized. My work presented in this thesis, together with parallel reports constitutes a solid research indicating the importance of miR-21 during PD fibrogenesis.

References

1. Agarwal, V., Bell, G. W., Nam, J. W. & Bartel, D. P. (2015) Predicting effective microRNA target sites in mammalian mRNAs. *Elife*, 4.
2. Aguilera, A., Yáñez-Mo, M., Selgas, R., Sánchez-Madrid, F. & López-Cabrera, M. (2005) Epithelial to mesenchymal transition as a triggering factor of peritoneal membrane fibrosis and angiogenesis in peritoneal dialysis patients. *Curr Opin Investig Drugs*, 6(3), 262-8.
3. Akat, K. M., Moore-McGriff, D., Morozov, P., Brown, M., Gogakos, T., Correa Da Rosa, J., Mihailovic, A., Sauer, M., Ji, R., Ramarathnam, A., Totary-Jain, H., Williams, Z., Tuschl, T. & Schulze, P. C. (2014) Comparative RNA-sequencing analysis of myocardial and circulating small RNAs in human heart failure and their utility as biomarkers. *Proc Natl Acad Sci U S A*, 111(30), 11151-6.
4. Altuvia, Y., Landgraf, P., Lithwick, G., Elefant, N., Pfeffer, S., Aravin, A., Brownstein, M. J., Tuschl, T. & Margalit, H. (2005) Clustering and conservation patterns of human microRNAs. *Nucleic Acids Res*, 33(8), 2697-706.
5. Araki, S., Eitel, J. A., Batuello, C. N., Bijangi-Vishehsaraei, K., Xie, X. J., Danielpour, D., Pollok, K. E., Boothman, D. A. & Mayo, L. D. (2010) TGF-beta1-induced expression of human Mdm2 correlates with late-stage metastatic breast cancer. *J Clin Invest*, 120(1), 290-302.
6. Aroeira, L. S., Aguilera, A., Selgas, R., Ramírez-Huesca, M., Pérez-Lozano, M. L., Cirugeda, A., Bajo, M. A., del Peso, G., Sánchez-Tomero, J. A., Jiménez-Heffernan, J. A. & López-Cabrera, M. (2005) Mesenchymal conversion of mesothelial cells as a mechanism responsible for high solute transport rate in peritoneal dialysis: role of vascular endothelial growth factor. *Am J Kidney Dis*, 46(5), 938-48.
7. Aroeira, L. S., Aguilera, A., Sánchez-Tomero, J. A., Bajo, M. A., del Peso, G., Jiménez-Heffernan, J. A., Selgas, R. & López-Cabrera, M. (2007) Epithelial to mesenchymal transition and peritoneal membrane failure in peritoneal dialysis patients: pathologic significance and potential therapeutic interventions. *J Am Soc Nephrol*, 18(7), 2004-13.
8. Asahina, K., Zhou, B., Pu, W. T. & Tsukamoto, H. (2011) Septum transversum-derived mesothelium gives rise to hepatic stellate cells and perivascular mesenchymal cells in developing mouse liver. *Hepatology*, 53(3), 983-95.
9. Asangani, I. A., Rasheed, S. A. K., Nikolova, D. A., Leupold, J. H., Colburn, N. H., Post, S. & Allgayer, H. (2008) MicroRNA-21 (miR-21) post-transcriptionally downregulates tumor suppressor Pdcd4 and stimulates invasion, intravasation and metastasis in colorectal cancer. *Oncogene*, 27(15), 2128-2136.
10. Bajaj, M. S., Pendurthi, U., Koenig, K., Pueblitz, S. & Idell, S. (2000) Tissue factor pathway inhibitor expression by human pleural mesothelial and mesothelioma cells. *Eur Respir J*, 15(6), 1069-78.
11. Bajo, M. A., Pérez-Lozano, M. L., Albar-Vizcaino, P., del Peso, G., Castro, M. J., Gonzalez-Mateo, G., Fernández-Perpén, A., Aguilera, A., Sánchez-Villanueva, R., Sánchez-Tomero, J. A., López-Cabrera, M., Peter, M. E., Passlick-Deetjen, J. & Selgas, R. (2011) Low-GDP peritoneal dialysis fluid ('balance') has less impact in vitro and ex vivo on epithelial-to-mesenchymal transition (EMT) of mesothelial cells than a standard fluid. *Nephrol Dial Transplant*, 26(1), 282-91.
12. Bao, J. F., Hao, J., Liu, J., Yuan, W. J. & Yu, Q. (2015) The abnormal expression level of microRNA in epithelial-mesenchymal transition of peritoneal mesothelial cells induced by high glucose. *Eur Rev Med Pharmacol Sci*, 19(2), 289-92.
13. Baroni, G., Schuinski, A., de Moraes, T. P., Meyer, F. & Pecoits-Filho, R. (2012) Inflammation and the peritoneal membrane: causes and impact on structure and function during peritoneal dialysis. *Mediators Inflamm*, 2012, 912595.
14. Bartel, D. P. (2004) MicroRNAs: genomics, biogenesis, mechanism, and function. *Cell*, 116(2), 281-97.
15. Bartel, D. P. (2009) MicroRNAs: target recognition and regulatory functions. *Cell*, 136(2), 215-33.

16. Beelen, R. H., Oosterling, S. J., van Egmond, M., van den Born, J. & Zareie, M. (2005) Omental milky spots in peritoneal pathophysiology (spots before your eyes). *Perit Dial Int*, 25(1), 30-2.
17. Beltrami, C. (2014) *The identification of miRNA biomarkers of chronic kidney disease and development of minimally-invasive methods of molecular detection*. Philosophiae Doctor Cardiff University.
18. Beltrami, C., Clayton, A., Phillips, A. O., Fraser, D. J. & Bowen, T. (2012) Analysis of urinary microRNAs in chronic kidney disease. *Biochem Soc Trans*, 40(4), 875-9.
19. Benaud, C., Gentil, B. J., Assard, N., Court, M., Garin, J., Delphin, C. & Baudier, J. (2004) AHNAK interaction with the annexin 2/S100A10 complex regulates cell membrane cytoarchitecture. *J Cell Biol*, 164(1), 133-44.
20. Bernstein, E., Caudy, A. A., Hammond, S. M. & Hannon, G. J. (2001) Role for a bidentate ribonuclease in the initiation step of RNA interference. *Nature*, 409(6818), 363-6.
21. Betel, D., Koppal, A., Agius, P., Sander, C. & Leslie, C. (2010) Comprehensive modeling of microRNA targets predicts functional non-conserved and non-canonical sites. *Genome Biol*, 11(8), R90.
22. Betel, D., Wilson, M., Gabow, A., Marks, D. S. & Sander, C. (2008) The microRNA.org resource: targets and expression. *Nucleic Acids Res*, 36(Database issue), D149-53.
23. Bharadwaj, A., Bydoun, M., Holloway, R. & Waisman, D. (2013) Annexin A2 heterotetramer: structure and function. *Int J Mol Sci*, 14(3), 6259-305.
24. Bierie, B. & Moses, H. L. (2006) Tumour microenvironment: TGFbeta: the molecular Jekyll and Hyde of cancer. *Nat Rev Cancer*, 6(7), 506-20.
25. Blake, P. G., Jain, A. K. & Yohanna, S. (2013) Biocompatible peritoneal dialysis solutions: many questions but few answers. *Kidney Int*, 84(5), 864-6.
26. Boivin, G. P., Molina, J. R., Ormsby, I., Stemmermann, G. & Doetschman, T. (1996) Gastric lesions in transforming growth factor beta-1 heterozygous mice. *Lab Invest*, 74(2), 513-8.
27. Borchert, G. M., Lanier, W. & Davidson, B. L. (2006) RNA polymerase III transcribes human microRNAs. *Nat Struct Mol Biol*, 13(12), 1097-101.
28. Bos, H. J., Struijk, D. G., Tuk, C. W., de Veld, J. C., Helmerhorst, T. J., Hoefsmit, E. C., Arisz, L. & Beelen, R. H. (1991) Peritoneal dialysis induces a local sterile inflammatory state and the mesothelial cells in the effluent are related to the bacterial peritonitis incidence. *Nephron*, 59(3), 508-9.
29. Bosson, A. D., Zamudio, J. R. & Sharp, P. A. (2014) Endogenous miRNA and target concentrations determine susceptibility to potential ceRNA competition. *Mol Cell*, 56(3), 347-59.
30. Bottles, K. D., Laszik, Z., Morrissey, J. H. & Kinasewitz, G. T. (1997) Tissue factor expression in mesothelial cells: induction both in vivo and in vitro. *Am J Respir Cell Mol Biol*, 17(2), 164-72.
31. Boulanger, E., Wautier, M. P., Wautier, J. L., Boval, B., Panis, Y., Wernert, N., Danze, P. M. & Dequiedt, P. (2002) AGEs bind to mesothelial cells via RAGE and stimulate VCAM-1 expression. *Kidney Int*, 61(1), 148-56.
32. Bowen, T., Jenkins, R. H. & Fraser, D. J. (2013) MicroRNAs, transforming growth factor beta-1, and tissue fibrosis. *J Pathol*, 229(2), 274-85.
33. Bradford, M. M. (1976) A rapid and sensitive method for the quantitation of microgram quantities of protein utilizing the principle of protein-dye binding. *Anal Biochem*, 72, 248-54.
34. Brown, B. D. & Naldini, L. (2009) Exploiting and antagonizing microRNA regulation for therapeutic and experimental applications. *Nat Rev Genet*, 10(8), 578-85.
35. Brønnum, H., Andersen, D. C., Schneider, M., Sandberg, M. B., Eskildsen, T., Nielsen, S. B., Kalluri, R. & Sheikh, S. P. (2013) miR-21 promotes fibrogenic epithelial-to-mesenchymal transition of epicardial mesothelial cells involving Programmed Cell Death 4 and Sprouty-1. *PLoS One*, 8(2), e56280.

36. Brück, K., Stel, V. S., Gambaro, G., Hallan, S., Völzke, H., Ärnlöv, J., Kastarinen, M., Guessous, I., Vinhas, J., Stengel, B., Brenner, H., Chudek, J., Romundstad, S., Tomson, C., Gonzalez, A. O., Bello, A. K., Ferrieres, J., Palmieri, L., Browne, G., Capuano, V., Van Biesen, W., Zoccali, C., Gansevoort, R., Navis, G., Rothenbacher, D., Ferraro, P. M., Nitsch, D., Wanner, C., Jager, K. J. & Consortium, E. C. B. (2016) CKD Prevalence Varies across the European General Population. *J Am Soc Nephrol*, 27(7), 2135-47.
37. Burgos, K. L., Javaherian, A., Bomprezzi, R., Ghaffari, L., Rhodes, S., Courtright, A., Tembe, W., Kim, S., Metpally, R. & Van Keuren-Jensen, K. (2013) Identification of extracellular miRNA in human cerebrospinal fluid by next-generation sequencing. *RNA*, 19(5), 712-22.
38. Byrne, C., Steenkamp, R., Castledine, C., Ansell, D. & Feehally, J. (2010) UK Renal Registry 12th Annual Report (December 2009): chapter 4: UK ESRD prevalent rates in 2008: national and centre-specific analyses. *Nephron Clin Pract*, 115 Suppl 1, c41-67.
39. Böttinger, E. P., Letterio, J. J. & Roberts, A. B. (1997) Biology of TGF-beta in knockout and transgenic mouse models. *Kidney Int*, 51(5), 1355-60.
40. Cai, X., Hagedorn, C. H. & Cullen, B. R. (2004) Human microRNAs are processed from capped, polyadenylated transcripts that can also function as mRNAs. *RNA*, 10(12), 1957-66.
41. Cannistra, S. A., Ottensmeier, C., Tidy, J. & DeFranzo, B. (1994) Vascular cell adhesion molecule-1 expressed by peritoneal mesothelium partly mediates the binding of activated human T lymphocytes. *Exp Hematol*, 22(10), 996-1002.
42. Capocasale, R. J., Lamb, R. J., Vonderheid, E. C., Fox, F. E., Rook, A. H., Nowell, P. C. & Moore, J. S. (1995) Reduced surface expression of transforming growth factor beta receptor type II in mitogen-activated T cells from Sézary patients. *Proc Natl Acad Sci U S A*, 92(12), 5501-5.
43. Carlsson, H., Petersson, S. & Enerbäck, C. (2005) Cluster analysis of S100 gene expression and genes correlating to psoriasin (S100A7) expression at different stages of breast cancer development. *Int J Oncol*, 27(6), 1473-81.
44. Carmeliet, P., Ferreira, V., Breier, G., Pollefeyt, S., Kieckens, L., Gertsenstein, M., Fahrig, M., Vandenhoeck, A., Harpal, K., Eberhardt, C., Declercq, C., Pawling, J., Moons, L., Collen, D., Risau, W. & Nagy, A. (1996) Abnormal blood vessel development and lethality in embryos lacking a single VEGF allele. *Nature*, 380(6573), 435-9.
45. Chaib, H., Rubin, M. A., Mucci, N. R., Li, L., Taylor JMG, Day, M. L., Rhim, J. S. & Macoska, J. A. (2001) Activated in prostate cancer: a PDZ domain-containing protein highly expressed in human primary prostate tumors. *Cancer Res*, 61(6), 2390-4.
46. Chan, T. M. & Yung, S. (2007) Studying the effects of new peritoneal dialysis solutions on the peritoneum. *Perit Dial Int*, 27 Suppl 2, S87-93.
47. Chau, Y. Y., Bandiera, R., Serrels, A., Martínez-Estrada, O. M., Qing, W., Lee, M., Slight, J., Thornburn, A., Berry, R., McHaffie, S., Stimson, R. H., Walker, B. R., Chapuli, R. M., Schedl, A. & Hastie, N. (2014) Visceral and subcutaneous fat have different origins and evidence supports a mesothelial source. *Nat Cell Biol*, 16(4), 367-75.
48. Chen, C., Ridzon, D. A., Broomer, A. J., Zhou, Z., Lee, D. H., Nguyen, J. T., Barbisin, M., Xu, N. L., Mahuvakar, V. R., Andersen, M. R., Lao, K. Q., Livak, K. J. & Guegler, K. J. (2005) Real-time quantification of microRNAs by stem-loop RT-PCR. *Nucleic Acids Res*, 33(20), e179.
49. Chen, J., Kam-Tao, P., Kwan, B. C., Chow, K. M., Lai, K. B., Luk, C. C. & Szeto, C. C. (2012a) Relation between microRNA expression in peritoneal dialysis effluent and peritoneal transport characteristics. *Dis Markers*, 33(1), 35-42.
50. Chen, M., Liu, Y., Varley, P., Chang, Y., He, X. X., Huang, H., Tang, D., Lotze, M. T., Lin, J. & Tsung, A. (2015) High-Mobility Group Box 1 Promotes Hepatocellular Carcinoma Progression through miR-21-Mediated Matrix Metalloproteinase Activity. *Cancer Res*, 75(8), 1645-56.
51. Chen, W., Jin, W., Hardegen, N., Lei, K. J., Li, L., Marinos, N., McGrady, G. & Wahl, S. M. (2003) Conversion of peripheral CD4+CD25- naive T cells to CD4+CD25+ regulatory T cells by TGF-beta induction of transcription factor Foxp3. *J Exp Med*, 198(12), 1875-86.

52. Chen, X., Liang, H., Zhang, J., Zen, K. & Zhang, C. Y. (2012b) Secreted microRNAs: a new form of intercellular communication. *Trends Cell Biol*, 22(3), 125-32.
53. Chen, Y. T., Chang, Y. T., Pan, S. Y., Chou, Y. H., Chang, F. C., Yeh, P. Y., Liu, Y. H., Chiang, W. C., Chen, Y. M., Wu, K. D., Tsai, T. J., Duffield, J. S. & Lin, S. L. (2014) Lineage tracing reveals distinctive fates for mesothelial cells and submesothelial fibroblasts during peritoneal injury. *J Am Soc Nephrol*, 25(12), 2847-58.
54. Chendrimada, T. P., Gregory, R. I., Kumaraswamy, E., Norman, J., Cooch, N., Nishikura, K. & Shiekhattar, R. (2005) TRBP recruits the Dicer complex to Ago2 for microRNA processing and gene silencing. *Nature*, 436(7051), 740-4.
55. Clovis, Y. M., Enard, W., Marinaro, F., Huttner, W. B. & De Pietri Tonelli, D. (2012) Convergent repression of Foxp2 3'UTR by miR-9 and miR-132 in embryonic mouse neocortex: implications for radial migration of neurons. *Development*, 139(18), 3332-42.
56. Cnossen, T. T., Usvyat, L., Kotanko, P., van der Sande, F. M., Kooman, J. P., Carter, M., Leunissen, K. M. & Levin, N. W. (2011) Comparison of outcomes on continuous ambulatory peritoneal dialysis versus automated peritoneal dialysis: results from a USA database. *Perit Dial Int*, 31(6), 679-84.
57. Cortez, M. A., Bueso-Ramos, C., Ferdin, J., Lopez-Berestein, G., Sood, A. K. & Calin, G. A. (2011) MicroRNAs in body fluids--the mix of hormones and biomarkers. *Nat Rev Clin Oncol*, 8(8), 467-77.
58. Cottonham, C. L., Kaneko, S. & Xu, L. (2010) miR-21 and miR-31 converge on TIAM1 to regulate migration and invasion of colon carcinoma cells. *J Biol Chem*, 285(46), 35293-302.
59. Cui, L., Johkura, K., Liang, Y., Teng, R., Ogiwara, N., Okouchi, Y., Asanuma, K. & Sasaki, K. (2002) Biodefense function of omental milky spots through cell adhesion molecules and leukocyte proliferation. *Cell Tissue Res*, 310(3), 321-30.
60. Dai, C. & Liu, Y. (2004) Hepatocyte growth factor antagonizes the profibrotic action of TGF-beta1 in mesangial cells by stabilizing Smad transcriptional corepressor TGIF. *J Am Soc Nephrol*, 15(6), 1402-12.
61. Davies, S. J., Phillips, L., Griffiths, A. M., Russell, L. H., Naish, P. F. & Russell, G. I. (1998) What really happens to people on long-term peritoneal dialysis? *Kidney Int*, 54(6), 2207-17.
62. Davis, B. N., Hilyard, A. C., Lagna, G. & Hata, A. (2008) SMAD proteins control DROSHA-mediated microRNA maturation. *Nature*, 454(7200), 56-61.
63. Davis, B. N., Hilyard, A. C., Nguyen, P. H., Lagna, G. & Hata, A. (2010) Smad proteins bind a conserved RNA sequence to promote microRNA maturation by Drosha. *Mol Cell*, 39(3), 373-84.
64. De Vriese, A. S., Flyvbjerg, A., Mortier, S., Tilton, R. G. & Lameire, N. H. (2003) Inhibition of the interaction of AGE-RAGE prevents hyperglycemia-induced fibrosis of the peritoneal membrane. *J Am Soc Nephrol*, 14(8), 2109-18.
65. Decologne, N., Kolb, M., Margetts, P. J., Menetrier, F., Artur, Y., Garrido, C., Gauldie, J., Camus, P. & Bonniaud, P. (2007) TGF-beta1 induces progressive pleural scarring and subpleural fibrosis. *J Immunol*, 179(9), 6043-51.
66. Deguchi, M., Iizuka, T., Hata, Y., Nishimura, W., Hirao, K., Yao, I., Kawabe, H. & Takai, Y. (2000) PAPIN. A novel multiple PSD-95/Dlg-A/ZO-1 protein interacting with neural plakophilin-related armadillo repeat protein/delta-catenin and p0071. *J Biol Chem*, 275(38), 29875-80.
67. Del Peso, G., Jiménez-Heffernan, J. A., Bajo, M. A., Aroeira, L. S., Aguilera, A., Fernández-Perpén, A., Cirugeda, A., Castro, M. J., de Gracia, R., Sánchez-Villanueva, R., Sánchez-Tomero, J. A., López-Cabrera, M. & Selgas, R. (2008) Epithelial-to-mesenchymal transition of mesothelial cells is an early event during peritoneal dialysis and is associated with high peritoneal transport. *Kidney Int Suppl*(108), S26-33.
68. Deora, A. B., Kreitzer, G., Jacovina, A. T. & Hajjar, K. A. (2004) An annexin 2 phosphorylation switch mediates p11-dependent translocation of annexin 2 to the cell surface. *J Biol Chem*, 279(42), 43411-8.

69. Derveaux, S., Vandesompele, J. & Hellemans, J. (2010) How to do successful gene expression analysis using real-time PCR. *Methods*, 50(4), 227-30.
70. Derynck, R. & Zhang, Y. E. (2003) Smad-dependent and Smad-independent pathways in TGF-beta family signalling. *Nature*, 425(6958), 577-84.
71. Devuyst, O., Margetts, P. J. & Topley, N. (2010) The pathophysiology of the peritoneal membrane. *J Am Soc Nephrol*, 21(7), 1077-85.
72. Devuyst, O. & Rippe, B. (2014) Water transport across the peritoneal membrane. *Kidney Int*, 85(4), 750-8.
73. Dey, N., Ghosh-Choudhury, N., Kasinath, B. S. & Choudhury, G. G. (2012) TGFβ-stimulated microRNA-21 utilizes PTEN to orchestrate AKT/mTORC1 signaling for mesangial cell hypertrophy and matrix expansion. *PLoS One*, 7(8), e42316.
74. Deák, F., Mátés, L., Korpos, E., Zvara, A., Szénási, T., Kiricsi, M., Mendler, L., Keller-Pintér, A., Ozsvári, B., Juhász, H., Sorokin, L., Dux, L., Mermod, N., Puskás, L. G. & Kiss, I. (2014) Extracellular deposition of matrilin-2 controls the timing of the myogenic program during muscle regeneration. *J Cell Sci*, 127(Pt 15), 3240-56.
75. Di Leva, G., Garofalo, M. & Croce, C. M. (2014) MicroRNAs in cancer. *Annu Rev Pathol*, 9, 287-314.
76. Di Paolo, N., Garosi, G., Petrini, G., Traversari, L. & Rossi, P. (1995) Peritoneal dialysis solution biocompatibility testing in animals. *Perit Dial Int*, 15(7 Suppl), S61-9; discussion S69-70.
77. Eades, G., Yao, Y., Yang, M., Zhang, Y., Chumsri, S. & Zhou, Q. (2011) miR-200a regulates SIRT1 expression and epithelial to mesenchymal transition (EMT)-like transformation in mammary epithelial cells. *J Biol Chem*, 286(29), 25992-6002.
78. Ebert, M. S. & Sharp, P. A. (2012) Roles for microRNAs in conferring robustness to biological processes. *Cell*, 149(3), 515-24.
79. Ernst, M. & Jenkins, B. J. (2004) Acquiring signalling specificity from the cytokine receptor gp130. *Trends Genet*, 20(1), 23-32.
80. Fang, Y. T., Lin, C. F., Wang, C. Y., Anderson, R. & Lin, Y. S. (2012) Interferon-γ stimulates p11-dependent surface expression of annexin A2 in lung epithelial cells to enhance phagocytosis. *J Cell Physiol*, 227(6), 2775-87.
81. Feng, X. H. & Derynck, R. (2005) Specificity and versatility in tgf-beta signaling through Smads. *Annu Rev Cell Dev Biol*, 21, 659-93.
82. Fernandez de Castro, M., Selgas, R., Jimenez, C., Auxiliadora Bajo, M., Martinez, V., Romero, J. R., de Alvaro, F. & Vara, F. (1994) Cell populations present in the nocturnal peritoneal effluent of patients on continuous ambulatory peritoneal dialysis and their relationship with peritoneal function and incidence of peritonitis. *Perit Dial Int*, 14(3), 265-70.
83. Ferrandez-Izquierdo, A., Navarro-Fos, S., Gonzalez-Devesa, M., Gil-Benso, R. & Llombart-Bosch, A. (1994) Immunocytochemical typification of mesothelial cells in effusions: in vivo and in vitro models. *Diagn Cytopathol*, 10(3), 256-62.
84. Ferrari, G., Pintucci, G., Seghezzi, G., Hyman, K., Galloway, A. C. & Mignatti, P. (2006) VEGF, a prosurvival factor, acts in concert with TGF-beta1 to induce endothelial cell apoptosis. *Proc Natl Acad Sci U S A*, 103(46), 17260-5.
85. Filipenko, N. R., Kang, H. M. & Waisman, D. M. (2000) Characterization of the Ca2+-binding sites of annexin II tetramer. *J Biol Chem*, 275(49), 38877-84.
86. Finnegan, E. F. & Pasquinelli, A. E. (2013) MicroRNA biogenesis: regulating the regulators. *Crit Rev Biochem Mol Biol*, 48(1), 51-68.
87. Fragiadaki, M. & Mason, R. M. (2011) Epithelial-mesenchymal transition in renal fibrosis - evidence for and against. *Int J Exp Pathol*, 92(3), 143-50.
88. Franco-Montoya, M. L., Boucherat, O., Thibault, C., Chailley-Heu, B., Incitti, R., Delacourt, C. & Bourbon, J. R. (2011) Profiling target genes of FGF18 in the postnatal mouse lung: possible relevance for alveolar development. *Physiol Genomics*, 43(21), 1226-40.

89. Friedlander, M. A., Wu, Y. C., Elgawish, A. & Monnier, V. M. (1996) Early and advanced glycosylation end products. Kinetics of formation and clearance in peritoneal dialysis. *J Clin Invest*, 97(3), 728-35.
90. Fujita, S., Ito, T., Mizutani, T., Minoguchi, S., Yamamichi, N., Sakurai, K. & Iba, H. (2008) miR-21 Gene expression triggered by AP-1 is sustained through a double-negative feedback mechanism. *J Mol Biol*, 378(3), 492-504.
91. Fullár, A., Baghy, K., Deák, F., Péterfia, B., Zsák, Y., Tátrai, P., Schaff, Z., Dudás, J., Kiss, I. & Kovalszky, I. (2014) Lack of Matrilin-2 favors liver tumor development via Erk1/2 and GSK-3β pathways in vivo. *PLoS One*, 9(4), e93469.
92. Fusshoeller, A. (2008) Histomorphological and functional changes of the peritoneal membrane during long-term peritoneal dialysis. *Pediatr Nephrol*, 23(1), 19-25.
93. Gabbiani, G., Hirschel, B. J., Ryan, G. B., Statkov, P. R. & Majno, G. (1972) Granulation tissue as a contractile organ. A study of structure and function. *J Exp Med*, 135(4), 719-34.
94. Gangji, A. S., Brimble, K. S. & Margetts, P. J. (2009) Association between markers of inflammation, fibrosis and hypervolemia in peritoneal dialysis patients. *Blood Purif*, 28(4), 354-8.
95. García-López, E. & Lindholm, B. (2009) Icodextrin metabolites in peritoneal dialysis. *Perit Dial Int*, 29(4), 370-6.
96. García-López, E., Lindholm, B. & Davies, S. (2012) An update on peritoneal dialysis solutions. *Nat Rev Nephrol*, 8(4), 224-33.
97. Golper, T. A. (2013) The possible impact of the US prospective payment system ("bundle") on the growth of peritoneal dialysis. *Perit Dial Int*, 33(6), 596-9.
98. Gong, Y., Hart, E., Shchurin, A. & Hoover-Plow, J. (2008) Inflammatory macrophage migration requires MMP-9 activation by plasminogen in mice. *J Clin Invest*, 118(9), 3012-24.
99. González-Mateo, G. T., Loureiro, J., Jiménez-Hefferman, J. A., Bajo, M. A., Selgas, R., López-Cabrera, M. & Aroeira, L. S. (2009) Chronic exposure of mouse peritoneum to peritoneal dialysis fluid: structural and functional alterations of the peritoneal membrane. *Perit Dial Int*, 29(2), 227-30.
100. Gorelik, L. & Flavell, R. A. (2000) Abrogation of TGFbeta signaling in T cells leads to spontaneous T cell differentiation and autoimmune disease. *Immunity*, 12(2), 171-81.
101. Gotloib, L., Shostak, A., Wajsbrot, V. & Kushnier, R. (1999) High glucose induces a hypertrophic, senescent mesothelial cell phenotype after long in vivo exposure. *Nephron*, 82(2), 164-73.
102. Grassmann, A., Gioberge, S., Moeller, S. & Brown, G. (2005) ESRD patients in 2004: global overview of patient numbers, treatment modalities and associated trends. *Nephrol Dial Transplant*, 20(12), 2587-93.
103. Gregory, P. A., Bert, A. G., Paterson, E. L., Barry, S. C., Tsykin, A., Farshid, G., Vadas, M. A., Khew-Goodall, Y. & Goodall, G. J. (2008) The miR-200 family and miR-205 regulate epithelial to mesenchymal transition by targeting ZEB1 and SIP1. *Nat Cell Biol*, 10(5), 593-601.
104. Grgic, I., Duffield, J. S. & Humphreys, B. D. (2012) The origin of interstitial myofibroblasts in chronic kidney disease. *Pediatr Nephrol*, 27(2), 183-93.
105. Grimson, A., Farh, K. K., Johnston, W. K., Garrett-Engele, P., Lim, L. P. & Bartel, D. P. (2007) MicroRNA targeting specificity in mammals: determinants beyond seed pairing. *Mol Cell*, 27(1), 91-105.
106. Grishok, A., Pasquinelli, A. E., Conte, D., Li, N., Parrish, S., Ha, I., Baillie, D. L., Fire, A., Ruvkun, G. & Mello, C. C. (2001) Genes and mechanisms related to RNA interference regulate expression of the small temporal RNAs that control C. elegans developmental timing. *Cell*, 106(1), 23-34.
107. Groppe, J., Greenwald, J., Wiater, E., Rodriguez-Leon, J., Economides, A. N., Kwiatkowski, W., Affolter, M., Vale, W. W., Izpisua Belmonte, J. C. & Choe, S. (2002)

Structural basis of BMP signalling inhibition by the cystine knot protein Noggin. *Nature*, 420(6916), 636-42.
108. Grotendorst, G. R. (1997) Connective tissue growth factor: a mediator of TGF-beta action on fibroblasts. *Cytokine Growth Factor Rev*, 8(3), 171-9.
109. Grzegorzewska, A. E., Mariak, I., Dobrowolska-Zachwieja, A. & Szajdak, L. (1999) Effects of amino acid dialysis solution on the nutrition of continuous ambulatory peritoneal dialysis patients. *Perit Dial Int*, 19(5), 462-70.
110. Gu, S. & Kay, M. A. (2010) How do miRNAs mediate translational repression? *Silence*, 1(1), 11.
111. Gui, T., Sun, Y., Shimokado, A. & Muragaki, Y. (2012) The Roles of Mitogen-Activated Protein Kinase Pathways in TGF-β-Induced Epithelial-Mesenchymal Transition. *J Signal Transduct*, 2012, 289243.
112. Guo, H., Ingolia, N. T., Weissman, J. S. & Bartel, D. P. (2010) Mammalian microRNAs predominantly act to decrease target mRNA levels. *Nature*, 466(7308), 835-40.
113. Guo, H., Leung, J. C., Lam, M. F., Chan, L. Y., Tsang, A. W., Lan, H. Y. & Lai, K. N. (2007) Smad7 transgene attenuates peritoneal fibrosis in uremic rats treated with peritoneal dialysis. *J Am Soc Nephrol*, 18(10), 2689-703.
114. Ha, H., Cha, M. K., Choi, H. N. & Lee, H. B. (2002) Effects of peritoneal dialysis solutions on the secretion of growth factors and extracellular matrix proteins by human peritoneal mesothelial cells. *Perit Dial Int*, 22(2), 171-7.
115. Ha, H., Yu, M. R. & Lee, H. B. (2001) High glucose-induced PKC activation mediates TGF-beta 1 and fibronectin synthesis by peritoneal mesothelial cells. *Kidney Int*, 59(2), 463-70.
116. Hansen, T. B., Jensen, T. I., Clausen, B. H., Bramsen, J. B., Finsen, B., Damgaard, C. K. & Kjems, J. (2013) Natural RNA circles function as efficient microRNA sponges. *Nature*, 495(7441), 384-8.
117. Haque, T., Nakada, S. & Hamdy, R. C. (2007) A review of FGF18: Its expression, signaling pathways and possible functions during embryogenesis and post-natal development. *Histol Histopathol*, 22(1), 97-105.
118. Harada, N., Mizoi, T., Kinouchi, M., Hoshi, K., Ishii, S., Shiiba, K., Sasaki, I. & Matsuno, S. (2001) Introduction of antisense CD44S CDNA down-regulates expression of overall CD44 isoforms and inhibits tumor growth and metastasis in highly metastatic colon carcinoma cells. *Int J Cancer*, 91(1), 67-75.
119. Hausmann, M. J., Rogachev, B., Weiler, M., Chaimovitz, C. & Douvdevani, A. (2000) Accessory role of human peritoneal mesothelial cells in antigen presentation and T-cell growth. *Kidney Int*, 57(2), 476-86.
120. Heinrich, P. C., Behrmann, I., Haan, S., Hermanns, H. M., Müller-Newen, G. & Schaper, F. (2003) Principles of interleukin (IL)-6-type cytokine signalling and its regulation. *Biochem J*, 374(Pt 1), 1-20.
121. Hellemans, J., Mortier, G., De Paepe, A., Speleman, F. & Vandesompele, J. (2007) qBase relative quantification framework and software for management and automated analysis of real-time quantitative PCR data. *Genome Biol*, 8(2), R19.
122. Heller, F., Lindenmeyer, M. T., Cohen, C. D., Brandt, U., Draganovici, D., Fischereder, M., Kretzler, M., Anders, H. J., Sitter, T., Mosberger, I., Kerjaschki, D., Regele, H., Schlöndorff, D. & Segerer, S. (2007) The contribution of B cells to renal interstitial inflammation. *Am J Pathol*, 170(2), 457-68.
123. Herlihy, S. E., Starke, H. E., Lopez-Anton, M., Cox, N., Keyhanian, K., Fraser, D. J. & Gomer, R. H. (2015) PERITONEAL DIALYSIS FLUID AND SOME OF ITS COMPONENTS POTENTIATE FIBROCYTE DIFFERENTIATION. *Perit Dial Int*.
124. Hicklin, D. J. & Ellis, L. M. (2005) Role of the vascular endothelial growth factor pathway in tumor growth and angiogenesis. *J Clin Oncol*, 23(5), 1011-27.

125. Ho-dac-Pannekeet, M. M., Schouten, N., Langendijk, M. J., Hiralall, J. K., de Waart, D. R., Struijk, D. G. & Krediet, R. T. (1996) Peritoneal transport characteristics with glucose polymer based dialysate. *Kidney Int*, 50(3), 979-86.
126. Hohaus, A., Person, V., Behlke, J., Schaper, J., Morano, I. & Haase, H. (2002) The carboxyl-terminal region of ahnak provides a link between cardiac L-type Ca2+ channels and the actin-based cytoskeleton. *FASEB J*, 16(10), 1205-16.
127. Holmes, C. J. (1993) Biocompatibility of peritoneal dialysis solutions. *Perit Dial Int*, 13(2), 88-94.
128. Honda, K. & Oda, H. (2005) Pathology of encapsulating peritoneal sclerosis. *Perit Dial Int*, 25 Suppl 4, S19-29.
129. Hu, M. C., Qiu, W. R., Wang, Y. P., Hill, D., Ring, B. D., Scully, S., Bolon, B., DeRose, M., Luethy, R., Simonet, W. S., Arakawa, T. & Danilenko, D. M. (1998) FGF-18, a novel member of the fibroblast growth factor family, stimulates hepatic and intestinal proliferation. *Mol Cell Biol*, 18(10), 6063-74.
130. Humphreys, B. D., Lin, S. L., Kobayashi, A., Hudson, T. E., Nowlin, B. T., Bonventre, J. V., Valerius, M. T., McMahon, A. P. & Duffield, J. S. (2010) Fate tracing reveals the pericyte and not epithelial origin of myofibroblasts in kidney fibrosis. *Am J Pathol*, 176(1), 85-97.
131. Ichikawa, T., Suenaga, Y., Koda, T., Ozaki, T. & Nakagawara, A. (2008) DeltaNp63/BMP-7-dependent expression of matrilin-2 is involved in keratinocyte migration in response to wounding. *Biochem Biophys Res Commun*, 369(4), 994-1000.
132. Ijpenberg, A., Pérez-Pomares, J. M., Guadix, J. A., Carmona, R., Portillo-Sánchez, V., Macías, D., Hohenstein, P., Miles, C. M., Hastie, N. D. & Muñoz-Chápuli, R. (2007) Wt1 and retinoic acid signaling are essential for stellate cell development and liver morphogenesis. *Dev Biol*, 312(1), 157-70.
133. Iliopoulos, D., Jaeger, S. A., Hirsch, H. A., Bulyk, M. L. & Struhl, K. (2010) STAT3 activation of miR-21 and miR-181b-1 via PTEN and CYLD are part of the epigenetic switch linking inflammation to cancer. *Mol Cell*, 39(4), 493-506.
134. Inagi, R., Miyata, T., Yamamoto, T., Suzuki, D., Urakami, K., Saito, A., van Ypersele de Strihou, C. & Kurokawa, K. (1999) Glucose degradation product methylglyoxal enhances the production of vascular endothelial growth factor in peritoneal cells: role in the functional and morphological alterations of peritoneal membranes in peritoneal dialysis. *FEBS Lett*, 463(3), 260-4.
135. Ishibashi, Y., Sugimoto, T., Ichikawa, Y., Akatsuka, A., Miyata, T., Nangaku, M., Tagawa, H. & Kurokawa, K. (2002) Glucose dialysate induces mitochondrial DNA damage in peritoneal mesothelial cells. *Perit Dial Int*, 22(1), 11-21.
136. Ito, T., Yorioka, N., Yamamoto, M., Kataoka, K. & Yamakido, M. (2000) Effect of glucose on intercellular junctions of cultured human peritoneal mesothelial cells. *J Am Soc Nephrol*, 11(11), 1969-79.
137. Ivarsson, M. L., Holmdahl, L., Falk, P., Mölne, J. & Risberg, B. (1998) Characterization and fibrinolytic properties of mesothelial cells isolated from peritoneal lavage. *Scand J Clin Lab Invest*, 58(3), 195-203.
138. Jain, A. K., Blake, P., Cordy, P. & Garg, A. X. (2012) Global trends in rates of peritoneal dialysis. *J Am Soc Nephrol*, 23(3), 533-44.
139. Jenkins, R. H., Davies, L. C., Taylor, P. R., Akiyama, H., Cumbes, B., Beltrami, C., Carrington, C. P., Phillips, A. O., Bowen, T. & Fraser, D. J. (2014) miR-192 induces G2/M growth arrest in aristolochic acid nephropathy. *Am J Pathol*, 184(4), 996-1009.
140. Jiménez-Heffernan, J. A., Aguilera, A., Aroeira, L. S., Lara-Pezzi, E., Bajo, M. A., del Peso, G., Ramírez, M., Gamallo, C., Sánchez-Tomero, J. A., Alvarez, V., López-Cabrera, M. & Selgas, R. (2004) Immunohistochemical characterization of fibroblast subpopulations in normal peritoneal tissue and in peritoneal dialysis-induced fibrosis. *Virchows Arch*, 444(3), 247-56.
141. Jiménez-Heffernan, J. A., Perna, C., Auxiliadora Bajo, M., Luz Picazo, M., Del Peso, G., Aroeira, L., Aguilera, A., Tejerina, E., López-Cabrera, M. & Selgas, R. (2008) Tissue

distribution of hyalinazing vasculopathy lesions in peritoneal dialysis patients: an autopsy study. *Pathol Res Pract*, 204(8), 563-7.
142. Joannes, A., Brayer, S., Besnard, V., Marchal-Sommé, J., Jaillet, M., Mordant, P., Mal, H., Borie, R., Crestani, B. & Mailleux, A. A. (2016) FGF9 and FGF18 in idiopathic pulmonary fibrosis promote survival and migration and inhibit myofibroblast differentiation of human lung fibroblasts in vitro. *Am J Physiol Lung Cell Mol Physiol*, ajplung.00185.2015.
143. Johnson, D. W., Brown, F. G., Clarke, M., Boudville, N., Elias, T. J., Foo, M. W., Jones, B., Kulkarni, H., Langham, R., Ranganathan, D., Schollum, J., Suranyi, M. G., Tan, S. H., Voss, D. & Investigators, b. T. (2012) The effects of biocompatible compared with standard peritoneal dialysis solutions on peritonitis microbiology, treatment, and outcomes: the balANZ trial. *Perit Dial Int*, 32(5), 497-506.
144. Jonas, A., Thiem, S., Kuhlmann, T., Wagener, R., Aszodi, A., Nowell, C., Hagemeier, K., Laverick, L., Perreau, V., Jokubaitis, V., Emery, B., Kilpatrick, T., Butzkueven, H. & Gresle, M. (2014) Axonally derived matrilin-2 induces proinflammatory responses that exacerbate autoimmune neuroinflammation. *J Clin Invest*, 124(11), 5042-56.
145. Jones, S., Holmes, C. J., Krediet, R. T., Mackenzie, R., Faict, D., Tranaeus, A., Williams, J. D., Coles, G. A., Topley, N. & Group, B. L. S. (2001) Bicarbonate/lactate-based peritoneal dialysis solution increases cancer antigen 125 and decreases hyaluronic acid levels. *Kidney Int*, 59(4), 1529-38.
146. Jonjić, N., Peri, G., Bernasconi, S., Sciacca, F. L., Colotta, F., Pelicci, P., Lanfrancone, L. & Mantovani, A. (1992) Expression of adhesion molecules and chemotactic cytokines in cultured human mesothelial cells. *J Exp Med*, 176(4), 1165-74.
147. Kalluri, R. & Weinberg, R. A. (2009) The basics of epithelial-mesenchymal transition. *J Clin Invest*, 119(6), 1420-8.
148. Kasai, H., Allen, J. T., Mason, R. M., Kamimura, T. & Zhang, Z. (2005) TGF-beta1 induces human alveolar epithelial to mesenchymal cell transition (EMT). *Respir Res*, 6, 56.
149. Kato, M., Putta, S., Wang, M., Yuan, H., Lanting, L., Nair, I., Gunn, A., Nakagawa, Y., Shimano, H., Todorov, I., Rossi, J. J. & Natarajan, R. (2009) TGF-beta activates Akt kinase through a microRNA-dependent amplifying circuit targeting PTEN. *Nat Cell Biol*, 11(7), 881-9.
150. Kawaguchi, Y., Kawanishi, H., Mujais, S., Topley, N. & Oreopoulos, D. G. (2000) Encapsulating peritoneal sclerosis: definition, etiology, diagnosis, and treatment. International Society for Peritoneal Dialysis Ad Hoc Committee on Ultrafiltration Management in Peritoneal Dialysis. *Perit Dial Int*, 20 Suppl 4, S43-55.
151. Keil, R., Schulz, J. & Hatzfeld, M. (2013) p0071/PKP4, a multifunctional protein coordinating cell adhesion with cytoskeletal organization. *Biol Chem*, 394(8), 1005-17.
152. Keller, P., Gburcik, V., Petrovic, N., Gallagher, I. J., Nedergaard, J., Cannon, B. & Timmons, J. A. (2011) Gene-chip studies of adipogenesis-regulated microRNAs in mouse primary adipocytes and human obesity. *BMC Endocr Disord*, 11, 7.
153. Kerr, M., Bray, B., Medcalf, J., O'Donoghue, D. J. & Matthews, B. (2012) Estimating the financial cost of chronic kidney disease to the NHS in England. *Nephrol Dial Transplant*, 27 Suppl 3, iii73-80.
154. Kim, V. N., Han, J. & Siomi, M. C. (2009) Biogenesis of small RNAs in animals. *Nat Rev Mol Cell Biol*, 10(2), 126-39.
155. Kinashi, H., Ito, Y., Mizuno, M., Suzuki, Y., Terabayashi, T., Nagura, F., Hattori, R., Matsukawa, Y., Mizuno, T., Noda, Y., Nishimura, H., Nishio, R., Maruyama, S., Imai, E., Matsuo, S. & Takei, Y. (2013) TGF-β1 promotes lymphangiogenesis during peritoneal fibrosis. *J Am Soc Nephrol*, 24(10), 1627-42.
156. Kinnaert, P., De Wilde, J. P., Bournonville, B., Husson, C. & Salmon, I. (1996) Direct activation of human peritoneal mesothelial cells by heat-killed microorganisms. *Ann Surg*, 224(6), 749-54; discussion 754-5.

157. Klatt, A. R., Becker, A. K., Neacsu, C. D., Paulsson, M. & Wagener, R. (2011) The matrilins: modulators of extracellular matrix assembly. *Int J Biochem Cell Biol*, 43(3), 320-30.
158. Kong, W., Yang, H., He, L., Zhao, J. J., Coppola, D., Dalton, W. S. & Cheng, J. Q. (2008) MicroRNA-155 is regulated by the transforming growth factor beta/Smad pathway and contributes to epithelial cell plasticity by targeting RhoA. *Mol Cell Biol*, 28(22), 6773-84.
159. Korevaar, J. C., Feith, G. W., Dekker, F. W., van Manen, J. G., Boeschoten, E. W., Bossuyt, P. M., Krediet, R. T. & Group, N. S. (2003) Effect of starting with hemodialysis compared with peritoneal dialysis in patients new on dialysis treatment: a randomized controlled trial. *Kidney Int*, 64(6), 2222-8.
160. Kosaka, N., Iguchi, H. & Ochiya, T. (2010) Circulating microRNA in body fluid: a new potential biomarker for cancer diagnosis and prognosis. *Cancer Sci*, 101(10), 2087-92.
161. Kota, J., Chivukula, R. R., O'Donnell, K. A., Wentzel, E. A., Montgomery, C. L., Hwang, H. W., Chang, T. C., Vivekanandan, P., Torbenson, M., Clark, K. R., Mendell, J. R. & Mendell, J. T. (2009) Therapeutic microRNA delivery suppresses tumorigenesis in a murine liver cancer model. *Cell*, 137(6), 1005-17.
162. Kozomara, A. & Griffiths-Jones, S. (2014) miRBase: annotating high confidence microRNAs using deep sequencing data. *Nucleic Acids Res*, 42(Database issue), D68-73.
163. Krediet, R. T., Zweers, M. M., van der Wal, A. C. & Struijk, D. G. (2000) Neoangiogenesis in the peritoneal membrane. *Perit Dial Int*, 20 Suppl 2, S19-25.
164. Krichevsky, A. M. & Gabriely, G. (2009) miR-21: a small multi-faceted RNA. *J Cell Mol Med*, 13(1), 39-53.
165. Krist, L. F., Eestermans, I. L., Steenbergen, J. J., Hoefsmit, E. C., Cuesta, M. A., Meyer, S. & Beelen, R. H. (1995) Cellular composition of milky spots in the human greater omentum: an immunochemical and ultrastructural study. *Anat Rec*, 241(2), 163-74.
166. Kriz, W., Kaissling, B. & Le Hir, M. (2011) Epithelial-mesenchymal transition (EMT) in kidney fibrosis: fact or fantasy? *J Clin Invest*, 121(2), 468-74.
167. Krupa, A. (2010) *The role of microRNAs in renal fibrosis*. Philosophiae Doctor Cardiff University.
168. Krupa, A., Jenkins, R., Luo, D. D., Lewis, A., Phillips, A. & Fraser, D. (2010) Loss of MicroRNA-192 promotes fibrogenesis in diabetic nephropathy. *J Am Soc Nephrol*, 21(3), 438-47.
169. Ksiazek, K., Korybalska, K., Jörres, A. & Witowski, J. (2007) Accelerated senescence of human peritoneal mesothelial cells exposed to high glucose: the role of TGF-beta1. *Lab Invest*, 87(4), 345-56.
170. Kulkarni, A. B., Huh, C. G., Becker, D., Geiser, A., Lyght, M., Flanders, K. C., Roberts, A. B., Sporn, M. B., Ward, J. M. & Karlsson, S. (1993) Transforming growth factor beta 1 null mutation in mice causes excessive inflammatory response and early death. *Proc Natl Acad Sci U S A*, 90(2), 770-4.
171. Kulkarni, A. B. & Karlsson, S. (1993) Transforming growth factor-beta 1 knockout mice. A mutation in one cytokine gene causes a dramatic inflammatory disease. *Am J Pathol*, 143(1), 3-9.
172. Labib, M. & Berezovski, M. V. (2015) Electrochemical sensing of microRNAs: avenues and paradigms. *Biosens Bioelectron*, 68, 83-94.
173. Laemmli, U. K. (1970) Cleavage of structural proteins during the assembly of the head of bacteriophage T4. *Nature*, 227(5259), 680-5.
174. Lagos-Quintana, M., Rauhut, R., Lendeckel, W. & Tuschl, T. (2001) Identification of novel genes coding for small expressed RNAs. *Science*, 294(5543), 853-8.
175. Lai, K. N., Lai, K. B., Lam, C. W., Chan, T. M., Li, F. K. & Leung, J. C. (2000) Changes of cytokine profiles during peritonitis in patients on continuous ambulatory peritoneal dialysis. *Am J Kidney Dis*, 35(4), 644-52.

176. Lai, K. N., Lai, K. B., Szeto, C. C., Lam, C. W. & Leung, J. C. (1999) Growth factors in continuous ambulatory peritoneal dialysis effluent. Their relation with peritoneal transport of small solutes. *Am J Nephrol*, 19(3), 416-22.
177. Lamb, E. J., Cattell, W. R. & Dawnay, A. B. (1995) In vitro formation of advanced glycation end products in peritoneal dialysis fluid. *Kidney Int*, 47(6), 1768-74.
178. Lambie, M., Chess, J., Donovan, K. L., Kim, Y. L., Do, J. Y., Lee, H. B., Noh, H., Williams, P. F., Williams, A. J., Davison, S., Dorval, M., Summers, A., Williams, J. D., Bankart, J., Davies, S. J., Topley, N. & Investigators, G. F. S. (2013) Independent effects of systemic and peritoneal inflammation on peritoneal dialysis survival. *J Am Soc Nephrol*, 24(12), 2071-80.
179. Lameire, N., Van Biesen, W., Van Landschoot, M., Wang, T., Heimbürger, O., Bergström, J., Lindholm, B., Hekking, L. P., Havenith, C. E. & Beelen, R. H. (1998) Experimental models in peritoneal dialysis: a European experience. *Kidney Int*, 54(6), 2194-206.
180. Lamouille, S., Xu, J. & Derynck, R. (2014) Molecular mechanisms of epithelial-mesenchymal transition. *Nat Rev Mol Cell Biol*, 15(3), 178-96.
181. Landgraf, P., Rusu, M., Sheridan, R., Sewer, A., Iovino, N., Aravin, A., Pfeffer, S., Rice, A., Kamphorst, A. O., Landthaler, M., Lin, C., Socci, N. D., Hermida, L., Fulci, V., Chiaretti, S., Foà, R., Schliwka, J., Fuchs, U., Novosel, A., Müller, R. U., Schermer, B., Bissels, U., Inman, J., Phan, Q., Chien, M., Weir, D. B., Choksi, R., De Vita, G., Frezzetti, D., Trompeter, H. I., Hornung, V., Teng, G., Hartmann, G., Palkovits, M., Di Lauro, R., Wernet, P., Macino, G., Rogler, C. E., Nagle, J. W., Ju, J., Papavasiliou, F. N., Benzing, T., Lichter, P., Tam, W., Brownstein, M. J., Bosio, A., Borkhardt, A., Russo, J. J., Sander, C., Zavolan, M. & Tuschl, T. (2007) A mammalian microRNA expression atlas based on small RNA library sequencing. *Cell*, 129(7), 1401-14.
182. Larsson, J., Goumans, M. J., Sjöstrand, L. J., van Rooijen, M. A., Ward, D., Levéen, P., Xu, X., ten Dijke, P., Mummery, C. L. & Karlsson, S. (2001) Abnormal angiogenesis but intact hematopoietic potential in TGF-beta type I receptor-deficient mice. *EMBO J*, 20(7), 1663-73.
183. Leavesley, D. I., Stanley, J. M. & Faull, R. J. (1999) Epidermal growth factor modifies the expression and function of extracellular matrix adhesion receptors expressed by peritoneal mesothelial cells from patients on CAPD. *Nephrol Dial Transplant*, 14(5), 1208-16.
184. LeBleu, V. S., Taduri, G., O'Connell, J., Teng, Y., Cooke, V. G., Woda, C., Sugimoto, H. & Kalluri, R. (2013) Origin and function of myofibroblasts in kidney fibrosis. *Nat Med*, 19(8), 1047-53.
185. Lee, R. C., Feinbaum, R. L. & Ambros, V. (1993) The C. elegans heterochronic gene lin-4 encodes small RNAs with antisense complementarity to lin-14. *Cell*, 75(5), 843-54.
186. Lee, Y., Ahn, C., Han, J., Choi, H., Kim, J., Yim, J., Lee, J., Provost, P., Rådmark, O., Kim, S. & Kim, V. N. (2003) The nuclear RNase III Drosha initiates microRNA processing. *Nature*, 425(6956), 415-9.
187. Lee, Y., Jeon, K., Lee, J. T., Kim, S. & Kim, V. N. (2002) MicroRNA maturation: stepwise processing and subcellular localization. *EMBO J*, 21(17), 4663-70.
188. Lee, Y., Kim, M., Han, J., Yeom, K. H., Lee, S., Baek, S. H. & Kim, V. N. (2004) MicroRNA genes are transcribed by RNA polymerase II. *EMBO J*, 23(20), 4051-60.
189. Lessan, K., Aguiar, D. J., Oegema, T., Siebenson, L. & Skubitz, A. P. (1999) CD44 and beta1 integrin mediate ovarian carcinoma cell adhesion to peritoneal mesothelial cells. *Am J Pathol*, 154(5), 1525-37.
190. Leung, J. C., Chan, L. Y., Li, F. F., Tang, S. C., Chan, K. W., Chan, T. M., Lam, M. F., Wieslander, A. & Lai, K. N. (2005) Glucose degradation products downregulate ZO-1 expression in human peritoneal mesothelial cells: the role of VEGF. *Nephrol Dial Transplant*, 20(7), 1336-49.
191. Leung, J. C., Chan, L. Y., Tam, K. Y., Tang, S. C., Lam, M. F., Cheng, A. S., Chu, K. M. & Lai, K. N. (2009) Regulation of CCN2/CTGF and related cytokines in cultured peritoneal cells under conditions simulating peritoneal dialysis. *Nephrol Dial Transplant*, 24(2), 458-69.

192. Levey, A. S., Coresh, J., Balk, E., Kausz, A. T., Levin, A., Steffes, M. W., Hogg, R. J., Perrone, R. D., Lau, J., Eknoyan, G. & Foundation, N. K. (2003) National Kidney Foundation practice guidelines for chronic kidney disease: evaluation, classification, and stratification. *Ann Intern Med*, 139(2), 137-47.
193. Lewis, B. P., Burge, C. B. & Bartel, D. P. (2005) Conserved seed pairing, often flanked by adenosines, indicates that thousands of human genes are microRNA targets. *Cell*, 120(1), 15-20.
194. Li, J. Y., Yong, T. Y., Michael, M. Z. & Gleadle, J. M. (2010) Review: The role of microRNAs in kidney disease. *Nephrology (Carlton)*, 15(6), 599-608.
195. Li, Y., Wang, J. & Asahina, K. (2013) Mesothelial cells give rise to hepatic stellate cells and myofibroblasts via mesothelial-mesenchymal transition in liver injury. *Proc Natl Acad Sci U S A*, 110(6), 2324-9.
196. Liang, Y., Ridzon, D., Wong, L. & Chen, C. (2007) Characterization of microRNA expression profiles in normal human tissues. *BMC Genomics*, 8, 166.
197. Liberek, T., Topley, N., Luttmann, W. & Williams, J. D. (1996) Adherence of neutrophils to human peritoneal mesothelial cells: role of intercellular adhesion molecule-1. *J Am Soc Nephrol*, 7(2), 208-17.
198. Lin, F., Wu, X., Zhang, H., You, X., Zhang, Z., Shao, R. & Huang, C. (2015) A microrna screen to identify regulators of peritoneal fibrosis in a rat model of peritoneal dialysis. *BMC Nephrol*, 16(1), 48.
199. Liu, H., Zhang, N. & Tian, D. (2014) MiR-30b is involved in methylglyoxal-induced epithelial-mesenchymal transition of peritoneal mesothelial cells in rats. *Cell Mol Biol Lett*, 19(2), 315-29.
200. Liu, L., Shi, C. X., Ghayur, A., Zhang, C., Su, J. Y., Hoff, C. M. & Margetts, P. J. (2009) Prolonged peritoneal gene expression using a helper-dependent adenovirus. *Perit Dial Int*, 29(5), 508-16.
201. Liu, X., Sempere, L. F., Ouyang, H., Memoli, V. A., Andrew, A. S., Luo, Y., Demidenko, E., Korc, M., Shi, W., Preis, M., Dragnev, K. H., Li, H., Direnzo, J., Bak, M., Freemantle, S. J., Kauppinen, S. & Dmitrovsky, E. (2010) MicroRNA-31 functions as an oncogenic microRNA in mouse and human lung cancer cells by repressing specific tumor suppressors. *J Clin Invest*, 120(4), 1298-309.
202. Liu, Y., Guo, R., Hao, G., Xiao, J., Bao, Y., Zhou, J., Chen, Q. & Wei, X. (2015) The expression profiling and ontology analysis of noncoding RNAs in peritoneal fibrosis induced by peritoneal dialysis fluid. *Gene*, 564(2), 210-9.
203. Liu, Z., Xu, J., Colvin, J. S. & Ornitz, D. M. (2002) Coordination of chondrogenesis and osteogenesis by fibroblast growth factor 18. *Genes Dev*, 16(7), 859-69.
204. Livak, K. J. & Schmittgen, T. D. (2001) Analysis of relative gene expression data using real-time quantitative PCR and the 2(-Delta Delta C(T)) Method. *Methods*, 25(4), 402-8.
205. Lopez-Anton, M., Bowen, T. & Jenkins, H. R. (2015) microRNA Regulation of Peritoneal Cavity Homeostasis in Peritoneal Dialysis. *BioMed Research International*.
206. Lopez-Anton, M., style="font-size:12.0pt, s. l. E.-U., line-height:150%, font-family:"Calibri", s.-s., mso-ascii-theme-font:minor-latin, mso-fareast-font-family:Calibri, mso-fareast-theme-font:, minor-latin, mso-hansi-theme-font:minor-latin, Roman", m.-b.-f.-f. T. N., mso-bidi-theme-font:minor-bidi, mso-ansi-language:EN-US, mso-fareast-language:, EN-US, style="font-size:12.0pt, m.-b.-l. A.-S. s. l. E.-U., line-height:150%, font-family:"Calibri", s.-s., mso-ascii-theme-font:minor-latin, mso-fareast-font-family:Calibri, mso-fareast-theme-font:, minor-latin, mso-hansi-theme-font:minor-latin, Roman", m.-b.-f.-f. T. N., mso-bidi-theme-font:minor-bidi, mso-ansi-language:EN-US, mso-fareast-language:, EN-US, mso-bidi-language:AR-SA">Lambie, M., style="font-size:12.0pt, s. l. E.-U., line-height:150%, font-family:"Calibri", s.-s., mso-ascii-theme-font:minor-latin, mso-fareast-font-family:Calibri, mso-fareast-theme-font:, minor-latin, mso-hansi-theme-font:minor-latin, Roman", m.-b.-f.-f. T. N., mso-bidi-theme-font:minor-bidi, mso-ansi-language:EN-US, mso-fareast-language:, EN-US, style="font-size:12.0pt, m.-b.-l. A.-S. s. l. E.-

U., line-height:150%, font-family:"Calibri", s.-s., mso-ascii-theme-font:minor-latin, mso-fareast-font-family:Calibri, mso-fareast-theme-font:, minor-latin, mso-hansi-theme-font:minor-latin, Roman", m.-b.-f.-f. T. N., mso-bidi-theme-font:minor-bidi, mso-ansi-language:EN-US, mso-fareast-language:, EN-US, mso-bidi-language:AR-SA">Lopez-Cabrera, M., style="font-size:12.0pt, s. l. E.-U., line-height:150%, font-family:"Calibri", s.-s., mso-ascii-theme-font:minor-latin, mso-fareast-font-family:Calibri, mso-fareast-theme-font:, minor-latin, mso-hansi-theme-font:minor-latin, Roman", m.-b.-f.-f. T. N., mso-bidi-theme-font:minor-bidi, mso-ansi-language:EN-US, mso-fareast-language:, EN-US, style="font-size:12.0pt, m.-b.-l. A.-S. s. l. E.-U., line-height:150%, font-family:"Calibri", s.-s., mso-ascii-theme-font:minor-latin, mso-fareast-font-family:Calibri, mso-fareast-theme-font:, minor-latin, mso-hansi-theme-font:minor-latin, Roman", m.-b.-f.-f. T. N., mso-bidi-theme-font:minor-bidi, mso-ansi-language:EN-US, mso-fareast-language:, EN-US, mso-bidi-language:AR-SA">Schmitt, C. P., style="font-size:12.0pt, s. l. E.-U., line-height:150%, font-family:"Calibri", s.-s., mso-ascii-theme-font:minor-latin, mso-fareast-font-family:Calibri, mso-fareast-theme-font:, minor-latin, mso-hansi-theme-font:minor-latin, Roman", m.-b.-f.-f. T. N., mso-bidi-theme-font:minor-bidi, mso-ansi-language:EN-US, mso-fareast-language:, EN-US, style="font-size:12.0pt, m.-b.-l. A.-S. s. l. E.-U., line-height:150%, font-family:"Calibri", s.-s., mso-ascii-theme-font:minor-latin, mso-fareast-font-family:Calibri, et al *MicroRNA-21 promotes fibrogenesis in peritoneal dialysis by targeting PDCD4,* peer review edition. The Journal of Pathology.

207. Lorenzen, J., Kumarswamy, R., Dangwal, S. & Thum, T. (2012) MicroRNAs in diabetes and diabetes-associated complications. *RNA Biol*, 9(6), 820-7.
208. Loureiro, J., Aguilera, A., Selgas, R., Sandoval, P., Albar-Vizcaíno, P., Pérez-Lozano, M. L., Ruiz-Carpio, V., Majano, P. L., Lamas, S., Rodríguez-Pascual, F., Borras-Cuesta, F., Dotor, J. & López-Cabrera, M. (2011) Blocking TGF-β1 protects the peritoneal membrane from dialysate-induced damage. *J Am Soc Nephrol*, 22(9), 1682-95.
209. Loureiro, J., Schilte, M., Aguilera, A., Albar-Vizcaíno, P., Ramírez-Huesca, M., Pérez-Lozano, M. L., González-Mateo, G., Aroeira, L. S., Selgas, R., Mendoza, L., Ortiz, A., Ruíz-Ortega, M., van den Born, J., Beelen, R. H. & López-Cabrera, M. (2010) BMP-7 blocks mesenchymal conversion of mesothelial cells and prevents peritoneal damage induced by dialysis fluid exposure. *Nephrol Dial Transplant*, 25(4), 1098-108.
210. Lu, X., Luo, F., Liu, Y., Zhang, A., Li, J., Wang, B., Xu, W., Shi, L., Liu, X., Lu, L. & Liu, Q. (2015) The IL-6/STAT3 pathway via miR-21 is involved in the neoplastic and metastatic properties of arsenite-transformed human keratinocytes. *Toxicol Lett*, 237(3), 191-9.
211. Lv, Z. D., Yang, Z. C., Wang, H. B., Li, J. G., Kong, B., Wang, X. G., Liu, X. Y., Niu, Z. H., Wang, Y. & Nie, G. (2012) The cytotoxic effect of TGF-β1 on mesothelial cells via apoptosis in early peritoneal carcinomatosis. *Oncol Rep*, 27(6), 1753-8.
212. López-Cabrera, M., Aguilera, A., Aroeira, L. S., Ramírez-Huesca, M., Pérez-Lozano, M. L., Jiménez-Heffernan, J. A., Bajo, M. A., del Peso, G., Sánchez-Tomero, J. A. & Selgas, R. (2006) Ex vivo analysis of dialysis effluent-derived mesothelial cells as an approach to unveiling the mechanism of peritoneal membrane failure. *Perit Dial Int*, 26(1), 26-34.
213. Löffler, D., Brocke-Heidrich, K., Pfeifer, G., Stocsits, C., Hackermüller, J., Kretzschmar, A. K., Burger, R., Gramatzki, M., Blumert, C., Bauer, K., Cvijic, H., Ullmann, A. K., Stadler, P. F. & Horn, F. (2007) Interleukin-6 dependent survival of multiple myeloma cells involves the Stat3-mediated induction of microRNA-21 through a highly conserved enhancer. *Blood*, 110(4), 1330-3.
214. Lúdvíksson, B. R., Seegers, D., Resnick, A. S. & Strober, W. (2000) The effect of TGF-beta1 on immune responses of naïve versus memory CD4+ Th1/Th2 T cells. *Eur J Immunol*, 30(7), 2101-11.
215. Ma, C., Tarnuzzer, R. W. & Chegini, N. (1999) Expression of matrix metalloproteinases and tissue inhibitor of matrix metalloproteinases in mesothelial cells and their regulation by transforming growth factor-beta1. *Wound Repair Regen*, 7(6), 477-85.

216. Ma, L., Teruya-Feldstein, J. & Weinberg, R. A. (2007) Tumour invasion and metastasis initiated by microRNA-10b in breast cancer. *Nature*, 449(7163), 682-8.
217. Macfarlane, L. A. & Murphy, P. R. (2010) MicroRNA: Biogenesis, Function and Role in Cancer. *Curr Genomics*, 11(7), 537-61.
218. Madureira, P. A., O'Connell, P. A., Surette, A. P., Miller, V. A. & Waisman, D. M. (2012) The biochemistry and regulation of S100A10: a multifunctional plasminogen receptor involved in oncogenesis. *J Biomed Biotechnol*, 2012, 353687.
219. Mann, H. H., Sengle, G., Gebauer, J. M., Eble, J. A., Paulsson, M. & Wagener, R. (2007) Matrilins mediate weak cell attachment without promoting focal adhesion formation. *Matrix Biol*, 26(3), 167-74.
220. Margetts, P. J. & Bonniaud, P. (2003) Basic mechanisms and clinical implications of peritoneal fibrosis. *Perit Dial Int*, 23(6), 530-41.
221. Margetts, P. J., Bonniaud, P., Liu, L., Hoff, C. M., Holmes, C. J., West-Mays, J. A. & Kelly, M. M. (2005) Transient overexpression of TGF-{beta}1 induces epithelial mesenchymal transition in the rodent peritoneum. *J Am Soc Nephrol*, 16(2), 425-36.
222. Margetts, P. J. & Churchill, D. N. (2002) Acquired ultrafiltration dysfunction in peritoneal dialysis patients. *J Am Soc Nephrol*, 13(11), 2787-94.
223. Margetts, P. J., Hoff, C., Liu, L., Korstanje, R., Walkin, L., Summers, A., Herrick, S. & Brenchley, P. (2013) Transforming growth factor β-induced peritoneal fibrosis is mouse strain dependent. *Nephrol Dial Transplant*, 28(8), 2015-27.
224. Margetts, P. J., Kolb, M., Galt, T., Hoff, C. M., Shockley, T. R. & Gauldie, J. (2001) Gene transfer of transforming growth factor-beta1 to the rat peritoneum: effects on membrane function. *J Am Soc Nephrol*, 12(10), 2029-39.
225. Martínez-Aguilar, J., Clifton-Bligh, R. & Molloy, M. P. (2015) A multiplexed, targeted mass spectrometry assay of the S100 protein family uncovers the isoform-specific expression in thyroid tumours. *BMC Cancer*, 15, 199.
226. Massagué, J. (2000) How cells read TGF-beta signals. *Nat Rev Mol Cell Biol*, 1(3), 169-78.
227. Massagué, J., Seoane, J. & Wotton, D. (2005) Smad transcription factors. *Genes Dev*, 19(23), 2783-810.
228. McLoughlin, R. M., Hurst, S. M., Nowell, M. A., Harris, D. A., Horiuchi, S., Morgan, L. W., Wilkinson, T. S., Yamamoto, N., Topley, N. & Jones, S. A. (2004) Differential regulation of neutrophil-activating chemokines by IL-6 and its soluble receptor isoforms. *J Immunol*, 172(9), 5676-83.
229. McLoughlin, R. M., Witowski, J., Robson, R. L., Wilkinson, T. S., Hurst, S. M., Williams, A. S., Williams, J. D., Rose-John, S., Jones, S. A. & Topley, N. (2003) Interplay between IFN-gamma and IL-6 signaling governs neutrophil trafficking and apoptosis during acute inflammation. *J Clin Invest*, 112(4), 598-607.
230. Medcalf, J. F., Walls, J., Pawluczyk, I. Z. & Harris, K. P. (2001) Effects of glucose dialysate on extracellular matrix production by human peritoneal mesothelial cells (HPMC): the role of TGF-beta. *Nephrol Dial Transplant*, 16(9), 1885-92.
231. Meng, F., Henson, R., Wehbe-Janek, H., Ghoshal, K., Jacob, S. T. & Patel, T. (2007) MicroRNA-21 regulates expression of the PTEN tumor suppressor gene in human hepatocellular cancer. *Gastroenterology*, 133(2), 647-58.
232. Mercado-Pimentel, M. E. & Runyan, R. B. (2007) Multiple transforming growth factor-beta isoforms and receptors function during epithelial-mesenchymal cell transformation in the embryonic heart. *Cells Tissues Organs*, 185(1-3), 146-56.
233. Mignone, F., Gissi, C., Liuni, S. & Pesole, G. (2002) Untranslated regions of mRNAs. *Genome Biol*, 3(3), REVIEWS0004.
234. Mitamura, T., Watari, H., Wang, L., Kanno, H., Kitagawa, M., Hassan, M. K., Kimura, T., Tanino, M., Nishihara, H., Tanaka, S. & Sakuragi, N. (2014) microRNA 31 functions as an endometrial cancer oncogene by suppressing Hippo tumor suppressor pathway. *Molecular Cancer*, 13.

235. Mitchell, P. S., Parkin, R. K., Kroh, E. M., Fritz, B. R., Wyman, S. K., Pogosova-Agadjanyan, E. L., Peterson, A., Noteboom, J., O'Briant, K. C., Allen, A., Lin, D. W., Urban, N., Drescher, C. W., Knudsen, B. S., Stirewalt, D. L., Gentleman, R., Vessella, R. L., Nelson, P. S., Martin, D. B. & Tewari, M. (2008) Circulating microRNAs as stable blood-based markers for cancer detection. *Proc Natl Acad Sci U S A*, 105(30), 10513-8.
236. Mizuiri, S., Ohashi, Y., Hemmi, H., Arita, M., Yamada, K., Aoki, T., Miyagi, M., Sakai, K. & Aikawa, A. (2009) Effects of new peritoneal dialysis solutions, pyridoxamine and AT1 receptor blocker, on TGF-beta1 and VEGF expression in rat peritoneal mesothelial cells. *Am J Nephrol*, 30(3), 295-302.
237. Morgan, L. W., Wieslander, A., Davies, M., Horiuchi, T., Ohta, Y., Beavis, M. J., Craig, K. J., Williams, J. D. & Topley, N. (2003) Glucose degradation products (GDP) retard remesothelialization independently of D-glucose concentration. *Kidney Int*, 64(5), 1854-66.
238. Morishita, Y., Yoshizawa, H., Watanabe, M., Imai, R., Imai, T., Hirahara, I., Akimoto, T., Ookawara, S., Muto, S. & Nagata, D. (2016) MicroRNA expression profiling in peritoneal fibrosis. *Transl Res*, 169, 47-66.
239. Mukherjee, A., Dong, S. S., Clemens, T., Alvarez, J. & Serra, R. (2005) Co-ordination of TGF-beta and FGF signaling pathways in bone organ cultures. *Mech Dev*, 122(4), 557-71.
240. Mutsaers, S. E. (2002) Mesothelial cells: their structure, function and role in serosal repair. *Respirology*, 7(3), 171-91.
241. Mutsaers, S. E. (2004) The mesothelial cell. *Int J Biochem Cell Biol*, 36(1), 9-16.
242. Mutsaers, S. E., Birnie, K., Lansley, S., Herrick, S. E., Lim, C. B. & Prêle, C. M. (2015) Mesothelial cells in tissue repair and fibrosis. *Front Pharmacol*, 6, 113.
243. Mátés, L., Nicolae, C., Mörgelin, M., Deák, F., Kiss, I. & Aszódi, A. (2004) Mice lacking the extracellular matrix adaptor protein matrilin-2 develop without obvious abnormalities. *Matrix Biol*, 23(3), 195-204.
244. Nagy, J. A. & Jackman, R. W. (1998) Anatomy and Physiology of the Peritoneal Membrane

245. Seminars in Dialysis Volume 11, Issue 1. *Seminars in Dialysis*, 11(1), 49-56. Available online: http://onlinelibrary.wiley.com/doi/10.1111/j.1525-139X.1998.tb00210.x/abstract [Accessed 01].
246. Nakamura, S. & Niwa, T. (2004) Advanced glycation end-products and peritoneal sclerosis. *Semin Nephrol*, 24(5), 502-5.
247. Nakayama, M., Kawaguchi, Y., Yamada, K., Hasegawa, T., Takazoe, K., Katoh, N., Hayakawa, H., Osaka, N., Yamamoto, H., Ogawa, A., Kubo, H., Shigematsu, T., Sakai, O. & Horiuchi, S. (1997) Immunohistochemical detection of advanced glycosylation end-products in the peritoneum and its possible pathophysiological role in CAPD. *Kidney Int*, 51(1), 182-6.
248. Nam, J. W., Rissland, O. S., Koppstein, D., Abreu-Goodger, C., Jan, C. H., Agarwal, V., Yildirim, M. A., Rodriguez, A. & Bartel, D. P. (2014) Global analyses of the effect of different cellular contexts on microRNA targeting. *Mol Cell*, 53(6), 1031-43.
249. Nie, J., Dou, X., Hao, W., Wang, X., Peng, W., Jia, Z., Chen, W., Li, X., Luo, N., Lan, H. Y. & Yu, X. Q. (2007) Smad7 gene transfer inhibits peritoneal fibrosis. *Kidney Int*, 72(11), 1336-44.
250. Nitta, T., Kim, J. S., Mohuczy, D. & Behrns, K. E. (2008) Murine cirrhosis induces hepatocyte epithelial mesenchymal transition and alterations in survival signaling pathways. *Hepatology*, 48(3), 909-19.
251. Nomura, M. & Li, E. (1998) Smad2 role in mesoderm formation, left-right patterning and craniofacial development. *Nature*, 393(6687), 786-90.
252. Offner, F. A., Feichtinger, H., Stadlmann, S., Obrist, P., Marth, C., Klingler, P., Grage, B., Schmahl, M. & Knabbe, C. (1996) Transforming growth factor-beta synthesis by human peritoneal mesothelial cells. Induction by interleukin-1. *Am J Pathol*, 148(5), 1679-88.

253. Ogata, R., Hiramatsu, N., Hayakawa, K., Nakajima, S., Yao, J., Kobayashi, T. & Kitamura, M. (2011) Impairment of MCP-1 expression in mesothelial cells exposed to peritoneal dialysis fluid by osmotic stress and acidic stress. *Perit Dial Int*, 31(1), 80-9.
254. Oshima, M., Oshima, H. & Taketo, M. M. (1996) TGF-beta receptor type II deficiency results in defects of yolk sac hematopoiesis and vasculogenesis. *Dev Biol*, 179(1), 297-302.
255. Padua, D. & Massagué, J. (2009) Roles of TGFbeta in metastasis. *Cell Res*, 19(1), 89-102.
256. Papadimitriou, E., Vasilaki, E., Vorvis, C., Iliopoulos, D., Moustakas, A., Kardassis, D. & Stournaras, C. (2012) Differential regulation of the two RhoA-specific GEF isoforms Net1/Net1A by TGF-β and miR-24: role in epithelial-to-mesenchymal transition. *Oncogene*, 31(23), 2862-75.
257. Paraskevopoulou, M. D., Georgakilas, G., Kostoulas, N., Vlachos, I. S., Vergoulis, T., Reczko, M., Filippidis, C., Dalamagas, T. & Hatzigeorgiou, A. G. (2013) DIANA-microT web server v5.0: service integration into miRNA functional analysis workflows. *Nucleic Acids Res*, 41(Web Server issue), W169-73.
258. Pasquinelli, A. E. (2012) MicroRNAs and their targets: recognition, regulation and an emerging reciprocal relationship. *Nat Rev Genet*, 13(4), 271-82.
259. Pasquinelli, A. E., Reinhart, B. J., Slack, F., Martindale, M. Q., Kuroda, M. I., Maller, B., Hayward, D. C., Ball, E. E., Degnan, B., Müller, P., Spring, J., Srinivasan, A., Fishman, M., Finnerty, J., Corbo, J., Levine, M., Leahy, P., Davidson, E. & Ruvkun, G. (2000) Conservation of the sequence and temporal expression of let-7 heterochronic regulatory RNA. *Nature*, 408(6808), 86-9.
260. Patel, P., Sekiguchi, Y., Oh, K. H., Patterson, S. E., Kolb, M. R. & Margetts, P. J. (2010a) Smad3-dependent and -independent pathways are involved in peritoneal membrane injury. *Kidney Int*, 77(4), 319-28.
261. Patel, P., West-Mays, J., Kolb, M., Rodrigues, J. C., Hoff, C. M. & Margetts, P. J. (2010b) Platelet derived growth factor B and epithelial mesenchymal transition of peritoneal mesothelial cells. *Matrix Biol*, 29(2), 97-106.
262. Pereira, B. J. G., Sayegh, M. H. & Blake, P. G. (2005) *Chronic kidney disease, dialysis, and transplantation : a companion to Brenner and Rector's the kidney*, 2nd ed. edition. Philadelphia, Pa. ; [Great Britain]: Elsever Saunders.
263. Perfumo, F., Altieri, P., Degl'Innocenti, M. L., Ghiggeri, G. M., Caridi, G., Trivelli, A. & Gusmano, R. (1996) Effects of peritoneal effluents on mesothelial cells in culture: cell proliferation and extracellular matrix regulation. *Nephrol Dial Transplant*, 11(9), 1803-9.
264. Peterson, S. M., Thompson, J. A., Ufkin, M. L., Sathyanarayana, P., Liaw, L. & Congdon, C. B. (2014) Common features of microRNA target prediction tools. *Front Genet*, 5, 23.
265. Pfeffer, S., Zavolan, M., Grässer, F. A., Chien, M., Russo, J. J., Ju, J., John, B., Enright, A. J., Marks, D., Sander, C. & Tuschl, T. (2004) Identification of virus-encoded microRNAs. *Science*, 304(5671), 734-6.
266. Piecha, D., Wiberg, C., Mörgelin, M., Reinhardt, D. P., Deák, F., Maurer, P. & Paulsson, M. (2002) Matrilin-2 interacts with itself and with other extracellular matrix proteins. *Biochem J*, 367(Pt 3), 715-21.
267. Pietenpol, J. A., Stein, R. W., Moran, E., Yaciuk, P., Schlegel, R., Lyons, R. M., Pittelkow, M. R., Münger, K., Howley, P. M. & Moses, H. L. (1990) TGF-beta 1 inhibition of c-myc transcription and growth in keratinocytes is abrogated by viral transforming proteins with pRB binding domains. *Cell*, 61(5), 777-85.
268. Posthuma, N., ter Wee, P. M., Niessen, H., Donker, A. J., Verbrugh, H. A. & Schalkwijk, C. G. (2001) Amadori albumin and advanced glycation end-product formation in peritoneal dialysis using icodextrin. *Perit Dial Int*, 21(1), 43-51.
269. Quaggin, S. E. & Kapus, A. (2011) Scar wars: mapping the fate of epithelial-mesenchymal-myofibroblast transition. *Kidney Int*, 80(1), 41-50.

270. Que, J., Wilm, B., Hasegawa, H., Wang, F., Bader, D. & Hogan, B. L. (2008) Mesothelium contributes to vascular smooth muscle and mesenchyme during lung development. *Proc Natl Acad Sci U S A*, 105(43), 16626-30.
271. Rabindranath, K. S., Adams, J., Ali, T. Z., Daly, C., Vale, L. & Macleod, A. M. (2007) Automated vs continuous ambulatory peritoneal dialysis: a systematic review of randomized controlled trials. *Nephrol Dial Transplant*, 22(10), 2991-8.
272. Ramalingam, P., Palanichamy, J. K., Singh, A., Das, P., Bhagat, M., Kassab, M. A., Sinha, S. & Chattopadhyay, P. (2014) Biogenesis of intronic miRNAs located in clusters by independent transcription and alternative splicing. *RNA*, 20(1), 76-87.
273. Randall, R. A., Germain, S., Inman, G. J., Bates, P. A. & Hill, C. S. (2002) Different Smad2 partners bind a common hydrophobic pocket in Smad2 via a defined proline-rich motif. *EMBO J*, 21(1-2), 145-56.
274. Reczko, M., Maragkakis, M., Alexiou, P., Grosse, I. & Hatzigeorgiou, A. G. (2012) Functional microRNA targets in protein coding sequences. *Bioinformatics*, 28(6), 771-6.
275. Reinhart, B. J., Slack, F. J., Basson, M., Pasquinelli, A. E., Bettinger, J. C., Rougvie, A. E., Horvitz, H. R. & Ruvkun, G. (2000) The 21-nucleotide let-7 RNA regulates developmental timing in Caenorhabditis elegans. *Nature*, 403(6772), 901-6.
276. Ribas, J., Ni, X., Castanares, M., Liu, M. M., Esopi, D., Yegnasubramanian, S., Rodriguez, R., Mendell, J. T. & Lupold, S. E. (2012) A novel source for miR-21 expression through the alternative polyadenylation of VMP1 gene transcripts. *Nucleic Acids Res*, 40(14), 6821-33.
277. Richmond, J., Tuzova, M., Cruikshank, W. & Center, D. (2014) Regulation of cellular processes by interleukin-16 in homeostasis and cancer. *J Cell Physiol*, 229(2), 139-47.
278. Ruvkun, G. (2001) Molecular biology. Glimpses of a tiny RNA world. *Science*, 294(5543), 797-9.
279. Réty, S., Sopkova, J., Renouard, M., Osterloh, D., Gerke, V., Tabaries, S., Russo-Marie, F. & Lewit-Bentley, A. (1999) The crystal structure of a complex of p11 with the annexin II N-terminal peptide. *Nat Struct Biol*, 6(1), 89-95.
280. Salmena, L., Poliseno, L., Tay, Y., Kats, L. & Pandolfi, P. P. (2011) A ceRNA hypothesis: the Rosetta Stone of a hidden RNA language? *Cell*, 146(3), 353-8.
281. Sandberg, R., Neilson, J. R., Sarma, A., Sharp, P. A. & Burge, C. B. (2008) Proliferating cells express mRNAs with shortened 3' untranslated regions and fewer microRNA target sites. *Science*, 320(5883), 1643-7.
282. Sanford, L. P., Ormsby, I., Gittenberger-de Groot, A. C., Sariola, H., Friedman, R., Boivin, G. P., Cardell, E. L. & Doetschman, T. (1997) TGFbeta2 knockout mice have multiple developmental defects that are non-overlapping with other TGFbeta knockout phenotypes. *Development*, 124(13), 2659-70.
283. Saxena, R. & West, C. (2006) Peritoneal dialysis: a primary care perspective. *J Am Board Fam Med*, 19(4), 380-9.
284. Schelch, K., Hoda, M. A., Klikovits, T., Münzker, J., Ghanim, B., Wagner, C., Garay, T., Laszlo, V., Setinek, U., Dome, B., Filipits, M., Pirker, C., Heffeter, P., Selzer, E., Tovari, J., Torok, S., Kenessey, I., Holzmann, K., Grasl-Kraupp, B., Marian, B., Klepetko, W., Berger, W., Hegedus, B. & Grusch, M. (2014) Fibroblast growth factor receptor inhibition is active against mesothelioma and synergizes with radio- and chemotherapy. *Am J Respir Crit Care Med*, 190(7), 763-72.
285. Schlueter, J. & Brand, T. (2013) Subpopulation of proepicardial cells is derived from the somatic mesoderm in the chick embryo. *Circ Res*, 113(10), 1128-37.
286. Schwarzenbach, H., Nishida, N., Calin, G. A. & Pantel, K. (2014) Clinical relevance of circulating cell-free microRNAs in cancer. *Nat Rev Clin Oncol*, 11(3), 145-56.
287. Schwenger, V., Morath, C., Salava, A., Amann, K., Seregin, Y., Deppisch, R., Ritz, E., Bierhaus, A., Nawroth, P. P. & Zeier, M. (2006) Damage to the peritoneal membrane by glucose degradation products is mediated by the receptor for advanced glycation end-products. *J Am Soc Nephrol*, 17(1), 199-207.

288. Seeger, T., Fischer, A., Muhly-Reinholz, M., Zeiher, A. M. & Dimmeler, S. (2014) Long-term inhibition of miR-21 leads to reduction of obesity in db/db mice. *Obesity (Silver Spring)*, 22(11), 2352-60.
289. Selgas, R., Bajo, A., Jiménez-Heffernan, J. A., Sánchez-Tomero, J. A., Del Peso, G., Aguilera, A. & López-Cabrera, M. (2006) Epithelial-to-mesenchymal transition of the mesothelial cell--its role in the response of the peritoneum to dialysis. *Nephrol Dial Transplant*, 21 Suppl 2, ii2-7.
290. Sherif, A. M., Nakayama, M., Maruyama, Y., Yoshida, H., Yamamoto, H., Yokoyama, K. & Kawakami, M. (2006) Quantitative assessment of the peritoneal vessel density and vasculopathy in CAPD patients. *Nephrol Dial Transplant*, 21(6), 1675-81.
291. Shi, R. & Chiang, V. L. (2005) Facile means for quantifying microRNA expression by real-time PCR. *Biotechniques*, 39(4), 519-25.
292. Shi, Y. & Massagué, J. (2003) Mechanisms of TGF-beta signaling from cell membrane to the nucleus. *Cell*, 113(6), 685-700.
293. Shmaryahu, A., Carrasco, M. & Valenzuela, P. D. (2014) Prediction of bacterial microRNAs and possible targets in human cell transcriptome. *J Microbiol*, 52(6), 482-9.
294. Shull, M. M., Ormsby, I., Kier, A. B., Pawlowski, S., Diebold, R. J., Yin, M., Allen, R., Sidman, C., Proetzel, G. & Calvin, D. (1992) Targeted disruption of the mouse transforming growth factor-beta 1 gene results in multifocal inflammatory disease. *Nature*, 359(6397), 693-9.
295. Slack, F. J., Basson, M., Liu, Z., Ambros, V., Horvitz, H. R. & Ruvkun, G. (2000) The lin-41 RBCC gene acts in the C. elegans heterochronic pathway between the let-7 regulatory RNA and the LIN-29 transcription factor. *Mol Cell*, 5(4), 659-69.
296. Stevens, P. E., O'Donoghue, D. J., de Lusignan, S., Van Vlymen, J., Klebe, B., Middleton, R., Hague, N., New, J. & Farmer, C. K. (2007) Chronic kidney disease management in the United Kingdom: NEOERICA project results. *Kidney Int*, 72(1), 92-9.
297. Strippoli, R., Benedicto, I., Foronda, M., Perez-Lozano, M. L., Sánchez-Perales, S., López-Cabrera, M. & Del Pozo, M. (2010) p38 maintains E-cadherin expression by modulating TAK1-NF-kappa B during epithelial-to-mesenchymal transition. *J Cell Sci*, 123(Pt 24), 4321-31.
298. Strippoli, R., Benedicto, I., Perez Lozano, M. L., Pellinen, T., Sandoval, P., Lopez-Cabrera, M. & del Pozo, M. A. (2012) Inhibition of transforming growth factor-activated kinase 1 (TAK1) blocks and reverses epithelial to mesenchymal transition of mesothelial cells. *PLoS One*, 7(2), e31492.
299. Strippoli, R., Benedicto, I., Pérez Lozano, M. L., Cerezo, A., López-Cabrera, M. & del Pozo, M. A. (2008) Epithelial-to-mesenchymal transition of peritoneal mesothelial cells is regulated by an ERK/NF-kappaB/Snail1 pathway. *Dis Model Mech*, 1(4-5), 264-74.
300. Stylianou, E., Jenner, L. A., Davies, M., Coles, G. A. & Williams, J. D. (1990) Isolation, culture and characterization of human peritoneal mesothelial cells. *Kidney Int*, 37(6), 1563-70.
301. Sulaiman, H., Dawson, L., Laurent, G. J., Bellingan, G. J. & Herrick, S. E. (2002) Role of plasminogen activators in peritoneal adhesion formation. *Biochem Soc Trans*, 30(2), 126-31.
302. Sun, P. D. & Davies, D. R. (1995) The cystine-knot growth-factor superfamily. *Annu Rev Biophys Biomol Struct*, 24, 269-91.
303. Surette, A. P., Madureira, P. A., Phipps, K. D., Miller, V. A., Svenningsson, P. & Waisman, D. M. (2011) Regulation of fibrinolysis by S100A10 in vivo. *Blood*, 118(11), 3172-81.
304. Szeto, C. C., Chow, K. M., Lai, K. B., Szeto, C. Y., Kwan, B. C. & Li, P. K. (2006) Connective tissue growth factor is responsible for transforming growth factor-beta-induced peritoneal mesothelial cell apoptosis. *Nephron Exp Nephrol*, 103(4), e166-74.
305. Taccioli, C., Garofalo, M., Chen, H., Jiang, Y., Tagliazucchi, G. M., Di Leva, G., Alder, H., Fadda, P., Middleton, J., Smalley, K. J., Selmi, T., Naidu, S., Farber, J. L., Croce, C. M. & Fong,

L. Y. (2015) Repression of Esophageal Neoplasia and Inflammatory Signaling by Anti-miR-31 Delivery In Vivo. *J Natl Cancer Inst*, 107(11).
306. Tam, C. W., Liu, V. W., Leung, W. Y., Yao, K. M. & Shiu, S. Y. (2008) The autocrine human secreted PDZ domain-containing protein 2 (sPDZD2) induces senescence or quiescence of prostate, breast and liver cancer cells via transcriptional activation of p53. *Cancer Lett*, 271(1), 64-80.
307. Tan, R., Zhang, X., Yang, J., Li, Y. & Liu, Y. (2007) Molecular basis for the cell type specific induction of SnoN expression by hepatocyte growth factor. *J Am Soc Nephrol*, 18(8), 2340-9.
308. Termén, S., Tan, E. J., Heldin, C. H. & Moustakas, A. (2013) p53 regulates epithelial-mesenchymal transition induced by transforming growth factor β. *J Cell Physiol*, 228(4), 801-13.
309. Thum, T., Gross, C., Fiedler, J., Fischer, T., Kissler, S., Bussen, M., Galuppo, P., Just, S., Rottbauer, W., Frantz, S., Castoldi, M., Soutschek, J., Koteliansky, V., Rosenwald, A., Basson, M. A., Licht, J. D., Pena, J. T., Rouhanifard, S. H., Muckenthaler, M. U., Tuschl, T., Martin, G. R., Bauersachs, J. & Engelhardt, S. (2008) MicroRNA-21 contributes to myocardial disease by stimulating MAP kinase signalling in fibroblasts. *Nature*, 456(7224), 980-4.
310. Tietze, L., Elbrecht, A., Schauerte, C., Klosterhalfen, B., Amo-Takyi, B., Gehlen, J., Winkeltau, G., Mittermayer, C. & Handt, S. (1998) Modulation of pro- and antifibrinolytic properties of human peritoneal mesothelial cells by transforming growth factor beta1 (TGF-beta1), tumor necrosis factor alpha (TNF-alpha) and interleukin 1beta (IL-1beta). *Thromb Haemost*, 79(2), 362-70.
311. Topley, N., Jörres, A., Luttmann, W., Petersen, M. M., Lang, M. J., Thierauch, K. H., Müller, C., Coles, G. A., Davies, M. & Williams, J. D. (1993) Human peritoneal mesothelial cells synthesize interleukin-6: induction by IL-1 beta and TNF alpha. *Kidney Int*, 43(1), 226-33.
312. Toyoshima, H. & Hunter, T. (1994) p27, a novel inhibitor of G1 cyclin-Cdk protein kinase activity, is related to p21. *Cell*, 78(1), 67-74.
313. Tsukazaki, T., Chiang, T. A., Davison, A. F., Attisano, L. & Wrana, J. L. (1998) SARA, a FYVE domain protein that recruits Smad2 to the TGFbeta receptor. *Cell*, 95(6), 779-91.
314. Turchinovich, A., Weiz, L., Langheinz, A. & Burwinkel, B. (2011) Characterization of extracellular circulating microRNA. *Nucleic Acids Res*, 39(16), 7223-33.
315. Usui, H., Shibayama, M., Ohbayashi, N., Konishi, M., Takada, S. & Itoh, N. (2004) Fgf18 is required for embryonic lung alveolar development. *Biochem Biophys Res Commun*, 322(3), 887-92.
316. Valle, M. T., Degl'Innocenti, M. L., Bertelli, R., Facchetti, P., Perfumo, F., Fenoglio, D., Kunkl, A., Gusmano, R. & Manca, F. (1995) Antigen-presenting function of human peritoneum mesothelial cells. *Clin Exp Immunol*, 101(1), 172-6.
317. van de Luijtgaarden, M. W., Noordzij, M., Stel, V. S., Ravani, P., Jarraya, F., Collart, F., Schön, S., Leivestad, T., Puttinger, H., Wanner, C. & Jager, K. J. (2011) Effects of comorbid and demographic factors on dialysis modality choice and related patient survival in Europe. *Nephrol Dial Transplant*, 26(9), 2940-7.
318. Vargha, R., Endemann, M., Kratochwill, K., Riesenhuber, A., Wick, N., Krachler, A. M., Malaga-Dieguez, L. & Aufricht, C. (2006) Ex vivo reversal of in vivo transdifferentiation in mesothelial cells grown from peritoneal dialysate effluents. *Nephrol Dial Transplant*, 21(10), 2943-7.
319. Virchow, R. (1858) *Die Cellularpathologie in ihrer Begründung auf physiologische und pathologische Gewebelehre : [zwanzig Vorlesungen gehalten während der Monate Februar - April 1858]*. Berlin: A. Hirschwald.
320. Vousden, K. H. & Lane, D. P. (2007) p53 in health and disease. *Nat Rev Mol Cell Biol*, 8(4), 275-83.

321. Wang, D., Lu, M., Miao, J., Li, T., Wang, E. & Cui, Q. (2009) Cepred: predicting the co-expression patterns of the human intronic microRNAs with their host genes. *PLoS One*, 4(2), e4421.
322. Wang, Q., Ding, Y., Gao, F., Jiang, S., Zhang, B. & Ni, J. (2013) A sensitive DNA biosensor based on a facile sulfamide coupling reaction for capture probe immobilization. *Anal Chim Acta*, 788, 158-64.
323. Wang, X. & El Naqa, I. M. (2008) Prediction of both conserved and nonconserved microRNA targets in animals. *Bioinformatics*, 24(3), 325-32.
324. Weiskirchen, R. & Meurer, S. K. (2013) BMP-7 counteracting TGF-beta1 activities in organ fibrosis. *Front Biosci (Landmark Ed)*, 18, 1407-34.
325. Wightman, B., Ha, I. & Ruvkun, G. (1993) Posttranscriptional regulation of the heterochronic gene lin-14 by lin-4 mediates temporal pattern formation in C. elegans. *Cell*, 75(5), 855-62.
326. Wilfinger, W. W., Mackey, K. & Chomczynski, P. (1997) Effect of pH and ionic strength on the spectrophotometric assessment of nucleic acid purity. *Biotechniques*, 22(3), 474-6, 478-81.
327. Williams, J. D., Craig, K. J., Topley, N., Von Ruhland, C., Fallon, M., Newman, G. R., Mackenzie, R. K., Williams, G. T. & Group, P. B. S. (2002) Morphologic changes in the peritoneal membrane of patients with renal disease. *J Am Soc Nephrol*, 13(2), 470-9.
328. Wilm, B., Ipenberg, A., Hastie, N. D., Burch, J. B. & Bader, D. M. (2005) The serosal mesothelium is a major source of smooth muscle cells of the gut vasculature. *Development*, 132(23), 5317-28.
329. Witowski, J. & Jörres, A. (2006) Peritoneal cell culture: fibroblasts. *Perit Dial Int*, 26(3), 292-9.
330. Witowski, J., Jörres, A., Coles, G. A., Williams, J. D. & Topley, N. (1996) Superinduction of IL-6 synthesis in human peritoneal mesothelial cells is related to the induction and stabilization of IL-6 mRNA. *Kidney Int*, 50(4), 1212-23.
331. Witowski, J., Korybalska, K., Wisniewska, J., Breborowicz, A., Gahl, G. M., Frei, U., Passlick-Deetjen, J. & Jörres, A. (2000) Effect of glucose degradation products on human peritoneal mesothelial cell function. *J Am Soc Nephrol*, 11(4), 729-39.
332. Wong, N. & Wang, X. (2015) miRDB: an online resource for microRNA target prediction and functional annotations. *Nucleic Acids Res*, 43(Database issue), D146-52.
333. Wong, T. Y., Phillips, A. O., Witowski, J. & Topley, N. (2003) Glucose-mediated induction of TGF-beta 1 and MCP-1 in mesothelial cells in vitro is osmolality and polyol pathway dependent. *Kidney Int*, 63(4), 1404-16.
334. Wu, L. & Belasco, J. G. (2008) Let me count the ways: mechanisms of gene regulation by miRNAs and siRNAs. *Mol Cell*, 29(1), 1-7.
335. Xiao, L., Zhou, X., Liu, F., Hu, C., Zhu, X., Luo, Y., Wang, M., Xu, X., Yang, S., Kanwar, Y. S. & Sun, L. (2015) MicroRNA-129-5p modulates epithelial-to-mesenchymal transition by targeting SIP1 and SOX4 during peritoneal dialysis. *Lab Invest*.
336. Xu, J., Lamouille, S. & Derynck, R. (2009) TGF-beta-induced epithelial to mesenchymal transition. *Cell Research*, 19(2), 156-172.
337. Xu, N., Meisgen, F., Butler, L. M., Han, G., Wang, X.-J., Soderberg-Naucler, C., Stahle, M., Pivarcsi, A. & Sonkoly, E. (2013) MicroRNA-31 Is Overexpressed in Psoriasis and Modulates Inflammatory Cytokine and Chemokine Production in Keratinocytes via Targeting Serine/Threonine Kinase 40. *Journal of Immunology*, 190(2), 678-688.
338. Yamada, A., Irie, K., Hirota, T., Ooshio, T., Fukuhara, A. & Takai, Y. (2005) Involvement of the annexin II-S100A10 complex in the formation of E-cadherin-based adherens junctions in Madin-Darby canine kidney cells. *J Biol Chem*, 280(7), 6016-27.
339. Yamaoka, H., Nishizawa, S., Asawa, Y., Fujihara, Y., Ogasawara, T., Yamaoka, K., Nagata, S., Takato, T. & Hoshi, K. (2010) Involvement of fibroblast growth factor 18 in dedifferentiation of cultured human chondrocytes. *Cell Prolif*, 43(1), 67-76.

340. Yang, A. H., Chen, J. Y. & Lin, J. K. (2003) Myofibroblastic conversion of mesothelial cells. *Kidney Int*, 63(4), 1530-9.
341. Yang, J., Dai, C. & Liu, Y. (2005) A novel mechanism by which hepatocyte growth factor blocks tubular epithelial to mesenchymal transition. *J Am Soc Nephrol*, 16(1), 68-78.
342. Yang, J. & Weinberg, R. A. (2008) Epithelial-mesenchymal transition: at the crossroads of development and tumor metastasis. *Dev Cell*, 14(6), 818-29.
343. Yang, J., Zhu, T., Liu, X., Zhang, L., Yang, Y., Zhang, J. & Guo, M. (2015) Heat shock protein 70 protects rat peritoneal mesothelial cells from advanced glycation end-products-induced epithelial-to-mesenchymal transition through mitogen-activated protein kinases/extracellular signal-regulated kinases and transforming growth factor-β/Smad pathways. *Mol Med Rep*, 11(6), 4473-81.
344. Yang, W. S., Kim, B. S., Lee, S. K., Park, J. S. & Kim, S. B. (1999a) Interleukin-1beta stimulates the production of extracellular matrix in cultured human peritoneal mesothelial cells. *Perit Dial Int*, 19(3), 211-20.
345. Yang, X., Letterio, J. J., Lechleider, R. J., Chen, L., Hayman, R., Gu, H., Roberts, A. B. & Deng, C. (1999b) Targeted disruption of SMAD3 results in impaired mucosal immunity and diminished T cell responsiveness to TGF-beta. *EMBO J*, 18(5), 1280-91.
346. Yang, X., Popescu, N. C. & Zimonjic, D. B. (2011) DLC1 interaction with S100A10 mediates inhibition of in vitro cell invasion and tumorigenicity of lung cancer cells through a RhoGAP-independent mechanism. *Cancer Res*, 71(8), 2916-25.
347. Yao, Q., Cao, S., Li, C., Mengesha, A., Kong, B. & Wei, M. (2011) Micro-RNA-21 regulates TGF-β-induced myofibroblast differentiation by targeting PDCD4 in tumor-stroma interaction. *Int J Cancer*, 128(8), 1783-92.
348. Yao, Q., Pawlaczyk, K., Ayala, E. R., Styszynski, A., Breborowicz, A., Heimburger, O., Qian, J. Q., Stenvinkel, P., Lindholm, B. & Axelsson, J. (2008) The role of the TGF/Smad signaling pathway in peritoneal fibrosis induced by peritoneal dialysis solutions. *Nephron Exp Nephrol*, 109(2), e71-8.
349. Yee, D. S., Narula, N., Ramzy, I., Boker, J., Ahlering, T. E., Skarecky, D. W. & Ornstein, D. K. (2007) Reduced annexin II protein expression in high-grade prostatic intraepithelial neoplasia and prostate cancer. *Arch Pathol Lab Med*, 131(6), 902-8.
350. Yeung, M. L., Tam, T. S., Tsang, A. C. & Yao, K. M. (2003) Proteolytic cleavage of PDZD2 generates a secreted peptide containing two PDZ domains. *EMBO Rep*, 4(4), 412-8.
351. Yi, R., Qin, Y., Macara, I. G. & Cullen, B. R. (2003) Exportin-5 mediates the nuclear export of pre-microRNAs and short hairpin RNAs. *Genes Dev*, 17(24), 3011-6.
352. Yiannoullou, P., Kanesalingam, K., van Dellen, D. & Augustine, T. (2015) Encapsulating peritoneal sclerosis: presentation without preceding symptoms. *Saudi J Kidney Dis Transpl*, 26(2), 329-34.
353. Young, V. J., Ahmad, S. F., Brown, J. K., Duncan, W. C. & Horne, A. W. (2015) Peritoneal VEGF-A expression is regulated by TGF-β1 through an ID1 pathway in women with endometriosis. *Sci Rep*, 5, 16859.
354. Yu, J. W., Duan, W. J., Huang, X. R., Meng, X. M., Yu, X. Q. & Lan, H. Y. (2014) MicroRNA-29b inhibits peritoneal fibrosis in a mouse model of peritoneal dialysis. *Lab Invest*, 94(9), 978-90.
355. Yu, M. A., Shin, K. S., Kim, J. H., Kim, Y. I., Chung, S. S., Park, S. H., Kim, Y. L. & Kang, D. H. (2009) HGF and BMP-7 ameliorate high glucose-induced epithelial-to-mesenchymal transition of peritoneal mesothelium. *J Am Soc Nephrol*, 20(3), 567-81.
356. Yung, S., Chen, X. R., Tsang, R. C., Zhang, Q. & Chan, T. M. (2004) Reduction of perlecan synthesis and induction of TGF-beta1 in human peritoneal mesothelial cells due to high dialysate glucose concentration: implication in peritoneal dialysis. *J Am Soc Nephrol*, 15(5), 1178-88.
357. Yung, S., Li, F. K. & Chan, T. M. (2006) Peritoneal mesothelial cell culture and biology. *Perit Dial Int*, 26(2), 162-73.

358. Yáñez-Mó, M., Lara-Pezzi, E., Selgas, R., Ramírez-Huesca, M., Domínguez-Jiménez, C., Jiménez-Heffernan, J. A., Aguilera, A., Sánchez-Tomero, J. A., Bajo, M. A., Alvarez, V., Castro, M. A., del Peso, G., Cirujeda, A., Gamallo, C., Sánchez-Madrid, F. & López-Cabrera, M. (2003) Peritoneal dialysis and epithelial-to-mesenchymal transition of mesothelial cells. *N Engl J Med*, 348(5), 403-13.
359. Zeisberg, M. & Duffield, J. S. (2010) Resolved: EMT produces fibroblasts in the kidney. *J Am Soc Nephrol*, 21(8), 1247-53.
360. Zeisberg, M., Hanai, J., Sugimoto, H., Mammoto, T., Charytan, D., Strutz, F. & Kalluri, R. (2003) BMP-7 counteracts TGF-beta1-induced epithelial-to-mesenchymal transition and reverses chronic renal injury. *Nat Med*, 9(7), 964-8.
361. Zhang, H., Liu, F. Y., Liu, Y. H., Peng, Y. M., Liao, Q. & Zhang, K. (2005) Effect of TGF-β1 Stimulation on the Smad Signal Transduction Pathway of Human Peritoneal Mesothelial Cells. *Int J Biomed Sci*, 1(1), 8-15.
362. Zhang, K., Zhang, H., Zhou, X., Tang, W. B., Xiao, L., Liu, Y. H., Liu, H., Peng, Y. M., Sun, L. & Liu, F. Y. (2012) miRNA589 regulates epithelial-mesenchymal transition in human peritoneal mesothelial cells. *J Biomed Biotechnol*, 2012, 673096.
363. Zhang, L., Liu, F., Peng, Y., Sun, L. & Chen, G. (2013) Changes in expression of four molecular marker proteins and one microRNA in mesothelial cells of the peritoneal dialysate effluent fluid of peritoneal dialysis patients. *Exp Ther Med*, 6(5), 1189-1193.
364. Zhang, X., Ibrahimi, O. A., Olsen, S. K., Umemori, H., Mohammadi, M. & Ornitz, D. M. (2006) Receptor specificity of the fibroblast growth factor family. The complete mammalian FGF family. *J Biol Chem*, 281(23), 15694-700.
365. Zhou, Q., Fan, J., Ding, X., Peng, W., Yu, X., Chen, Y. & Nie, J. (2010) TGF-{beta}-induced MiR-491-5p expression promotes Par-3 degradation in rat proximal tubular epithelial cells. *J Biol Chem*, 285(51), 40019-27.
366. Zhou, Q., Yang, M., Lan, H. & Yu, X. (2013) miR-30a negatively regulates TGF-β1-induced epithelial-mesenchymal transition and peritoneal fibrosis by targeting Snai1. *Am J Pathol*, 183(3), 808-19.
367. Zhou, X., Ren, Y., Liu, A., Han, L., Zhang, K., Li, S., Li, P., Kang, C., Wang, X. & Zhang, L. (2014) STAT3 inhibitor WP1066 attenuates miRNA-21 to suppress human oral squamous cell carcinoma growth in vitro and in vivo. *Oncol Rep*, 31(5), 2173-80.
368. Zhu, F., Li, T., Qiu, F., Fan, J., Zhou, Q., Ding, X., Nie, J. & Yu, X. (2010) Preventive effect of Notch signaling inhibition by a gamma-secretase inhibitor on peritoneal dialysis fluid-induced peritoneal fibrosis in rats. *Am J Pathol*, 176(2), 650-9.
369. Zweers, M. M., de Waart, D. R., Smit, W., Struijk, D. G. & Krediet, R. T. (1999) Growth factors VEGF and TGF-beta1 in peritoneal dialysis. *J Lab Clin Med*, 134(2), 124-32.

Appendix: Buffers and Reagents

Reduccing Gel Loading Buffer 3x

0.5 M Tris-HCl, pH 6.8 ..... 1 ml

Glycerol ..... 2.4 ml

10% (w/v) SDS..... 4.8 ml

0.05% (w/v) Bromophenol Blue .... 2 drops

Beta-mercaptoethanol..... 1.2 ml

TBS (10x)

Tris..... 24.2 g/l

NaCl ..... 80 g/l

pH 7.4

Running Buffer (10x)

Tris-HCl ..... 30 g/l

Glycine..... 144 g/l

SDS ..... 10 g/l

pH 8.3

YTx2

Tryptone ..... 16 g/l

Yeast extract ..... 10 g/l

NaCl ..... 5 g/l

Transfer Buffer (10x)

Tris-HCl ..... 30 g/l

Glycine..... 144 g/l

pH 8.3 (no adjustment necessary)

YTx2 agar plates

Tryptone ..... 16 g/l

Yeast extract ..... 10 g/l

NaCl ..... 5 g/l

Agar ..... 20 g/l

Transfer Buffer (1x)

Transfer Buffer 10x ..... 100 ml/l

Methanol..... 200 ml/l